Infrared Spectroscopic Assessment of Capillary-Alveolar Membrane Permeability in Acute Lung Injury: A Biophysical Perspective

By

Jing Wang

A Thesis Submitted to the Faculty of Graduate Studies:
Partial Fulfillment of the Requirements for the Degree of

DOCTOR OF PHILOSOPHY

Interdisciplinary Program
University of Manitoba
Winnipeg, Manitoba

THE UNIVERSITY OF MANITOBA

FACULTY OF GRADUATE STUDIES

*****

COPYRIGHT PERMISSION PAGE

INFRARED SPECTROSCOPIC ASSESSMENT OF CAPILLARY-ALVEOLAR MEMBRANE PERMEABILITY IN ACUTE LUNG INJURY:

A BIOPHYSICAL PERSPECTIVE

BY

JING WANG

A Thesis/Practicum submitted to the Faculty of Graduate Studies of The University of Manitoba in partial fulfillment of the requirements of the degree of

DOCTOR OF PHILOSOPHY

Synopsis

Increased permeability of the alveolar-capillary membrane results in diffuse alveolar damage that leads to non-cardiogenic low-pressure pulmonary edema. Clinically, this is referred to as acute lung injury (ALI). The well-described phenomenon of acute respiratory distress syndrome (ARDS) is a severe form of acute lung injury, often associated with a high mortality rate in the critical care population. Currently, there are very few practical techniques available to provide a rapid and direct measure of pulmonary microvascular permeability in the critical care setting.

In this study, a novel diagnostic technique involving the administration of hydroxyethyl starches (HES) to patients with ALI/ARDS is introduced. The infrared (IR) spectroscopic determination of hydroxyethyl starch-based macromolecules in patient's bronchial washing fluids is used to assess the pulmonary alveolar-capillary permeability in acute lung injury. The technique is also capable of monitoring the effectiveness of oncotic fluid management for ARDS patients during their treatment course in the ICU.

Hydroxyethyl starches are used clinically as colloid plasma expanders. The large size of infused HES, under normal circumstances, restricts these molecules to the intravascular space. Under conditions of increased pulmonary vascular permeability, high molecular weight fractions of the polymer with plasma protein components and water will leak into the pulmonary interstitium. The leakage of plasma protein and water result in pulmonary interstitial edema. Eventually, the leakage expands into the alveolar space and in severe cases may lead to ARDS. Recovery of HES in a patient's bronchial alveolar fluid or in the bronchial washing fluids therefore suggests capillary-alveolar membrane

abnormalities and lung edema. The HES molecules have a unique vibrational absorption signature that can be easily detected by IR spectroscopy.

IR spectroscopy and IR microscopy were applied to animal injury experiments for pulmonary permeability assessment. The investigations on animal bronchoalveolar fluids and tissue provide physiological, pathological and histochemical evidences of starch-based macromolecule infiltration into the interstitium through the damaged capillary endothelial barrier. From there, these molecules gain access into the alveolar space.

From the baseline study, two groups were recognized as "leak" and "non-leak" based on the spectral signature of HES in bronchial washing fluid. By applying a spectral pattern recognition methodology a training set was constructed based on a set of bronchial washings for leak and non-leak groups. Linear discriminant analysis was then used to establish a prediction model which was tested and applied to clinical investigations.

Autopsy tissue from a patient with acute lung injury confirmed that investigation of a patient's bronchial washing fluid is able to provide an early diagnosis of ARDS. A prospective randomized study on an injured patient population was also conducted. An IR spectral database for bronchial washing fluids resulted from this investigation. Two cases of ALI/ARDS were examined by the new methodology emphasizing the importance of early diagnosis. The results of these case studies demonstrate the potential value of IR spectroscopy for assessing pulmonary permeability in critically ill patients.

The experimental and clinical investigations demonstrate that IR spectroscopy provides a direct measure of capillary-alveolar membrane permeability in acute lung injury. This technique is advantageous because no radioactive tracers are employed and

little sample preparation is required. It is a rapid, simple, and a minimally invasive technique with high sensitivity for diagnosing ARDS. Furthermore, the assay method is very specific in evaluating pulmonary vascular permeability in acute lung injury cases. The simplicity of this method makes it convenient to use and applicable to the critical care environment. This study of the use of IR spectroscopy in the assessment of capillary-alveolar membrane permeability in acute lung injury patients represents a new and significant application of this technique to clinical sciences. There is already ample evidence that the IR technique will add invaluable diagnostic information about a challenging lung disease as well as providing an easy method of monitoring treatment during its clinical course.

Acknowledgments

I wish to acknowledge first and foremost my supervisor, Dr. H. H. Mantsch. His scientific guidance and constant encouragement have been steadfast throughout my time at the Institute for Biodiagnostics, the National Research Council of Canada. His work ethic and particular attention to detail has been of great inspiration to me. I am very grateful that he has provided me with the opportunity to work under his supervision, using the extensive research facilities at the National Research Council of Canada.

I wish to express my very special thanks to Dr. L. Oppenheimer for giving me the chance to collaborate on this significant research project. I have learned a great deal from his detailed knowledge of physiology, biophysics and clinical science and in turn, this has broadened my appreciation of the different ways that clinical and basic sciences merge. He has provided guidance and constructive suggestions throughout all the phases of this research project, and use of his laboratory and research facilities provided important contributions to my research. Without his support, it would have been difficult to finish my graduate studies.

I would also like to thank other advisory committee members, Dr. E. Kroeger and Dr. G. Tabisz, who have provided me with valuable advice on physiology and physics throughout the period of my graduate study. I thank too Dr. A. Ismail for agreeing to be my external examiner and spending time reading my thesis.

I also wish to express my gratitude to my clinical collaborators, Drs. Bracken, Pintin, Yip, Court and Fata, for their friendship, and without whose strong support of this research the project would have been completed. Drs. Fata and Court, in particular have

spent much of their valuable time in supporting this research and in reading and correcting my thesis. Their assistance and friendship will have a special place in my heart. I have gained much clinical knowledge from all these surgical research fellows and am very appreciative of this extended scholarship.

I would like to express my appreciation to my colleagues at the Institute for Biodiagnostics, Drs. M. Sowa, A. Shaw, M. Jackson, H. Eysel, L-P. Choo-Smith, Mr. J. Mansfield and the rest of spectroscopy group for their help and support of my work. I have benefited greatly in many ways by working with the group. I would like to express special thanks to Dr. C. Schultz, for many useful discussions, suggestions and friendship. I have learned a great deal from him. My thanks are also extended to Dr. K. Scott for assistance proof-reading in some parts of my thesis.

There are many people at the Institute who have provided very useful feedback: Mr. R. Summers, Drs. A. Nikouline and R. Somorjai from the Informatics group for their help in data statistical analysis and the use of software developed by the group. I would like to express my gratitude to all of those people at the Institute who assisted me during my graduate study.

I would also like to thank Ms. M. Dajic, the research laboratory technician at Health Sciences Center, for her consistent technical support and attention to detail. Having her constant support in the lab made the animal experiments possible.

Finally, this work is dedicated to my wife, Limei Hu, my daughter, Qian Wang, and my family, whose support and understanding have been unconditional throughout this undertaking.

Abbreviations

ALI, acute lung injury

ANTU, alpha-naphthyl thiourea

ARDS. acute respiratory distress syndrome

BALF, bronchial alveolar lavage fluid

BWF, bronchial washing fluids

CM, center of mass

COP, colloid osmotic pressure

CT, x-ray-computed tomography

ELF, epithelial lining fluid

EVLW, extravascular volume of lung water

FiO_2, fraction of inspired oxygen

FT-IRS, Fourier transform infrared spectroscopy

H & E, hematoxylin and eosin

HES, hydroxyethyl starch

HMW, high molecular weight

ICU, intensive care units

IR, infrared

LDA, linear discriminant analysis

LIS, lung injury score

LMW, low molecular weight

MCT, mercury cadmium telluride

PaO_2, partial pressure of arterial oxygen

PAS, periodic acid-Schiff

PEEP, positive end-expiratory pressure

SICU, surgical intensive care unit

List of Figures

List of Tables

Table of Contents:

Introduction

The mechanics of transcapillary exchange are based upon the principles of classical transport and statistical thermodynamics. These encompass the mechanisms of molecular diffusion, forces acting across membranes, solute transport through membranes and fluid osmotic flow. Together, these theories form a complete hypothesis of molecular transport through membrane barriers. This is referred to as the pore theory of the membrane. Macromolecule transport mechanics can be expressed mathematically in terms of hydrostatic and osmotic pressure gradients, a filtration coefficient and a reflection coefficient. These expressions are well known as fluid filtration equations and are extensively used to describe the fluid distribution between intravascular and extravascular compartments under normal and abnormal conditions.

In the normal situation, fluid transport dynamics in a microcirculatory system is described as a capillary-tissue-lymphatic system. In this model, fluid from the blood passes through the capillary wall under the influence of pressure. This fluid consists of water, electrolytes, small molecules such as glucose and dissolved oxygen or carbon dioxide, and large protein molecules. The protein concentration is much lower in the interstitial space than within the capillaries. This maintains the pressure gradients (hydrostatic and osmotic) in favor of continuous fluid filtration into the interstitium, thus providing for the physiological needs of tissues and organs. Excess fluid from the interstitium is returned into circulation by the lymphatic flow.

Under abnormal conditions, such as in the case of an inflammatory reaction or other physical and chemical insult, the membrane barriers between the tissues and the

capillaries are damaged. This allows large plasma protein components and water to leak into the interstitial spaces. The accumulated fluid in the interstitium forms interstitial edema. This theory explains the pathophysiology of permeability edema.

The term ALI/ARDS describes the acute abnormalities of pulmonary function. This condition is the result of diffuse alveolar damage resulting in noncardiogenic pulmonary edema. It is characterized by increased pulmonary vascular permeability due to the breakdown of capillary endothelial and epithelial membrane barriers. Pulmonary edema, hypoxemia, and decreased gas exchange function across the alveolar membrane are common clinical features related to this syndrome. Despite advances in medical therapy, there is still a high mortality rate, in excess of 50% (Marino, *ICU Book*, 1995), in the critical care population.

The treatment of ALI/ARDS patients is primarily supportive. A new therapeutic strategy was recently introduced based on application of the principles of transvascular fluid filtration and macromolecular exchange. Oncotic fluid manipulation is designed to increase the osmotic pressure gradient between the intravascular and extravascular compartments, and thereby mobilize fluid from extravascular (interstitial) spaces into the intravascular space. This process will reabsorb excess fluid from the interstitium and reduce edema. The colloid materials often used to increase capillary osmotic pressure are large macromolecules with high colloidal properties. Recent studies indicate that plasma expanders, namely hydroxyethyl starches (HES), exert the greatest influence in oncotic manipulation for ARDS therapy.

Currently ALI/ARDS diagnosis is largely dependent on the patient's pulmonary function, and is measured by a lung injury scoring system designed by John Murray

(Murray *et al.*, 1988). The system includes four parameters, chest X-ray evaluation, hypoxemia score, the respiratory system compliance score and the optimal positive end-expiratory pressure (PEEP) score. Although the scoring system performs adequately in clinical terms, it provides no direct measure of pulmonary vascular permeability, the pathognomonic feature of ALI/ARDS.

In this thesis, a new approach to capillary-alveolar permeability determination in acute lung injury is introduced. The approach is based on the use of IR spectroscopic technique combined with the administration of hydroxyethyl starch. The hypothesis of this study is that under the conditions of exaggerated capillary-alveolar permeability which occur in acute lung injury, large macromolecules such as hydroxyethyl starches can gain access to the interstitium of the lung and then enter the alveolar space. Therefore, recovery of hydroxyethyl starch in significant quantities from the alveolar space constitutes evidence of capillary-alveolar leakage. This should provide diagnostic information of acute lung injury and ARDS. Excessive leakage of hydroxyethyl starch-based macromolecules into the alveolar space reduces the intravascular osmotic pressure gradient, thus reducing effectiveness of oncotic management. Monitoring hydroxyethyl starch alveolar infiltration should not only provide a measure of lung vascular permeability but it should also identify patient population in which oncotic management will be most effective. The objective of this thesis is to evaluate an IR spectroscopic technique for the diagnosis and management of ALI and ARDS.

IR spectroscopy is one of the most useful physical methods in chemical and biochemical analysis. It plays an important role in the elucidation of structures and in the identification of organic, inorganic and biochemical materials. Due to improvements in

instrumentation and data evaluation, quantitative analysis of samples can be reliable and straightforward even at the picogram level. The technique has recently been applied to biomedical problems and demonstrates great potential for diagnosing diverse clinical diseases. This technique has an advantage in that analysis is not hindered by the physical state of the sample. Gaseous, liquid, solid, or even inhomogeneous specimens can be studied. A number of clinical investigations using IR spectroscopy have been successfully performed utilizing biofluids such as plasma, urine, cerebrospinal fluid, synovial fluid, and also tissues.

The starch-based macromolecules are weighted averaged polymers. The average molecular weight of these polymers is generally high enough to minimize their filtration into the interstitial space. The molecular compositions of these polymers are not uniformly distributed. Their broad range of distributions theoretically includes molecules small enough to be filtered into the interstitium. This suggests that fractions of various molecular sizes of these polymers may penetrate into the interstitium through the pores on the damaged membrane barrier.

In this study, IR spectroscopic assessment of pulmonary permeability in ALI/ARDS patients is based on determination of low molecular weight hydroxyethyl starch (LMW HES) infiltrating the alveolar space. LMW HES is a substituted glucose polymer that is structurally similar to glycogen. It has an average molecular weight of 200,000-300,000 Daltons. Clinically LMW HES is primarily used as a colloid plasma volume expander. In the normal situation, the size of infused HES largely confines these molecules to the intravascular spaces until they are hydrolyzed by the serum α-amylases into subunits small enough to be filtered and eliminated by kidney. Certain pathological

conditions capable of producing an increase in capillary permeability might be expected to be associated with leakage of larger HES macromolecules into the interstitial space. The detection of HES in patient's lung fluid indicates the presence of pulmonary vascular leakage. Thus, HES could be essentially used as a tracer of increased pulmonary capillary permeability. These polymers have a unique infrared absorption signature that is easily monitored by IR spectroscopy.

Considerable attention has been paid to the determination of lung microvascular permeability in critical ill patients. In spite of this the demonstration of the presence of increased capillary permeability still remains a challenge. Several methods have been introduced to measure pulmonary capillary permeability in abnormal states. Most methods rely on the use of radioactive isotopes as tracers. Indicator-dilution methods introduce specifically labeled components, typically $^{3}H_2O$, ^{14}C-urea, ^{125}I-albumin and ^{51}Cr labeled red blood cells, into the circulation system. The time course of these tracers in the blood then is followed in a single pass requiring rapid and precisely timed arterial blood sampling. Based on partitioning models for the variously labeled components, the permeable surface area for urea and the extravascular volume of lung water (EVLW) can be determined. It has been difficult, however, to clinically establish the soundness of these determinations. This is especially true for the critical care population where vascular tone and tissue permeability characteristics vary considerably. In addition, measuring EVLW by indicator-dilution methods is a costly and tedious bedside procedure. It has a reliability of <70% in the best case series (*Handbook of Critical Care*, Dukes, 1996). External pulmonary gamma counting has the advantage of providing a more direct measure of tracer infiltration into the lung. The technique is, however,

cumbersome and thus ill suited to routine patient monitoring in a critical care environment. The reliance of both of these methods on the use of radioactive tracers carries with it some safety concerns. There are also associated ethical issues concerning the use of these tracers on a control population.

In contrast to other methods used to determine pulmonary microvascular permeability, IR based HES assay uses no radioactive tracers and requires little sample preparation. The instrumentation is compact and the method rapidly provides a measure of pulmonary capillary permeability that makes it suitable for routine operation in a critical care environment. Therefore, this study would illustrate a new application of IR spectroscopy in the clinical sciences.

The scope of the research includes (1) The investigation of an animal model of acute injury model to provide the background for a controlled physiological/biophysical environment. (2) The establishment of an IR spectral database of patient's bronchial washing for capillary leak and non-leak patient populations. (3) The application of multivariate statistical classification methods to the IR spectral database to ascertain the optimal data classification scheme and the establishment of a prediction model. (4) The application of the prediction model to a randomized patient population as well as case studies to evaluate the clinical significance of the IR-bronchial washing assay technique. The most important impact of the study would be its clinical application to ALI/ARDS patients. Once the IR-bronchial washing method is calibrated, it may provide a diagnostic tool for identification and treatment of a poorly defined and often misdiagnosed clinical problem that commonly encountered in the ICU population.

This thesis includes six chapters. In the first chapter, pulmonary permeability properties and pulmonary edema formation in acute lung injury are reviewed. The second chapter describes fluid transport mechanics across membranes from the physical perspective. The transport of macromolecules through a membrane is derived from certain mathematical relationships known as capillary filtration equations. Some practical considerations of the use of a filtration equation will be point of out in this chapter. The biophysical therapeutic treatment strategies of ALI/ARDS are discussed, as well as the physical, and chemical properties of the treatment reagent HES. The third chapter will introduces a tool for evaluating pulmonary permeability. It includes a brief theory of IR spectroscopy and its biomedical applications. The fourth chapter includes IR spectroscopic characterization of HES, the IR spectroscopic and microspectroscopic investigations of an animal injury model by use of HES. The pathologic conformation and significance of the investigations are also discussed in this chapter. The fifth chapter introduces the IR-bronchial washing assay method for assessing pulmonary permeability in patients. A model for predicting pulmonary leakage is built based on spectral pattern recognition. The sixth chapter covers the clinical application of this new method. A randomized, prospective study and two case studies are discussed. The significance of this technique in clinical applications is analyzed using statistical methods. The final chapter concludes the relevant clinical and experimental findings using this technique and possible future applications.

Chapter 1

Pathophysiological Background: Pulmonary Vascular Permeability and Acute Lung Injury

The properties of capillary permeability to macromolecules in both normal and abnormal situations have been the subject of interest to physiologists for decades. To date, many attempts to describe these properties have been proposed theoretically, experimentally, and clinically. Theoretical work focuses largely on developing physical and mathematical models based on idealized system to describe the macromolecular exchange mechanism through the capillary wall. Experimental investigations have concentrated on measuring permeability properties in various organ systems. The ultimate goal is to develop a practical method to evaluate changes in permeability properties in the capillary leak syndrome.

1.1 Structure of the Capillary Membrane Wall

In this section, the ultrastructure, composition, function and permeability properties of normal alveolocapillary membrane barriers will be reviewed, with a special focus on the pulmonary capillary system.

1.1.1 Capillary Structure and Transport Pathways

The capillaries are the principal sites of substrate exchange between the blood plasma and the tissue fluid. Although the microcirculation varies in different organs, the microcirculatory system in general, can be described simply as consisting of small arteries (radii > 40 μm), which further bifurcate into smaller arteries called *capillaries*. The capillaries then separate into small venules. A diagram of the microcirculation and cellular components of the blood is presented in Fig.1.1.1. This division forms an extensive network with very little resistance and a large surface area for absorption. The large area of capillary beds permits exchange of small molecules such as glucose, lipid soluble molecules and water with the interstitial space. Although solute and solvent can leave and enter the microcirculation through both small arteries and venules, physiologists believe that the capillaries are the principal sites of water and solute exchange. The capillary wall consists of extremely attenuated endothelial cells with their basal lamina supported by a sparse network of reticular fibers composed of loose collagen.

Scattered along the outside of capillary cells are the *pericytes*. Pericytes are enclosed in a thin external lamina that is continuous with the basal lamina of the endothelium except at the gap junctions between their processes and the underlying endothelial cells. The average diameter of the capillaries is from 7 to 10 μm. This diameter is just large enough to permit unimpeded passage of the cellular elements of the blood. Large cell components like red blood cells can squeeze through capillaries.

Capillaries are complex structures offering several pathways for exchange. The transport pathway in the capillary refers to the channel of microcirculatory exchange of

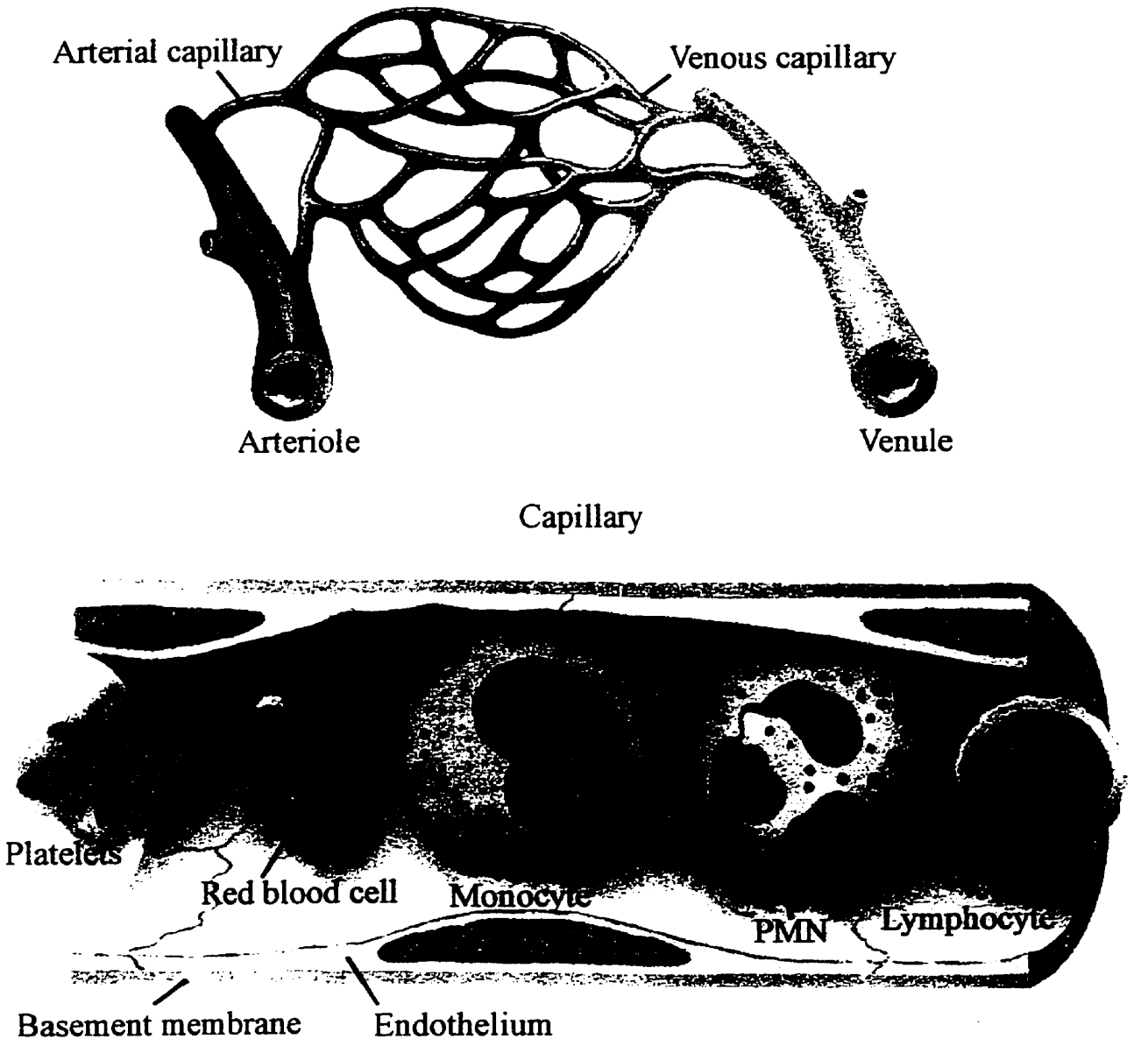

Fig. 1.1.1 The microcirculation and cell components of the blood (From Rubin, 2nd edition, 1994, with permission)

fluid and protein components between capillary and tissue. Capillary walls are defined as having continuous, fenestrated, or discontinuous barriers, as demonstrated in Fig. 1.1.2. The continuous capillaries have dense continuous basement membranes. They are the most widely distributed capillaries in mammalian tissues and can be found in the muscle, lung, kidney, heart, and most organs in the body. The major transport pathways in the continuous basement membrane are the intercellular junctions, often called intercellular *clefts*. The clefts are the thin slits between adjacent endothelial cells and are the major component of the transport pathway. Structurally, each of these "clefts" is interrupted periodically by short ridges of protein attachments that hold the endothelial cells together. Each ridge is in turn broken after a short distance so that the fluid can move through the clefts. The average spacing is normally about 6-7 nm. These intercellular clefts occupy no more than 1/1000 of the total surface area of the capillary (Guyton and Hall, 1996). The "clefts" are very permeable to small solutes such as glucose, water, and NaCl. By contrast, large protein molecules in plasma are excluded from these clefts.

Large macromolecules can gain access to the interstitium through transendothelial channels in the continuous capillaries. These large transendothelial channels most likely represent the capillary "*pores*" as described in physiological studies.

Fenestrated capillaries are commonly found in the interstitial mucosa, endocrine, and exocrine glands and the glomerulus. Fenestrated capillaries are normally located in organs where large fluxes of small solute and fluid constantly occur. Certain features of the fenestrated capillary wall such as the inter-endothelial channels may serve as transport pathways for macromolecules. These capillaries, however, are no more leaky to plasma proteins than the continuous capillary membranes (Taylor *et al.*, 1985).

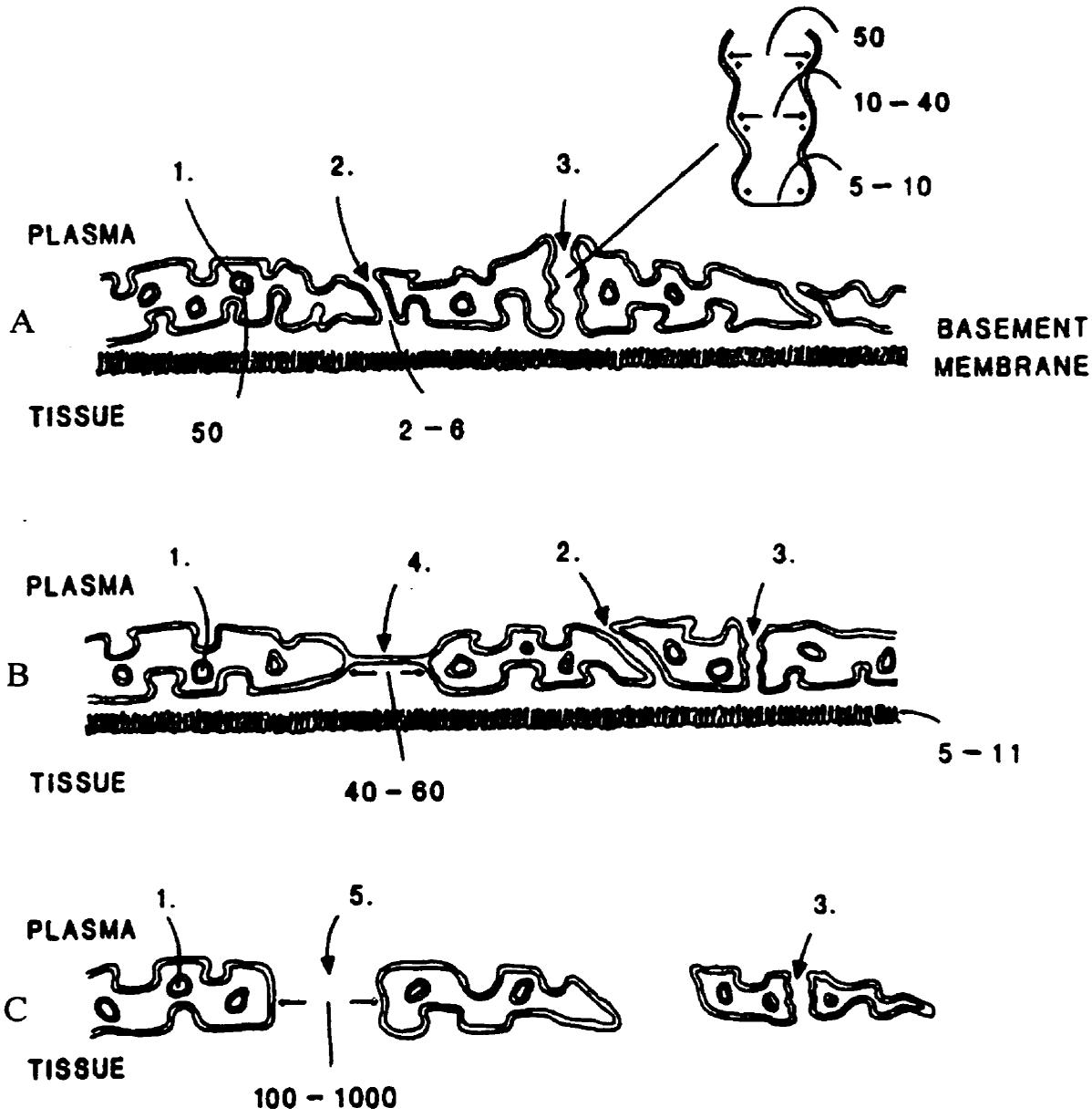

Fig. 1.1.2 Diagram of representation of continuous (A), fenestrated (B), and discontinuous (C) capillaries. 1.indicates plasmalemmal vesicles; 2. Inter-endothelialchannels; 3. Transendothelial channels(pores); 4. diaphragms; and 5. large gaps in discontinuous capillaries. The sizes of pore radii are given at each site with units in nm (Reproduced from Taylor *et al.*, 1991).

Discontinuous capillaries are characterized by large gaps, between endothelial cells, ranging from 100 to 1000 nm. No basement membrane is present. These large gaps are highly permeable to plasma proteins. Protein concentrations are almost the same in the tissues and the plasma across the discontinuous capillaries (Taylor,1985).

Continuous and fenestrated capillaries are highly selective barriers to plasma proteins. Only small amounts of protein escape from these capillaries in the tissues. Discontinuous capillaries are highly permeable to plasma proteins but are found in only a few organs. Capillary walls, therefore, provide an excellent partitioning of proteins and fluid between the plasma and the interstitial fluid. Permeability properties of capillary walls, however, are difficult to describe simply by analyzing structural characteristics.

1.1.2 Microscopic Structure of the Pulmonary System

Microscopically, the respiratory portion of the lung is composed of respiratory bronchioles, alveolar ducts, and alveoli (see Fig.1.1.3). Anatomically, the respiratory tract divides from the trachea into principal bronchi and subsequently into smaller terminal bronchi that constitute the transition from the conduction system above to the respiratory portion of the lungs where gas exchange actually occurs. The walls of the respiratory bronchioles are interrupted by very thin alveoli. Gas exchange can take place within these thin walls. With each branching, the number of alveoli increases, thus increasing the surface area for gas exchange.

The respiratory bronchioles further branch into alveolar ducts. The alveolar ducts contain numerous alveoli. The alveoli are so closely spaced that the limits of the ducts are discernible in section only by the alignment of thickenings of the free edges of the septa between adjacent alveoli.

Fig. 1.1.3 Microscopic structure of pulmonary system. RB: Bronchiole; AD: Alveolar ducts; AS: Alveolar sacs; A: Alveoli; V: Blood vessels. Reproduced from Histology (Fawcett,1994). 14× magnification

These inter-alveolar septa have thickened adluminal edges, which are covered by a few bronchial epithelial cells. These cells overlie delicate strands of smooth muscle within the septal connective tissue.

Pulmonary alveoli are physiologically the most important components of the lung. The alveolus is a very thin-walled component at the termination of the arborescent branching of the bronchioles and the respiratory bronchioles. Here the exchange of oxygen and carbon dioxide takes place between the blood and the inspired air. About 200 to 500 million alveoli are present in the two human lungs. The alveolus is in close apposition to the capillaries as demonstrated in Fig1.1.4. The diameter of a capillary segment is about 10 μm, just enough for a red blood cell. The usual thin microscopic cross-section shows the red blood cells in the capillaries (see Fig. 1.1.4B). There is a high concentration of red blood cells at any given cross-section since these cells are responsible for oxygen distribution to the tissues. This microstructure facilitates oxygen diffusion into the capillaries in exchange for CO_2 destined for the alveolus

The septa between adjacent alveoli contain a dense network of capillaries supported by collagenous and elastic fibers, see Fig 1.1.4A and Fig. 1.15A. This layer of vessels and connective tissue is covered on either side by a thin pulmonary epithelium. The epithelium is made up of type-I and type-II alveolar cells. The type-I alveolar cells are less than 0.2 μm in thickness. The type-I cells represent only 10% of the total cell population in the lung, but they occupy about 95% of the total alveolar surface. The type-II cells are commonly located near the angles between neighboring alveolar septa. The type-II cells constitute 12% of all cells in the lung, but they occupy only 5% of the alveolar surface.

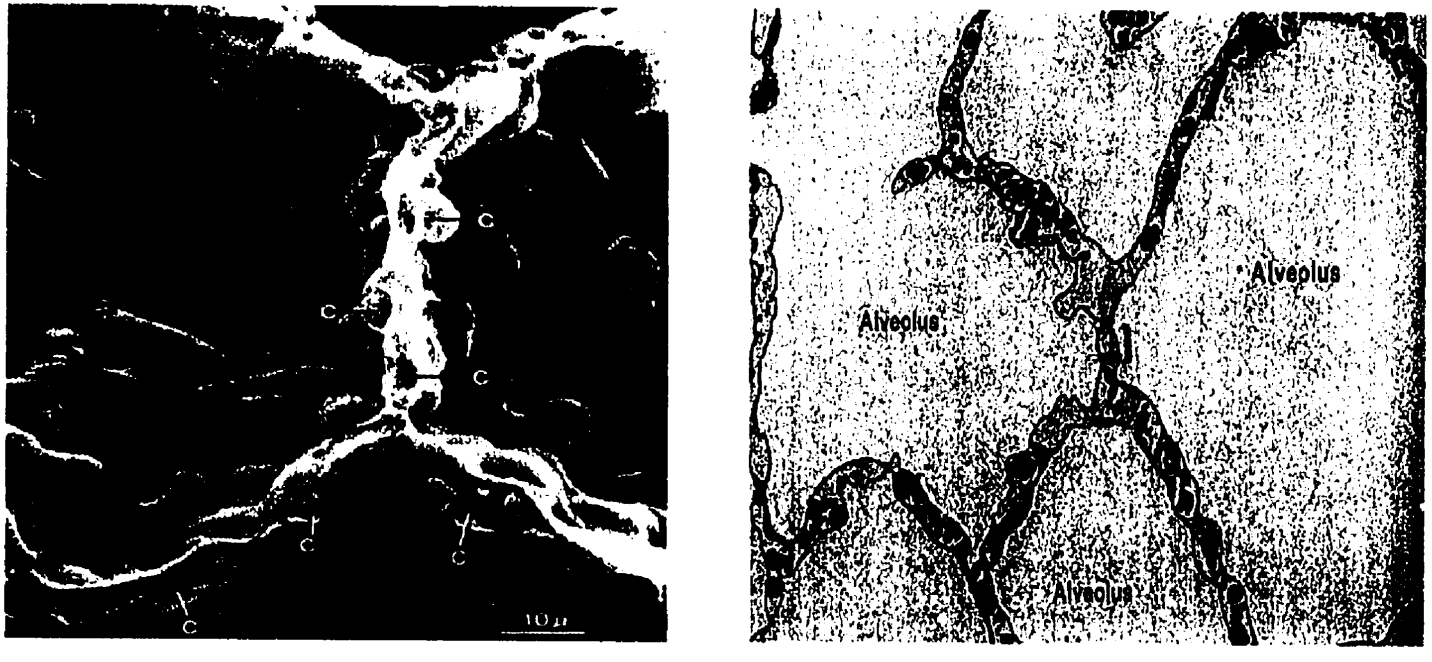

A B

Fig. 1.1.4 A: A high magnification of several alveoli in mammalian lung. B: Electron micrograph of several alveoli in equine lung showing erythrocyte-filled capillaries in the inter-alveolar septa (B: Reproduced from Fawcett, 1994).

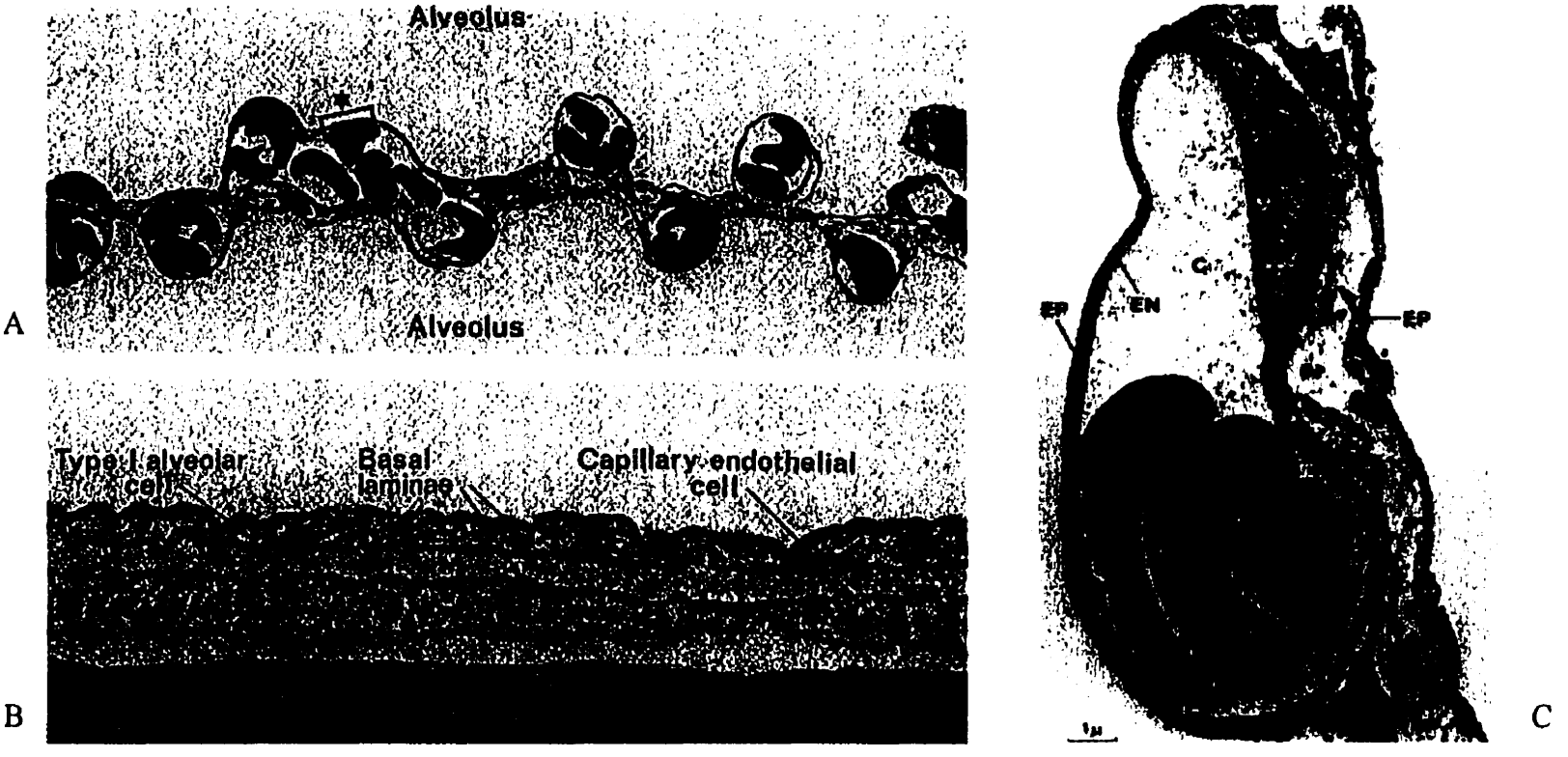

Fig. 1.1.5 A: Micrograph of the septum between two alvoeli of rabbit lung. Capillaries covered by type-I alveolar cells bulge into the lumen, exposing a large surface to the inspired air. B: a high magnification of area indicated by the rectangle in A. (Reproduced from Fawcett, 1994). C: Electron photomicrograph of a human lung, capillaries containing red blood cells are suspended in the inter-alveolar septum between two alveolar spaces. The basement membranes of the epithelium and endothelium appears to be fused over the thin portion of the septum containing the interstitial space.

The type-II alveolar cells synthesize and secrete pulmonary surfactant. The lamellar bodies are their secretory granules (Fawcett, 1994). A detailed discussion of the structure and functions of these cells is beyond the scope of this study and will not be discussed further.

The capillary is lacking connective tissue and the epithelium is separated from the vessel wall by the apposed basal laminae, see Fig. 1.1.5B. These thin areas are favourable for gas exchange. The tissue between the two layers of epithelium on the alveolar septa is defined as the pulmonary interstitium. It contains interstitial fibroblasts (septal cells), mast cells, and a few lymphocytes (Fawcett, 1994). In some species, there may be occasional smooth muscle cells but they are rarely found in the human lung. The septal cells are the most abundant cell type of the interstitium. Their principal function is the production of type-III collagen, elastin and proteoglycans of the extracellular matrix of the alveolar septa.

The capillary-alveolar barrier refers to the barrier separating the pulmonary capillary lumen and the alveolar space. It comprises the capillary endothelium and the alveolar epithelium. The interstitial space lies between and is arranged asymmetrically around the capillaries (Fig. 1.1.5B and 1.1.5C). On one side of the capillary, the interstitial space is obliterated and the width of the barrier is less that 0.5 μm, which facilitates efficient gas exchange. On the other side, the space is larger,1-2 μm, and is thought to be the site of fluid flux between the capillary and the interstitium, Fig.1.1.5C. (MacNaughton, 1996).

1.2 Pulmonary Permeability and Acute Lung Injury

Edema refers to the presence of excess fluid in body tissue. It occurs mainly in the extracellular fluid compartment. Edema formation in the lung can be physiologically classified into hydrostatic edema and permeability edema. Hydrostatic edema is induced by a change in capillary hydrostatic pressure. When caused by left heart failure, it is referred to as cardiogenic edema (presumably no change in capillary-alveolar membrane permeability). Permeability edema results from changes in capillary permeability usually associated with an inflammatory response. It is characterized by abnormal leakage of fluid and protein across capillary membrane into the interstitium. The failure of the lymphatic system to return the excess fluid back to the plasma from the interstitium can also result in pulmonary interstitial edema. Edema caused by lymphatic blockage is a critical factor, because accumulated macromolecules in the interstitium cannot be removed and consequently cause an increase in osmotic pressure of the interstitium that results in more fluid being drawn into the interstitial space.

The acute lung injury and edema formation is a complicated process affected by multiple factors including biochemical and biophysical influences.

1.2.1 Capillary Permeability Properties

1. Semipermeable Membrane

In the transcapillary movement, of the capillary membranes are selective to all plasma proteins molecules averaging from 3.7 nm (albumin) to 12 nm (β-lipoprotein) in radius (Taylor, 1994). The smaller plasma proteins are less restricted than these large macromolecules during their movements across capillary walls.

The concept of "*semipermeable*" membranes has been introduced to describe the selective property of the capillary membrane. The consequence of such selective permeability to plasma proteins is to change the osmotic pressure gradient across membrane barriers and thus influence fluid movements across the capillary membrane. In fluid transport theory the term *osmotic reflection coefficient* (σ) has been introduced to interpret this selective property and to correct the imperfect semipermeable membrane model. By characterizing the capillary membrane in this way, the transport theory has the capacity to physically describe the ability of the membrane to restrict the passage of different-sized molecules. This obviates the assumption that solutes are either freely permeable or impermeable. Fig. 1.2.1 describes the physical interpretation of the selective permeability properties and the reflection coefficient in a membrane barrier. The value of the reflection coefficient ranges from 0 to 1. A value of zero indicates that solutes have no reflection, i.e. all solutes pass through the barrier. At this value, the effect is a protein osmotic pressure of zero. A value of one means total reflection occurs and no solute passes. The protein osmotic pressure is then in the range of 0.7-0.9 mmHg (Staub, 1992). In the case of increased capillary permeability (an injury state), the coefficient will decrease and the osmotic pressure gradient will drop dramatically. The introduction of reflection coefficient into the fluid transport theory emphasizes the value of introducing the osmotic effect. The reflection coefficient is normally defined for a specific solute.

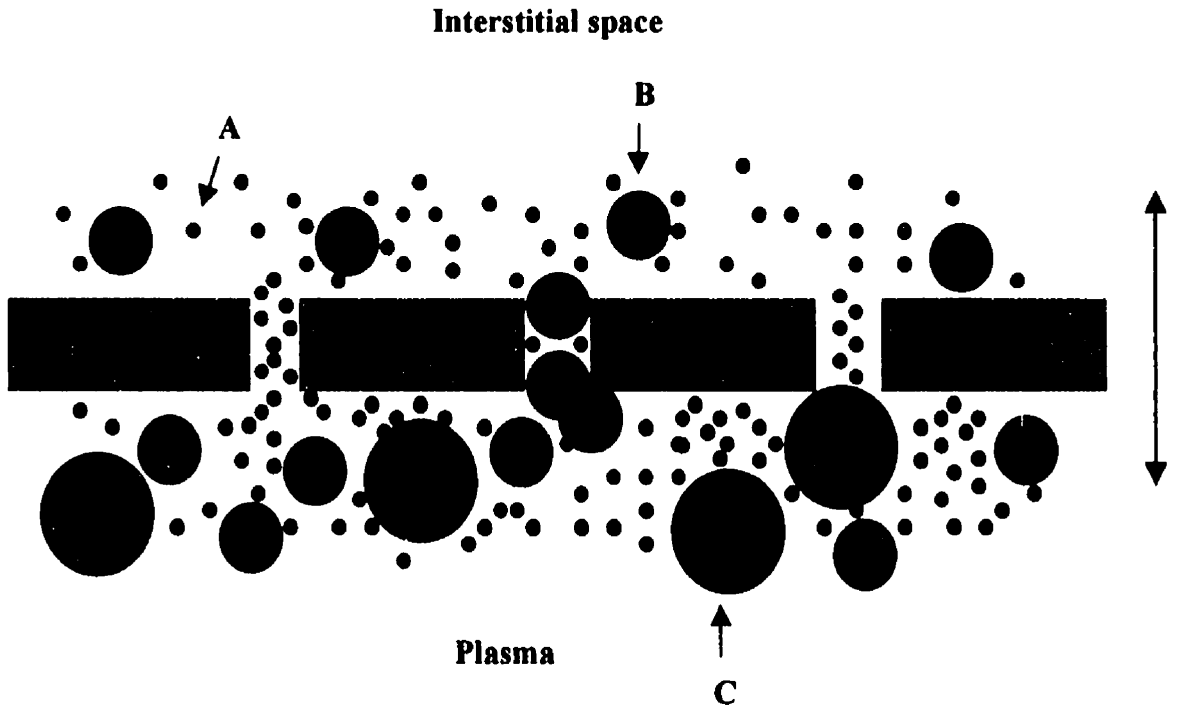

Fig. 1.2.1 Representation of selectivity of a semipermeable membrane. A: small molecules are not restricted to pass, reflection coefficient $\sigma = 0$; B: Molecules pass with some restrictions, $0 < \sigma < 1$; C: Larger molecules are restricted to pass, $\sigma = 1$.

2. Capillary Permeability Properties

A biophysical description of the capillary permeability properties is characterized by capillary pore sizes, permeability-surface area product, reflection coefficient of permeating molecules and filtration coefficient of capillary. Most capillary networks have a large number of small pores with radius about 5 nm which is sufficiently large for albumin to escape into the interstitium, but restricts the large plasma protein components such as β-lipoprotein to the vascular space.

A relatively small number of large pores with radius approximately 20 nm, exist in most capillaries and almost all plasma proteins can penetrate into the interstitium through these channels. The large pore systems are similar between organs and may exist to permit large gamma globulin to enter the tissues in order to deliver the various metabolic substrates and hormones that are carried on their surfaces to parenchymal cells.

The permeability-surface area product of permeating molecules is a function of both permeability of the capillary wall to the molecules and the surface area for exchange. In a normal situation, the permeability-surface area product for small molecules, such as glucose and NaCl, are high in all tissues. Permeability-surface area product (*PS*) will be increased when the capillary walls are damaged and protein will equilibrate more rapidly within the tissue.

The reflection coefficients have a value of one, since small molecules and water are not highly restricted by capillaries. The σ value for albumin in most tissues is near one, and is equal to 1 in the central nervous system capillaries. In the lung and cardiac muscles, the σ values are lower, 0.75 and 0.45 respectively. High protein permeability in these tissues allows plasma protein to better serve as lipid "shuttles" for cardiac

metabolism and surfactant production in lung type II cells (Taylar *et al.*, 1994). The decreased value of σ results in a reduced absorptive force, which will cause the magnitude of transcapillary fluid flux to be underestimated if σ is assumed to be one. This would be the case in states such as increased pulmonary capillary permeability and lung edema formation

The molecular sizes of transported substances are the major factor for the transendothelial exchange. Based on experimental observations, the rates of passage of water-soluble molecules could be accounted for by postulating two fluid-filled systems of pores tranversing the endothelium: (i) "small pores" about 9 nm in diameter and of relatively high frequency. (ii) "large pores" up to 70 nm in diameter and of lower frequency. Although there is general agreement that the vesicles in muscle capillaries and the pores of fenestrated capillaries are the structural equivalents of the "large pores" that are postulated by physiologists. Disagreement is still present as to the location of the "small pore" permitting passage of molecules that are smaller than 9 nm. One possibility is that molecules of this size may pass through discontinuities in the intercellular junctions (Roselli *et al.*, 1969; 1989, 1989).

The transendothelial permeability is also influenced by factors other than molecular size, such as the chemical nature of the molecules, their net charge, and the charge in the pathways involved in the transportation (Taylor *et al.*, 1994).

1.2.2 Changes of Capillary Permeability

Pulmonary pathophysiologic problems related to increased capillary-alveolar membrane permeability resulting in lung edema and alveolar flooding can be induced by various inflammatory mediators. Inflammation in the microcirculation results in movement of

fluid and leukocytes from the blood into extravascular tissues. Under normal conditions, the inflammatory response eliminates the pathogenic insult and removes injured tissue components. Such a process accomplishes regeneration of the normal tissue architecture and return of physiologic normal function. Under certain pathological conditions, the ability to clear injured tissue of foreign agents is impaired or the regulatory mechanism of the inflammatory response is altered. In these circumstances, inflammation is harmful to the host and leads to excessive tissue destruction and injury (Rubin and Farber, 1994).

One of the primary morphological abnormalities in all types of inflammation is the presentation of defects as large "gaps" or "widened slits" in the endothelial cell junctions. Such changes in the structure of capillary membrane walls induce changes of capillary permeability that lead to increasing volumes of fluid filtered into the interstitium. The capillary-alveolar permeability changes have been well documented after anoxia, shock, trauma, anaphylaxis, toxin, endotoxins and enzymes.

It has been determined that hypoxia, inflammatory mediators, autocoids (Rabinovici *et al.*, 1991; Willoughby *et al.*, 1973), a number of cytokines, eicosanoids, endotoxins, and toxins; as well as certain poisons (Carlson *et al.*, 1975; Carlson *et al.*, 1981; Carlson *et al.*, 1990) cause deformation of capillary endothelial cells resulting in larger endothelial "gaps". As a consequence, leakage of protein-rich plasma fluids into the interstitium results. The deformation of capillary endothelial cells occurs by contraction of cytoskeletal fibrils, which have attachments from nucleus to cell wall membrane (Majno *et al.*, 1961 and 1969; Joris, *et al.*, 1972 and 1987). These microfilamemnts are made up of actomyosin, and their contraction deforms and pulls the endothelial cell junction apart forming the "gaps". Morphological studies have shown

that all types of inflammation abnormalities in the endothelial membrane are present in the larger cell junction gaps or pores. Although these large pores may represent evidence of inflammation of the capillary endothelial membrane walls, they may or may not be responsible for causing the capillary leakage that permits macromolecules to penetrate into the interstitium.

Vasoactive mediators that originate from both plasma and cellular sources include histamine, serotonin, bradykinin etc. These mediators bind to specific receptors on vascular endothelial and smooth muscle causing endothelial cell contraction and increased gap formation. The post-capillary venule is the primary site at which vasoactive mediators induce endothelial changes. According to Majno, vascular leakage is a "cardinal" effect of certain inflammatory mediators, "and it is well established that it occurs almost exclusively in the post-capillary venules with a diameter in the range of 10-50 μm" (Majno *et al.*, 1969). Responses of the microvasculature to injury is illustrated in Fig.1.2.2.

The concept of capillary endothelial cell contraction, creating cell junctional gaps, is now generally accepted and leakage of macromolecules such as albumin has been demonstrated with radioisotopic active labels (Dauber *et al.*, 1985 and Mintun *et al.*, 1990). In an electron micrograph by Majno after leukotrience E_4 and intravenous injection of colloid carbon, this large molecule tracer appears between the contracted capillary endothelial cells extravasating through the induced "gap" and resting against the basement membrane and pericyte (Majno, 1969).

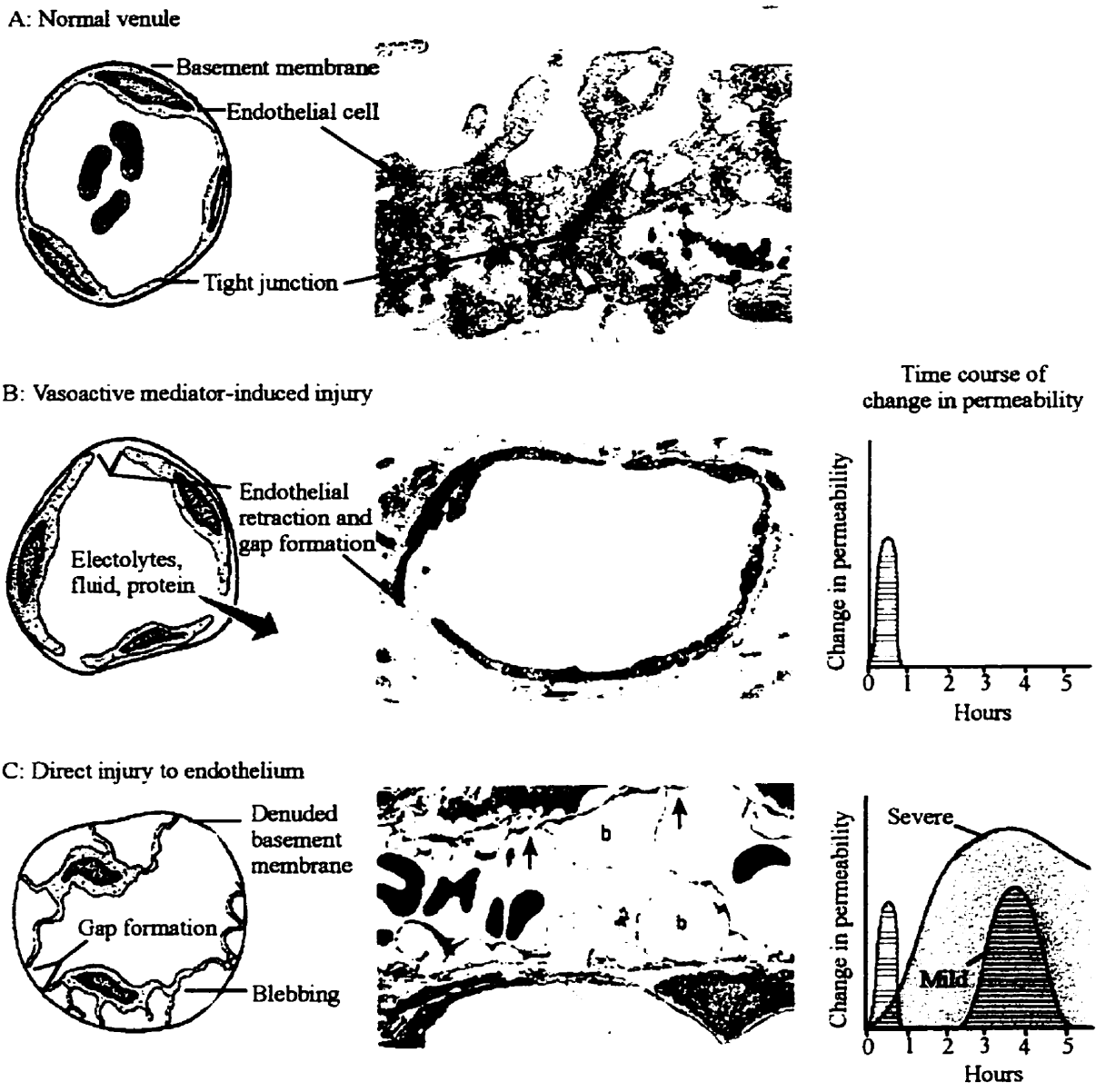

Fig.1.2.2 Response of the microvasculature to injury. A: The wall of the normal venule is sealed by tight junction between adjacent endothelial cells; B: During mild vascuactive mediator induced injury, the endothelial cells separate and permit the passage of fluid constituents of blood. C: With severe direct injury, the endothelial cells form blebs and separate from the underlying basement membrane. Areas of denuded basement membrane (arrows) allow a prolonged escape of fluid elements from the microvasculature. (From Pathology Rubin and Farber, 1994, with permission)

Inflammatory mediators affect the interstitial gel matrix which occupies the interstitial space and is made up of proteoglycans, elastic fibers, reticular filaments, etc. As the fluid enters the interstitial space, one would expect changes in the matrix. Much work has been done on the inflammatory response and the injury process. The description of the detailed process of the inflammation is beyond the scope of this review.

1.2.3 Permeability and Acute Lung Injury

Inflammatory mediators may stimulate dramatic changes in the architecture of the capillary-alveolar endothelial and epithelial barriers. A common conclusion of acute lung injury by various investigators is that increases in capillary-alveolar permeability occur as a result of the release of inflammatory mediators from cells either endogenous or exogenous to the lung.

In the early phases of acute injury, the normal exchange rate of solute and water is greatly accelerated, causing plasma fluid and proteins to rapidly spill into the interstitial spaces through the capillary endothelium. The excess fluid starts to accumulate in the pulmonary interstitium. When the interstitial space becomes sufficiently expanded, as a result, interstitial edema will be formed. The changes of increase in capillary membrane permeability are reversible following mild injury. In severe injury states, however, the excess fluid in the interstitial space eventually breaks the alveolar epithelial membrane resulting in alveolar flooding, and will deteriorate gas exchange between inspired air and the blood.

The disturbance of gas exchange in pulmonary edema is often described as acute lung injury and usually represents the total effects of numerous pathophysiological processes. The development of hypoxemia (decreased PaO_2) and reduced respiratory

system compliance represent deterioration of gas exchange function. The well-known term ARDS is a specific form of acute injury with diverse causes characterized pathologically by diffuse alveolar damage.

This mechanism of non-cardiogenic pulmonary edema which results from increased pulmonary capillary permeability is widely accepted. Since the vascular permeability plays an important role in non-cardiogenic acute lung injury, it is necessary to determine permeability characteristics during early edema formation in order to understand the role it plays in the pathophysiological process. This determination might provide a measure of how abnormal the pulmonary vascular permeability must be before it reliably predicts the presence of edema in the appropriate clinical setting.

1.3 Pulmonary Permeability Determinations

Increased permeability of the pulmonary endothelium to macromolecules is an important factor in many types of lung injury. A number of experimental and clinical approaches to pulmonary permeability in both healthy and injurious states have been investigated. Each approach provides important and useful information on permeability properties, and each of these techniques has unique advantages and limitations, especially for clinical applications. An outline of the major approaches is given in the discussion that follows.

1.3.1 Experimental Approaches

Determination of reflection coefficient (σ), and permeability surface area product (PS) through a monolayer membrane system: Determination of biophysical properties of permeability on pulmonary capillary membrane barriers would be very helpful for analysis on lung fluid balance. The determination of protein permeability on the

pulmonary endothelial and epithelial cell monolayers is a model that is closest to an ideal system for measuring the biophysical properties of a membrane. Many investigations have focussed on in the determination of protein permeability σ and PS (Peterson, 1992). The advantage of the monolayer method is that the surface area, the concentration gradient of solute, the hydrostatic and oncotic pressure gradients are easily obtained. Using such a model also permits the study of a particular solute at a time, and allows the parameters σ and P to be easily calculated for a specific solute.

Lymph studies in an in vivo system: The lymph study of macromolecule permeability is based on the determination of protein content in lymph. It is assumed that the composition of lymph is identical to that of interstitial fluid under steady-state conditions (Russenyak *et al.*, 1967 and Yoffey *et al.*,1970). Experimental data comparisons of interstitial fluid samples with lymph collected simultaneously from the same tissue generally support the assumption that concentrations of macromolecules in lymph and interstitial fluid are identical. In studying an *in vivo* system, measurements of the vascular pressures, lymph flow, and protein concentration in the lymph and plasma provide estimates of fluid flux, pressure gradients acting across the membrane, and the protein concentration in the filtration equation. Such a body of work has been conducted in determining endothelial *PS* by analyzing plasma-lymph albumin kinetics in normally hydrated dog or sheep lung (Staub *et al.*, 1975; Parker *et al.*, 1984). Similar work has also been carried out by other investigators (Brigham *et al.*, 1977 and Renkin *et al.*, 1977).

Using the lymph fluid to estimate *PS* and σ provides important information as to the physiological state of the *in vivo* system. The disadvantages of such a study includes the variation of protein concentration in the lymph as it passes through the lymph node,

which will induce experimental errors (Adair *et al.*, 1982). The reason for this alteration can be attributed to the height of the lymphatic cannula, affecting lymph flow (Drake *et al.*, 1985). The inability to measure directly the hydrostatic pressure in the fluid exchange vessels and the interstitium (Gaar *et al.*, 1967) are other disadvantages of using this method to estimate PS and σ from lymphatic flow.

Isogravimetric method in isolated lung: The isogravimetric methodology can be used to measure the filtration coefficient K_{fc} ($ml.min^{-1}.cmH_2O^{-1}$). The work was initially undertaken by Drake (1978) and is based on constantly monitoring the weight change through a perfused lung which is suspended from a stain gauge. The lymphatics are ligated and the perfusion pressures are adjusted to keep the weight of the lung constant. In this situation, assuming the hydrostatic and osmotic pressure gradients are balanced so that there is no net fluid filtration occurs, a sudden increase in hydrostatic pressure ΔP or decrease in osmotic pressure will result in the weight increasing. This is interpreted as the change of fluid flux ΔJ_v. This method allows the evaluation of the filtration coefficient K_{fc} simply as $K_{fc} = \frac{\Delta J_v}{\Delta P}$. This assumes that the entire increase in the driving pressure is due to the increase in hydrostatic pressure.

The rapid change of weight of the lung may be due to the sudden increase in blood volume flow. An alternate way to perform the experiment is to weight every 10 min. for the volume change to subside (Drake *et al.*, 1980) or extrapolating the late data to zero (Drake *et al.*, 1978). Determination of filtration coefficient in a perfused isolated lung was also performed whereby the lung fluid filtration was monitored by measuring the change of labeled albumin concentration (Oppenheimer *et al.*, 1983).

An isolated lung system has the advantage of well defined physical parameters and it may provide a more accurate result. The disadvantages of this technique are that the isolated lung behaves differently from the intact lung and the filtration coefficient K_{fc} is an average of the properties of different parts of the pulmonary circulation.

General Morphology studies: Morphological examination of lung tissue by light and electron microscopy provides an invaluable adjunct to physiological studies. The morphometric analyses are more laborious but they provide qualitative assessments of cell populations and cellular changes that are important aspects of lung injury, however it provides little or no qualitative information about the degree of injury. A number of investigations were performed along this line. A freeze-fracture technique can also be applied and provides detailed assessment of the integrity of endothelial and epithelial tight junctions. Such information is valuable in determining the pathophysiology of permeability changes. Fixation of lung tissues provides a useful information in morphological studies of lung permeability by electron microscopy (Hayat *et al.*, 1981).

Other morphological investigations involve microscopic visualization of macromolecule leakage. The microscopic visualization of macromolecule leakage was introduced by Landis (Landis and Pappenheimer, 1963; Landis, 1964). Since then, the microscopic technique for observing macromolecule extravasation in tissue has been proven to be one of the more important tools for the determination of the location of leaks, along the length of the capillary. Using dyes or fluorescent compounds with an affinity for binding macromolecules, this technique allows one to correlate macromolecule extravasation with vessel structure. Furthermore, by varying the size of the dye-labeled macromolecule, one can correlate the degree or rate of extravasation with

solute size. One of the major limitations of the microscopic visualization method is that the results obtained from the method are generally qualitative in nature, and the reliability of the conclusions largely depend on the assumption that the dye is entirely bound to the macromolecule with negligible unbound dye (Landis, 1964; Levick and Michel 1973).

1.3.2 Clinical Approaches

Tracer techniques: Tracer techniques are used in conjunction with physiological measurements and the general ultrastructural morphology provides information about the specific sites of leakage of these tracers. The presence of tracer provides strong evidence of the site of leakage in the injured state, as well as evidence for the importance of vesicular transportation in a normal situation. However, use of the tracer method to determine leakage could result in data which is easily misinterpreted. A number of reasons, such as delay in lymphatic clearance, could potentially lead to accumulation of a tracer in an alveolus, and this could be interpreted as evidence of leakage. However, this is actually a false positive result. It is also very difficult to precisely identify the position of leakage because it is possible that the tracer leaked into the air spaces via anther route and then moved into its final location during the edemagenic process.

Clinically, indicator-dilution methods introduce specifically labeled components, typically $^{3}H_2O$, ^{14}C-urea, ^{125}I-albumin and ^{51}Cr labeled red blood cells, into the blood stream. The time course of these tracers in the blood stream is then followed by single pass requiring rapid and precisely timed arterial blood sampling. Based on partitioning models for the various labeled components, permeability surface-area for urea and extravascular volume of lung water can be determined. However, the soundness of this model's assumptions is based on measurements the permeability surface area and

extravascular volume of lung water which have been shown to be difficult to assess clinically. This is especially the case concerning the critical care population where vascular tone and tissue permeability characteristics vary considerably. External pulmonary gamma counting has the advantage of providing a more direct measure of tracer infiltration into the lung. The technique, however, is cumbersome and thus ill-suited to routine patient monitoring in an intensive care unit environment. The reliance of both of these methods on radioactive tracers carries with it some safety questions as well as the associated ethical issues concerning the use of these tracers on a control population.

Radiographic assessment of increased lung permeability: Radiographic assessment of increased lung permeability is based on the use of chest roetgenogram or x-ray-computed tomograph (CT). The chest x-ray has wide clinical application, but provides no quantitative information about the biophysical parameters, K_{fc}, σ and provides little or no qualitative indices of altered integrity. Alberle (Alberle *et al.*, 1988) studied whether the chest x-ray has ability to discriminate permeability changes. Radiological examination was performed in 15 patients with hydrostatic edema and 30 patients with increased permeability edema as assessed by measurement of the protein concentration in the edema fluid with 30 min. intubation. The results indicated that radiological examination alone correctly identifies 87% of the patients with hydrostatic edema, but only 60% of increased permeability edema patients were identified. This results concludes that chest radiography has little value in determining changes in lung permeability, except to identify patients who have pulmonary edema. The chest x-ray alone cannot distinguish

permeability edema from hydrostatic edema unless other clinical parameters are considered.

Analysis of bronchial alveolar lavage fluid: Analyzing bronchial alveolar lavage fluid (BALF) is intended to provide information from the epithelial lining fluid of lungs concerning the presence of edema. Such measurement of epithelial lining fluid volume has been difficult in experimental and clinical settings. The problem associated with this technique is the unknown dilution factor, which is present during the lavage-fluid collection procedure. Gorin and Stewart were able to solve this dilemma by using labeled albumin (Gorin *et al.*, 1980). In this way, the data is normalized to the endogenous albumin concentration, resulting in a measure of the rate of equilibration of the labeled albumin with the endogenous albumin. Other investigators, such as Baughman and Rennard have attempted to modify the lavage technique (Baughman *et al.*, 1983; Rennard *et al.*, 1986). Their improvements consist of measuring the concentration of endogenous proteins in the ELF by devising ways to measure the degree of dilution of the ELF by the saline lavage. Involving a $^{99m}TcO_4^-$ tracer (Peterson *et al,.* 1990) developed a rewash lavage procedure that allows estimation of the dilution of the epithelial lining fluid by the saline.

Once the dilution factor is known, the epithelial-lining fluid protein or tracer concentration can be evaluated from the measured protein concentration in the collected bronchial alveolar lavage fluid. The technique of BALF has previously been used in animal experiments for measuring epithelial fluid protein concentration in control and injured (increasing pulmonary permeability) populations. The results were consistent with morphological estimates (Peterson *et al.*, 1990; Weibel, 1973).

Clinically, measurements of the protein concentration of epithelial lining fluid were limited to conditions where there was sufficient lung injury to cause alveolar and airway flooding to allow direct sampling of edema fluid. This information is useful for understanding the pathophysiologic aspects of lung edema, but more useful information would probably come from studies of changes in epithelial lining fluid that occur before the alveolar and airway flooding occurs. Another aspect related to the protein concentration is that this concentration depends on the injury causing the flooding and is affected by alveolar clearance.

The discussion of pulmonary vascular permeability has focused primarily on descriptive pathophysiology and structural characteristics of the alveolar-capillary barrier. The following chapter will explore the mechanics of fluid transport across the membrane in mathematical and physical descriptions. This discussion will yield a comprehensive background for the principles applied to diagnostic and treatment strategies applied in the critical care setting.

Chapter 2

Physical Background: Mechanics of Fluid Transport across Membranes

The biophysical description of microvascular fluid exchange can be interpreted using fundamental physics principles. The theory describing the process is referred to as the *pore theory*. The discussion is restricted only to the transport phenomena due to pressure gradients, the transport process can be explained by fluid diffusion and filtration mechanics such as Poiseuillean flow, osmotic diffusion and osmotic flow.

The energy for the microvascular transport process is supplied by the heart. The tissue cells are responsible for metabolic uptake to produce nutrients and metabolites. Blood flow through capillaries maintains the gradient of solute concentration and hydrostatic pressure between the capillary lumen and the cells of the body tissues. The potential energy stored in these pressure gradients is dissipated as the solute and water overcome the frictional resistance within pathways for passive transport across the capillary wall.

Pore theory is the theoretical foundation for fluid movement in biological systems. This theoretical development is based on the striking similarities between the permeability characteristics of capillary walls and artificial porous membranes. This theory attempts to interpret transcapillary transport events in terms of permeation through rigid fluid-filled pores using physical fluid transport principles. The mechanics of

Poiseuillean flow, osmotic diffusion and osmotic flow in the pores caused by interaction between solutes and the pore walls play fundamental roles in the formulation of this theory.

2.1 Fluid Movement across the Capillary Membrane

Physically, the transport process describes some physical quantity, such as mass, energy, momentum or electrical charge, that is transported from one region of the system to another. An example of such a process is the mass transport that occurs in the flow of a fluid through a pipe resulting from a pressure difference between the ends of the pipe. Diffusion is another form of mass transportation which takes place in a mixture when a concentration gradient is generated. Each type of physical transportation process can be described by a certain physics law. For example, Ohm's law describes the electrical current flow, fluid flow is interpreted by Poiseille's law, and Fick's law explains the diffusional process.

2.1.1 Poiseuillean Flow

Poiseuille's law was developed to describe fluid flowing in cylindrical pores. In order to apply the law to biological membrane transport systems, the principal assumption in the derivation of the pore theory is that the hydrodynamic relations describing flow and viscous drag forces in macroscopic flow are applicable in channels of molecular dimensions.

Consider a fluid viscously flow in a cylindrical pore, with the forces acting on the fluid element being body forces caused by the pressure gradients in the axial direction and viscous forces described by Newton's law of viscosity. In case of steady flow, P =

$P(z)$ and $\frac{dp}{dz}$ is constant, i.e. the fluid is not accelerated. The equation of motion along the axial direction for the flow, in cylindrical coordinates, can be written as

$$\eta\frac{d^2V_r}{dr^2}+\frac{\eta}{r}\frac{dV_r}{dr}+\frac{dP}{dz}=0 \qquad 2.1.1$$

where η is fluid viscosity in unite dyn•s•cm^{-2}, P is pressure, and V(r) is velocity profile of fluid. The boundary conditions are given:

$$\frac{dV(r)}{dr}=0 \quad \text{at} \quad r=0 \qquad \text{and}$$

$$V(r)=0 \qquad \text{at} \quad r=r_p \qquad 2.1.2$$

where r_p is the radius of the pore. The first requirement for the equation of motion is the assumption that the velocity profile is symmetrical about the axis. The second requirement is that there is no slip between the fluid and the pore wall and the material forming the channel boundary. Then, solving the equation with respect to r, and applying the boundary conditions, one can find the velocity profile in a cylindrical pore to be

$$V(r)=\frac{r_p^2}{4\eta}(1-r^2/r_p^2)\frac{dP}{dz} \qquad 2.1.3$$

The above expression provides the fluid velocity at any radial position in the pore. Total volume flow per unit of time, defined as J_v, through a pore channel is then determined by

$$J_v=\int V(r)dA=\int_0^{r_p}V(r)2\pi r dr$$

$$=\int_0^{r_p}\frac{dP}{dz}\frac{r_p^2}{4\eta}(1-\frac{r^2}{r_p})2\pi r dr=\frac{dP}{dz}\frac{\pi r_p^2}{2\eta}\int_0^{r_p}(1-\frac{r^2}{r_p})r dr=\frac{\pi r_p^4}{8\eta}\frac{\Delta P}{\Delta z} \qquad 2.1.4$$

The evaluated integration gives the total volume flow through a pore of length Δz induced by a pressure difference ΔP. The dependence of J_v on r_p^4 in the above equation indicates that the small changes in the pore radius causes large changes in flow.

For N parallel pores each of area $S = \pi r_p^2$, the area over which fluid exchange occurs is $A_p = N_p \pi r_p^2$. Therefore, the volume flow per unit area is

$$J_v/S = \frac{N_p \frac{\pi r_p^4}{8\eta}\left(\frac{\Delta P}{\Delta z}\right)}{S} = \frac{A_p r_p^2}{8\eta S}\left(\frac{\Delta P}{\Delta z}\right) \qquad 2.1.5a$$

The equation can be rearranged as

$$J_v/S\Delta P = \frac{A_p r_p^2}{S\Delta z 8\eta} = \frac{N_p \pi r_p^4}{S\Delta z 8\eta} = L_p \qquad 2.1.5b$$

where L_p is defined as hydraulic conductivity of the membrane in unit $gm^{-1}\cdot cm^{-1}\cdot sec$, and it characterizes the membrane transport property. The pore radius can be evaluated by rearranging this equation. The calculated pore radius, $r_{p,eq.}$ from the equation is called the equivalent radius; it defines the frictional resistance to fluid flow through the channels in a porous membrane, and is given by

$$r_{p,eq.} = \sqrt{\left(\frac{J_v/S}{\Delta P}\right)\left(\frac{8\eta S}{A_p/\Delta z}\right)} = \sqrt{L_p \frac{8\eta}{A_p/(\Delta z S)}} \qquad 2.1.6$$

This equivalent radius may be not be characteristic of the membrane structure if the viscous force in the membrane is modified by long-range structure of fluid within the channels or if radial velocity gradients at the pore wall differ from the no-slip condition (the boundary condition given by Eq. 2.1.2). The calculation of the equivalent pore radius from equation 2.1.6 has been proven to be close to the equivalent radius estimated from

three independent methods applied to artificial porous membranes; (1) the pressure required to balance the surface tension of an immiscible fluid within the channels of the membrane, (2) the upper limit of solute size that will just penetrate the membrane, and (3) the channel size estimated by the earliest attempts to measure channel dimensions in an artificial membrane by electron microscopy (Pappenheimer *et al.*, 1951). These results indicate that the equivalent pore radius calculated from Poiseuille's law could be used to interpret the physical properties of membranes for a variety of processes. However, it is important to know that the physical basis of this result remains very poorly understood; this is largely due to the presence of randomly oriented, multiply connected regions whose geometry cannot be simply described.

2.1.2 Osmotic Diffusion

Osmotic transport is a molecular diffusive process. A general form of the diffusion process can be written as: Flux = mobility×concentration×total driving force, where flux is the amount of substance, which per unit time penetrates a unit area normal to the direction of transport. The mathematical expression of flux can be written as

$$\Phi = -Mc\nabla\mu = -Mc\frac{\partial\mu}{\partial x} \qquad 2.1.7$$

where M represents the mobility, c is the molecule concentration, and μ represents the chemical potential of fluid with $\mu = \mu_0 + RT\ln(c/c_0)$, where R is the gas constant, T is the absolute temperature. The minus sign indicates that when the chemical potential increases in the direction we consider as positive, the flux will proceed in the opposite direction.

The osmotic pressure is derived from statistical mechanical arguments. In an equilibrium state, the osmotic pressure can be written as $\Pi = -\frac{RT}{v_w}\ln X_F$, where v_w is the partial molar volume of water, and X_F is the molar fraction with $X_F = \frac{n_w}{n_s + n_w}$ (n_w is the number of mole water molecules and n_s is the number of mole solute molecules). Then

$$\Pi = \frac{RT}{\upsilon_w}\ln\left(1 - \frac{n_s}{n_s + n_w}\right) \qquad 2.1.8a$$

For small $\frac{n_s}{n_s + n_w}$ and $n_s << n_w$, the approximate osmotic pressure can be written as:

$$\Pi = \frac{RTn_s}{\upsilon_w n_w} = RTC_s \qquad 1.1.8b$$

where C_s is the molar concentration. This is the well-known Van't Hoff's formula for osmotic pressure, and it represents a very good approximation for dilute solutions. Osmotic diffusion occurs when a molecular concentration difference, ΔC, is generated across membrane segments, so that an osmotic pressure gradient is produced across that segment with a magnitude of $RT\Delta C$. The force acting on each molecule is given by

$$F = \frac{RT\Delta C}{N_A C\Delta x} \qquad 2.1.9$$

where N_A is Avogadro's number; C is the molar solute concentration within the region and Δx is the thickness of the region. For a particle moving under the influence of this acting force F in a viscous medium with a resistance force fv, where v is the velocity of the particle, and f is molecular friction coefficient with units that are the reciprocal of solute mobility, a steady condition is reached when the driving force and the frictional force acting on the particle are equal. In this case, the particle is moving in a constant

velocity given by $v=F/f$. If the particle is spherical with radius r, the friction coefficient is defined by Stokes formula and given by $f=6\pi\eta r$, thus the velocity of the particle can be determined as $v=\frac{F}{6\pi\eta r}$. Therefore the particle velocity multiplied by the molar concentration of the substance gives the flux of the substance in moles per unit area, per unit time, i.e. flux = vC. Then the flux is given by

$$\Phi = {}^{J_s}\!/_{S} = -\frac{C}{6\pi\eta r}\frac{RT\Delta C}{N_A C\Delta x} = -\frac{RT}{N_A 6\pi\eta r}\frac{\Delta C}{\Delta x} \qquad 2.1.10$$

This equation represents Fick's first law of diffusion, where J_s/S represents the solute diffusion per unit area. Often the flux equation is written in the form $\Phi = {}^{J_S}\!/_{S} = -D\frac{\partial c}{\partial x}$, where $D=\frac{RT}{N_A 6\pi\eta r}$. This is the Stokes-Einstein diffusion coefficient. It allows one to evaluate the Stokes-Einstein radius of an equivalent hydrodynamic sphere, and given by

$$r_{eq.} = \frac{RT}{N_A 6\pi\eta D} \qquad 2.1.11$$

2.1.3 Osmotic Flow and Filtration Equations

Fluid transport in the biological membrane system is considered to consist of both viscous and diffusive motion. Such transport mechanics are referred to as "osmotic flow". A model for osmotic flow in porous membrane can be developed based on classical transport and thermodynamic relations (Anderson and Malone, 1974).

Considering solute molecules transport through a cylindrical pore of radius r, the non-uniform pressures and concentration conditions along the radial direction of the cylindrical pore provide the driving force for osmotic flow. The general equation of motion for osmotic flow in a pore can be written in the form

$$\frac{\eta}{r}\frac{\partial}{\partial r}\left(r\frac{\partial V}{\partial r}\right)-\frac{\partial P}{\partial z}=0 \qquad 2.1.12$$

where V represents the axial flow velocity and P is the pressure term that consists of both hydrostatic and osmotic terms. Since radial mechanical equilibrium exists within the pore, the Gibbs-Duhem equation related pressure and potential gradients is

$$\frac{\partial P}{\partial r}+c(r,z)\frac{\partial \mu}{\partial r}=0 \qquad 2.1.13a$$

where c is the solute concentration, and μ is the chemical potential. The Boltzmann equation is given by

$$c(r,z)=c_0(z)\exp\left[-\frac{\mu(r)-\mu(0)}{RT}\right] \qquad 2.1.13b$$

where $c_0(z)$ is the concentration along the axis of the cylinder. The subscript zero indicates the pore center (r = 0). Substituting Equation 2.1.13b into the Gibbs-Duhem equation (Eq. 2.1.13a) and subsequently integrating over r and z, one can obtain

$$P(r,z)-P_0(z)=-RTC_0(z)\int_0^r \exp\left[-\left(\frac{\mu(r)-\mu(0)}{RT}\right)\right]$$

or

$$P(r,z)=P_0(z)-\Pi_0(z)\left[1-e^{-(v(r)-v(0))}\right] \qquad 2.1.14$$

$\Pi_0 = RTc_0(z)$ is osmotic pressure, $P_0(z)$ is the pressure at r = 0. $v(r)=\mu(r)/RT$ is the potential term. Equation 2.1.14 relates the solute concentration to pressure that creates the driving force for bulk flow. Substituting Eq. 2.1.14 into the equation of motion, Eq. 2.1.12, gives

$$\frac{\eta}{r}\frac{\partial}{\partial r}\left(r\frac{\partial V}{\partial r}\right)-\frac{\partial P_0}{\partial z}+\frac{\partial \Pi_0}{\partial z}\left(1-e^{-[v(r)-v(0)]}\right)=0 \qquad 2.1.15$$

The flow velocity is calculated by solving this differential equation with a radial distributed pressure at any position along the pore, and applying the boundary condition that there is no slip on the pore wall, i.e. $V(r_p, z) = 0$. Assuming that osmotic pressure does not depend on radial distance, one can obtain the velocity at any given radius as the solution of Eq. 2.1.15 with this boundary condition:

$$V(r,z) = -\frac{\left(r_p^2 - r^2\right)}{4\eta}\frac{\partial P_0}{\partial z} + \frac{1}{\eta}\frac{d\Pi_0}{dz}\int_r^{r_p}\frac{dr'}{r'}\int_0^{r'} r''\left(1 - e^{-[v(r'')-v(0)]}\right)dr'' \qquad 2.1.16$$

This equation emphasizes the fact that the fluid velocity is dependent on both the axial osmotic pressure gradient $\frac{\partial \Pi_0(z)}{\partial z}$ and the radial variation in chemical potential of the solute.

The average velocity through a uniform cylindrical pore is evaluated by integrating Eq. 2.1.16 over the cross section area of the pore, πr_p^2.

$$\begin{aligned}\overline{V} &= \int_0^{r_p} V(r,z)2\pi r\,dr \\ &= -\left(\frac{r_p^2}{8\eta}\right)\frac{\partial P_0}{\partial z} + \frac{1}{\eta r_p^2}\frac{d\Pi_0}{dz}\int_0^{r_p} 2r\,dr\int_r^{r_p}\frac{dr'}{r'}\int_0^{r'} r''\left(1 - e^{-[v(r'')-v(0)]}\right)dr''\end{aligned} \qquad 2.1.17$$

In order to use the equation to produce a relation between volume flow and pressure and osmotic differences, certain bulk parameters have to be introduced into the model. Applying the Bolzmann and Gibbs-Duhem relations at the pore ends, and equating hydrostatic and osmotic pressure at the ends of the pore to their respective values in the bulk fluid, we obtain the following (Anderson and Malone, 1974):

$$\begin{aligned}
&\Pi_0(0) = \Pi_{0\infty} e^{-v(0)}, \\
&\Pi_0(l) = \Pi_{l\infty} e^{-v(0)}, \\
&P_0(l) = P_{0\infty} - \Pi_{0\infty}\left(1 - e^{-v(0)}\right), \\
&P_0(l) = P_{l\infty} - \Pi_{l\infty}\left(1 - e^{-v(0)}\right).
\end{aligned} \qquad 2.1.18$$

where $\Pi_{0\infty}$, $\Pi_{l\infty}$ are the osmotic pressures in the bulk fluid on each side of the membrane, and similarly $P_{0\infty}$, $P_{l\infty}$.

Substitute these parameters into equation 2.1.17 and multiply the pore volume, the resultant volume flow through a pore can be obtained as

$$J_v = \frac{\pi r_p^4}{8\eta l}\left\{\Delta P_\infty - \Delta\Pi_\infty\left[1 - \frac{8\pi}{r_p^2}\int_r^{r_p}\frac{dr'}{r'}\int_{r_0}^{r'}\left(1 - e^{-[v(r'')-v(0)]}\right)dr''\right]\right\} \qquad 2.1.19$$

where the term $\frac{\pi r_p^4}{8\eta l} = K_f$ is defined as the hydraulic conductivity of a cylindrical pore, and ΔP_∞, $\Delta\Pi_\infty$ are the differences in bulk pressures on either side of the membrane. Often the volume flow equation is written without the subscript ∞.

Osmotic flow in the biological membrane system occurs when the membrane is semipermeable, which implies that only molecules of selected size can penetrate the pore membrane. Such a membrane property results in the change of the osmotic pressure gradient on both sides of the membrane. The integration term in Eq. 2.1.19 is a description of such a semipermeable property and is defined as the osmotic reflection coefficient which is given by

$$\sigma(r) = 1 - \frac{8\pi}{r_p^2}\int_r^{r_p}\frac{dr'}{r'}\int_{r_0}^{r'}\left(1 - e^{-[v(r'')-v(0)]}\right)dr'' \qquad 2.1.20$$

This definition indicates that the reflection coefficient is a function of both pore radius and the solute chemical potential. Therefore, particular molecules and certain sizes of pore characterize the osmotic filtration process.

Taking into account the filtration equation and the definition of the osmotic reflection coefficient, equation of 2.1.19 can be then rewritten as

$$J_v(r) = K_f[\Delta P - \sigma(r)\Delta\Pi] \qquad 2.1.21$$

which is known as the *Starling* equation and is often referred to as the filtration equation for fluid flux. The osmotic flow occurs when an additional amount of solute exists in the solution that lowers the chemical potential of water. As long as the concentration difference is maintained, a steady osmotic flow of water occurs across the membrane. On the other hand, to prevent osmotic flow and to achieve the equilibrium state, one has to raise the pressure on the solution by an amount, ΔP, that is sufficient to equalize the potential energy of water on each side of the membrane.

The equation provides a simple linear description of biological membrane transport mechanics in terms of the physical parameters ΔP, $\Delta\Pi$, ΔC, K_f, and J_v, which are explicitly defined. The equation indicates that the fluid flow in biological membranes is related to both hydrostatic and osmotic pressures rather than just a hydrostatic driven force as described by the Poiseuille's equation or a pure osmotic diffusive force as characterized by Fick's law of diffusion. The linear filtration equation also introduces the osmotic reflection coefficient, σ, into the system that can be used to characterize the membrane and solute properties.

2.2 Practical Considerations

The nature of fluid movement across biological membrane barriers is controversial. Generally, two types of flow mechanics are concerned when describing the capillary transport phenomenon: viscous flow and diffusion. A number of investigations have been carried out in order to determine the relative contribution of the two types of flow with respect to the driven pressure gradients and the concentration differences across membranes (Mauro, 1957; Robbins and Mauro, 1960; Ticknor, 1958). The type of flow largely depends on the size of the permeating molecules, the pore size on the membrane and the amount of bonding the permeating species displays for the membrane material. Some of the experimental work indicates that the rate of diffusion flow and the rate of viscous flow would be equal when the pore radii of the membrane capillaries are nearly twice the radius of the permeating molecules. It was surmised that when the pore radius becomes much larger than the molecular radius the flow will be viscous and when they are nearly equal the flow will be diffusive (Ticknor, 1958). In the situation of large pore sizes, or leaky membranes, the solvent is assumed to be a continuum with respect to the pore dimension. The fluid transport is assumed to be viscous flow rather than diffusive, which could also be the case when the solute molecules are small enough or the pores are large enough.

Certain results have been produced that distinguish the types of flow in various situations including the influence of pressure and solute concentration gradients, variations of pore sizes of membranes, and the sizes of permeating molecules. The flow mechanics in microvascular exchange system are still contestable.

It is reasonable to assume that both types of flow occur simultaneously during the transport process. The mechanics of osmotic flow is used to elucidate such a transport state. The basic principle behind osmotic flow is the semipermeable property of the transport surface within a porous membrane, which creates osmotic pressure gradients in solution that are normal to the transport surface maintaining thermodynamic equilibrium across the membrane. The introduction of the osmotic reflection coefficient into the osmotic flow equation realistically reflects the semipermeable property of membranes and the transport process. It is recognized that in reality the pores represent a complex structural system. Therefore, when using the osmotic flow mechanics to interpret three-dimensional fluid flow phenomena, and perusing the physiological significance of fluid flux in biological membrane systems, one should keep in mind that it is derived specifically for cylindrical pores of circular cross section, and its applicability to other geometries remains uncertain.

The osmotic flow mechanics agree with the Kedem-Katchalsky equations which were developed based on statistical thermodynamics principles (Kedem, and Katchalsky, 1958). Both approaches provide the same relation for the fluid flux across capillary membrane barriers. The Kedem-Katchalsky equation consists of two sets of equations related to volume flow and solute transport mechanics

$$J_v = K_f\left(\Delta P - \sigma\ \Delta\Pi\right) \qquad 2.2.1$$

$$J_s = J_v(1-\sigma)C_s + PS\Delta C \qquad 2.2.2$$

where ΔP and $\Delta\Pi$ are the hydraulic pressure gradient and the osmotic pressure gradient between capillary and interstitial spaces. As discussed earlier, the osmotic pressure is thermodynamically related to the solute concentration difference across the membrane.

For an ideal situation $\Delta\Pi=RT\Delta C$. PS is the permeability coefficient-surface area product, ΔC is the solute concentration difference, and C_s is the average molar concentration within the porous membrane. The term $J_v(1-\sigma)C_s$ is defined as the connective solute flux and $PS\Delta C$ is given as the diffusive solute flux. The reflection coefficient σ can be evaluated experimentally by

$$\sigma = 1 - \left.\frac{J_s}{J_v C_s}\right|_{\Delta C=0} \qquad 2.2.3$$

Non-linear filtration equations can be derived based on the linear filtration equations. Mathematically, they are derived by converting the Kedem-Katchalsky equations into a differential form, which can be applied to any infinitesimal lamina of a thick homogeneous membrane such as

$$J_v = -L'\left(\frac{dp}{dx}\right) - sRT\frac{dc}{dx} \qquad 2.2.4a$$

$$J_s = -w'RT\frac{dc}{dx} + (1-\sigma)cJ_v \qquad 2.2.4b$$

Rearranging these equations into a first order differential equation yields

$$\frac{dc}{dx} - \frac{J_v(1-\sigma)}{w'RT}c = -\frac{J_s}{w'RT} \qquad 2.2.5$$

If the membrane is homogeneous, L'_p, ω' and σ are concentration independent. Solving this differential equation with proper boundary conditions yields

$$J_v = -L_p(\Delta p - \sigma R\Delta c)$$

$$c_2 = c_1 \exp\left\{\frac{\left[(1-\sigma)J_v x\right]}{\omega RT}\right\} + \frac{J_s}{(1-\sigma)J_v}\left\{1 - \exp\frac{\left[(1-\sigma)J_v x\right]}{\omega RT}\right\} \qquad 2.2.6$$

For a homogeneous capillary-tissue membrane system, the solute transport equation can be written as

$$J_s = J_v(1-\sigma)\left[\frac{(c_P - c_L)e^{-x}}{1-e^{-x}}\right] \qquad 2.2.7$$

where c_P and c_L represent the concentrations of solute in the plasma and tissue, respectively. x is the Péclet number and $x=(1-\sigma)J_v/PS$. PS is the permeability surface product.

These equations are used to describe the steady state flow of solvent and for a single, neutral solute across a simple membrane system as derived by Patlak (Patlak *et al.*, 1963). Within these equations, Patlak had determined a variety of qualitative properties of the system for two special cases: (1) A pure active transport case where the concentrations in the outer solutions are the same and the solute pump is functioning and (2) a pure osmotic flow case where the concentrations in the outer solutions are different and the solute pump is inactive. In the first case, there will be solute flow across the membrane system, which may be hypertonic, isotonic, or hypotonic. In the second case, the solvent flow is not linearly related to the concentration difference between the outer solutions.

Although both linear and non-linear filtration equations reasonably explain the biological fluid transport mechanics in some particular applications, certain advantages of the linear filtration equations make them more attractive to investigators in the field. The first advantage is that the equations describe the fluid transport phenomenon in a simple fashion that involves only linear relations, unlike Patlak's non-linear filtration equations and other model systems that contain complex exponential functions. The second

advantage is that the Kedem-Katchalsky equation for solute flux, equation 1.1.18, is conveniently separated into two parts, the diffusive *(PSΔC)* part, and the connective part $J_v(1-\sigma_d)\overline{C}_s$ of solute fluxes. Practically, the Patlak equation has to be rearranged in a complex way in order to separate into these two parts (Patlak *et al.*, 1963). The most attractive feature of the linear equations is that the analysis developed is based on the irreversible thermodynamics principle that there is no assumption made regarding geometric structure of the capillary membrane pores. The approach can be applied to both biological and artificial membrane systems.

A number of physiological investigations showed that the analysis based on the linear filtration equations, derived by Kedem and Katchalsky, provide a reasonable solution to explain the exchange of fluid and macromolecules across capillary membrane barriers in both normal and abnormal situations.

Although the linear volume flow equation, 2.2.1 has been extensively used in physiological and clinical investigations, one should keep in the mind that this fluid transport mechanics has been developed based on an idealized system. The assumptions made from flow dynamics or from thermodynamics do not truly reflect the complicated transport phenomenon present in the biological membrane system. In ordinary situations, it is difficult to assess the nature of fluid flux occurring across three-dimensional capillary membrane barriers, subjected to one-dimensional hydrostatic and osmotic pressure gradients without considering other contributing factors. Generally, the permeating molecules are assumed to be of rigid spherical shape in order to simplify the mathematical derivations. Realistically, permeating molecules can take any kind of geometric appearance. The capillary membrane structures are also complicated by a

variety of sizes and shapes of pores. The transport phenomenon in capillary membrane barriers is so complex that it is still not fully and realistically understood or described. Therefore, results produced by linear filtration equations are approximate, and may not provide an accurate description of fluid movement across membrane barriers. However, the mechanics do provide a simple way to understand microvascular transport with acceptable results in most situations. In this thesis, the linear filtration equations will be used in providing a theoretical description of the capillary leak phenomenon and the oncotic fluid management in acute lung injury patients. The concept of capillary-alveolar permeability is also developed based on the linear filtration relations.

2.3 Fluid Dynamics and Pulmonary Interstitial Edema

Understanding the ultrastructural pathways and mechanisms that constitute the transendothelial pores or the clefts between the cell junctions to water and solute has been a major problem in the microvessel transport for over 30 years, and still remains unclear.

2.3.1 Fluid Circulatory Dynamics

In the normal situation, the fluid and protein movement occurring across capillary walls is described by a capillary-tissue-lymphatic dynamic system. In such a system, capillaries continuously lose plasma fluid and proteins through the different sizes of "pores" on the capillary wall into the interstitial space. Proteins and fluid are then returned to the circulatory system by the lymphatic system in the tissue. Through this system, exchange of nutrients and other substances between blood and tissue is regulated.

Interstitial space, in the pulmonary system, is considered as a compartment between vessels and airspace. It is not only a compartment of water but also composed of

cellular elements, collagen, elastin, glycosamines, and proteoglycans such as hyaluronate (Pickerel *et al.*, 1981). These components form a complex meshwork that provide an organized structure within the interstitium, which is called the interstitial matrix. The interstitium of the lung is different from that of solid tissue organs in that the distribution of stress along any hydrostatic level varies over time with inflation and deflation and it is not uniform. The interstitial pressure around extra-alveolar vessels is more negative than that around alveolar vessel. (Oppenheimer and Goldberg, 1989).

The amount of hyaluronate in the tissue is in a dynamic state, that changes from time to time, because increased capillary filtration can remove large amounts of fluid from the interstitial compartment. When this occurs, the swelling characteristics of the interstitium will be altered, and the assumption that the interstitium is a static system will no longer be valid, simply because of this reaction to capillary filtration by shrinking or swelling.

Most organs, in the human body, have an extensive lymphatic system. The interstitial fluid filtrates initially into lymphatic capillaries with no restriction of even large plasma proteins in the large endothelial gaps located in the initial lymphatics; that means the initial lymphatic capillaries have very large pores, which allows even the largest protein components to enter from the tissues. Larger lymphatics contain valves and lymph always flows away from the tissue through one valved segment to another. Larger lymphatics also consist of smooth muscle cells in their walls, and lymph is propelled between different valved segments of the lymphatic when the smooth muscle contracts. Tissue motion increases the lymph flow because of the valved nature of the lymphatic system (Guyton, 1975; Staub, 1974). Lymph finally drains into the large veins

in the chest. Because the total amount of albumin contained in plasma crosses the capillary walls, it enters the tissues and is carried back into the circulation. Any alteration in the ability of the lymphatic system to remove capillary filtrate will greatly affect the plasma volume.

In the normal situation when plasma passes through the capillaries, some fluid, small solutes, O_2 and CO_2 exchange rapidly with the interstitial space. A small amount of the large proteins contained in plasma move into the interstitium to be returned into circulation by the lymphatic system. About 150 mL of plasma filtrate enters the tissue each hour. Therefore, the plasma-tissue-lymphatic system is a dynamic fluid system that is constantly changing. Yet, even with this extensive movement of fluid and solute between plasma and the tissues, the interstitial spaces do not normally shrink or swell to any significant extent.

Considering the transport under only physical influences, Starling first postulated that fluid moves between plasma and tissues under the influence of hydrostatic and osmotic pressure gradients (Starling, 1896). His hypothesis was simply expressed as $P_c - P_t = \Pi_p - \Pi_c$. where P_c and P_t are the hydrostatic pressures and Π_p and Π_t are the osmotic pressure in the tissue and plasma respectively. The assumption he made was that the plasma protein and fluid loss into the interstitium was small, so that the hydrostatic and protein osmotic pressure are always balanced, and the capillary exchange of fluid is a self-regulating system with physiological limits. Realistically, this assumption was not completely correct, but under normal conditions the explanation of fluid transport across the membrane by this relation seems satisfactory. Because the plasma fluid and protein penetrate into the tissue in small amounts, and the fluid always returns the plasma by

lymphatic flow from the tissues, there is no accumulation of protein in the interstitial space. Therefore, the net result is maintenance of an almost constant flow in normal tissues.

The linear filtration equations provide an appropriate description of solute and water movements across membranes with the consideration of the semipermeable properties of membranes. The difference between the hydrostatic and osmotic pressures acting across capillary determines whether the fluid is filtering into the interstitium or absorbed from the interstitium. The hydrostatic pressure gradient operating across the capillary wall is an oversimplification since the hydrostatic pressure in the plasma and in the tissue differ between organs and even with the various portions of the microcirculation within a particular organ. Furthermore, several different proteins are present in plasma and they must be considered when a more exact analysis of transcapillary exchange is needed.

It should be noted that applying the linear filtration equations to analyze fluid dynamics and protein transport across a capillary wall should always consider implications and limitations of using a single value to describe microcirculatory permeability or capillary filtration. However, for most situations, a simplified analysis system may be sufficient to predict how an intervention affects transcapillary fluid and protein movement.

2.3.2 Fluid Filtration is Affected by Physical Factors and Pulmonary Interstitial Edema

The major causes of the abnormal leakage of protein and fluid into the interstitium can be described by three categories: (1) increased capillary pressure, (2) decreased plasma

proteins concentration, and (3) increased capillary permeability. According to the fluid flux equation, $J_v = K_{fc}[(P_c - P_{in}) - \sigma(\Pi_c - \Pi_{in})]$, the primary forces determining fluid movement across capillary membranes are (1) the capillary pressure (P_c) which tends to force fluid outward through the capillary wall, (2) the interstitial fluid pressure (P_{in}) which tends to force fluid inward through the capillary wall, (3) the plasma colloid osmotic pressure (Π_c) which tends to cause osmosis of fluid inward through the capillary wall, and (4) the interstitial fluid osmotic pressure (Π_{in}) which tends to cause osmotic flow outward through the membrane. The lymph flow is another important factor that affects capillary filtration. The ability of lymphatics to remove capillary filtrate is not only a function of lymph flow, it is also a function of the filtration properties of both the capillary walls and the interstitium. Physiologically, the forces governing the fluid flow across membranes and the rate of capillary filtration into the interstitium as well as the lymphatic flow rate are defined as edema factors that predict and prevent edema formation.

The dynamics of fluid exchange through the capillaries are qualitatively the same as for peripheral tissues. The pulmonary capillary hydrostatic pressure is about 7 mm Hg, in comparison with 17 mm Hg for the functional capillary pressure in the peripheral tissues. The interstitial fluid hydrostatic pressure determined by a pipette inserted into the pulmonary interstitium gives a value of –5 mm Hg in the lung. It presents a lower negative value than in the peripheral subcutaneous tissues that have a value of –3 mm Hg. The colloid osmotic pressure in the pulmonary interstitial fluid is about 14 mm Hg which is higher than that in other peripheral tissues; this is largely due to the fact that pulmonary capillaries have relatively high filtration rates (Guyton, *et al.*, 1975; Meyer, *et al.*, 1968

Parker, *et al.*, 1978). Table 2.3.1 summarizes the interrelations between interstitial fluid and any other pressures acting in the pulmonary system.

Table 2.3.1. Forces that govern fluid flow across capillary Wall

Forces acting across capillary wall	Values (mm Hg)
Forces that govern fluid move from capillary into the interstitium:	
Capillary hydrostatic pressure	7
Interstitial colloid osmotic pressure	14
Interstitial hydrostatic pressure	8
Net filtration pressure	29
Forces that govern fluid move from interstitium into the capillary: Plasma colloid osmotic pressure (net absorption pressure)	28
Net filtration pressure across capillary membrane barrier:	1

Under normal conditions, the result net filtration pressure (1 mm Hg) causes a continual fluid flow from the pulmonary capillaries into the interstitial spaces, and this fluid is filtered back to the circulation through the pulmonary lymphatic system. Keeping the alveoli "dry" is an important factor in pulmonary function in order to maintain the normal function of the lung for gas exchange. In the pulmonary capillaries and pulmonary lymphatic system, the interstitial pressure maintains a negative value. Because of this low pressure, if extra fluid appears in the alveoli, it will infiltrate into the pulmonary interstitial space through the small openings between the epithelial cells. Then the excess fluid is either carried away through the pulmonary lymphatics or absorbed into pulmonary capillaries. Therefore, under normal circumstances, the alveoli are maintained in a constant "dry" state except for a small amount of fluid that seeps from the epithelium into the lining surfaces of the alveoli to keep them moist.

The interstitial fluid volume of the lung usually cannot increase more than about 50% before the alveolar epithelial membrane will rupture and fluid begins to pour from the interstitial spaces into the alveoli. This is due to the slight tensional strength of the pulmonary alveolar epithelium, so that even the slightest positive pressure in the interstitial spaces causes immediate rupture of the pulmonary epithelium. Thus, except in the mildest cases of pulmonary edema, edema fluid always enters the alveoli if the edema becomes severe enough and it can cause death by suffocation (Staub, 1974; Guyton, *et al.*, 1971, 1979).

Pulmonary edema induced by increasing capillary hydrostatic pressure occurs when the heart fails to pump blood from the veins into the arteries which results in higher venous and capillary pressures. The interstitial hydrostatic pressure is increased as a consequence of elevated capillary pressure that results from a high filtration rate. Small changes in interstitial volume will cause large increases in interstitial fluid pressure. In a normal situation, the interstitial fluid hydrostatic pressure, P_{in}, is less than the atmospheric pressure (defined as a negative pressure) by an average amount of about 3 mm Hg. This negative pressure holds the tissues together. Although the changes in the interstitial fluid volume are small, the interstitial hydrostatic pressure is expected to have a relatively larger change, so that the pressure will oppose future fluid filtration into the tissue. Tissue can expand to some critical volume until tissue pressure will no longer increase to any significant extent and an excessive amount of fluid begins to accumulate in the interstitium. This occurs because the normally hydrated tissues have a low tissue compliance to resist expansion. However, the situation will be very different in the edema formation state since forces that normally resist the expansion of the interstitium are no

longer active. Since the normal value of the interstitial hydrostatic pressure is –3 mm Hg, the safety range that the interstitial pressure can maximally expand to is about 3 mm Hg. If this value is exceeded, interstitial fluid will accumulate in the tissue to induce edema (Guyton, 1963; Parker, *et al.*, 1978).

If the interstitial hydrostatic pressure rises above atmospheric pressure, the compliance of the tissue increases dramatically, and huge amounts of plasma fluid will start to accumulate in tissues with relatively small additional increases in interstitial hydrostatic pressure. The negative safety factor will be lost because of the large increase in compliance of tissues.

As increased amounts of fluid are filtered into the interstitium, the interstitial pressure in normal capillaries, Π_{in} decreases to a limiting value that is a function of the permeability of these capillary walls when capillary filtration increases. Π_t approaches 5% to 10% of Π_{in} when capillary filtration is large in most organs. This causes the effective osmotic gradient $\sigma(\Pi_c - \Pi_{in})$, acting across the capillary wall, to become almost equal to the plasma colloid osmotic pressure. When capillary walls are damaged, the reflection coefficient is decreased as well as Π_{in}, and the capillary filtration increases because more protein will leak into the interstitium from the damaged capillaries. This results in a $\sigma\ (\Pi_c - \Pi_{in})$ term that will not increase to any appreciable extent as capillary filtration increases. The reflection coefficient can decrease to values as low as 0.4 in severely damaged capillary walls. As a result, the capillary absorption forces are reduced to 60% of measured differences between Π_c and Π_{in}. When this occurs, Π_c - Π_{in} can not change sufficiently to oppose capillary pressure and edema. This type of edema is

usually referred to as low pressure edema or "leaky capillary syndrome" (Taylor *et al.*, 1994).

Lymph flow steadily increases capillary filtration as capillary filtration attains a plateau and the lymphatic system's ability to remove fluid is maximized. In the lung, lymph flow may actually decline as fluid enters the interstitial lumen, the alveoli, or the airways (Guyton, *et al.*, 1975; Laine, *et al.*, 1986). The importance of lymph flow in removing excess capillary filtration is not well understood and varies from tissue to tissue. For a long time, the lymphatic system was not considered to be an important factor in the removal of fluid from the system because volume of lymph flow is very low in some organs. In the case of fluid accumulation in the tissue, lymph flow can increase 10 to 50 fold, which allows the lymphatics to carry away large amounts of fluid and protein in response to the increased capillary filtration, preventing the interstitial pressure from rising to a positive range.

As increased amounts of fluid are filtered into the interstitium, the interstitial fluid pressure increases, causing lymph flow to increase. In most tissues, the protein concentration of the interstitium decreases as lymph flow is increased since larger amounts of protein are carried away than the amounts that are filtrated out of plasma. This occurs because the capillaries are more restricted to protein compared with the lymph vessels. Since the interstitial fluid colloid osmotic pressure caused by the protein tends to draw fluid out of the capillary, decreasing the interstitium fluid protein concentration lowers the net filtration force across the capillaries and tends to prevent future accumulation of fluid.

2.4 Oncotic Manipulation of Capillary Leakage

Increased pulmonary capillary permeability resulting in pulmonary interstitial edema is a biochemically mediated phenomenon. It can be analyzed as a physical model of capillary leakage of intravascular fluids through damaged membranes as discussed in the last section. An application of the physical description of fluid transport mechanics is the fluid oncotic manipulation in the management of edema patients.

2.4.1 Biophysical Therapeutic Strategies

One of the biophysical approaches to capillary leak patients was introduced by Zikria (Zikria *et al.*, 1988). The approach is based on the hypothesis that "intravascularly injected biodegrable macromolecules of appropriate size, acting as sealers (or molecular plugs) for the leaking capillaries, may reduce the albumin, fluid, and electrolytes in many acute states of injury". In his experiments, variably sized macromolecules of hydroxyethyl starch and dextran were used intravenously in rats to study their effectiveness in sealing capillary membrane defects. The observed phenomenon of reduction of albumin leakage from injured capillaries in the experiments was attributed to this so called "sealing effect". He believes that "the molecule size-dependent beneficial effect favors the presumption that the capillary pores, or holes, are sealed by a biophysical event." He concluded that this capillary "sealing" phenomenon was shown to be independent of the colloid osmotic pressure effect in the capillary system. The osmotic effect, however, was not clearly investigated in his work.

Based on experimental studies, Zikria favored macromolecules as large as or larger than 300,000 Daltons that would be appropriate to use in order to provide the best sealing effect. Although the role of transvascular colloid osmotic pressure in fluid

exchange remains controversial, a number of experimental and clinical investigations have shown that it contributes significantly to the fluid movement.

A new treatment strategy, called oncotic fluid manipulation, was introduced based on the theoretical framework of transvascular fluid movement (Oppenheimer *et al.*, 1996). The brief theory behind this treatment strategy can be explained as follows: in order to prevent capillary leakage and limit edema formation, the physical parameters that govern the fluid movement across membrane barriers must be in the range to cause the extravascular fluid to return to the circulatory system. Manipulating physical forces to promote re-absorption of the excess fluid becomes a therapeutic strategy in pulmonary edema management.

This treatment is designed to increase the plasma osmotic pressure (COP) and maintain the osmotic pressure gradient between the blood and extravascular tissue favoring the movement of the extra lung fluid from the extravascular (interstitial and intracellular) compartment back into the intravascular space, thus reducing the lung edema. Theoretically, increasing the plasma colloid osmotic pressure can be achieved by administrating poorly diffusible molecules with a high reflection coefficient σ. The implication of infusing poorly diffusive molecules is that larger macromolecules are confined to the intravascular space, since they are larger than the disturbed membrane cell junctions. These macromolecules exert a pressure confined to the intravascular space, to draw fluid back into the vasculature where it can be mobilized. Thus only very small molecular fractions will escape into the interstitial space. This principle of oncotic management has been successfully applied to patients with very severe ARDS. The management difficulty encountered in treating these patients is that the interstitial fluid is

inaccessible. By generating an oncotic gradient to promote redistribution, fluid may be removed through medical diuretics or hemodialysis, but only once it has returned to the circulatory system.

To achieve increases in capillary osmotic pressure, clinically, a variety of synthetic macromolecular plasma volume expanders are normally used. These plasma volume expanders have unique molecular properties that have been reported to improve perfusion and oxygen transport in critical care patients. Oppenheimer *et al* (1996) have been successful in re-establishing oncotic gradients in conditions of increased capillary permeability to protein in animal experiments by use of 6% Hetastarch (a high molecular weight plasma expander). A study of pulmonary vascular filtration using starch-based macromolecules that affect the lung fluid balance were reported by McGrath (McGrath *et al.*, 1996). It showed the beneficial oncotic properties of starch-based plasma volume expanders including Hetastarch, Pentafraction, and Dextran-70. According to their observation, "Pentafraction and Hetastarch demonstrated greater oncotic effectiveness because of restricted plasma-to-lymph macromolecular filtration and limited transvascular fluid flux". In comparison with other plasma volume expanders, they concluded that "Pentafraction appears to possess filtration properties that optimize critical care fluid management compared to currently available colloid solutions". The treatment has been successfully applied to patients with very severe ARDS (Oppenheimer, *et al.*, 1996).

Although the use of very large macromolecules produces a "sealing" effect on capillary leak patients, the manipulation of the osmotic pressure gradient to cause the fluid re-absorption is controversial. There is a great deal of evidence present to support

their application by using starch-based large colloid macromolecules to the capillary leak syndrome to prevent further leakage and reduce edema.

2.4.2 Properties of Starch-Based Colloid Macromolecules

The polydispersed colloid macromolecules include hydroxyethyl starches and dextran. Hydroxyethyl starches are modified natural polymers, derived from a waxy species of maize or sorghum. The major components of the starch-based polymers are amylopectin (98%) which is composed of linked glucose units. Amylopectin is rapidly degraded to glucose by amylase in the plasma and tissue fluids. Native starches in solution are unstable and are rapidly hydrolyzed by the ubiquitous amylase. The hydroxyethyl starches are the most stable modified polymers that improve the properties of the native polymers. With minimal substitution of hydroxyethyl radicals on glucose units, the solution stability is excellent but hydrolysis is rapid and the half-life is very short (Quon, 1988).

The molecular weight of these molecules is an important factor determining their colloidal effect and pharmacokinetics. The average molecular size of poly-dispersified solutions may be determined by properties related to the number of average molecules weight or properties influenced more by large molecules, or weight average molecules, the large the difference between these molecules weight, the higher the polydispersity.

The hydroxyethyl starches have hydroxyethyl radicals attached throughout the molecule, reducing the speed of breakdown and thus lengthening their half-life in the plasma. The rate of degradation is an inverse function of the degree of substitution. The chemical and physical characteristics of hydroxyethyl starches are defined by their molar

substitution ratios, which is the major determinant of their half-life, and by their molecular weight that determines the colloidal activity.

The kinetics of elimination may improve by higher substitution, which is better quantified by the molar substitution ratio, rather than by the substitution degree. The molar substitution ratio expresses the proportion of molecular mass that comprises by each of the two constituents. The introduction of hydroxyethyl ether groups into the molecule dramatically increases the water affinity in proportion to the molar substitution degree. The presence of these hydrophilic groups inside and outside the molecule produces a water coat surrounding the molecule and binds water inside. Consequently, for a given molecular weight, the scale of the molecule will depend on the amount bound inside, which in turn depends on the molar substitution ratio (Quon, 1988; Lederer, *et al.*, 1985).

Table 2.4.1 Structure and Properties of Some Polysaccharides Polymers

Polymer	Unit Linkage	Structure	Size (Dalton)
Starches:			
Amylose	α-1,4 linkages	fixed, out of level, linear	A few thousand to 500,000
Amylopectin	α-1,4 linkages, with α-1,6 branches every 24-30 residues	left-hand helix with an open core	up to 10^6
Glycogen	α-1,4 linkages with α-1,6 branches every 8-12 residues	left-hand helix with an open core	varies (Several million)
Dextran	α-1,6 linkages	not fixed, flexible	a few thousand to 260,00

HETASPAN® is a high molecular weight (HMW) hydroxyethyl starch which is formulated as 6 gm hetastarch/100 ml, The average molecular weight is approximately 450,000, with 90% of the polymer units falling within the range of 10,000 to 1,000,000.

The degree of substitution is 0.7, which means that hetastarch has 7 hydroxyethyl groups for every 10 glucose units.

Low molecular weight (LMW) hydroxyethyl starches have various terminal half-lifes. The major difference in comparison with HMW HES is the much faster elimination rate. PENTASPAN® is a low molecular weight hydroxyethyl starch, which is available commercially in a formulation of 10 g pentastarch/100 ml. It is a low molar substitution hydroxyethyl starch having an average molecular weight of 200,000 to 300,000, and a degree of substitution of 0.40 to 0.5. It means PENTASPAN® has approximately 45 hydroxyethyl groups for every 100 glucose units. PENTASPAN® is extensively used clinically as LMW HES, and has high volume expansion effect due to its lower molecular weight and shorter duration effect related to its lower molar substitution ratio. The chemical structure of PENTASPAN® is given in Fig. 2.4.1.

The rate of elimination of hydroxyethyl starches from serum depends entirely on molar substitution and not on the average molecular weight. By using the technique of size exclusion chromatography and low-angle laser light scattering techniques, the rate of break down of starch in human serum can be obtained. Table 2.4.2 provides information of HES 200/0.5 in human serum. In the Table, $\overline{M}_w$ is the weight average molecular weight, and $\overline{M}_n$ is the number average molecular weight. The diameter of the equivalent sphere of HES was calculated in Table 2.4.2 under the assumption that the branch starch molecule is a globular shape (Lederer, *et al*, 1985).

The understanding of transport mechanics across normal and injured membranes is important for the development of this novel diagnostic strategy using infrared spectroscopy. This methodology is based on the physiologic principles of fluid flux and

macromolecular exchange. Movement of large macromolecules such as hydroxyethyl starches across a more permeable membrane and the ability to recognize this event is of utmost importance to developing this hypothesis. The following chapter elaborates on the instrumental background to clarify how hydroxyethyl starch molecules may further contribute to our knowledge of a complex disease.

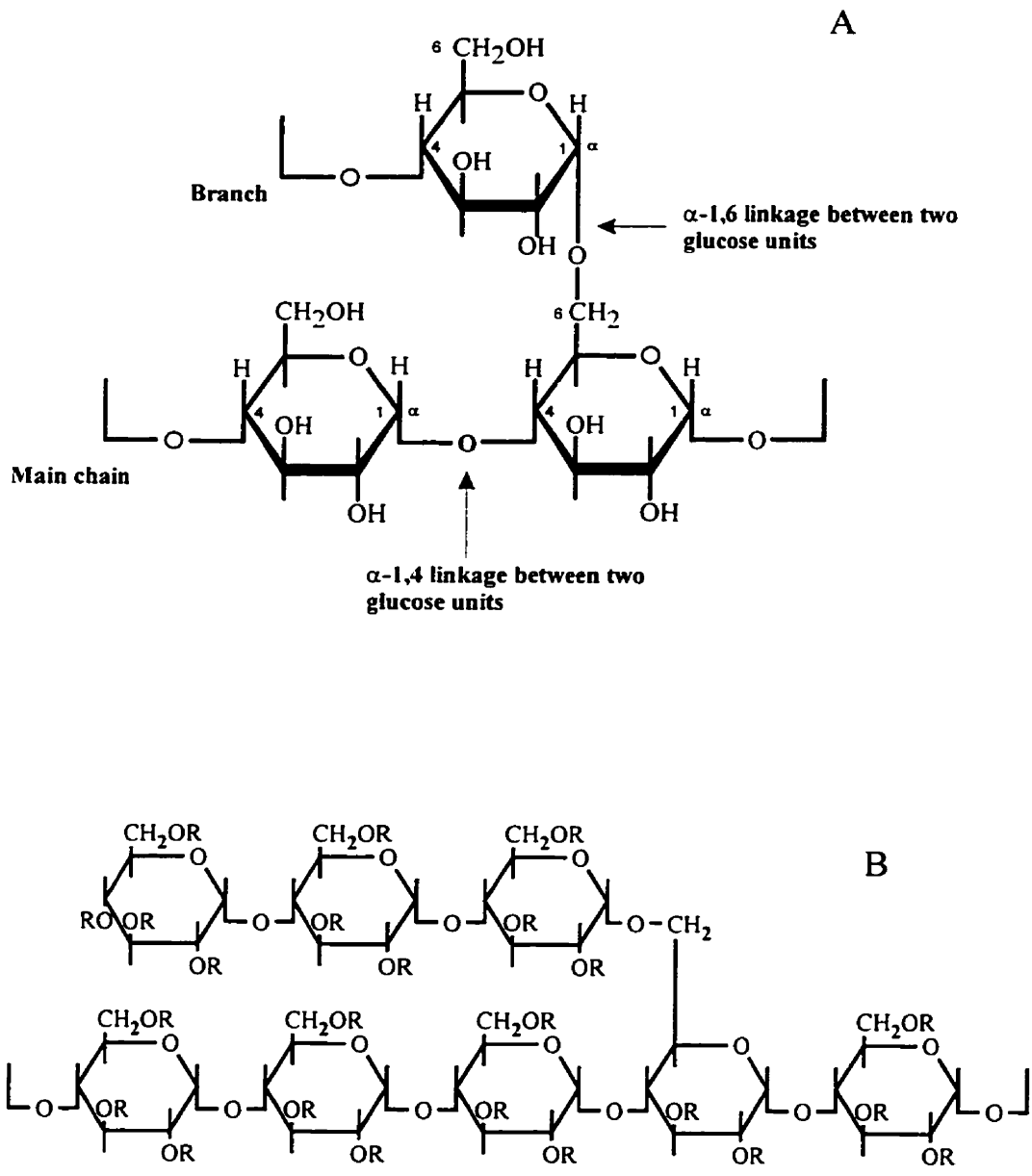

Fig.2.4.1 A:Linkage between two glucose units; B: Structure of PENTASPAN

Table 2.4.2 Dynamics of 200/0.5 HES in human serum

TIME	M_w (Dalton)	M_n (Dalton)	Volume (nm^3)	Diameter (nm)
0	411898	155073	7403	24.18
1 min	214228	93383	3062	18.02
30 min	147543	76947	1850	15.23
1 hour	126366	73401	1501	14.21
2 hours	108870	71204	1227	13.28
3 hours	98860	67471	1077	12.72
4 hours	93400	66537	979	12.32
5 hours	92116	65368	998	12.40
6 hours	86512	65314	900	11.98
9 hours	89495	64877	942	12.16
12 hours	75784	63743	752	11.28
1 day	71783	62556	699	11.01
2 days	72957	65364	715	11.09
3 days	74241	65251	732	11.18

* Referenced from *Arzneim*; Ferber, *et al.*, 1985

Chapter 3

Instrumental Background: Fundamentals of IR Spectroscopy and Biomedical Applications

The application of variably sized macromolecules, such as hydroxyethyl starches, for oncotic fluid manipulation has shown significant potential in treating pulmonary edema patients. This therapeutic strategy has lead in turn, to a new diagnostic methodology for ALI/ARDS patients. The rationale behind this diagnostic methodology is that increased pulmonary capillary permeability allows the starch-based colloid plasma expander to gain access to the pulmonary interstitium from the capillaries and then, at a severe stage, to enter the alveolar spaces. The detection of starch-based macromolecules in the alveolar space therefore provides evidence of capillary-alveolar leakage and this provides diagnostic information about pulmonary leakage in acute lung injury. To achieve this, a tool is required that can be used to identify starch-based macromolecules in a patient's lung fluid and plasma.

Infrared spectroscopy is a well-established and widely applied technique in the analytical chemistry laboratory, commonly used to analyze chemical/biochemical compositions in a mixture. The fundamental principle of IR spectroscopy is based on the fact that when a molecule absorbs IR radiation, there are resulting intra-molecular motions, such as vibrational motions and rotational motions. The absorption frequencies and intensities in the IR spectrum correspond directly to the chemical functional groups

in the molecule, such as C-H, O-H, N-H, C-C groups and provide information on its composition. They also depend on variations in the chemical and physical environment such as pH, temperature, and solvent. Recently, this technique has been applied to medical science to provide diagnostic information. In this study, IR spectroscopy is used as a tool to evaluate exaggerated lung permeability, since starch-based polymers have a unique infrared absorption feature that can easily be detected using IR spectroscopy.

In this chapter, the theory of Fourier transform infrared (FT-IR) instrumentation and the methodologies of spectral analysis will be reviewed. Some biomedical applications of IR spectroscopy will also be outlined.

3.1 IR Spectroscopy

Infrared radiation is a form of electromagnetic radiation that falls within the range of 0.7 to 500 μm (wavelength) or 14,300 to 20 cm^{-1} (wavenumbers). The wavenumber ($\bar{\nu}$) is a unit commonly used in IR spectroscopy and is the number of waves per unit length, expressed in cm^{-1}. The relationship between wavelength (λ), frequency (ν), and wavenumber can be expressed as

$$\bar{\nu} = \frac{\nu}{(c/n)} \quad \text{and} \quad \bar{\nu} = \frac{1}{\lambda}$$

where the term *c/n* is the velocity of light in a medium whose refractive index is *n*.

3.1.1 Brief Theory

The interaction between electromagnetic radiation and matter is that of energy transfer from the radiation to energy states of matter and vice versa. Light radiation is considered theoretically as discrete quanta of energy called photons, the energy of which is proportional to the frequency of the radiation. Photons can be emitted or absorbed when an atom or molecule changes energy levels. Spectral lines and bands are evidence of quantized energy states in matter and of quantized energy transfer between radiation and matter.

The energy states of molecules have components of electronic, vibrational, and rotational energy. They can be expressed as

$$E_{total} = E_{el} + E_{rot} + E_{vib}$$

where E_{el} is the electronic energy of the molecule, E_{rot} is the energy associated with the rotation of the molecule around its center of mass, and E_{vib} is the energy of the molecule due to inter-atomic vibrations. For each electronic energy state of a given molecule, there are several possible vibrational energy states, and for each of these, there are several possible rotational states. Consequently, the number of possible energy levels for a molecule is much larger than that for an atomic particle. The molecular energy levels are shown schematically in Fig. 3.1.1. The electronic energy is larger than either the rotational or the vibrational energies and requires energies corresponding to ultraviolet or visible radiation. The rotational and the vibrational transitions involve energies corresponding to infrared radiation.

Energy levels represent the current characteristic state of the molecule. The properties of the characteristic states are related to the identity of the molecules, the structure of the molecules and to the activity of any chemical processes that molecules undergo.

The energy of quanta of light may be transferred to a molecule, resulting in changes of energy states. According to quantum mechanics, in order to reach the first vibrational excited state (V_1) from the ground vibrational state (V_0), a molecule must take up an amount of photon energy $\Delta E = h\nu$ or $\Delta E = hc\bar{\nu}$ (h is Plank's constant and h = 6.6256×10^{-34} joule-sec.). Light quanta in the infrared region with a wavelength of 2.5 to 50 μm possess energies of $hc\bar{\nu}$ with $\bar{\nu}$ from 200 to 4000 cm^{-1}. A molecule may absorb light quanta having this energy, and the molecule is then excited from the ground vibrational state to the high vibrational states.

The work can be performed on a molecule in the form of displacement of charge. This requirement introduces the selection rule for infrared activity: a molecule will absorb IR radiation only if the change in vibrational state is associated with a change in the electronic dipole moment of the molecule. When a molecule vibrates, the charge distribution may or may not change with respect to the selected origin of the system, depending on the relative displacements of atoms. Only vibrations that cause the electric dipole moment to change will be associated with IR absorption.

When molecules absorb only one quantum of vibrational energy, the IR absorption bands occur in the region from 200 to 4000 cm^{-1}, and this is referred to as the fundamental or mid-IR region. Absorption bands induced by absorption of several vibrational quanta occur at higher frequencies, in the combination/overtone or near-IR

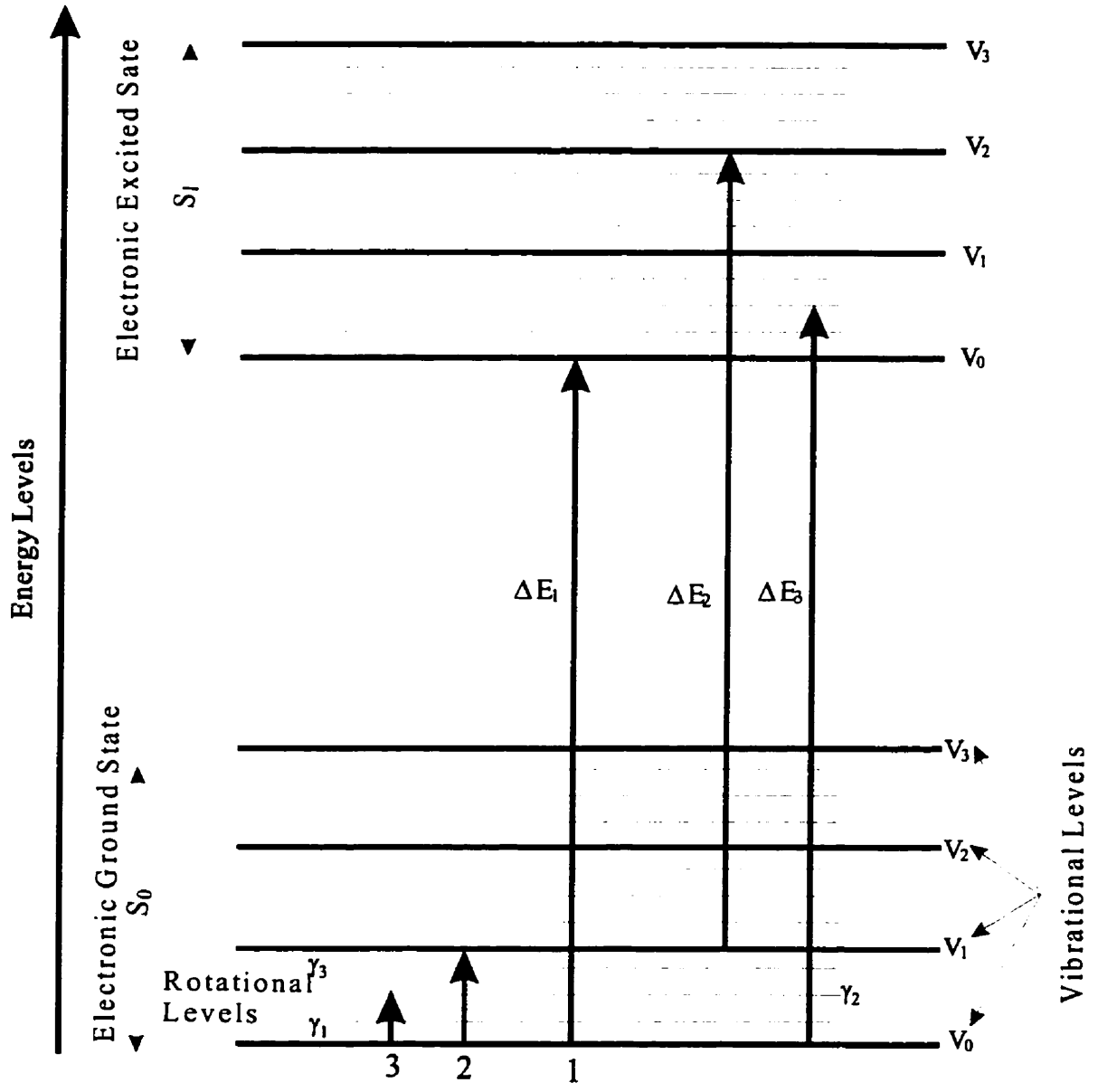

Fig. 3.1.1 Molecular energy levels showing electronic (1), vibrational (2), and rotational transitions (3).

region. In this study, we are particularly interested in the mid-IR region between 900 and 4000 cm^{-1}. Almost all of the fundamental vibrational motions of all chemical functional groups are included in this region, often referred to as the "fingerprint" region.

3.1.2 Normal Mode Molecular Vibrations

Molecules consist of many atoms, connected by chemical bonds. At any given moment, atoms and groups of atoms undergo complex motions. Generally, each atom possesses three degrees of freedom of motion, and an N-atom molecule therefore has 3N degrees of freedom.

The first kind of molecular motion is the translational motion, which corresponds to the movement of the entire molecule while the positions of the atoms in the molecule relative to each other remain fixed. The translational energy is independent of the energy responsible for the intra-molecular interactions. The translation motion possesses three degrees of translation freedom. Molecules also undergo rotational motions. During the rotational transitions, the inter-atomic distances remain constant but the entire molecule rotates with respect to three perpendicular axes that pass through the center of mass of the molecule. Therefore, polyatomic molecules generally have three degrees of rotational freedom. The last type of molecular motion is the vibration. The vibration of a molecule is a simultaneous motion of the atoms or functional groups with no shifting of the center of mass, i.e. the average position and orientation of the molecule remain unchanged. Therefore an N-atom polyatomic molecule involves 3N-6 vibrational degrees of freedom.

The vibrations of atoms in a molecule are closely related to the type of vibrating atoms, the forces of their interaction, and the structure of the molecule. The structure

reflects the molecule's spatial arrangement and is characterized by certain well-defined symmetry properties. Classification of a given vibration describes the properties of the vibration and depends on the symmetry of the molecule. The symmetry elements of a molecule include the axis of rotation, the plane of symmetry, the center of inversion and the rotation-inversion axis. Frequently, one vibration may be connected with movement of atoms joined by several chemical bonds.

In classical theory, the motions of a polyatomic molecule consisting of N atoms are characterized by choosing 3N ordinary Cartesian coordinates and describing the displacement from the equilibrium position of each of the atoms in the molecule. The 3N coordinate system is a set of coordinates such as X_1, Y_1, Z_1 for atom 1, X_2, Y_2, Z_2 for atom 2, and X_N, Y_N, Z_N for atom N, more generally given by the coordinates q_1, q_2, q_3, ..., q_{3N}. In classical mechanics, the equation of motion can be written in the Lagrange form that involves the kinetic energy (T) and potential energy (V) terms

$$\frac{d}{dt}\left(\frac{\partial T}{\partial \dot{q}}\right) + \frac{\partial V}{\partial q_i} = 0 \qquad 3.1.1$$

where q_i are the coordinates. In the 3N coordinate system, the equation of motion can be expressed as

$$\sum_{j=1}^{3N} m_{ij}\ddot{q} + \sum_{j=1}^{3N} f_{ij} q_j = 0 \qquad 3.1.2$$

$$\text{with} \quad \frac{\partial V}{\partial q_i} = \sum_{j=1}^{3N} f_{ij} g_j \quad \text{and} \quad \frac{d}{dt}\left(\frac{\partial T}{\partial \dot{q}}\right) = \sum m_{ij}\ddot{q}_j$$

where $\dot{q}$ is $\frac{dq}{dt}$, $\ddot{q}$ is $\frac{d}{dt}\left(\frac{dq}{dt}\right)$ and q_j is the j^{th} coordinates, the f_{ij} are force constants and m_{ij} is the term of atomic mass. These 3N equations have the general solution

$$q_j = A_j \sin\left(\sqrt{2\pi\nu t} + \alpha\right) \qquad 3.1.3$$

which is an equation characteristic of simple harmonic motion with a frequency ν, a maximum amplitude A_j and a phase constant α. This equation indicates that each atom oscillates about its equilibrium position with the same frequency ν and phase constant α, but with amplitude A_j, which differs for each coordinates. This means all the atoms go through their equilibrium positions simultaneously, such a motion is called a *normal mode of vibration*. The detailed solution and the complete theory of molecular vibrations are well developed (Herzberg, 1945).

Fundamental molecular normal mode vibrations include stretching and bending. The bending vibrations are often further subdivided into scissoring, wagging, rocking, and twisting. Fig. 3.1.2 demonstrates these types of vibrations. The arrows represent the relative displacements of the atoms. The stretching vibration is associated with a motion of atoms causing stretching and shortening of the chemical bond. In a three atom system, the stretching motion can be classified as symmetric or asymmetric (see Fig. 3.1.2a) in nature. A bending vibrational mode describes a motion of atoms during which the angle between the bonds changes. A wagging vibration (Fig. 3.1.2c) is an in-phase, out of phase motion of atoms, occurring while other atoms of the molecule are in the plane. A rocking vibration (Fig. 3.1.2d) describes atom in-plane swinging back and forth in phase within the symmetry plane of the molecule. If the plane is twisted, then the vibration is called a

twisting vibration (Fig. 3.1.2e). The frequency associated with a normal mode vibration is known as normal frequency of a molecule.

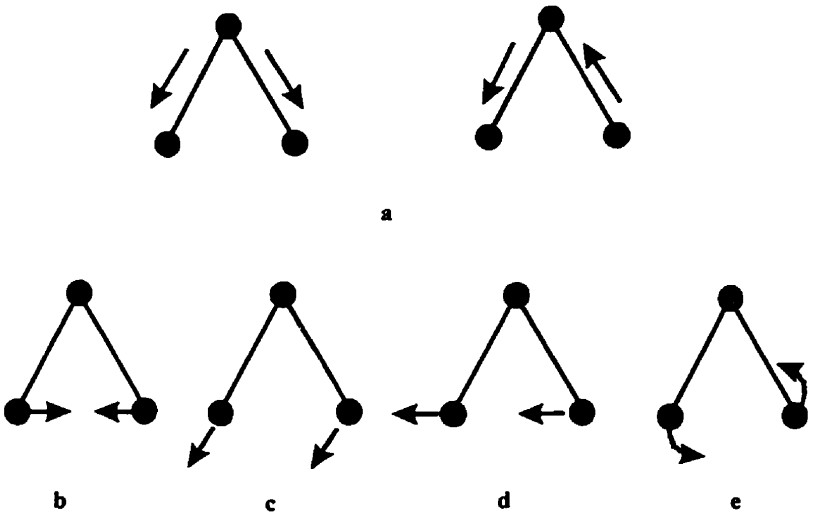

Fig. 3.1.2 Molecular vibrational modes (a) stretching (symmetric and asymmetric); (b) scissoring; (c) wagging; (d) rocking; (e) twisting.

3.2 FT-IR Spectrometers

The instrument used to record IR spectra is the infrared spectrometer, which contains hardware and software components. The hardware consists of an IR radiation source, a detector, optical components, sample accessories, electronic devices and a computer for data storage and evaluation. The software of an IR spectrometer is mainly used for spectral data analysis. A Fourier transform infrared (FT-IR) spectrometer is a particular type of IR spectrophotometer developed about 40 years ago. A diagram of an FT-IR spectrometer is illustrated in Fig. 3.2.1.

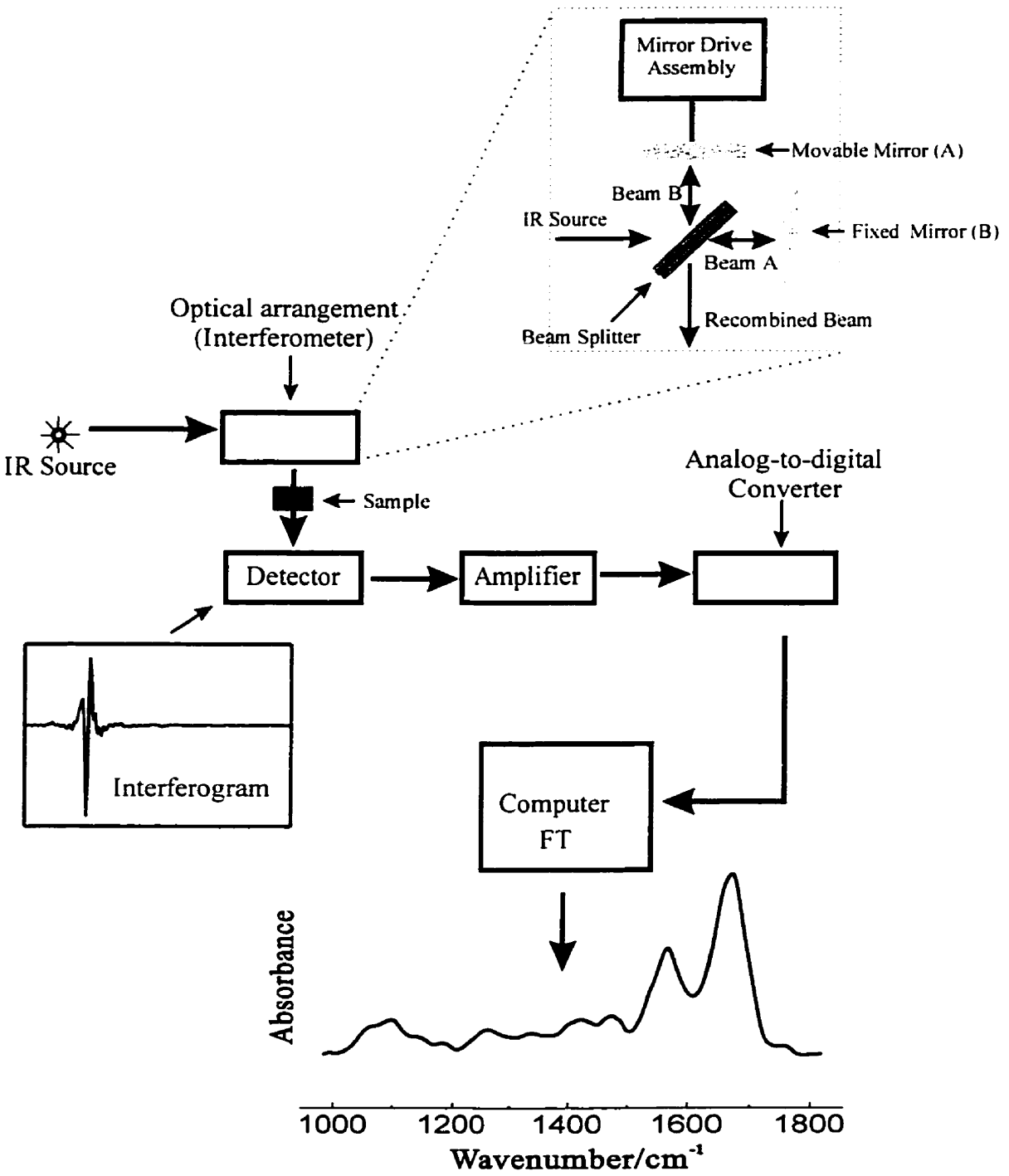

Fig. 3.2.1 Schematic Diagram of a FT-IR spectrometer

The optical arrangement of the typical FT-IR spectrometer is the Michelson interferometer consisting of two plane mirrors, one fixed and one moveable, and a beam splitter. The beam splitter transmits half of the radiation and reflects the other half.

The transmitted and reflected beams from the beam splitter strike two mirrors oriented perpendicular to each beam, and are reflected back to the beam splitter (see Fig.3.2.2). Interference occurs at the beam splitter where the radiation from the two mirrors recombine. The intensity of the beams passing to the detector is the sum of the intensities of the beams passing to the fixed and movable mirrors. When the two mirrors are equidistant from the beam splitter, the two beams are in-phase upon recombination at the beam splitter. At this position, so-called constructive interference occurs and the detector has a maximum output (see Fig.3.2.2A).

Destructive interference occurs when the recombined beams are out of phase at the beam splitter, producing a minimum detector output. Moving the moveable mirror from equidistant generates an optical path length difference of beams which is reflected from the mirrors. This optical path difference is called the *retardation.*

In order to understand how an interferogram is constructed, let us first consider a monochromatic radiation source with wavelength λ. Let the moveable mirror progress from the equidistant point by a distance of $\lambda/4$. The retardation is then $\lambda/2$. The radiation wave components from the two mirrors combine at the beam splitter one-half a wavelength out-of-phase and destructive interference occurs, resulting in the recombined beam, at the detector, having minimum output (see Fig. 3.2.2B). If the moveable mirror is further moved $\lambda/4$, i.e. $\lambda/2$ from the equidistant point, then the total retardation is λ. The

wave components from the two mirrors recombine again in-phase, so that constructive interference occurs and a maximum output is detected once again.

The response signal at the detector is an interferogram that is a function of the retardation. Fig.3.2.2 demonstrates this process. The interferogram of a monochromatic radiation source is a cosine function (Fig.3.2.2D). The Fourier transform of a single cosine wave interferogram is a single wavelength of radiation emitted from the radiation source. If the radiation source emits monochromatic radiation of a different wavelength with a different intensity, the interferogram will be a cosine wave with a different maximum amplitude and a different retardation length for one detector signal cycle.

A polychromatic radiation source is considered as a multiple monochromatic source with closely spaced wavelengths, covering the whole wavelength region of the source. The interferogram of a polychromatic source can be considered as a sum of all cosine waves from the monochromatic emission components. The polychromatic interferogram has strong maximum intensity at zero retardation, where all the cosine components are in-phase.

A sample is normally placed between the interferometer and the detector. By performing a Fourier transform, a spectrum is then obtained from an interferogram recorded in finite optical path intervals. The theory and mathematical calculations of obtaining a spectrum from an interferogram are well developed and can be found elsewhere (Griffiths and Haseth 1986).

Normally a single scan (with the moveable mirror traveling once over its allowed range) produces a complete spectrum. Usually a number of scans are taken and single-averaged by the computer. This is done to reduce the noise (by the square root of the

number of scans). Resolution is a constant over the whole spectrum and is increased by increasing the distance traveled by the moveable mirror.

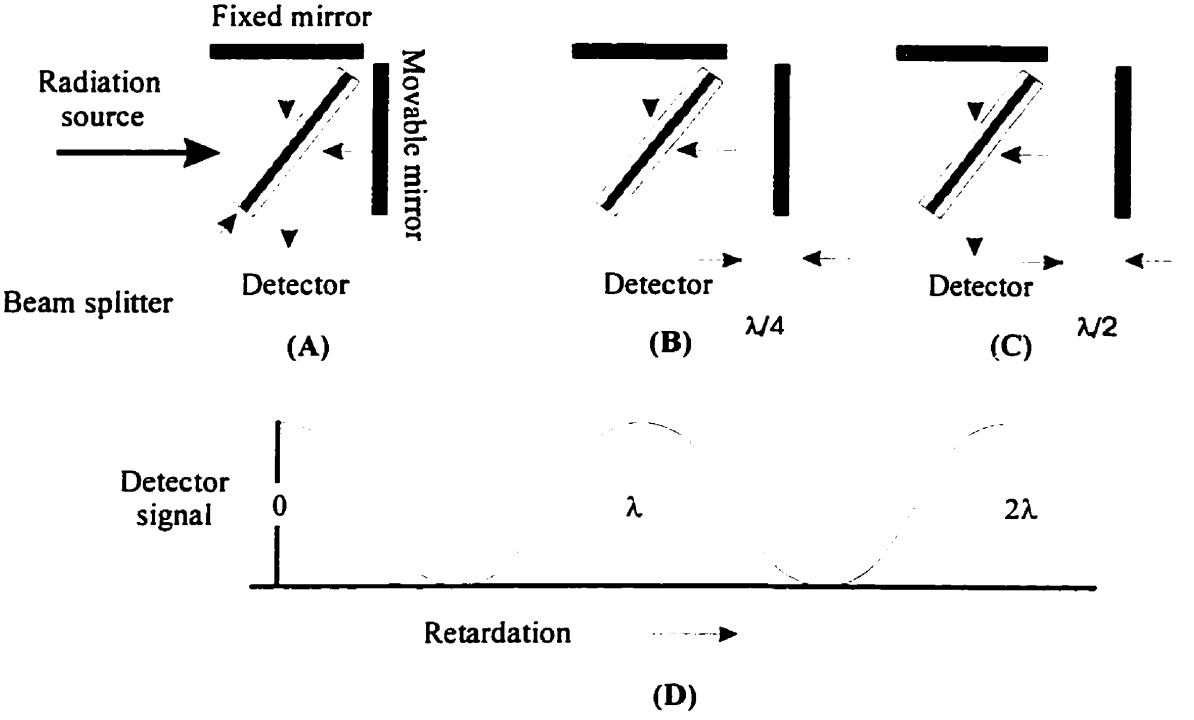

Fig. 3.2.2 Demonstration of the production of an interferogram from a monochromatic radiation source. (A) The mirrors are equidistant. (B) The moveable mirror is moved by λ/4. (C) The moveable mirror is moved by λ/2. (D) An interferogram for a monochromatic radiation source. The signal at the detector varies as a cosine function of the retardation. It reaches a maximum every time the retardation equals a whole number of wavelengths of radiation.

The IR detector is a device which measures the infrared radiation that has passed through the sample. The detector converts the infrared radiation energy into electrical energy which can be processed to obtain a spectrum. IR detectors are classified into two types: the photoconductive or quantum detectors and the thermal detectors. The most popularly used detectors are photoconductive cells, which have a very rapid response. They have been developed based on the quantum theory of the interaction of radiation with electrons in a solid, causing the electrons to be excited to a high-energy state. This

effect is due to the quantum nature of radiation. The energy of each photon is directly proportional to its wavelength and transition of electrons from one energy state to another will only occur if the wavelength is less than a certain critical value. Since the electrical properties differ when electrons are excited to another energy state, one method of detecting this quantum effect is by photoemission. This occurs when electrons acquire sufficient energy to escape from the bound states in the detector material, to free states, producing a current. The use of semiconductor technology is another method of detecting the quantum effect. Commonly used semiconductor detectors include PbS, PbSe, and mercury cadmium telluride (MCT).

Data analysis systems in a spectrometer are used both to store the recorded data and for spectral analysis, particularly useful in the analysis of complex spectra of biomolecules, biofluids and tissues.

3.3 Spectral Analysis

***Characteristic Positions of Vibrational Bands*:**

A vibrational band position is characterized by a particular vibrational mode of a given functional group, in a certain frequency region. It is possible, in a vibrating polyatomic molecule, to identify a particular functional group containing two or three atoms, for which the amplitude of a given normal vibration predominates over the amplitude

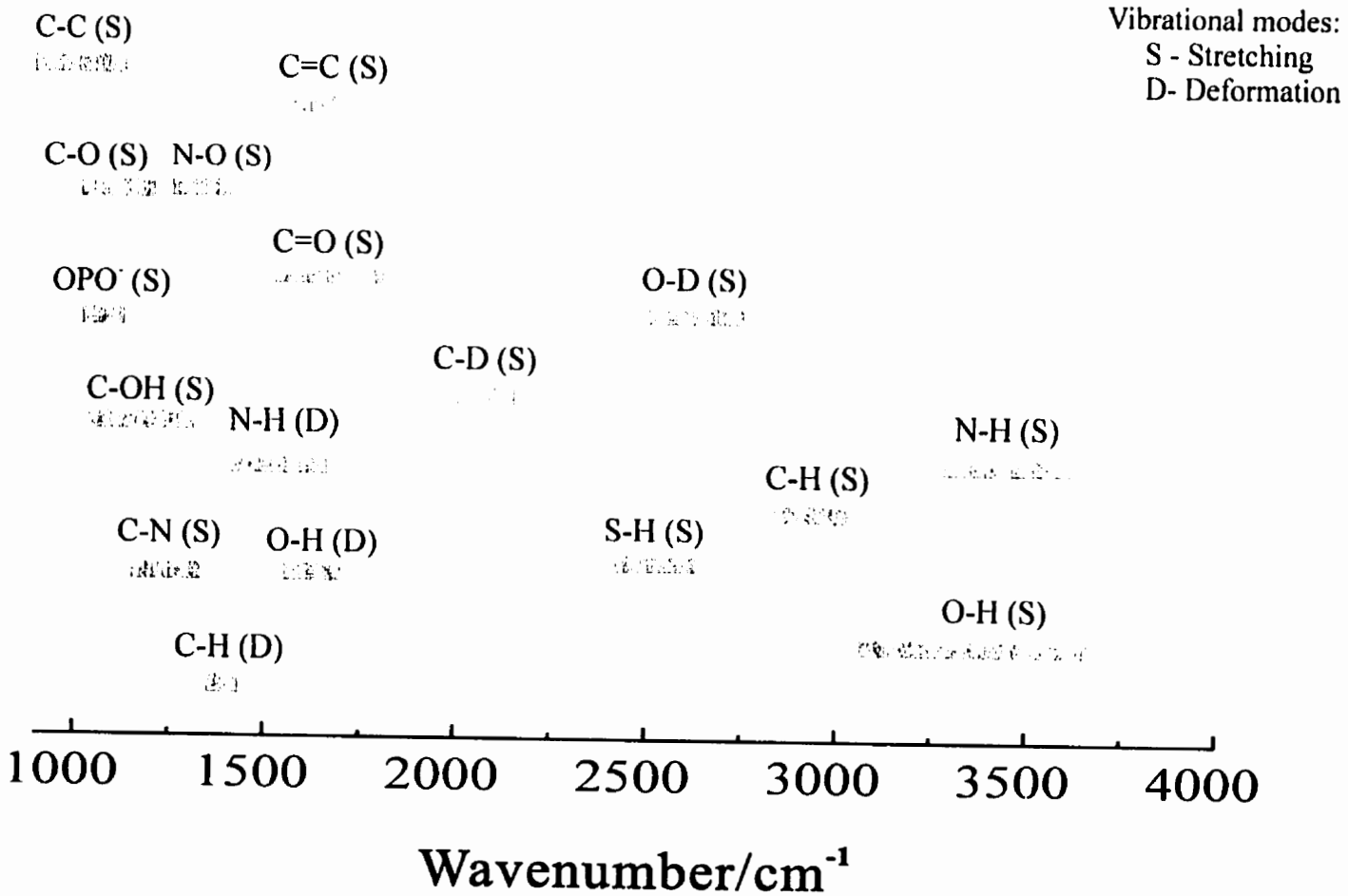

Fig. 3.3.1 Positions of some vibrational frequencies of various functional groups in the frequency region between 1000 to 4000 cm^{-1}

produced by other atoms in the molecule. A vibrational mode is then assigned to the particular vibration, which is specific for this functional group.

The corresponding IR frequency of an absorption band characterizes a particular vibrational mode of a functional group in a molecule. These characteristic positions of vibrational bands are of enormous practical significance for identification of functional groups in unknown molecules. Fig. 3.3.1 shows positions of some vibrational frequencies of various functional groups. Vibrations of functional groups of biomolecules in tissues and fluids will be discussed in a later section.

Quantitative Analysis:

A spectrum represents the absorption, or transmittance, as a function of the frequency (wavelength) of the recorded radiation. IR quantitative analysis is based on the absorption law (Beer's law). For a single solute in a non-absorbing solvent, the law is written as a function of absorption (A)

$$A = a(\bar{\nu})bc \qquad 3.3.1$$

which is the product of concentration c, the pathlength of a measured sample b, and the absorptivity $a(\bar{\nu})$, at a given wavelength. For multi-components, the law is written as

$$A = \sum_i a_i(\bar{\nu})bc_i \qquad 3.3.2$$

If I_0 is the intensity of radiation power entering a sample, and I is the intensity transmitted by the sample, the ratio I/I_0 is defined the transmittance of the sample and it is given by

$$T = I/I_0 = 10^{-a(\bar{\nu})bc} \qquad 3.3.3$$

Alternatively, this equation is transformed by taking the logarithm to the base 10, to obtain absorbance

$$A = \log_{10}\left(\frac{I_0}{I}\right) = \log_{10}\frac{1}{T} \qquad 3.3.4$$

Based on the absorption law, quantitative analysis can be summarized by the following:

(1) Peak height measurements: The peak height is determined by $A = \log_{10} {}^{I_0}/_{I}$. It reflects the concentration of a particular component in a mixture sample as indicated by Beer's law and is routinely used as a routine operation for quantitative analysis. It is sensitive, however, to changes of instrumental parameters such as resolution, and can vary from instrument to instrument.

(2) Integrated band area: The integrated band area is a measure of the total intensity of the infrared vibration, and is normally much less sensitive to instrumental variations. It is widely applied for quantitative analysis. It also has great theoretical significance, in that it is proportional to the square of the change in dipole moment with respect to the normal coordinates.

In practice, a band is measured as a function of linear coordinates of absorbance, $A = \log_{10}(I_0/I)$, versus wavenumber ($\bar{\nu}$). The band area then can be obtained by

$$Area = \int_{band} \log_{10}\left(\frac{I_0}{I}\right) d\bar{\nu} \qquad 3.3.5$$

The unit of the band area is Absorbance/cm.

(3) Ratio method: This method consists of the use of an intensity ratio of two bands, to determine relative amounts of molecules in a mixture. The advantage of the ratio method

is that it is not a function of the pathlength of the sample, since the absorbance ratio of two bands in the same spectrum should be independent of sample thickness.

Spectral Manipulation:

The purpose of performing spectral manipulations is to extract additional information, or to enhance spectral features in order to improve the efficiency of the spectral analysis. The most commonly used spectral manipulation methods are briefly described below.

(1) Baseline correction: baseline correction is used to correct spectra which have sloping or curved baselines that compromise quantitative analysis of the spectrum. The problem is normally caused by infrared light scattering on the sample by inappropriate choice of background and by instrument drifts.

Baseline correction can be achieved by generating a function which parallels the shape of the sloping baseline of the spectrum. It is then subtracted from the sample spectrum, yielding a result devoid of the sloped baseline. Software techniques such as function fits and interactive polynomials are used to generate the baseline correction function.

Often the baseline correction is performed in the simplest way, i.e. a two-point linear baseline correction. In this approach, once the baseline points are defined, the baseline is "flattened" with respect to the two points by subtracting the line defined by these two points.

(2) Spectral subtraction: Spectral subtraction is performed in order to obtain the spectrum of one component in a mixture. In performing spectral subtraction, two spectra are obtained. The spectrum of the mixture is termed "the sample" and the spectrum of the component to be subtracted from the sample is called "the reference". The absorption

values of the reference spectrum are subtracted point by point from the absorption values of the sample spectrum. One should keep in mind that the spectroscopic conditions of the reference spectrum (such as spectral resolution, spectral data points etc.) must be identical to the sample's spectrum.

(3) Derivative method: Derivative methods are introduced into spectral analysis to solve the difficulty of overlapping bands in the spectra. The derivative of an IR spectrum can be taken a number of times, producing derivatives of different orders (e.g. first or second derivatives).

As described in calculus theory the first derivative of a curve is the slope of that curve. A zero result of the first derivative indicates zero slope. In spectra, the first derivative determines the change of slope of the spectrum. Since the slope at the top of an absorbance band is zero, after performing the first derivative, the band position will be located at zero. As a result, the first derivative helps to indicate the peak positions of a band.

The second derivative, mathematically, is used to describe the concavity of a curve. In spectral analysis, it is also applied to indicate the position of an absorption peak. The corresponding positions in the second derivative are the same position as the wavenumber of the maximum absorbance of each band in the original spectrum, but are negative. A second derivative of an original spectrum is illustrated in Fig.3.3.2. This is a useful technique and is extensively applied in spectral analysis. It not only provides the position of an absorption band, but also indicates the shape changes of the absorption

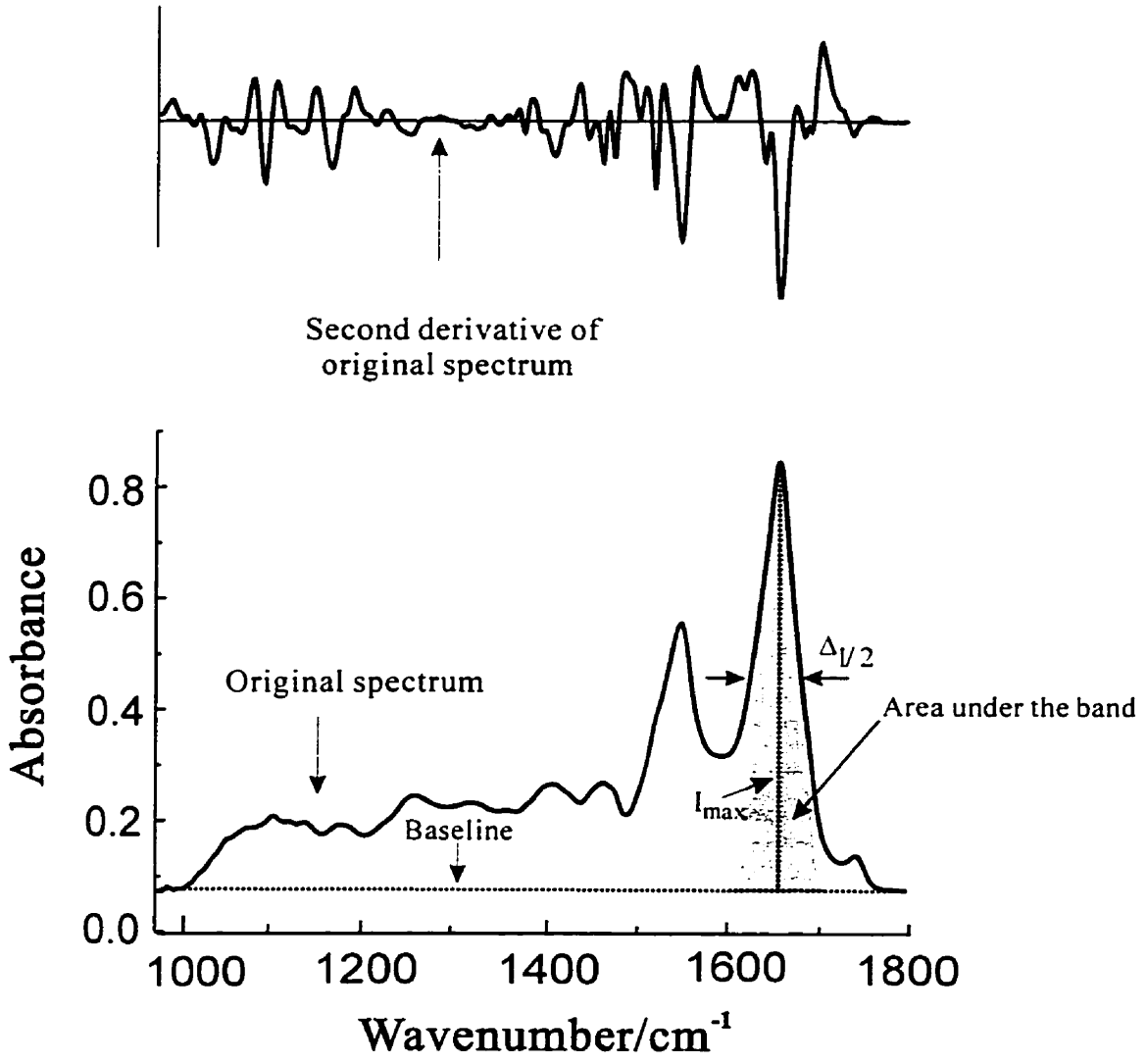

Fig.3.3.2 Illustration of IR spectral manipulations

band and separates possible overlapping bands. Other techniques to resolve the problem such as peak fitting and Fourier self-deconvolution are also well developed and are often applied. The accuracy of these methods, especially the peak fitting technique, remains controversial.

(4) Multivariate data analysis: Multivariate analysis is used for evaluation of complicated spectroscopic data sets, and is based on statistical methodologies. Techniques such as partial least square, and principal component analysis are particularly useful in analytical chemistry (Brereton, 1990). Classification methodologies, such as cluster analysis and linear discriminant analysis are very powerful and useful techniques in biomedical data assessment.

3.4 Biomedical Applications

IR spectroscopy has traditionally been one of the most important physical methods in the analytical chemical laboratory. One advantage of IR spectroscopic analysis is that the measurements are not affected by the physical states of the sample: gaseous, liquid, homogeneous, and inhomogeneous solid samples can all be conveniently studied (Wang *et al.*, 1996). Some recent investigations of the IR spectroscopic technique for *ex vivo* biomedical applications indicate that the technique has potential in the clinical sciences. Minimal sample preparation and reagent free assay are the most attractive factors for its ex *vivo* clinical application. These applications will be outlined in the following sections.

3.4.1 IR Characterization of Biofluid and Tissue Components

Application of IR spectroscopy to clinical sciences requires an understanding of the IR spectra of biofluids and tissues. It is thus important to have an understanding of the major biochemical components that comprise an IR spectrum of a biofluid.

Organs are composed of varying proportions of basic tissues including epithelial, connective and muscular tissues. The proportion of each type of tissue in an organ is dependent on the basic physiological function of that organ. The lung, for example, is composed mainly of epithelial cells and a thin-walled endothelium, allowing for gas exchange. Alveoli, the principal sites of oxygen uptake, are polyhedral or hexagonal, with one wall lacking to permit diffusion of air. These vestibules are packed so tightly that each alveolus does not have a separate wall and usually shares a common interalveolar septum. This septum contains an extensive capillary plexus, composed of endothelial cells and supported by a connective tissue skeleton framework. The major components of all type of tissues are proteins, lipids, water, and carbohydrates.

A biofluid is defined as a body fluid in the human body. Different types of fluids are present throughout the body such as cerebrospinal fluid, blood, pleural fluid, and peritoneal fluid. Although the concentration of individual components may vary among these fluids, body fluid is distributed between two major compartments, the *extracellular fluids* and the *intracellular fluids*. All the fluids outside the cells are collectively called the extracellular fluid. The extracellular fluid compartment is subdivided into the interstitial fluid compartment and the blood plasma. The extracellular fluid contains large amounts of NaCl, bicarbonate ions, and nutrients for the cells, such as oxygen, glucose,

fatty acids, and amino acids. The intracellular fluid contains large amounts of potassium, magnesium, and phosphate ions. (Guyton and Hall, 1994). In both fluid compartments the cells contain large amounts of protein.

Blood contains both extracellular fluid (the fluid in plasma) and intracellular fluid (the fluid within the red blood cells). However, the blood is considered a separate fluid compartment. To varying extents, the blood plasma also contains circulating lipids that have a tendency to contribute to IR spectra.

The IR spectra of human tissues or biofluids are generally complex. There is considerable overlap of absorption features from the major molecular species present. Understanding of the composition of the tissues and biofluids is required in order to enable correct assignment of the absorption bands. Although cellular and biochemical composition vary from tissue to tissue and from fluid to fluid, certain constituents are common to all human tissues and biofluids. These include lipids, proteins, nucleic acids, and carbohydrates. The IR spectra of most tissue and biofluids should theoretically be closely approximated by summation of these common constituents. Specialized tissues and biofluids may contain species that are not found in other tissues and biofluids, therefore the interpretation of spectroscopic results is facilitated if the investigator has a precise understanding of the histology, pathology, and biochemistry of the tissues and biofluids under investigation.

In the IR spectra of all tissues and biofluids, there is a series of absorption bands between 2800 and 3000 cm^{-1}. The O-H stretching band from the water component in tissues and fluids appears strongly at 3000-3400 cm^{-1}. Absorption bands between 2800 and 3000 cm^{-1} arise from asymmetric and symmetric stretching vibrations of CH_3 (2956

and 2871 cm^{-1}) and of CH_2 (2922 and 2851 cm^{-1}) groups present in protein and phospholipid components of cells and tissues. The so-called amide I and amide II absorption bands dominate the spectra of each tissue and biofluid sample. The amide I arises from the C=O stretching vibration weakly coupled to C-N stretching. The amide II band arises from the N-H bending vibrations coupled with the C-N stretching vibrations. Both amide I and amide II absorptions have been shown to be sensitive to conformation and are often used to predict protein secondary structure (Jackson and Mantsch, 1996). The amide absorptions in tissues and biofluids represent the average of the amide absorptions arising from all protein components that are present in a sample.

Other absorptions that are routinely seen in tissue and biofluid IR spectra are those attributed to C=O stretching vibrations of lipids (1740 cm^{-1}) and nucleic acids (1714 cm^{-1}). CH_2 and CH_3 asymmetric bending vibrations of lipids, protein, and nucleic acids appear as a complex absorption profile between 1450 and 1480 cm^{-1}. The carboxylate COO^- symmetric and asymmetric stretching vibrations of fatty acids and amino acids are observed at 1400 and 1550 cm^{-1}. The phosphate PO_2^- symmetric and asymmetric stretching vibrations of nucleic acids and phospholipids absorb at 1084 and 1225 cm^{-1} respectively (Fabian *et al.*, 1995). IR absorptions in the region between 900 and 1200 cm^{-1} arise from carbohydrate components in the tissues and biofluids. The major biological components contributing to IR spectra in this region include glucose, glycoprotein, glycolipid and DNA. Glycogen also has a strong IR absorption profile in this region.

A typical IR spectrum of human plasma is presented in Fig. 3.4.1. The major IR absorption band assignments of human plasma and bronchial alveolar lavage fluid are presented in Table 3.4.1.

3.4.2 IR Spectroscopic Analysis of Biofluids

IR spectroscopy offers a number of advantages for analysis of body fluids. Unlike most calorimetric or electrochemical/enzymatic clinical chemistry assays, IR spectroscopic analysis is applicable to a variety of biofluids: whole blood, plasma or serum, synovial fluid, aqueous humour, saliva and urine (Mantsch and Jackson, 1995).

Quantitative analysis of these biofluids can provide several clinically relevant parameters, for instance, analyses in blood may be used to indicate the metabolic status of the patient. It has already been demonstrated that multi-component analysis of several substrates in human EDTA-plasma can be performed with a precision well within the clinical acceptance tolerance limits using ATR infrared spectroscopy in the mid-IR region (Heise *et al.*, 1994; Heise and Bittner, 1995).

Other IR biological spectroscopic investigations have addressed the spectral range best suited for quantitative analysis. A recent study of the quantitative analysis of protein, creatinine, and urea in urine by IR spectroscopy, indicated that the results are as accurate as the reference methods currently used in the clinical chemistry laboratory (Shaw, *et al*, 1996). Another application of IR spectroscopy that has shown significant clinical potential is the prediction of fetal lung maturity by analyzing amniotic fluid (Lui, *et al.*, 1997).

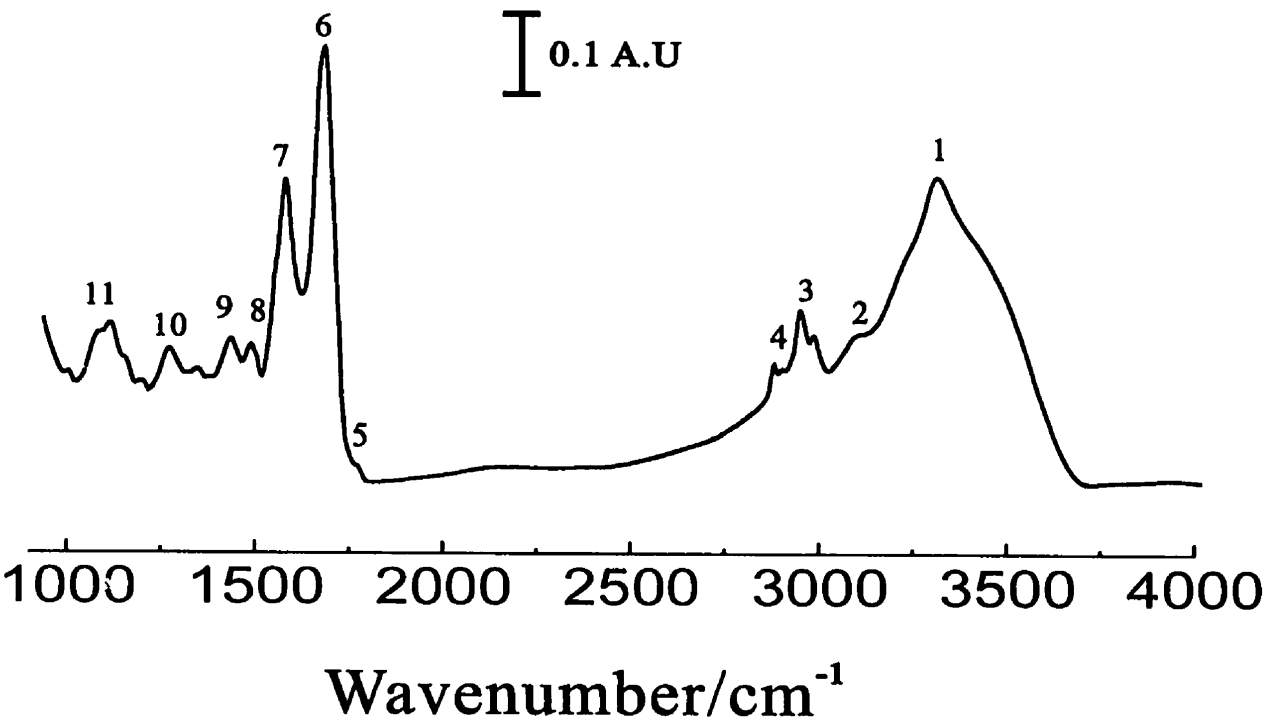

Fig. 3.4.1. Infrared spectrum of human plasma in the spectral region 900-4000 cm^{-1}

Table 3.4.1 Important IR Absorption Bands of Plasma and BALF

Vibrational mode	Observed frequencies for plasma (cm^{-1})	Observed frequencies for BALF (cm^{-1})	Position*
Amide A	3291	3293	1
Amide B	3073	3079	2
CH_3 asymmetric str.	2961	2959	3
CH_2 asymmetric str.	2929	2924	3
CH_3 symmetric str.	2874	2876	4
CH_2 symmetric str.	2854	2853	4
C=O str. (ester)	1735	1738	5
Amide I	1652	1652	6
Amide II.	1545	1546	7
COO^- symmetric str.	1400	1400	8
CH_3 symmetric bending	1452	1453	9
PO_2^- asymmetric str.	1243	1237	10
PO_2^- symmetric str.	1078	1079	
Sugar vibration modes (C-O-C, C-O etc)	1200-900	1200-900	11

* "Position " refers to the position indicated in Fig. 3.4.1

The advantages of using IR analysis include: (1) no reagents are required; (2) little or no sample preparation is needed and minimal technical skill is required of the operator; (3) it is non-destructive; (4) it lends itself readily to on-line measurements; and (5) once the methodology has been calibrated, it has the capacity for a rapid multi-component analysis to be carried out from a single measurement.

In specialized fluids, certain species that contribute a unique or distinguishable IR absorption pattern are often used as markers for diagnostic purposes. In these applications, the marker molecule is selected because it has a particular IR spectroscopic signature that can be distinguished from other biological components in the sample. This provides both quantitative and qualitative analytical results. The determination of thiocyanate levels in human saliva by IR spectroscopy is such an application (Schultz, *et al.*, 1996). In certain pathological conditions, the molecular structure of some biofluids changes from a normal to an altered state. While these changes in the IR spectra are sometimes obvious to the naked eye, most of the time this differentiation is difficult. This is due to the many components contributing to the IR absorption profile in biological samples. Normally the spectra are too complex to permit assignments of specific absorptions to individual constituents, and in these instances, a sophisticated statistical tool is used to analyze the spectrum and identify the regional differences corresponding to pathological changes.

Multivariate analysis methods such as cluster analysis and spectral pattern recognition approaches are the most successful statistical tools. Multivariate analysis of IR spectra of synovial fluid is an example of this application (Eysel *et al.*, 1996), as is IR spectroscopic characterization of chronic lymphocytic leukemia cells (Schultz, *et al.*,

1996). Spectroscopic classification of biomedical samples provides an objective aid in the diagnosis of disease, and has potential for staging the disease.

3.4.3 IR Investigation of Tissue and Cell Pathology

Pathology is the morphological study of the disease process. Although a distinct field, it is also related to other specialties such as cytology, histology, haematology, clinical chemistry, genetics, and microbiology. The instruments used in pathological studies are primarily optical and electron microscopy. With development of IR microspectroscopy, pathological and histochemical IR analyses are becoming increasingly attractive. Their usefulness is predicated upon the changes in tissues and cells compositions that characterize disease states.

FT-IR microspectroscopy is a new technique that combines IR spectroscopy and optical microscopy. The optical part of the instrument is used to select the area of interest for study, and the infrared part allows the focused IR source to be radiated onto the selected location. The aperture size of the focused IR beam can be adjusted to achieve the desired spatial resolution and the instrument is equipped with a computerized movable stage that allows for spectroscopic mapping of the tissue. Spatial resolution is an important factor in microspectroscopic mapping, relating primarily to the ability to measure spectra of small, isolated regions of specimens. With appropriate software, the spectroscopic mapping data of the specimen can be presented as a two-dimensional contour plot and an image of the sample can be generated from spectral information such as the band intensities or the peak height ratios. In this way, chemical structural information about the sample can be displayed as an IR image.

IR microspectroscopic examination of tissues is based on the IR absorption signature of the biochemical components of cells and tissues and involves the same complexities as IR analysis of biofluids. Spectra of tissue are typically complicated and involve overlap of absorptions from the major biochemical components in the tissue examined.

IR microspectroscopic analysis of tissue and cells provides additional pathological and histochemical diagnostic information about diseased tissues. Several clinical applications have been identified using isolated cells and tissues, which have provided significant additional information about the histopathology of the samples.

IR spectroscopy is well suited to the detection of cancer and IR has been used to investigate various cancers including colon, breast and cervical cancers. Investigation of cervical cancer has indicated that the asymmetric stretching vibration of the DNA phosphate group, PO_2^- changes. The absorption band position in the spectrum of healthy tissue (1240 cm^{-1}) shifts to a lower wavenumber (1225 cm^{-1}) in malignant tissue. It has been suggested that these spectral changes may indicate changes in the hydrogen bonding pattern of DNA, which implies structural alterations in the DNA of malignant cells as expected (Wong *et al.*, 1991,1993). Such a repositioning of the absorption band in the IR spectrum suggests that a significant proportion of the cellular components have undergone structural changes.

The use of IR in the investigation of human colon cancer has indicated distinct spectral differences between normal and malignant tissue in almost every region of the IR spectrum (Rigas *et al.*, 1990).

In addition to cancer, IR has been used to investigate neurological disorders such as multiple sclerosis and Alzheimer's disease. A study using synchrotron FT-IR microspectroscopy provides the first direct evidence of β-amyloid protein within a slice of human Alzheimer's diseased brain tissue (Choo *et al.*, 1996). This in situ protein structure analysis was based on the amide I band; the high spatial resolution (12 μm × 12 μm) achieved was close to the dimension of single cells.

The application of sophisticated multivariate statistical classification methods, such as linear discriminant analysis or artificial neural networks, increases the power and usefulness of IR pathological examinations. They allow the discrimination to be made in an objective manner and have been employed in several investigations (Romeo *et al.*, 1998, Lasch *et al.*, 1998, Schultz and Mantsch, 1997).

The determination of foreign materials in tissue presents another application for IR microspectroscopy. Polymetric materials used for surgical procedures are easily viewed with IR microscopy and FT-IR microspectroscopy has been used to confirm the presence of silicon polymers in skin biopsies (Ceteno *et al.*, 1992). Other polymers that have been located in bone biopsy tissue after reconstructive surgery include poly-glycolic acid and poly-dioxanon (Kalasinsky, 1996). The FT-IR microspectroscopic technique was also recently applied to the analysis of tissue sections from breast implant patients (Centeno, 1993; Hardt, 1994), since the presence of silicone gel or elastomer can be confirmed with "relatively distinct" IR absorption bands. These bands can also be used to visualize the presence of silicone in a spectral map.

It has been less than 10 years since investigations started to apply IR spectroscopy to clinical chemistry and pathology, but despite this relatively short period, it has already demonstrated significant potential. Further research in this area will likely reveal more possible clinical applications. In this study, IR spectroscopy and IR microspectroscopy are applied in the analysis of lung fluid and lung tissue to evaluate pulmonary permeability in the acute stages of lung injury.

Chapter 4

HES Pulmonary Leakage in the Animal Model and IR Analysis

The rationale for studying an animal lung injury model is to develop a methodology that follows pulmonary edema formation in a controlled physiological environment and to assess lung permeability. The lung-injury model experiments serve to test multiple hypotheses. The first question is whether the leakage of hydroxyethyl starch through a damaged pulmonary alveolar–capillary membrane barrier can be evaluated by examining lung tissue, pathologically and histochemically, based on the distribution of HES in the tissue. The second question is whether hydroxyethyl starch can be used as a marker to provide permeability information, by identifying it in bronchiolar lavage fluid using IR spectroscopy. Finally, the animal model of pulmonary edema is presented in order to assess whether the IR technique has a valid application in the clinical setting, to enhance the diagnostic potential for a critically ill population of patients.

Pathophysiologically, pulmonary vascular endothelial membrane damage is believed to be a cardinal feature of the ALI/ARDS. Quantifying and determining the composition of lung edema fluid through the animal injury model, will assist in the diagnosis and management of patients in the intensive care setting with suspected ALI/ARDS diagnoses.

The animal-injury model investigation focused on injured tissue histology and IR

histochemical analysis of injured tissue based on HES distribution. In addition, a methodology to assess pulmonary alveolar-capillary permeability through analysis of the bronchoalveolar lavage content using IR spectroscopy was developed. To achieve these objectives, it is important to know and distinguish the IR spectral signature of starch-based macromolecules in tissues and in biofluid. Thus, IR spectroscopic characterization of starch-based macromolecules will first be introduced in this chapter.

4.1 IR Spectroscopic Characterization of HES

PENTASPAN® (DuPont Pharma Inc, Mississauga, Ontario, Canada), a product of LMW HES, is used as an external tracer for lung permeability determination in this study. The polymeric product is 10% PENTASPAN® in 0.9 % sodium chloride solution and its clinical use is as a plasma volume expander. PENTASPAN has been used extensively following cardiac surgery and, currently is used preferentially for volume expansion in this setting. As well, PENTASPAN has been shown to have beneficial cardiorespiratory effects in sepsis, shock and for burn resuscitation. (Jean-Francois Baron, 1992.)

IR Absorption Profile of PENTASPAN®

The spectrum of a dried film of pure PENTASPAN® is presented in Fig. 4.1.1. In the region between 900-1200 cm^{-1}, the spectrum shows an intense feature (# 6 in Fig. 4.1.1), typical of glucose-based molecules. Often this region is referred to as the sugar absorption region. It represents complex vibrations arising from various functional

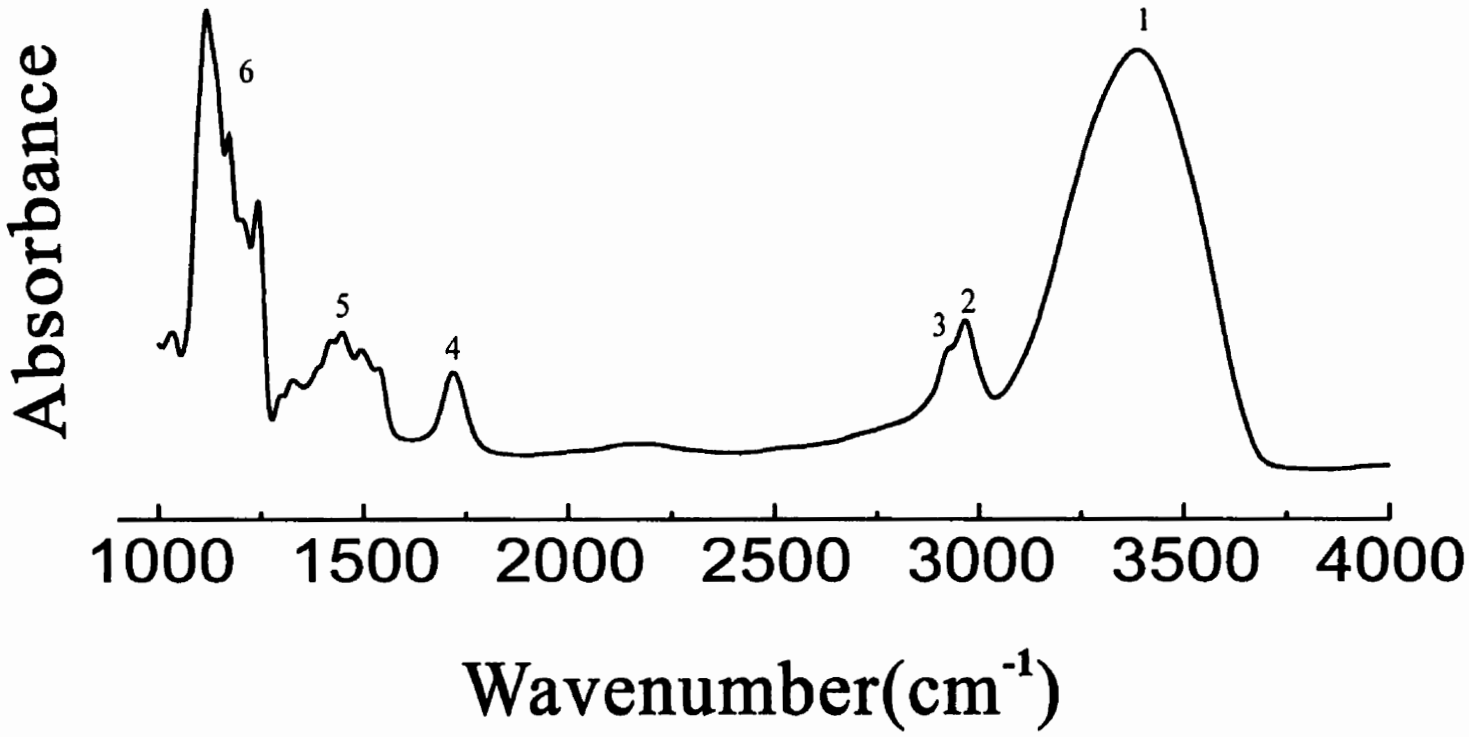

Fig. 4.1.1 Spectrum of a dried film of pure PENTASPAN in the region between 900 and 4000 cm^{-1} with important band positions marked.

groups in carbohydrate ring molecules, including moieties such as the C-O-C, C-C-C and C-C-O.

Proposed band assignments of PENTASPAN®: The peak at 3370 cm^{-1} corresponds to O-H stretching vibrations. The CH_2 asymmetric and symmetric stretching vibration bands, typical for PENTASPAN® are located at 2933 and 2875 cm^{-1} respectively. A weak band appears at 1645 cm^{-1} representing O-H bending vibrational modes. The major difficulty in assigning absorption bands for starch-based macromolecules is in the region between 900 and 1600 cm^{-1}, especially in the region of the sugar ring vibrations between 960 and 1200 cm^{-1}. There are many vibrational motions producing absorption bands, which all tightly overlap. Assigning the numerous bands is therefore very difficult and is only possible for simple sugar molecules.

A number of investigators have reported basic assignments of simple carbohydrate molecules such as glucose, maltose, etc in the region between 900 and 1600 cm^{-1}. These assignments can generally be summarized as follows: The bands located in the region between 1200 and 1474 cm^{-1} are due to the bending modes of O-C-H, C-C-H, and C-O-H proposed by Hineno (Hineno, 1977). The C-O stretching vibrations, perhaps coupled to C-C stretching vibrations, were assigned between 904 and 1153 cm^{-1} (Véronique, *et al.*, 1995). The band at 1149 cm^{-1} has been identified in many monosacharides as characteristic of pyranose sugars (Cael *et al.*, 1974). The band at 1103 cm^{-1} was assigned to be combined vibration modes including C-C, C-O, and C-O-H (Vasko *et al.*, 1972). Tentatively, C-O-C stretches and C-O-H grouping vibrations were assigned to a band at 1060 cm^{-1} (Mohamed and Koenig, 1986). Finally, the band at 1020 cm^{-1} may correspond to OH vibrations (Vasko *et al.*, 1971).

It is accepted practice to assign absorption bands by using the assignments from other molecules, which are simpler and structurally similar to the molecule which is under investigation. A problem associated with this approach is that assignments could be incorrect due to vibrational frequency shifts in the spectra of the comparison compound.

Thus, assignments made for complex molecules in this way are often controversial. The proposed band assignments of PENTASPAN® are presented in Table 4.1.1.

Table 4.1.1 Representative IR Absorption Bands for PENTASPAN

Vibration mode	Approx. observed frequencies (cm^{-1})	Position
OH (bound)	3370	1
CH_2 asymmetric str.	2933	2
CH_2 symmetric str.	2875	3
OH bending (bound)	1645	4
Ring skeletal bending vibrations C-O-H C-C-H O-C-H	1200-1470	5
Ring skeletal stretching vibrations C-C-C C-O-C C-C-O	960-1200	6

✸ Note: The positions indicated in Table 4.1.1 refer to Fig. 4.1.1

In most carbohydrate research, analyzing the skeletal vibrations arising from the ring structure of the glucose unit (the sugar ring), is much easier than working on assignments for each individual bond. The skeletal vibrations (including C-C and C-O stretching vibrations and C-O-C, C-C-O deformation vibrations) are often considered as a "fingerprint" of glucose-based molecules. In this study, the characteristic skeletal

vibrations of HES appearing in the region between 950-1200 cm^{-1} are most useful for determining hydroxyethyl starch in biofluids. The utility of this spectral region as a marker for hydroexyethyl starch in biofluids is demonstrated in this thesis.

Characterization of Glucose-Based Polymers in Biological Samples

Due to compositional similarities, the glucose-based molecules in biological samples generally have similar, but not identical, absorption features. Differences between PENTASPAN® and other glucose-based polymers exist in biological samples. To illustrate the nature of these differences, the IR spectra of films dried from some glucose-based macromolecules, hetastarch, pentastarch, and dextran, as well as from glycogen and glucose in human serum are presented in Fig. 4.1.2.

Despite the fact that the IR absorption features of these starch-based molecules are similar in biological samples (Fig. 4.1.2), some spectral differences do exist in the sugar region. This is mostly due to structural variations of these polymers. Such spectral variations can clearly be demonstrated in second derivative spectra of these polymers. For each of the polymers, the second derivative spectra calculated over the sugar region are presented in Fig. 4.1.3 together with the same region of the original IR spectra for comparison.

Major differences between samples are seen in 960-1065 cm^{-1} and 1090-1137 cm^{-1} regions (shadowed in the second derivative spectra of Fig 4.1.3). These spectral differences may be due to structural differences, such as the degree of polymerization of glucose in these polymers. The spectra of glycogen, PENTASPAN® and HETASPAN® in human plasma exhibit basic similarities in the sugar region (see Fig. 4.1.3 B, C, E).

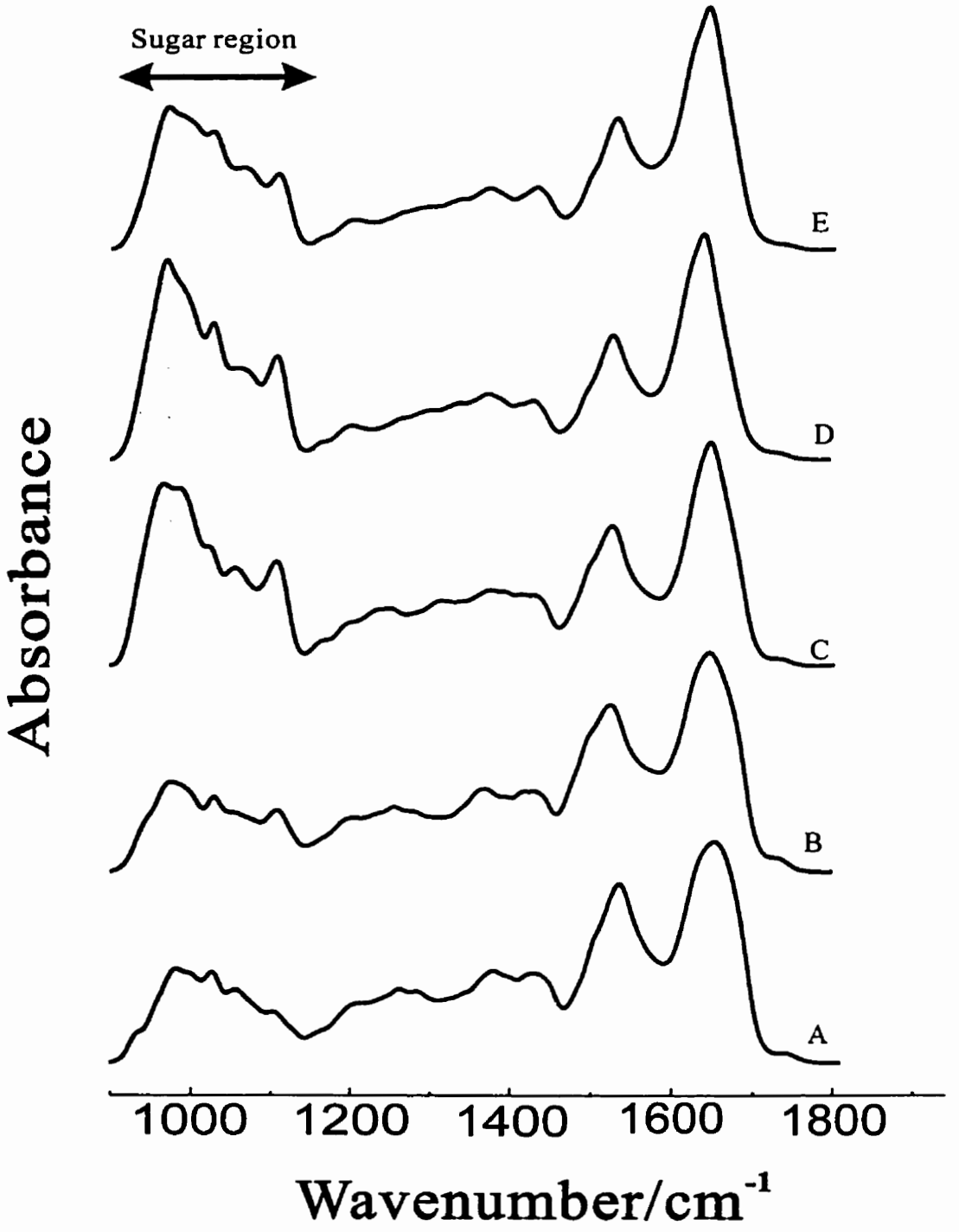

Fig. 4.1.2 IR spectra of glucose-based polymers in human plasma A: Glucose; B: Glycogen; C: Dextran; D: PENTASPAN; E: HETASPAN

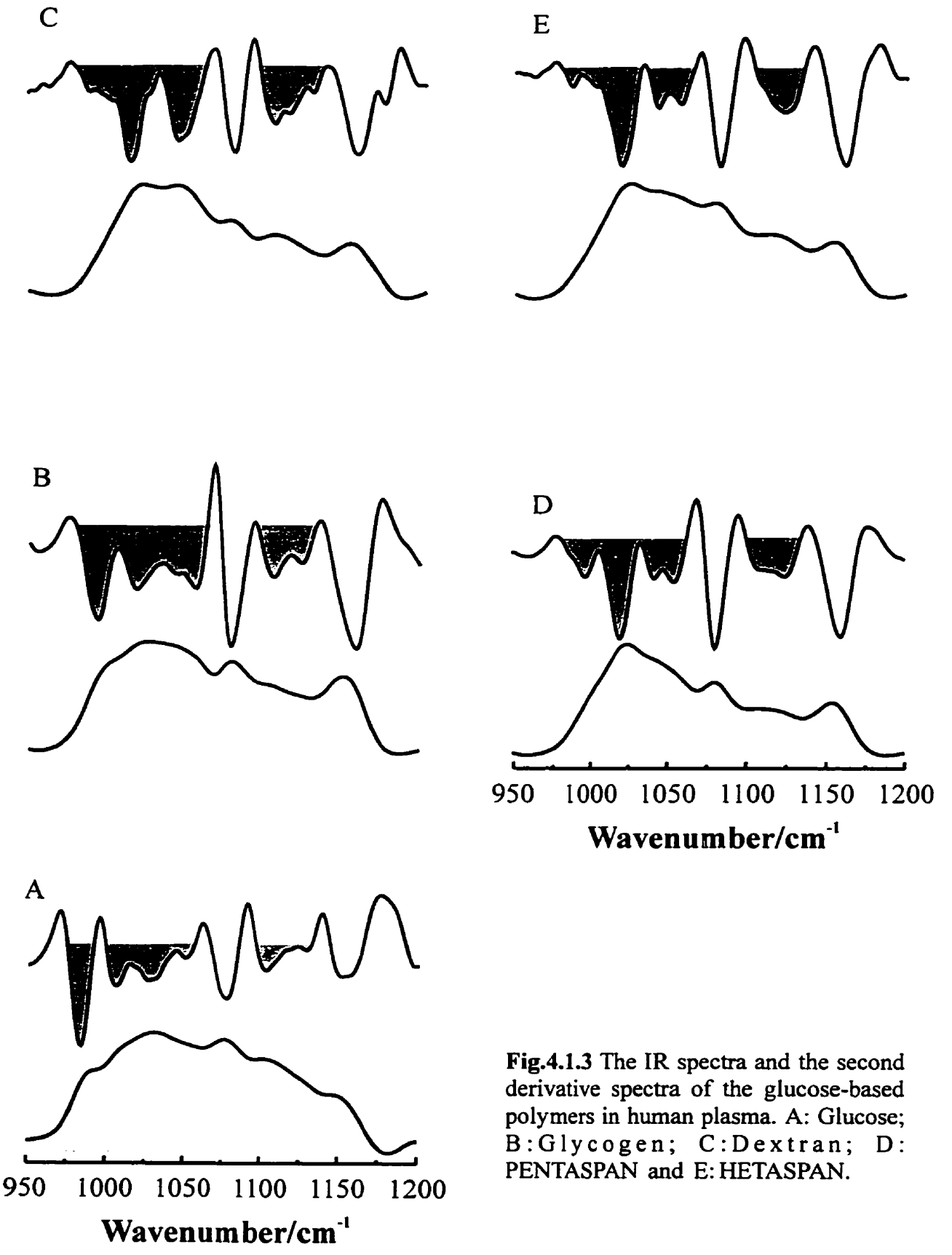

Fig.4.1.3 The IR spectra and the second derivative spectra of the glucose-based polymers in human plasma. A: Glucose; B: Glycogen; C: Dextran; D: PENTASPAN and E: HETASPAN.

This may be due to the same linkage of the glucose unit connection, all having chains of α-1,4 units connected with α-1,6 branches. The difference between glycogen and the starches is that the starches have larger residues in the 2- and 3-position in the rings, rather than hydrogen atoms, as discussed in Chapter 2.

Dextran (in the sugar region) differs from the other polymers, since the chain is only connected by α-1,6 linkages, resulting in a more flexible structure. The vibrational frequencies in the sugar region therefore differ slightly from those chains built of α-1,4 linked units.

An understanding of the IR characterization of HES in biological samples enables the investigator to evaluate spectra of tissues and of bronchoalveolar lavage fluids, based on the HES content. The animal injury model developed in the following section illustrates the application of this IR methodology.

4.2 Animal Permeability Edema Model

The protocol for the animal injury experiment of this investigation was approved by the animal care ethics committee of the University of Manitoba (983-128; "*Role of nuclear magnetic resonance and infrared spectroscopy in lung injury respiratory fatigue*"). The animal preparation for the experiments was performed at the surgical research laboratory, Health Sciences Center, University of Manitoba.

4.2.1 Animal Preparation

A canine model of the study was established using isolated left lower lung lobes. Mongrel dogs of both sexes, weighing between 15 and 23 kilograms were used for the

harvest of isolated lobes. Dogs for the study were anesthetized with intravenous sodium pentabarb (30 mg/kg) and intubated with a 7.0 Murphy endotracheal tube. The dogs were then ventilated with 100% O_2 using a Harvard pump (model 560) with a tidal volume of 350 cc at 16 breaths/min. A left lateral thoracotomy was performed through the fifth intercostal space using electrocautery. Prior to placement of the arterial cannula into the left lower lobe, the dog was given an intravenous dose of heparin (500 UI/Kg). A saline-filled arterial cannula was inserted into the pulmonary artery and secured. Care was taken to avoid air bubble entrapment, which could result in hemolysis and/or a lobar embolism. The cannula was unclamped momentarily, permitting it to passively fill with blood from the lobe. Once the cannula was shown to be in its proper position (achieved by pressure-flow filling of the cannula with blood), it was secured in place with a temporary tie.

The dog was then exsanguinated via the femoral artery and the blood retained for the autologous perfusion of the lobe. After exsanguination, the venous cannula was advanced into the left lower pulmonary vein and secured in place. The bronchus was exposed and incised, enabling placement of the airway cannula. The left lower lobe was carefully separated from the mediastinal tissues and transferred onto a trapeze constructed from lightweight metal and elastic burn net dressing.

The lobe was supported on a mesh trampoline with the hilum in the dependent position. The lobe was additionally suspended using EKG pads affixed to the surface of the lobe with cyanoacrylated adhesive. A suture was secured to the center of each pad following which the lobe was wrapped loosely in plastic. The system was then suspended from a Statham force transducer for continuous weight determination using both gravimetric and near-infrared techniques, and placed in a plastic tent into which

humidified air flowed to minimize evaporation. The bronchial cannula was attached to a humidified oxygen source and the lobe was statically inflated to a fixed transpulmonary pressure of 5 cm above water. A transient inflation of the lobe to 30 cm of water serves to eliminate any atelectatic (collapsed) areas in the lung, which may occur during the organ procurement and to maximize vascular recruitment. Lobar arterial and venous pressure was monitored continuously via pressure port catheters advanced through the cannulas to the hilum. The capillary osmotic pressure was measured using a colloid oncometer. The perfusion circuit consisted of a single reservoir of adjustable height to which the venous cannula was attached. A Masterflex Digistaltic pump was used to circulate blood from the venous reservoir through a heat exchanger, which was set at a fixed temperature (30 C°), macropore filter and then back into the arterial cannula. An 815 nm laser developed by Dr. L. Oppenheimer was interposed within the circuit (Oppenheimer *et al.*, 1993). This device is capable of measuring on-line hematocrit changes, which have already been demonstrated to correlate closely with volume exchange. Monitoring of the laser signal changes provides the confirmation of edema formation during the experiment. The setup is demonstrated in Fig. 4.2.1 and Fig. 4.2.2. The surgical research fellows and laboratory technician performed the animal experimental preparation.

4.2.2 Injury Induction and Sampling Protocol

The lobar injury was induced by injection of thiourea intravenously. The technique whereby thiourate derivatives induce permeability edema in dogs was introduced in mid 1940's. It is believed that thiourea is responsible for the damage of endothelial membrane in the capillary walls. Thiourea causes acute lung edema in dogs in a dose-dependent manner. This effect can be attributed to an increase in the passage of water and solute

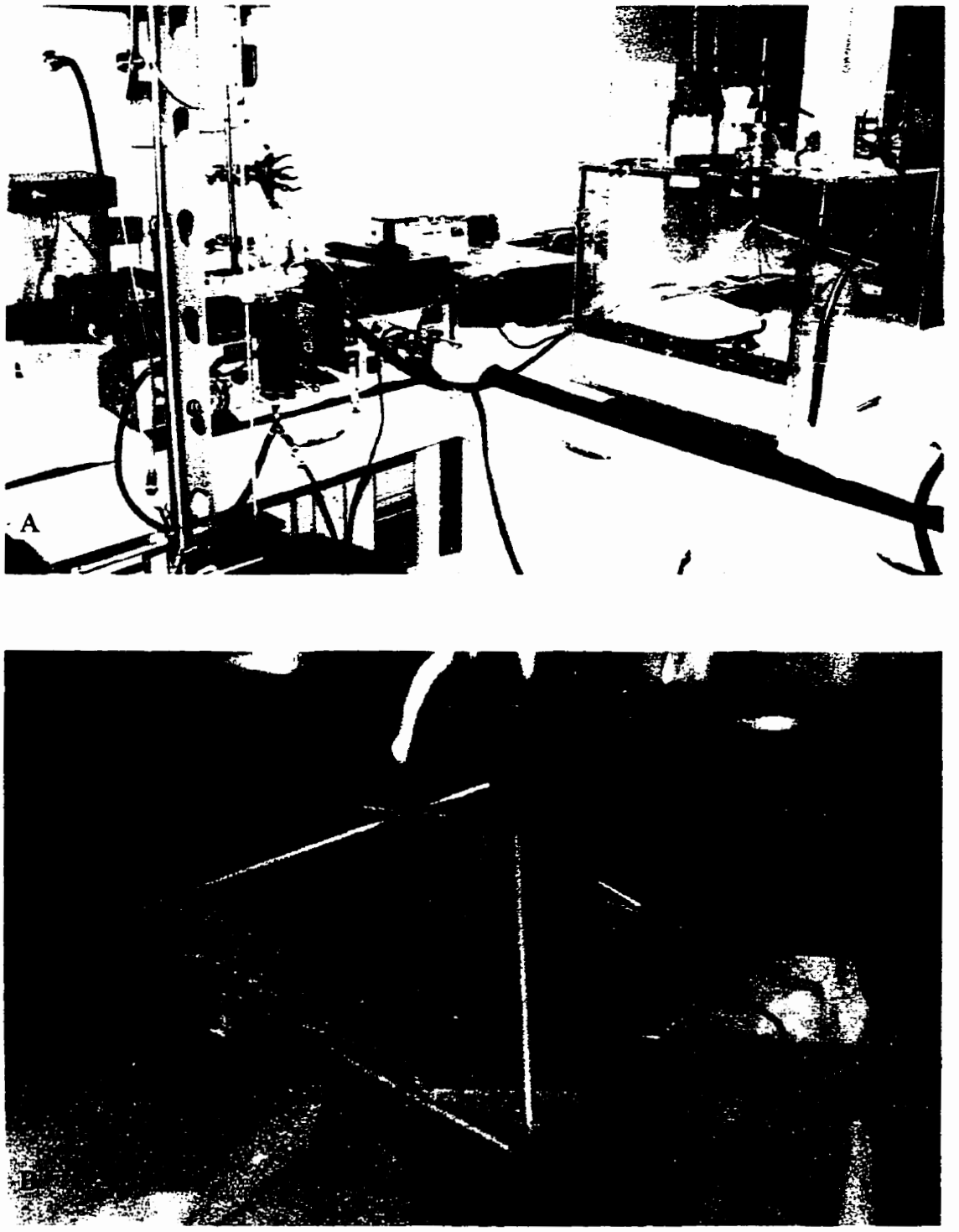

Fig. 4.2.1 Photograph of isolated lobe experiment. A: Experimental setting B: The isolated lobe

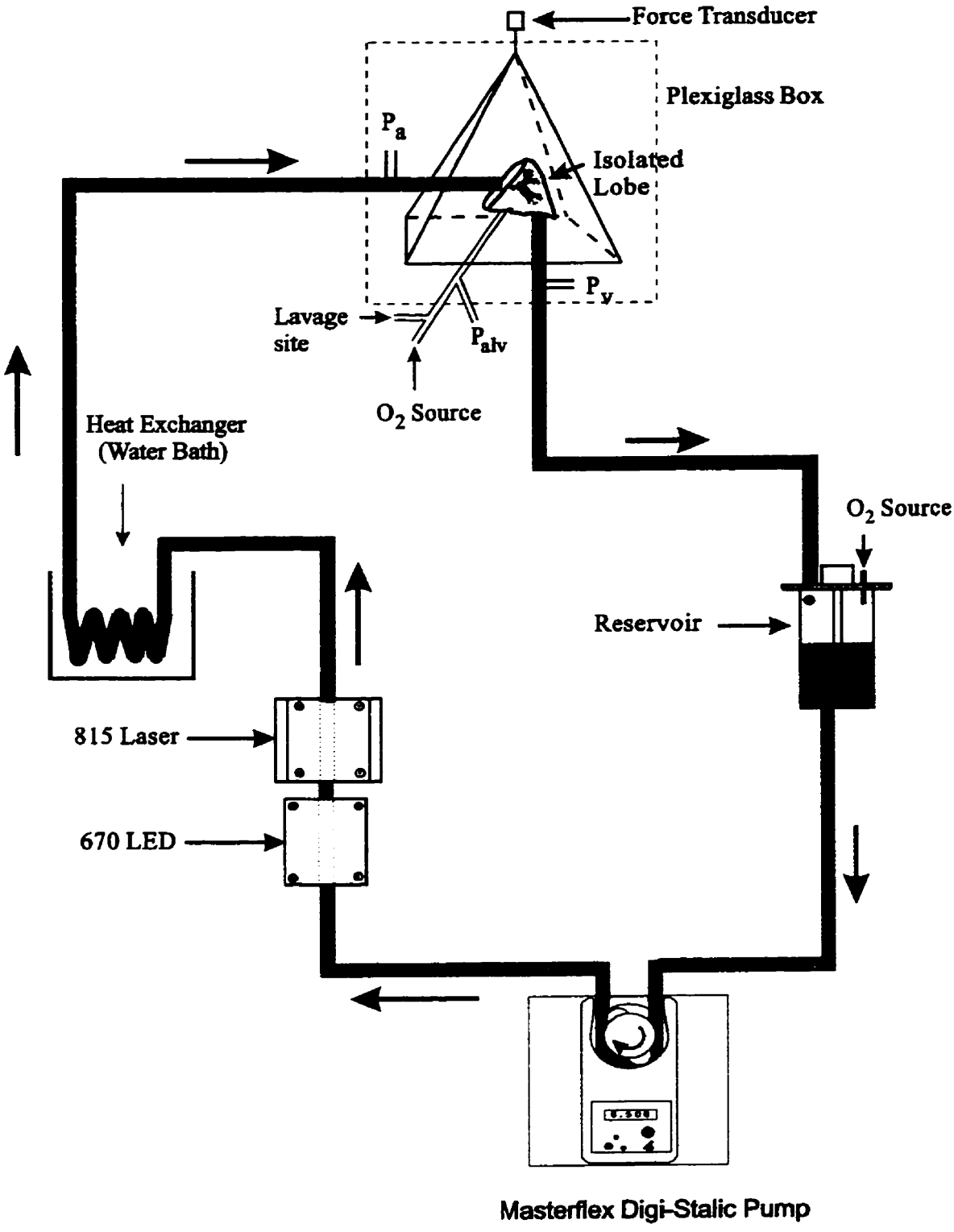

Fig. 4.2.2 Diagram of isolated lobe preparation for lung permeability determination

from the blood through the capillary walls. The chemical compound is an agent, which causes progressive, non-hemorrhagic and non-inflammatory leakage from the lung capillaries (Drinker and Hardenbergh, 1947).

After harvest, the isolated lobe was immediately reperfused. Stability of the system was attained for 30 minutes prior to administration of thiourea. Once the lobe was confirmed to be stable, a large diameter airway tube was inserted into the tracheal opening. This permitted a larger-sized lavage tubing to be used while at the same time allowing for adequate oxygenation of the lobe. (See Fig. 4.2.2). Two boluses of 1250 µl of thiourea were injected into the venous reservoir over a 10 minute time interval.

The colloid agent, PENTASPAN® was then given in 10 ml aliquots every half-hour for 40 ml. The polymer was administered intravenously, intended for use as a tracer to assess pulmonary permeability in the isolated lobe experiments. Before each intervention, a small sample of blood was taken from the venous reservoir for hematocrit, blood gas, and colloid osmotic pressure measurements. The total volume removed with each sampling was of 1.0 ml. Bronchoalveolar lavage fluid sampling was initiated once the presence of edema formation by the chart recorder was confirmed. The sampling procedure was performed by flushing of 1.0-ml volume of normal saline through the lavage tube with about 10 "flushes" and withdrawing the remaining volume. The residual volume was then measured by IR spectroscopy. The experiment was run for about 6-7 hours after the introduction of the first bolus of PENTASPAN®. This normally resulted in collection of about 6-7 bronchoalveolar lavage fluid samples. Upon termination the experiment, the lobe was weighed to obtain the wet weight, and air dried overnight. Lobes were then placed into an 80°C oven the following day to be thoroughly dried in

order to obtain the dry weight. This wet/dry weight ratio provides further evidence of edema formation.

4.3 Tissue Pathology

Lung tissue was analyzed by two methods: pathologically, and using IR microscopic examination. The IR microscopy is the combination of a FT-IR spectrometer with a microscope. This methodology is capable of elucidating the chemical composition within various biological materials such as tissues and cells, and can provide structural and dynamic information on the samples. The purpose of this investigation was to provide pathological and histochemical evidence of pulmonary edema and HES capillary leakage in the injured tissues.

4.3.1 Pathology of Microvascular Injury Induced Edema

The mechanism leading to pulmonary permeability edema is the injury to the capillaries of the alveolar septa. The edema results from primary injury to the vascular endothelium or damage to alveolar epithelial cells. This results in leakage of plasma fluid and proteins into the interstitial space and, in severe cases, into the alveoli. Most commonly, edema may remain localized, as it does in most forms of pneumonia. When the alveolar edema becomes diffuse however, it becomes an important factor contributing to a serious and sometimes fatal condition such as ARDS (Cotran *et al.*, 1994).

Morphology: In the acutely edematous stage, the lungs are grossly described as heavy, firm, red, and boggy. This has led many authors to describe diffuse alveolar damage using the term *congestive atelectasis.* This is the classic pathology of diffuse alveolar damage or ARDS. Microscopically, the term can be equally applicable and the lung

exhibits congestion, interstitial and intra-alveolar edema, and inflammation. Alveoli are collapsed and capillaries are engorged. The alveolar walls themselves become lined with waxy hyaline membranes, which consist of fibrin-rich edema fluid mixed with the cytoplasmic and lipid remnants of necrotic epithelial cells. Since it is the tight junctions between alveolar epithelial cells that are responsible for maintaining the alveoli in the dry state, segmental loss of epithelial cells will lead to interstitial fluid loss into the air space. This will inevitably displace and denature the surface-active layer and collapse the alveolus. Within a few days, type II epithelial cells (the stem cells) have regenerative capacity and undergo proliferation in an attempt to regenerate the alveolar lining. Once proliferation is complete, these cells will then differentiate into type I pneumocytes and re-epithelialize the surface of the basement membrane. There is organization of the fibrin exudate, with resultant intra-alveolar septa, caused by proliferation of interstitial cells and deposition of collagen. This process usually leads to interstitial scarring and fibrosis. Blood vessels undergo a similar process of fibrocellular intimal thickening and thrombosis. An increase in lung collagen is usually detected in ARDS patients surviving greater than 14 days and increases with the duration of disease. In survivors, this leads to eventual shrinkage of the lung; a process that has been termed atelectatic induration. (where the alveoli never reexpand as a result of extensive scarring). The lung will inevitably look similar to an end-stage fibrotic process, but this appearance is reached at a more accelerated rate (Wohl, M.E.B. 1990, NEJM) and fatal cases often have superimposed bronchopneumonia (Cotran, *et al.*, 1994). A representation of the pathological process of ARDS is presented in Fig.4.3.1.

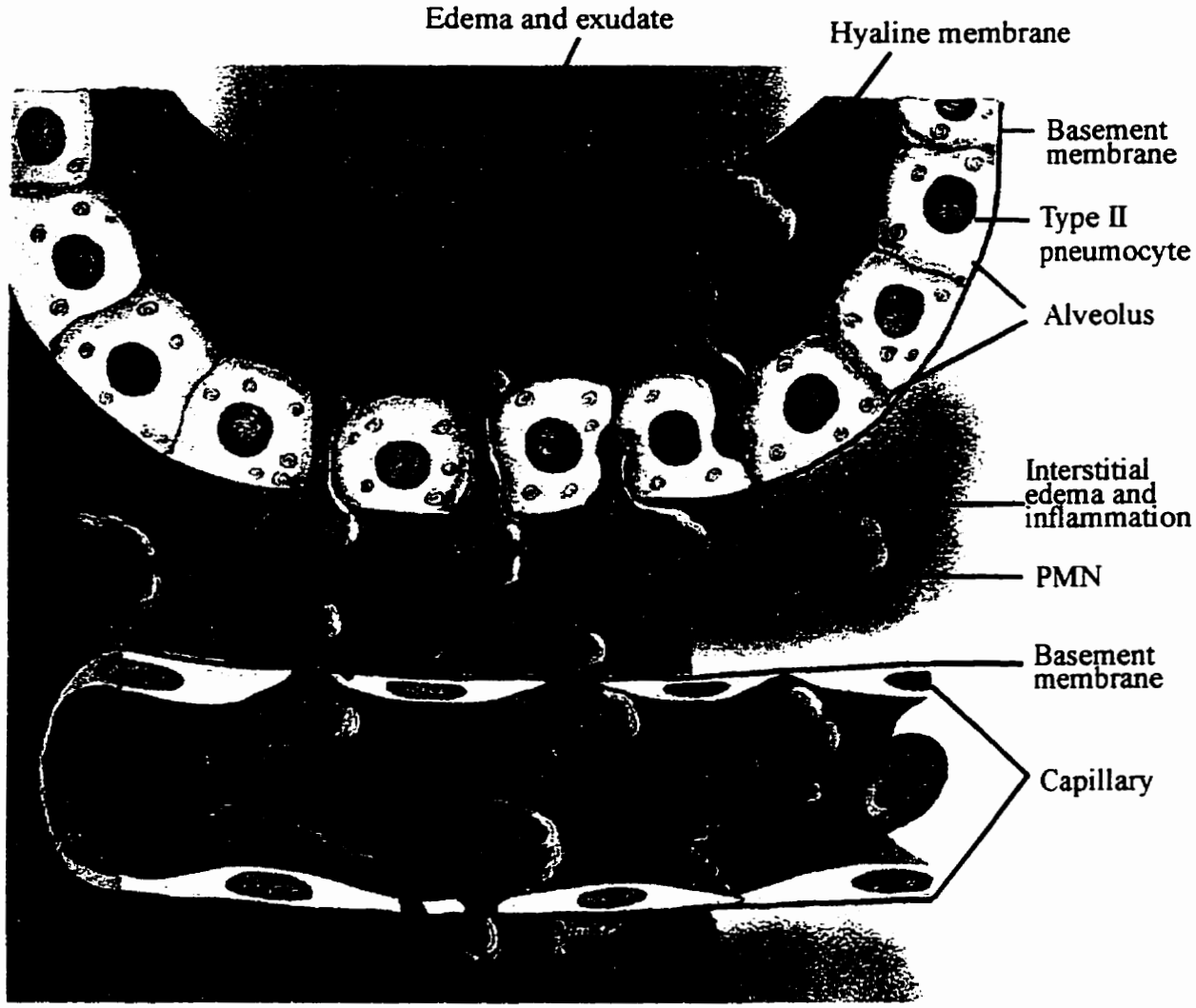

Fig. 4.3.1 Pathological process of ARDS. Type I cells die as a result of diffuse alveolar damage. Intra-alveolar edema follows, after which there is formation of hyline membranes composed of proteinaceous exudate and cell debris. In the acute phase the lungs are markedly congested and heavy. Type II cells multiply to line the alveolar surface. Interstitial inflammation is characteristic. The lesion may heal completely or progress to interstitial fibrosis. (Pathology, Rubin, *et al.*,1988. Adopted with permission)

Pathogenesis: The initial injury is either to capillary endothelium (most frequently) or alveolar epithelium (occasionally) and eventually both become clearly affected. Damage to these cells leads to an increase in capillary permeability, interstitial and then intra-alveolar edema, fibrin exudation and formation of hyaline membranes. The capillary defect is believed to be produced by an interaction of inflammatory cells and mediators, including leukocytes, cytokines, oxygen radicals, complement, and arachidonate metabolites. The interaction results in damage to the endothelium and allows fluids and proteins to leak into the alveolar space. Macrophages are an additional source of injury in ARDS. These cells are capable of producing toxic oxygen radicals, proteases, arachidonic acid metabolites, platelet-activating factor, and cytokines that mediate inflammation. It is also believed that neutrophilic inflammation in ARDS may be driven by macrophage-derived peptide cytokines (Cotran, *et al.*, 1994). Additional physiologic effects of these mediators induce vasoconstriction and platelet aggregation, both responsible for decreased blood flow to aerated regions of the lungs.

4.3.2 Tissue and Slice Preparation

To confirm the presence of lung injury, samples were obtained from animal tissues, namely, the normal lung, the lung exposed to PENTASPAN® alone, the injured lung treated with LMW HES, and the injured lung treated with alpha-napthyl thiourea. At the end of the experiment, the circuit was flushed with the remainder of the canine blood collected at the time of exsanguination. This step was necessary to ensure that any PENTASPAN® that may be detected would not be from the blood vessels. The flush was

carried out for 10 minutes. A sample of circuit blood pre and post wash was taken for comparison. The flush step greatly facilitates the procedure, as it removes one possible source of difficulty in interpretation. All remaining HES must be in the interstitium or the alveoli, and what becomes important is to determine the distribution in the lung tissue.

Tissues were obtained from four sections of the left lower lobe, and used for the IR microscopic examination. Initially, the samples selected were dissected using a No. 15 blade in 1 cm sections and were thought to be representative of different aeration and perfusion regions of the lung, see in Fig 4.3.2. The apical section of the lung, physiologically, has the highest oxygen tension. The dependent portion rests on the trapeze and, with the additional force of gravity, is the zone that receives the most supply and actually pools blood within the smaller capacitance vessels. In effect, the thiourea concentration should also be greater in dependent areas. Consequently, it is anticipated that the damage to the microcirculation would be greater in this area as well. The superior, middle and inferior portions of the lobe were chosen randomly in order to assess the degree of leakage and for comparison of injury across the lung.

Once the tissues were grossly cut, they were submerged in liquid nitrogen and sent to pathology for further processing and examination. Each specimen was prepared three sliced tissue sections, one stained with conventional *hematoxylin and eosin* (H & E) technique, one stained with the *periodic acid-Schiff* (PAS) technique, and an unstained section on a CaF_2 window for IR mapping. These stained tissue sections were used for pathologic examination. The purpose of IR tissue microscopic investigation was to determine whether IR microspectroscopy could add any new information to pathologic examination and, to eliminate any controversies surrounding diagnoses. That is, the

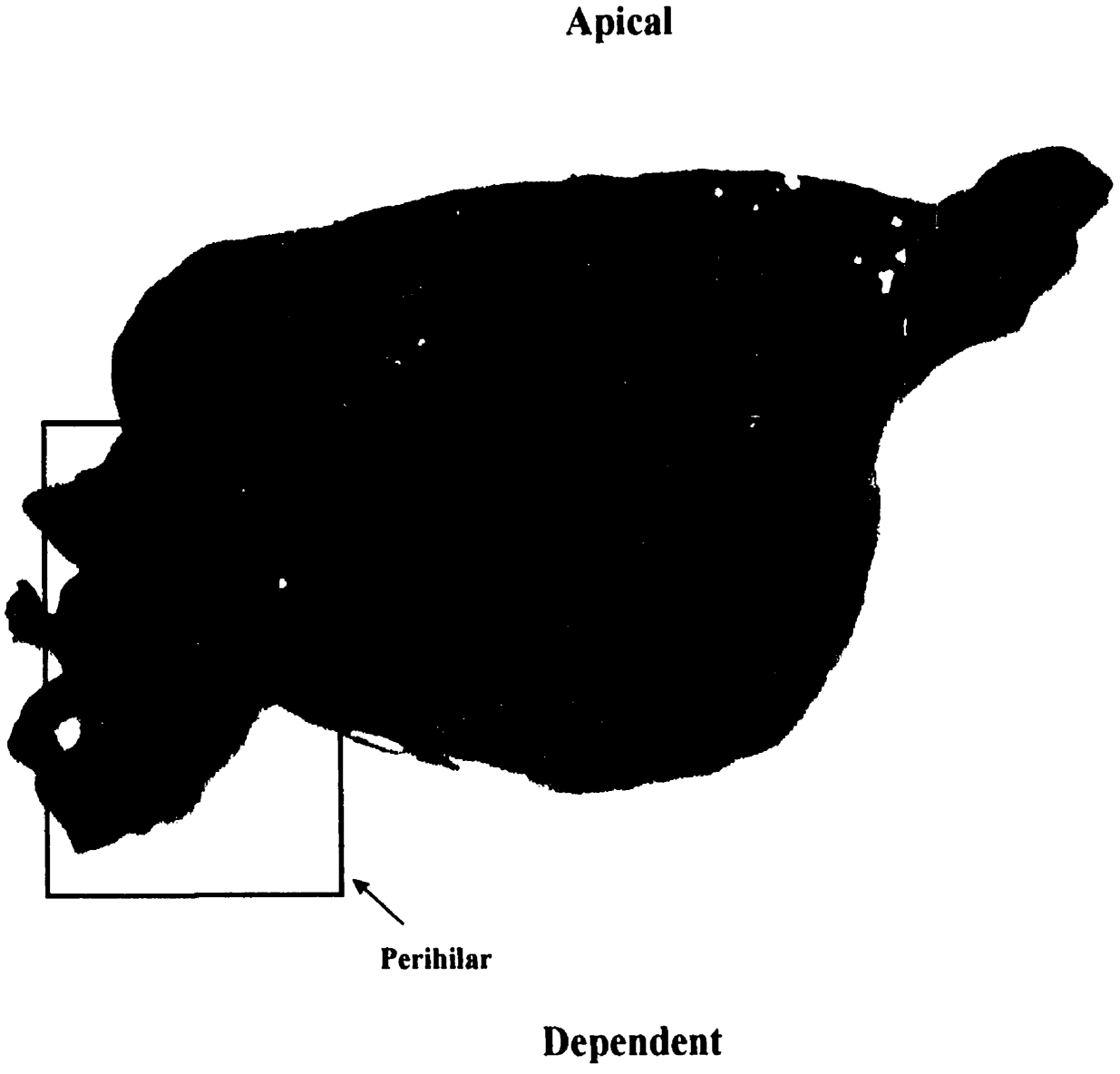

Fig. 4.3.2 Cross section of isolated left lower lobe as prepared for pathological examination of edema dependent areas.

diagnostic criteria for ARDS are nonspecific and IR microspectroscopy may assist when the diagnosis is uncertain. This work was a collaborative effort including the departments of surgery and pathology. A lung pathologist at Health Sciences Center was blinded as to the treatments received in each group of canine lungs as well as to which lungs had alpha-napthyl thiourea-induced lesions. The tissue mapping using IR microscopy was also conducted as a blind procedure, so that systematic bias would not be introduced. The dates of the procedure were recorded and the treatments recorded by a separate investigator. Only the experiment dates were known to the pathologist and for the purposes of IR mapping.

4.3.3 Pathological Significance

The pathologic significance of staining these lung biopsies is twofold. Firstly, the microscopic lesion may be confirmed and graded according to the degree of injury obtained. Despite all the different techniques used during the experiment to monitor and confirm edema formation, pathology remains the gold standard for qualifying the injury. Fig. 4.3.3A is included to demonstrate the appearance of a normal canine lung using a *hematoxlyn and eosin* stain. The air spaces are large, the alveolar septa are thin-walled, and very few inflammatory cells are present. For comparative purposes, normal lobes were also subjected to a *periodic acid-Schiff* stain, which demonstrates similar pathologic findings, and absence of deeply red staining starches (Fig. 4.3.3B). Examination of the injured tissue specimen reveals that normal alveolar spaces are collapsed and the interstitium is engorged with numerous inflammatory cells (Fig. 4.3.4A, B). The appearance of HES in the interstitial tissue is diffuse and recognized by the characteristic deep red color. When present in high concentration, the starch may also be identified with

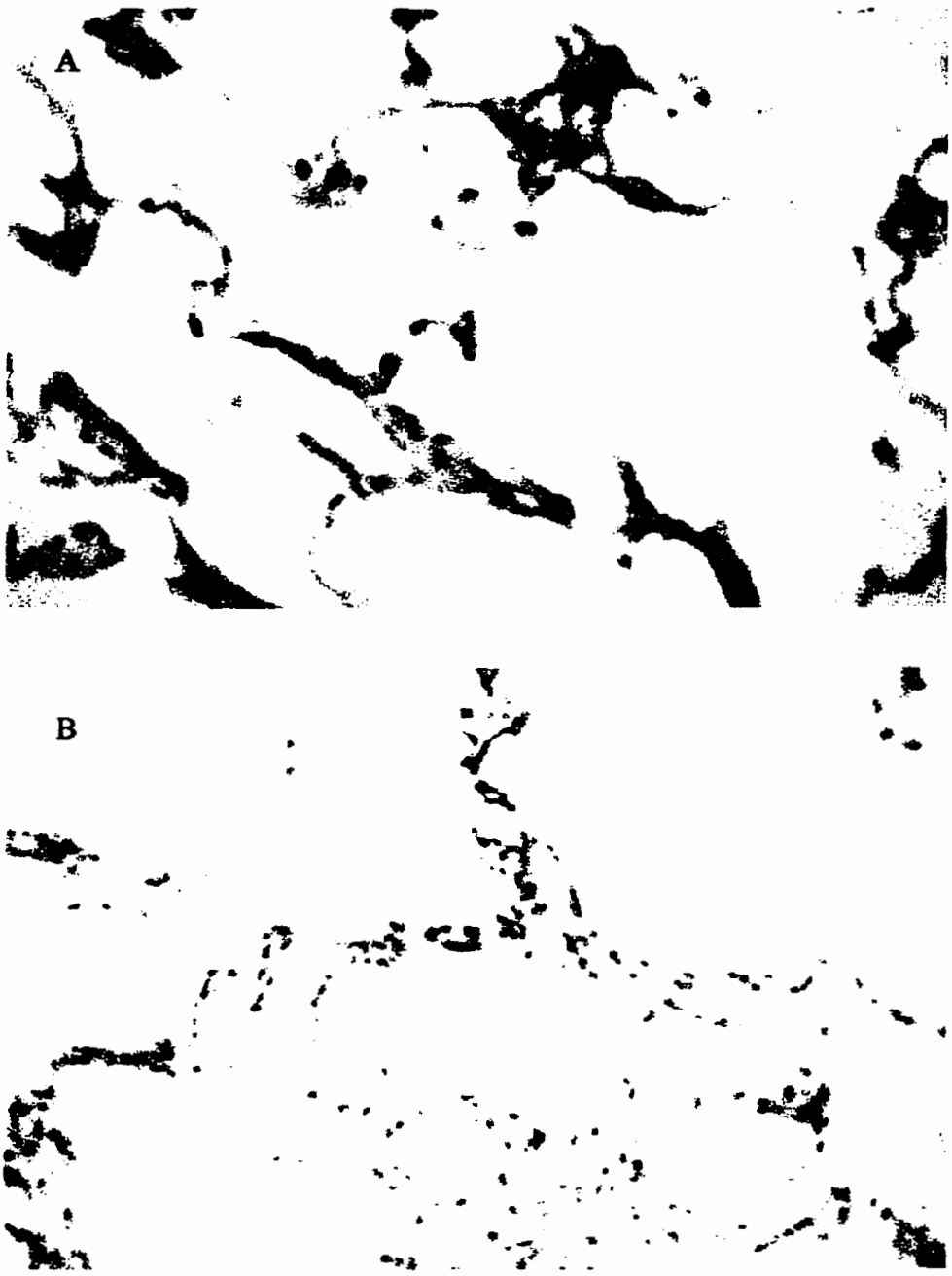

Fig. 4.3.3 Cross section at 200 × magnification. A: H & E stain of normal canine lobe. B: PAS stain of normal canine lobe

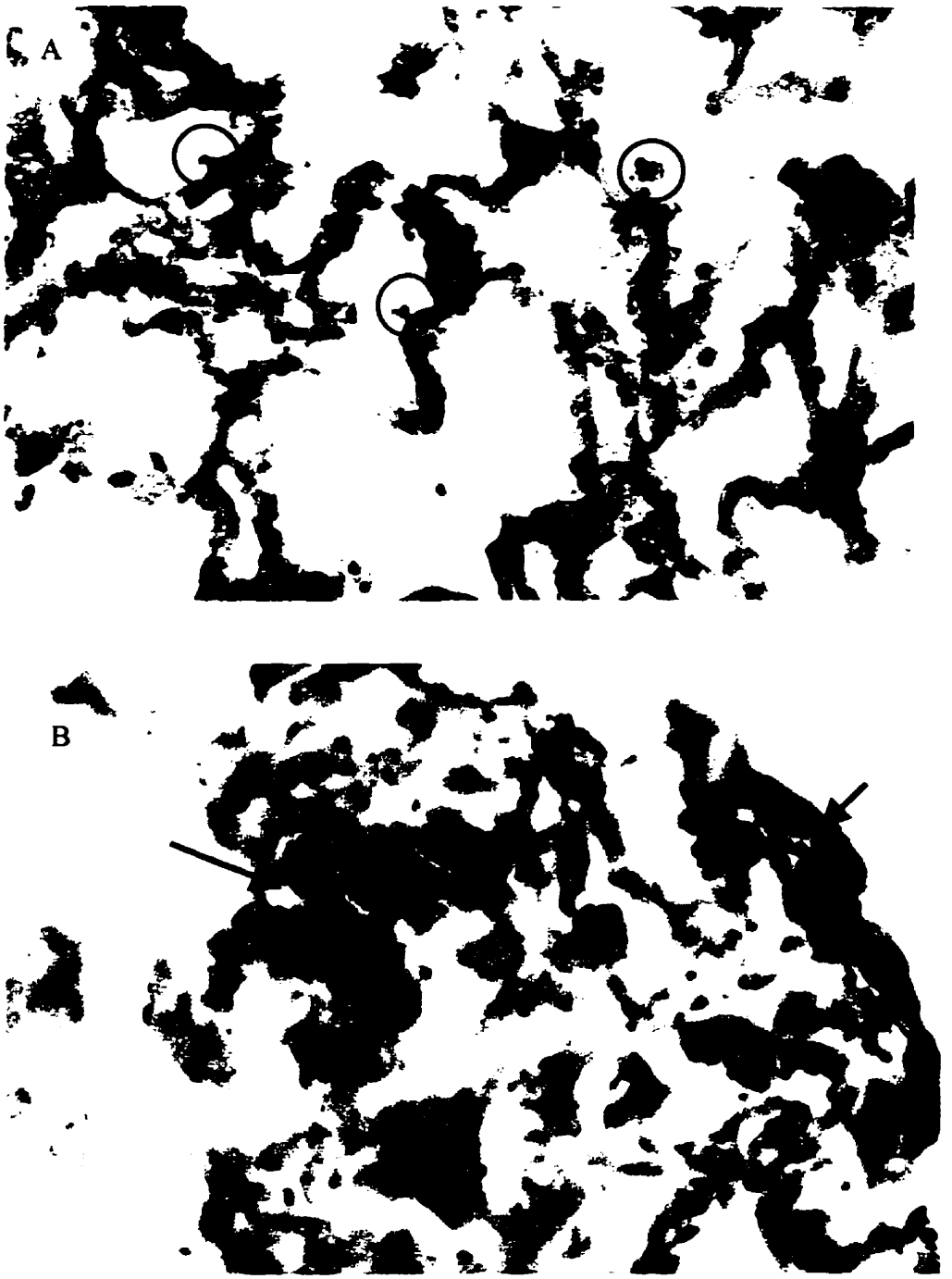

Fig. 4.3.4 Injured lobe treated with PENTASPAN®. A: H & E stained section. B: PAS stained section. Arrows indicate areas of HES leak. Encircled are actual HES fragments penetrating the alveolar spaces.

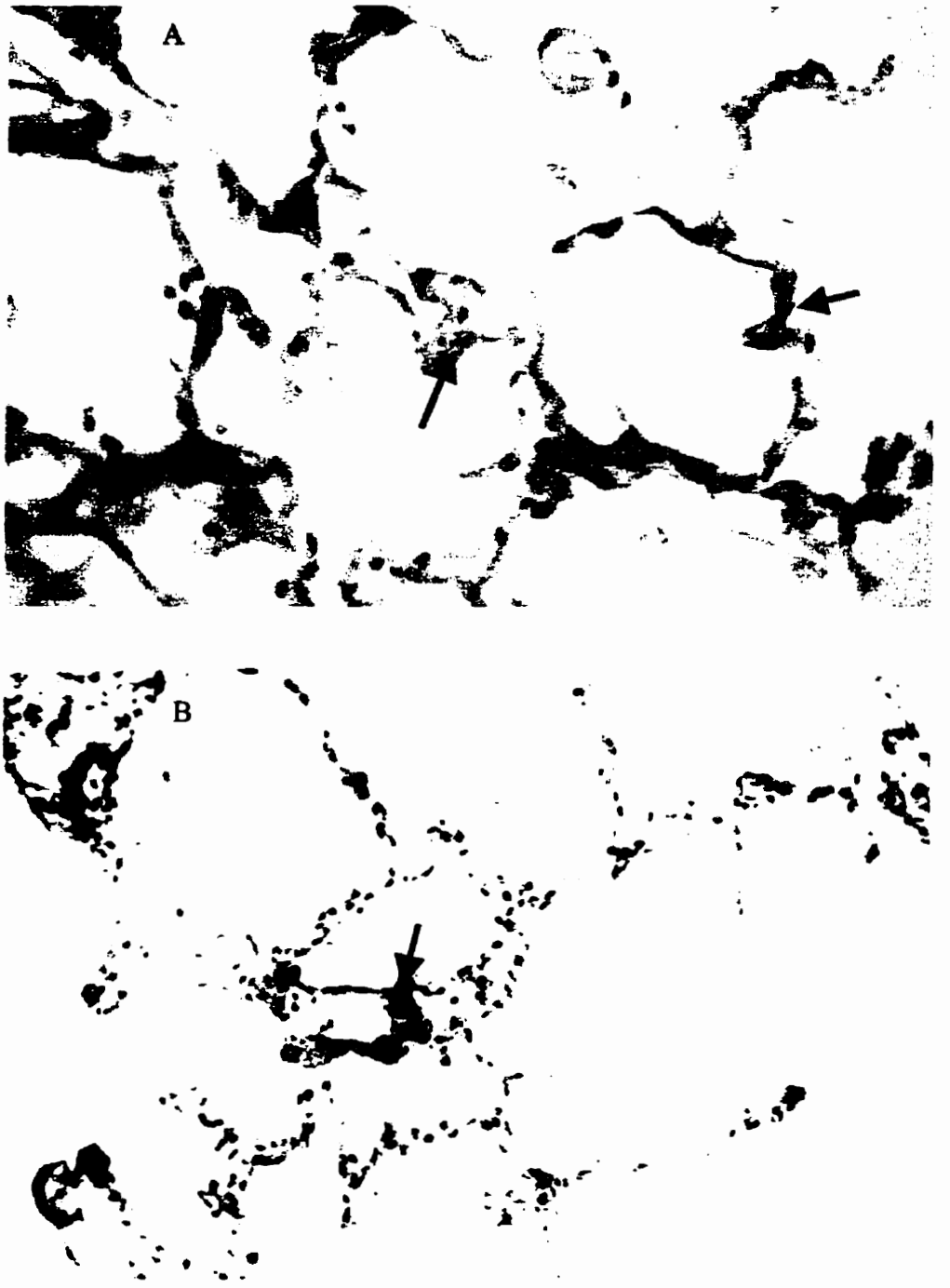

Fig. 4.3.5 Cross section of normal lung infused with PENTASPAN® at 200× magnification. A: H & E stain. B: PAS stain. The arrows indicate smaller fractions of HES penetrate to the membrane.

conventional *hematoxylin and eosin* staining. Furthermore, Fig. 4.3.4A, demonstrates the presence of starch in the alveolar spaces. The importance of this finding is evidence in support of the canine experiments and clinical trial to follow. These changes are reminiscent of the early lesions seen in acute lung injury. These changes are both present within the lobes exposed to alpha-napthyl thiourea.

With *periodic acid-Schiff* stained technique, HES in the injured lobe was identified in the interstitial space, see Fig 4.3.4B. The *hematoxlyn and eosin* stained slide on the same tissue section indicates capillary-alveolar membrane damage (see Fig. 4.3.4A). Comparing the PENTASPAN® group without injury (see Fig. 4.3.5A, B) demonstrates a normal lung with minimal areas where starch has leaked through, but has not permeated the alveoli. In severe pathologic states, PENTASPAN® should leak in large quantity through the interstitium into the alveolar space and bronchial tree where it may be detected using IR spectroscopic analysis.

In the animal injury model, high concentrations of PENTASPAN® was assumed in the interstitium, the experiment, however, could not be carried out for more than 4 hours, secondary to stability of the lobe itself. This period may have been too short to produce such a dramatic effect. By extrapolating the progression of injury from our knowledge of the pathophysiology of this disease, it is reasonable to conclude that given ample time PENTASPAN® would continue to leak into the airways. The presence of PENTASPAN® in the alveolar spaces, however, provides definitive evidence of disruption of the capillary-alveolar membrane. This injury and the subsequent leakage of PENTASPAN® are the rationale for analysis of bronchial alveolar lavage fluid. Normal lobes stained with *periodic acid-Schiff* following PENTASPAN® administration do not

show any colloid within the interstitium, nor the alveolar space. It follows then, that the presence of large amounts of PENTASPAN® in the alveolar space is suggestive of lung pathology. What is required then, is a simple, rapid and much less invasive method of determining which lobes are injured. This direct methodology would have a large impact on critical care management decisions.

4.3.4 Tissue Mapping and IR Histochemical Images

An EQUINOX 55 FT-IR spectrometer (Bruker, Germany) with an IR microscope attachment was used to perform the IR tissue mapping. For consistency, all maps were acquired using the same spectroscopic parameters. An eyepiece with a magnification of 4×, and a 15× IR objective were used for the mapping. Each IR spectrum was recorded at a resolution of 4 cm^{-1}, co-adding 16 scans, with a measurement time of about 15 sec/spectrum. All the spectra were recorded using a 30×30 μm rectangular aperture size.

Two sliced tissue sections (denoted tissue #1 and tissue #2) were mapped over the entire section, an area of 2370×2370 $(\mu m)^2$ each. The mapping procedure began at the grid-reference location 0,0 and progressed in steps of 30 μm by moving a computer-controlled stage, in the horizontal x-direction. At the end of each row, an increment of 30 μm in the vertical y-direction was made and the procedure was repeated until the entire area had been covered. Each map consisted of 6241 individual spectra.

Since there will be absorption to varying extents even in normal lung tissue in the sugar region, due to other biochemical components such as glycoprotein, phospholipids, etc., this would interfere with the detection of starch present in the tissue. Therefore, to be able to draw any inferences from the map, it is necessary to establish a baseline. A normalization procedure was therefore introduced. This procedure aids in offsetting the

intensity variations around the 1030 cm^{-1} region in normal lung tissue resulting from protein variations. The procedure involves the use of two intensities, the intensity at 1030 cm^{-1} and at 1550 cm^{-1} (amide II band). Using control tissue, a ratio factor, F, can be calculated from I_{1030}/I_{1550}, and this can be used to multiply the intensity of protein band (I_{1550}) at 1550 cm^{-1} in the tissue spectrum. This step will re-set protein absorption intensity to a value equal to the intensity at 1030 cm^{-1}. Then the equation, $I_{1030} - F \times I_{1550}$, will create a baseline which eliminates the variation resulting from components other than starch, i.e. due to protein variations in tissue.

If this procedure is utilized on an entire map, i.e. applied to every individual spectrum in the map, this will generate a baseline map with normal protein to sugar component distribution. A map generated in this way can be defined as

$$M_{HES} = M_{1030} - F \times M_{1550} \qquad 4.3.1$$

where M_{1030} is the map generated based on the absorption intensity at 1030 cm^{-1}; M_{1550} is the map generated based on the intensity of amide II band (1550 cm^{-1}) and F is the normalization factor. M_{HES} represents the tissue map for HES detection, called HES map and will hereafter be referred to as such.

The ratio factor, F, is obtained from normal tissue in a control lobe which had not been subjected to injury or PENTASPAN®. This control tissue section was measured over an area of 900×900 $(\mu m)^2$ with a 30×30 μm aperture size. This section produced 900 individual spectra. The ratio factor of the intensities at 1030 cm^{-1} to the intensities of the protein band at 1550 cm^{-1} is obtained from these 900 spectra. The mean ratio value of the two intensities was determined to be $F = 0.263 \pm 0.044$ std.

Two maps were generated from the control tissue section, the protein map and the HES map (see Fig. 4.3.6A, and B). The two maps represent the distribution of the protein and sugar components in normal lung tissue.

Two tissue sections were examined (tissue #1 and tissue #2). A protein map and a HES map of these tissue sections were generated in order to determine the protein and starch distributions. Fig. 4.3.7A, and Fig. 4.3.7C demonstrate the heterogeneous distribution of protein within these tissue sections. The air spaces are devoid of protein, and, the protein component in the interstitium itself, is also variable. This is especially true when injury is present. The pathophysiology of lung injury has been described in Chapter 1, and it follows that increased leakage of plasma proteins will occur with permeability edema. This will contribute to the variability of the protein component in the interstitial tissue. In contrast to the control tissue section Fig. 4.3.7A, Fig. 4.3.7C indicate a generally higher protein concentration for the tissues analyzed and in some areas even shows concentrated protein deposits. This suggests that there may be a lesion present in this tissue. From the HES maps, the images show that starch is present in both tissues and provides positive evidence for the presence of HES in these tissue sections. The tissue map #1 shows a widely distributed area containing large amounts of HES (Fig. 4.3.7 B). The presence of increased amounts of protein and starch when contrasted with the control, suggest major lung injury in this tissue. The presence of HES in higher concentrations implies that the lobe has been subjected to treatment with starch. The other image from tissue #2 (Fig. 4.3.7 D) shows only a few areas that possibly represent HES in the tissue, although the spectral pattern was not identical with the characteristic band pattern of HES. This specimen was retrieved from an injured lobe (confirmed later)

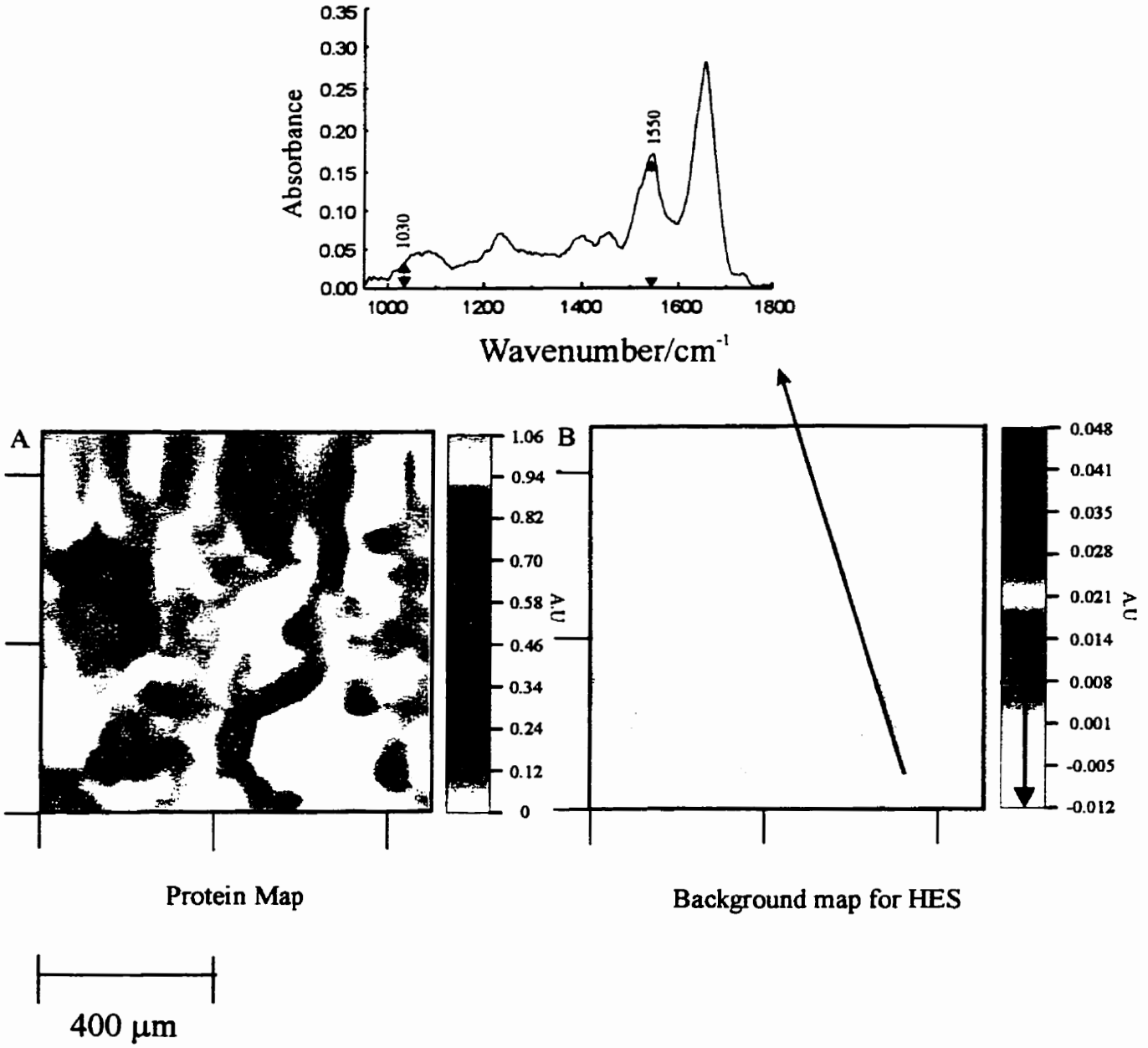

Fig. 4.3.6 Normal lung tissue maps. A: Protein distribution map based on amide II band. B: Tissue map for starch determination (arrow in the color bar indicates intensity fluctuations).

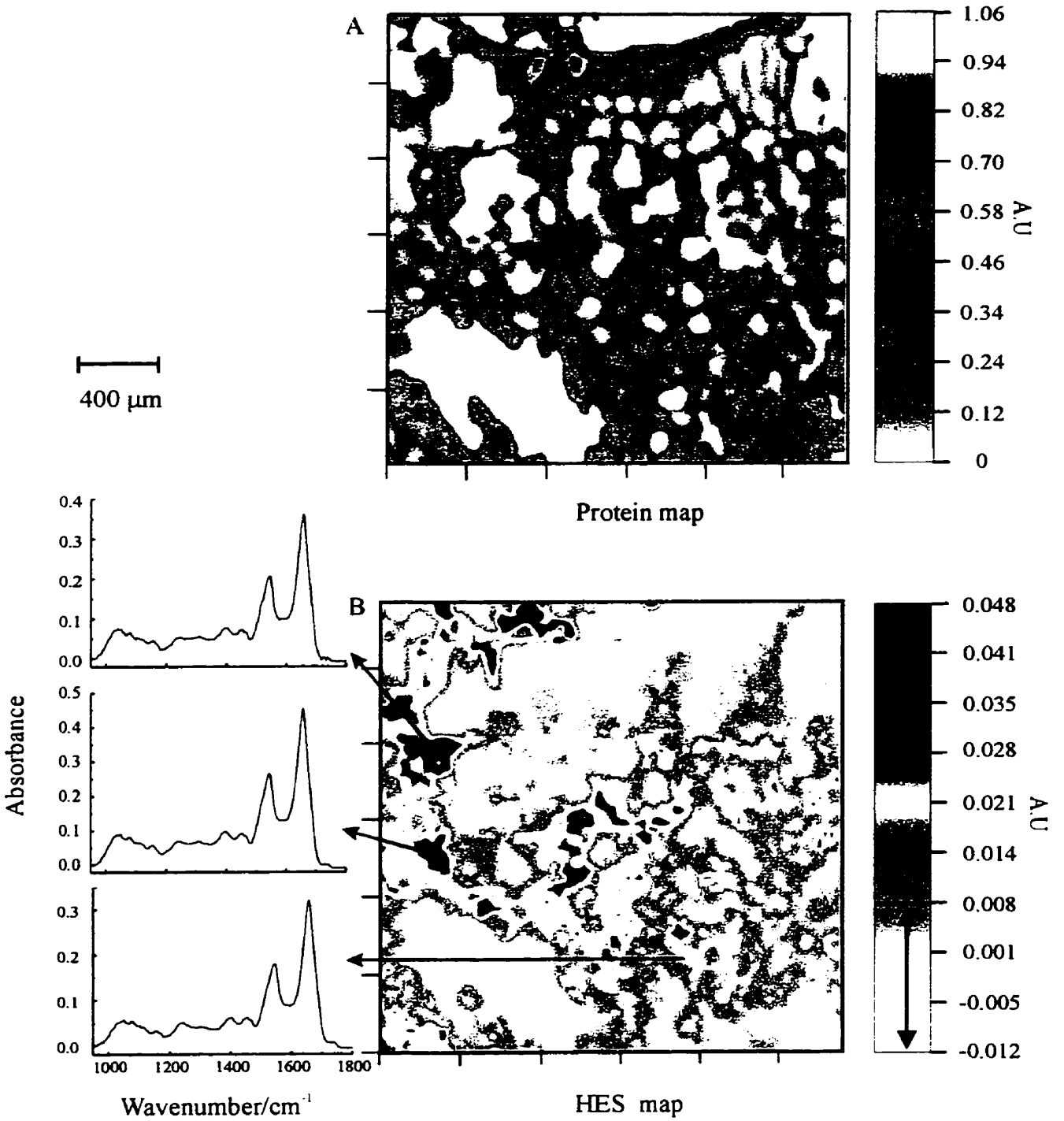

Tissue #1

Fig. 4.3.7 Two tissues were investigated from different experiment. A: protein distribution on the tissue #1. B: tissue map for HES from tissue #1. C: Protein map from tissue #2. D: tissue map for starch from tissue #2 .

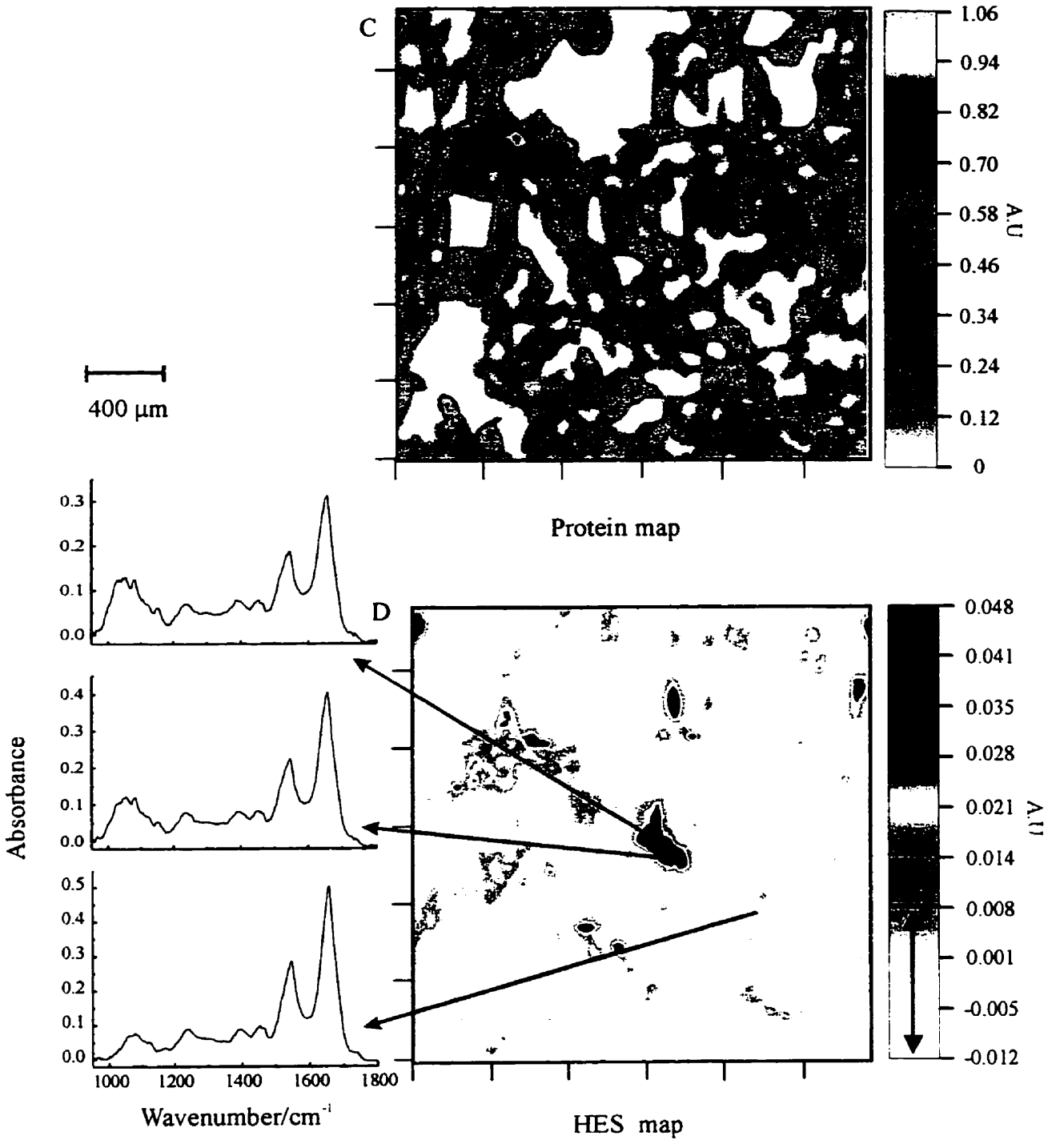

Tissue #2

Fig. 4.3.7 continued.

not subjected to PENTASPAN® infusion. However, this tissue clearly shows the effect of some kind of injury, indicated by elevated protein content and some regions of polysaccharide or other components deposition. A possible factor may be the presence of a large quantity of biochemical components other than starch, such as phospholipids and glycoproteins. It is also possibly due to the presence of glycogen from densely aggregated connective tissue. These compositional variations in the tissue section will enhance the absorption intensity of the sugar region, producing errors in the IR histochemical investigation for detecting HES in tissue.

The analysis of the lung specimens by IR microspectroscopy is a new method and is still in its inception. There are some difficulties surrounding its use in facilitating pathologic diagnosis in this investigation. There is a discrepancy in spatial resolution, e.g. while light microscopy can exceed magnification levels of 200 times, the conventional IR microspectroscopy is limited by an upper limit of 30×30μm (with 4 cm^{-1} resolution and 16 scans). This makes direct comparability difficult. In addition, the choice of the ratio factor, based on the protein band (amide II), is arbitrary since it is a relatively stable parameter in tissue. This choice was also made based on the assumption that the variation in the sugar region resulted from the protein variation and ignores the contribution from other components, for example the presence of phospholipids or glycolipids in lung tissue. The use of the protein band as reference may also introduce baseline map fluctuation due to tissue structural deformation.

However, IR microscopy was able to correctly identify both increased protein and HES leakage into the interstitium. With examination of further specimens, it will be possible to establish the reliability of this approach for generating a tissue map for the

purposes of detecting HES. Since the diagnostic criteria for ARDS can be applied to other nonpermeability conditions as well, the use of IR coupled with pathology may be useful in providing new information when a biopsy is available, or a diagnosis is in question.

4.4 Accessing HES Leakage through BALF

The pathological and histochemical confirmations of HES leakage into the alveolar space in acute lung injury strongly suggests that evidence of this HES leakage may be detected by analysis of the bronchial alveolar lavage fluid. If this could be accomplished, it should provide an index of pulmonary permeability to HES, which might yield diagnostic information. We investigated the alveolar-capillary leakage of injured lobes by analyzing bronchial alveolar lavage.

4.4.1 IR Measurements of BALF and Spectral Interpretation

Lavage samples were collected through a large diameter lavage tube inserted into the lobe; collection beginning once edema formation was confirmed on the chart recorder. Using 1.0 ml saline and 10 "flushes" followed by recollection of fluid, normally yielded an amount of 3.0 to 8.0 ml of lavage fluid. The bronchial alveolar lavage fluid samples were prepared with a volume of 3 μl placed on a 25×2 mm CaF_2 window and dried down for 4-5 minutes in a vacuum dissector to form a thin film. Each sample was prepared using three drops (3μl each) in order to check measurment reproducibility.

The measurements were performed using a Bio-Rad FTS-40 IR spectrometer (Biorad, Cambridge, MA) immediately following collection. All spectra were recorded at 8 cm^{-1} resolution and consisted of 128 co-added scans in the region between 900 and

4000 cm^{-1}. The IR spectroscopic parameters were used consistently for all the animals in the experiments.

Spectral Interpretations

Fig.4.4.1 demonstrates various concentrations of PENTASPAN® in the bronchial alveolar lavage fluid at different collection times, from an injured isolated lobe experiment. A comparison of samples containing PENTASPAN® with a group of samples in which the PENTASPAN® was not detected is illustrated in Fig. 4.4.2. Since an isolated lobe does not have enough biological secretions, the samples do not generally contain highly concentrated biological material (protein, lipid, etc.) and by nature, a very thin fluid containing mostly saline. An absorption spectrum obtained from these isolated lobes is therefore very weak (see Fig. 4.4.2) unless a severe leakage occurs.

In order to identify starch in a lavage sample, a computer model was established. Due to the biological similarity between animal and human lung fluid, 20 human lung-washing samples, which contained no starch (no PENTASPAN® infusion), were used to obtain a non-leak group. Then a pure PENTASPAN® spectrum was added to these spectra with various starch concentrations factor in the range from 1 to 10% to represent the leak population.

We observed that when the sample contains starch, the most intense absorption band in the sugar region is located around 1027.1±0.4 cm^{-1} and the band intensity increases rapidly as PENTASPAN® concentration increases. This band arises from skeletal vibrations of the sugar ring, and is proposed to be the C-O-H bending vibration.

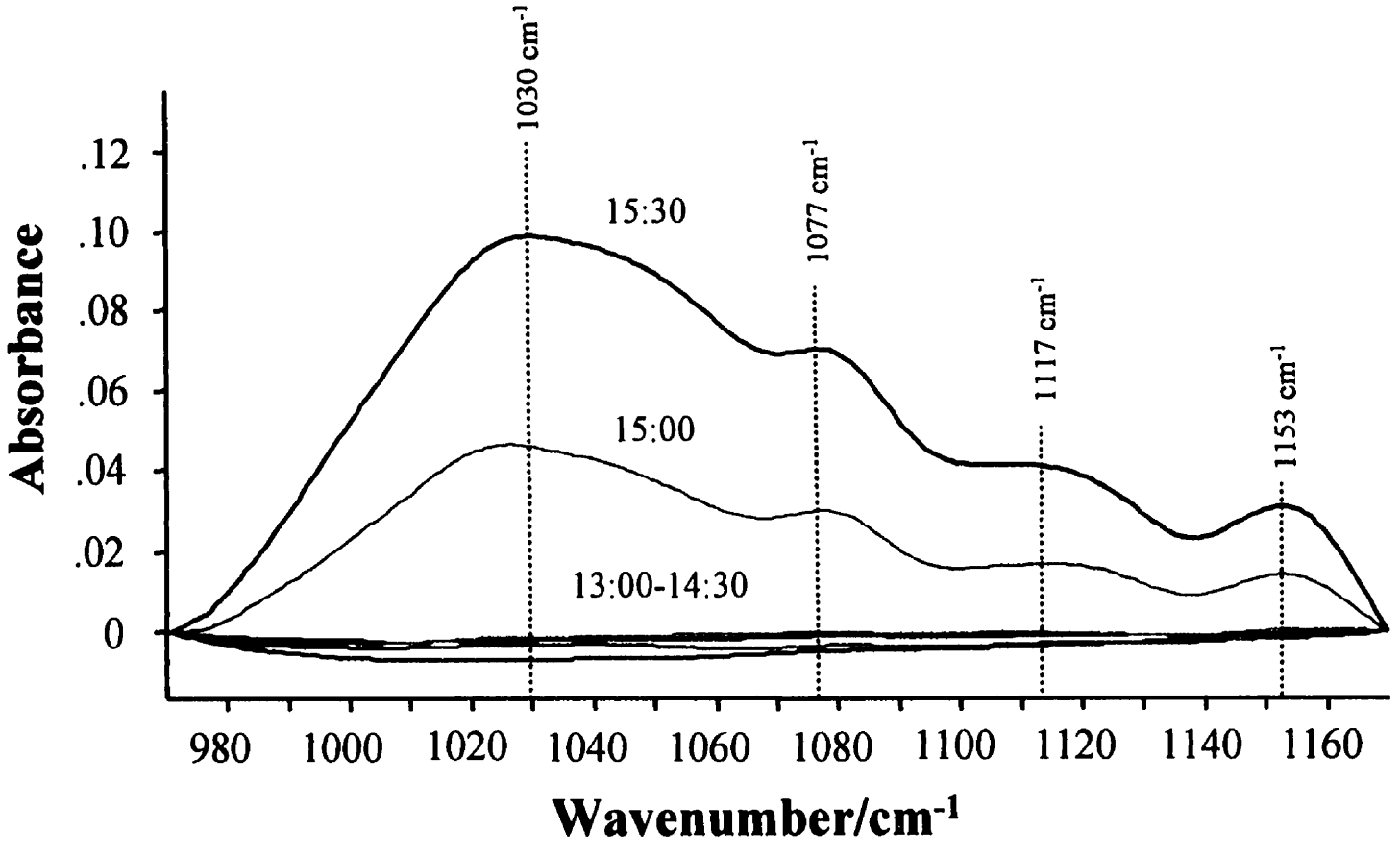

Fig. 4.4.1 Time courses of IR spectra containing various concentrations of PENTASPAN® from animal BALF. The final sample was collected from the airway. The collection time started at 13:00 (1 hour after PENTASPAN infusion) and was continued at half hourly intervals

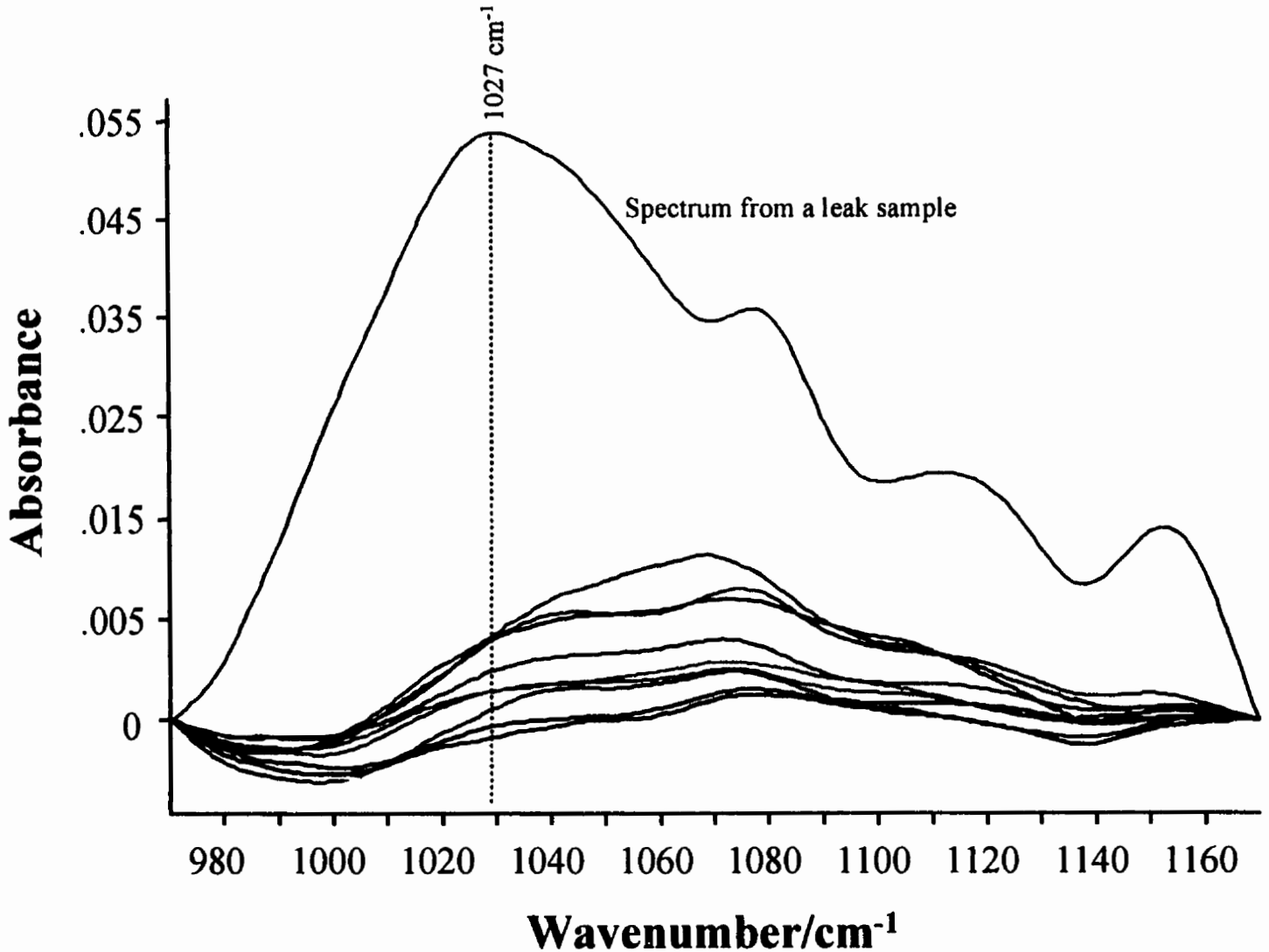

Fig. 4.4.2 Comparison of IR spectra (in the sugar region) of a leak sample containing PENTASPAN with a group of samples in which PENTASPAN was not detectable.

The original position of this band in pure PENTASPAN® is located at 1023.6±0.2 cm^{-1}. In contrast, in the spectra of the twenty lung washing fluid from human samples which contain no PENTASPAN®, the highest absorption band in the region appears around 1076.0±0.3 cm^{-1}. This band arises from phosphate PO_2^- symmetric stretching vibrations of nucleic acid and phospholipid components in the cells and the fluid. This suggests that the position of the most intense band in a spectrum may be used as an indicator for determining the PENTASPAN® content of in the samples.

A simple spectral analysis method for detecting starch in a lavage sample is introduced. The method is based on determining the absorption frequency differences between the band at 1024 cm^{-1}, set as baseline (pure PENTASPAN® absorption band), and the highest absorption band position of a spectrum from the sample under investigation. Generally, the smaller the differences between the bands in the two spectra (the narrower separation), the higher is the likelihood that the sample under investigation contains starch.

A computer program is used to perform this operation. A total of 40 human lung washing spectra are used, 20 of them containing no PENTASPAN® with the other 20 spectra containing various concentrations of PENTASPAN® ranging from 1 to 10% of starch, in steps of 0.5%. Initially, all spectra are truncated between 970 and 1170 cm^{-1} and the program then searches for the most intense absorption band in this region. The baseline frequency (1024 cm^{-1}) is then subtracted from the frequency of the highest absorption band in the region.

This was performed on all spectra in the model. Consequently, the model produced two distinct groups. A: the group containing no detectable PENTASPAN®, the

mean value of the distance between the most intense absorption band and the baseline frequency is 52.05 ±2.7 cm^{-1}(range 47.20 to 54.04 cm^{-1}). B: the group in which the PENTASPAN® is detectable; the mean value of the separation is 2.18 ±3.55 cm^{-1}(range -0.52 to 11.44 cm^{-1}) and varies with the PENTASPAN® concentrations in the sample. Fig. 4.4.3 demonstrates a statistical comparison of these two groups. It was determined that starch is not detectable when the PENTASPAN® concentration is less than 2.5% in the sample, and is detectable when the concentration is greater than or equal to 2.5%. The two mean values can be used to predict parameters for determining PENTASPAN® with a sensitivity of greater than or equal to 2.5% PENTASPAN® in the lavage sample.

Analyzing spectra in this simple way only produces a qualitative result. Due to the uncertainty in the amount of lavage fluid recovered, the dilution factor is essentially missing. This makes it difficult to produce quantitative results. A sophisticated spectral analysis method for qualitatively analysis of starch content in a lavage sample based on the spectral pattern recognition technique would be more appropriate. However, the spectral quality produced from these "IR-negative" isolated lobes was very poor (almost no IR absorption), which makes it impossible to apply such technique to this animal data set. The data set was also too small to use the multivariate statistical approach. The technique is only applicable to a spectral data set where every spectrum in the set has a significant IR absorption profile, and the data set is sufficiently large. Such an approach is applied to human studies in the next Chapter.

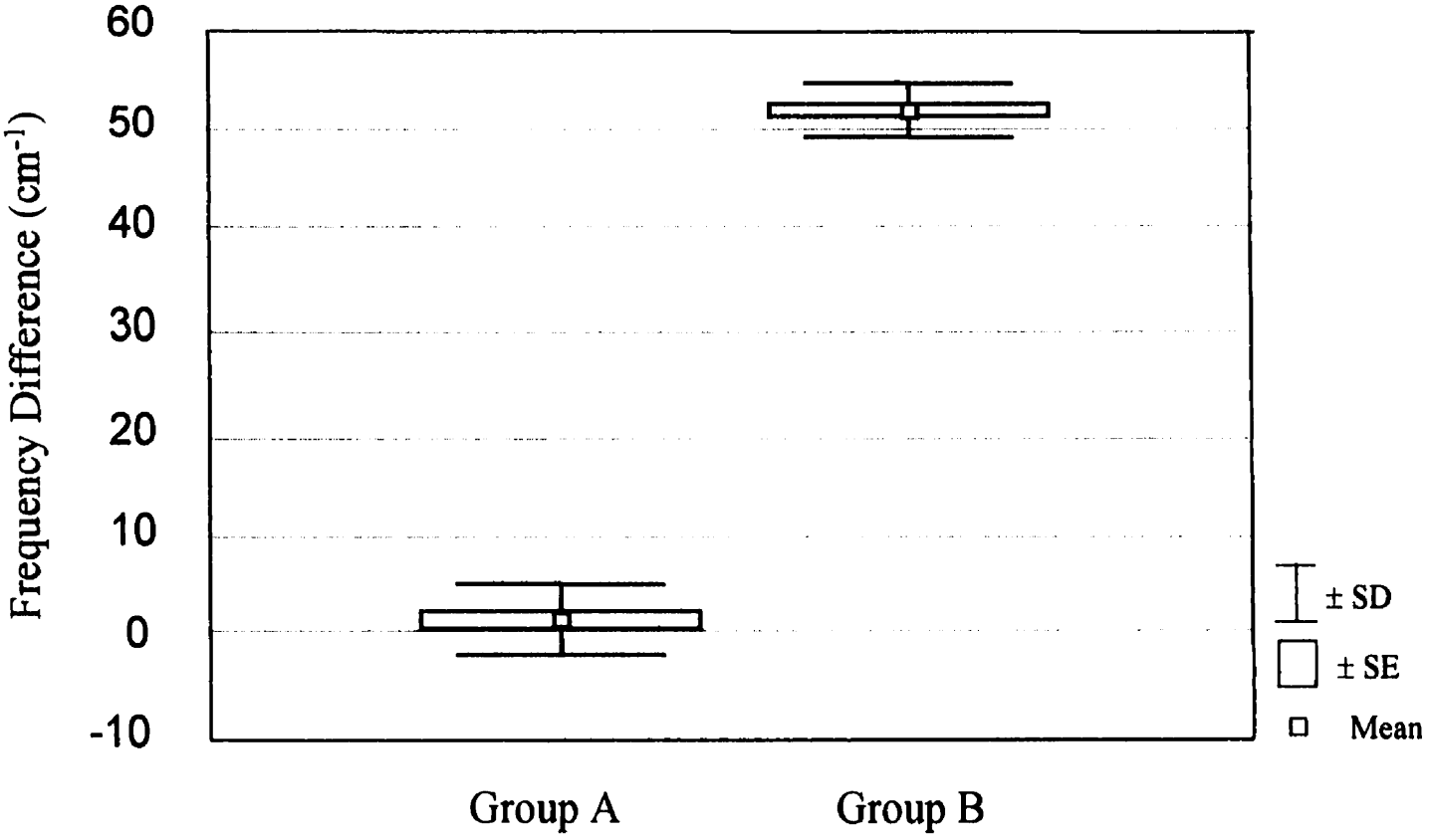

Fig. 4.4.3 Box & Whisker plot of the two groups

4.4.2 Data Analysis and Discussion

Twenty-seven isolated lobes were used for the injury model. All of the lobes for the injury study received thiourea, the reagent inducing injury, at a constant time and volume. Seven of these lobes (27% of the total injury population) were IR-positive for PENTASPAN® (infuse as colloid reagent) at various times. The remaining 20 lobes were categorized as IR-negative. Of these 20, ten lobes produced a measurable IR spectrum (significant intensity of amide I band, as well as the intensity of the sugar region), but no starch was detected in these spectra. The other 10 lobes did not produce significant lavage fluid, i.e. the fluid was composed of mostly saline that did not have an IR absorption signature. Since leakage is associated with large amounts of protein and cell components that leak out from the capillaries, these samples normally present significant amplitudes in the IR absorption region. Therefore, the lobes producing insignificant lavage fluid are grouped into the IR-negative group.

The wet-to-dry weight ratio of the lobes provides evidence of edema and these results correlated with those obtained by IR spectroscopy. The average wet-to-dry weight ratio for the IR-positive lobes was 9.29 (g) ± 1.51 SD. For those lobes that were IR-negative, the ratio values are 6.79 (g) ± 1.47 SD. The IR-positive and IR-negative groups are actually subgroups of one group, the injury group. In this experimental protocol, injury was established using thiourea and all lobes were subjected to PENTASPAN® boluses. The lobes did not have a uniform pattern of injury, more severe lesions being produced by the thiourea in some cases, as reflected by the difference in their final wet weight and wet-body weight ratios. The final wet weights were determined at the end of the experiment by weighing the lobe and the ratio, wet body weight ratio, is derived from

dividing the wet weight by the total weight of the animal. This adjustment normalizes the data set and partially corrects for random variation in individual canine weights. The raw data on body weight, wet weight, wet/body and wet/dry of IR-positive and IR-negative lobes is presented in Fig.4.4.4. In the experimental protocol, there were no control groups included, i.e. non-injured, untreated lobes. In a second set of experiments, a group of five canine lobes was isolated solely for control purposes. The final wet weights at the end of the experiment were 60.62 grams. The average wet-to-dry weight ratio for these lobes was 5.269 ± 0.751 SD. A simple one-way analysis of variance based on the final wet weights of the three groups, namely, the minimal injury group, the severely injured group and the control group demonstrates that significant differences exist between the injured groups ($p < 0.005$). However, no differences exist between the control group and the minimal injury group ($p = 0.47$), suggesting that either no injury was induced, or a very small lesion occurred. This lesion may have been too small for PENTASPAN® to be detected by the sampling technique. In any case, the clinical correlate of interest, namely ARDS, produces a much larger lesion.

A brief analysis of the results using a Spearman's rank correlation coefficient yields an $R=0.557216$. The corresponding p-level is <0.003 for IR-positive compared to wet-body weight ratios. Therefore, there is good correlation, using a non-parametric test, suggesting that using PENTASPAN® as a tracer for identifying pulmonary permeability injury is reasonable. For IR determination of bronchial washing content, a large lung injury is required. Since the IR-negative lobes may have produced a small lesion, which may have not been sampled using this procedure, a bronchoalveolar lavage under direct

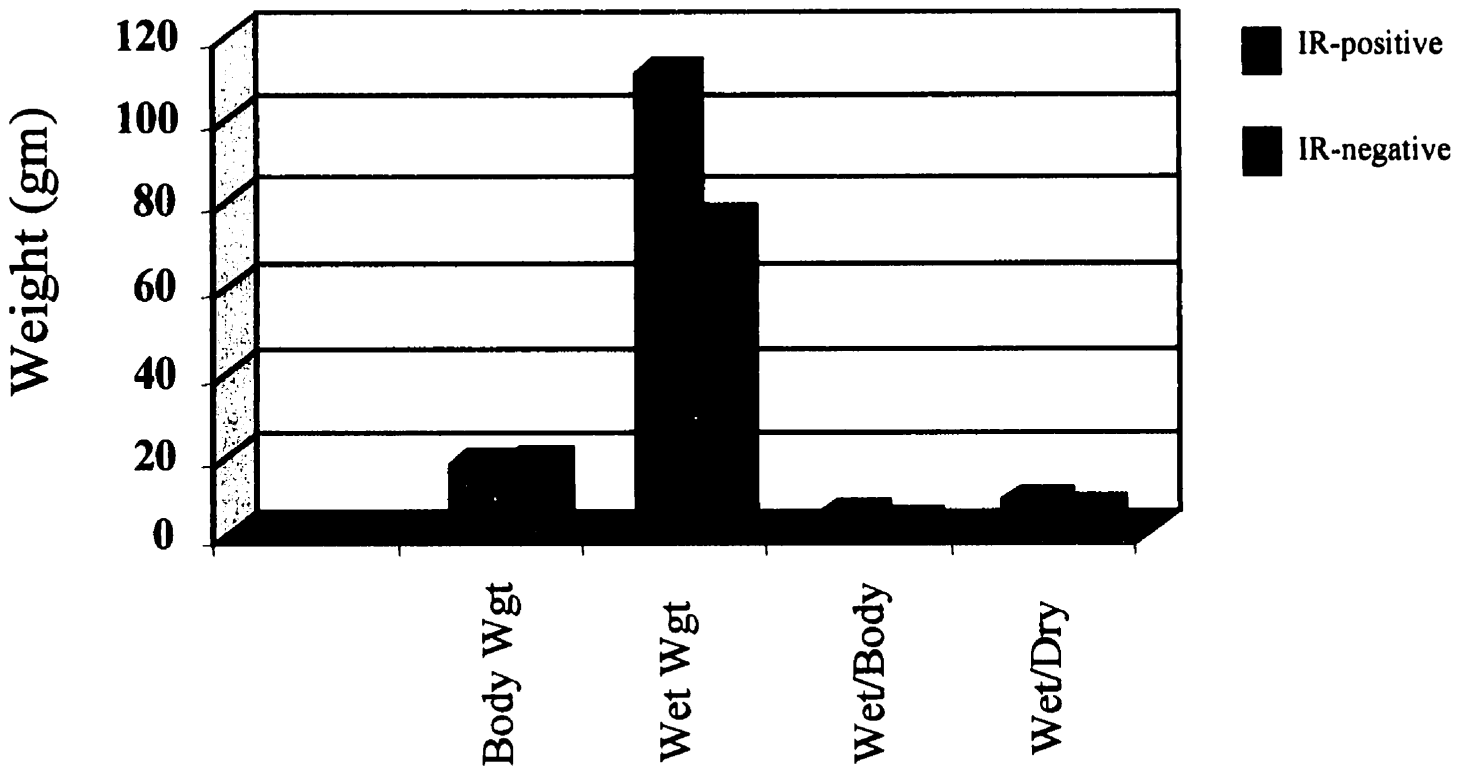

Fig.4.4.4 Raw data for IR-positive and IR-negative lobes. The average total body weights demonstrating no significant differences between groups at the start of the experiment, final wet weights, wet/ body weight ratios which account for variation in subjects,and wet/dry weight ratios are displayed.

vision may yield better results. This would have been impractical due to the small size of the canine lobe. However, when considering applicability in the clinical setting, the results must be interpreted as highly significant. Usually, in the setting of ARDS, injury is more diffuse, and IR identification of PENTASPAN® leakage in this case is feasible and highly practicable.

The low success rate of these experiments was largely due to the localized lavage site, which restricted the ability to determine if edema occurred elsewhere in the lobe. Quite possibly, since placement of the cannulae was a blind procedure and entirely random, different terminal bronchioles were selected with each experiment. This may have introduced a sampling error. In addition, the preparation did not allow for changing the lavage site during the course of the experiment. Furthermore, in addition to the technical difficulty of sampling, the success rate of using thiourea to induce pulmonary microvascular injury and lung edema are unknown in our experiments; it was variable from one preparation to another. This implies that not all of the lobes were able to produce significant edema simultaneously with respect to the degree of injury, and may not even have induced any edema during the experiment. The degree of lung injury produced by thiourea is dose-dependent; it is very possible that an insufficient amount was used. These factors must be taken into consideration concerning edema detection in mildly injured lungs (lobes). However, in the severe cases, described as high wet-to-dry weight ratio, the IR does pick up the signal of PENTASPAN® in BALF.

It must be acknowledged that the isolated lobe model does not perfectly represent the injury in the clinical setting. It is just what it claims to be, a model. However, the similarities are striking, especially considering the acute consequences of injury. The

most important contribution of this model is in developing a methodology for bronchial fluid assay using a rapid IR analysis. The study shows that PENTASPAN® can be detected in lavage samples in acute lung injury and provides a marker for assessing pulmonary permeability. If the technique can be applied to actual patients in a clinical setting, it would facilitate the early diagnosis of an often misdiagnosed disease, in which delay has a serious impact on morbidity and mortality. The impact of this application to the clinical setting and assessment of human lavage samples will be elucidated on in the following Chapters.

Chapter 5

A New Approach to Permeability Assessment in Acute Lung Injury

The objective of this chapter is to develop clinical and experimental protocols for assessing permeability by using a patient's bronchial washing fluid and to develop a diagnostic methodology for patients with ALI/ARDS. The focus of this part of thesis is to standardize the sample collection procedures and the sample experimental procedures. The spectral characterization of bronchial washing fluids of non-leak and leak situations will also be discussed. In order to make the approach of measuring bronchial washing fluids sensitive to the permeability evaluation, a powerful spectral pattern recognition methodology for recognizing the HES signal in the spectra of bronchial washing fluids will be introduced. This pattern recognition approach is a spectral classification approach and is based on the statistical method of linear discriminant analysis. The approach to this spectroscopic application is guided by a Genetic Algorithm, which will provide a general prediction model to determine HES in biofluids. In addition, this spectral pattern recognition approach for determination of the leakage of HES in bronchial washing fluids, is a new application of multivariate statistical analysis to IR spectra, and the prediction model introduced is a computerized diagnostic modelling system.

5.1 Sample Collection and IR Characterization of Bronchial Washing Fluids

With the development of the fiberoptic bronchoscope in the 1970s, instillation of small quantities of saline into the distal bronchial tree under direct vision became possible. Recovery of that fluid for cytological, microbiological, and biochemical examination has become a valuable clinical tool in the diagnosis and the management of certain acute and chronic lung conditions.

The technique of bronchoalveolar lavage fluid (BALF) collection involves the introduction of a flexible bronchoscope into the bronchial tree, often via an endotracheal tube in an anesthetized patient. The scope is advanced into a 4^{th} or 5^{th} generation subsegmental bronchus and "wedged" there. Once this is accomplished, the zone is lavaged repeatedly with 20cc aliquots of saline for a total of 100 cc. The lavage fluid is collected through the suction port of the bronchoscope using 50-80 mm Hg of negative pressure into a specimen trap. Although considered relatively safe, BALF remains an invasive, traumatic and time-consuming procedure, requiring the services of a skilled bronchoscopist.

Bronchial washing fluid represents aspiration of small amounts of saline and secretions from large airways. It can be performed quickly and easily in an intubated patient, and no adverse clinical effects of sample collection have been documented. In addition, the method of bronchial washing is standard pulmonary toilet in many intensive care units. The hypothesis of this investigation is that fluid from bronchial washings

contains comparable diagnostic information to that from bronchial alveolar lavage fluid in patients with ALI/ARDS.

Analysis of BALF and bronchial washing fluids yield very similar information with respect to cytological and microbiological aspects. This also suggests that determination of alveolar leakage through bronchial washing fluid from ALI/ARDS patients should provide the same information as BALF. Although the analysis of bronchial washing fluid may be less sensitive than BALF, it is relatively non-invasive, less traumatic to the airways, simple to perform and does not require a bronchoscopist and is already a part of the routine care of the ventilated patient.

5.1.1 Baseline Study

Purpose: The purpose of this part of the study is to define an IR spectral signature of bronchial washing fluids for a patient population with normal lung function, and to establish a sample collection protocol.

Patient Populations: A total of 23 patients were enrolled into the study from the Surgical Intensive Case Unit at Health Sciences Center (SICU), Winnipeg, Canada. The patient population of interest was comprised of primarily postoperative and trauma patients with as near normal pulmonary function as possible and normal or near normal chest x-rays. Patients who were diagnosed with acute or chronic pulmonary disease processes were excluded from the study. These patients did not receive PENTASPAN® before bronchial washings were collected.

Sample collection: All patients in the study were intubated and put on positive pressure ventilation. Bronchial washing samples were collected by advancing the inline suction catheter through the endotracheal tube until a slight resistance was felt, usually a distance

of 35 to 40 cm. At this distance, the tip of the catheter would be expected to lie in a segmental or sub-segmental bronchus. A volume of 10 to 20 cc of normal saline was then flushed down the catheter. After several respiratory cycles the catheter was aspirated using 50-75 mm Hg of negative pressure and then withdrawn. Aspirated fluid was collected in a Lukens trap, the usual yield being in the order of 3-4 cc. Once obtained, the samples were immediately refrigerated and transported for processing within 24 hours. At the time of bronchial washing fluid collection, a blood sample consisting of the arterial line discard was also collected in a stoppered syringe.

5.1.2 Sample Preparation and IR Measurement Protocol

IR spectra were recorded within 24 hours of specimen collection. Bronchial washing samples were homogenized (Variable speed homogenizer, Glas-Col®, Indiana, USA) for 2-3 minutes at 100 rpm and centrifuged at 15,000 rpm for 10 minutes. Plasma samples were diluted with distilled water to adjust for the analytical range of the instrument. A sample volume of 3 μl of prepared plasma or bronchial washing was placed on a 25×2 mm CaF_2 window and dried down for 4-5 minutes in a vacuum dissector to form a film. This procedure removes water and other volatile components from the sample, which can mask important features of the IR spectrum.

IR spectroscopic measurements were performed by using a Bio-Rad FTS-40A (Biorad, Cambridge, MA) spectrometer equipped with a conventional globar source, KBr beamsplitter, and mercury-cadmium-telluride detector (MCT). Spectra were recorded at 8 cm^{-1} resolution over the region between 900 and 4000 cm^{-1}, each spectrum consisted of 128 co-added scans. Data acquisition time corresponded to less than 3 minutes while the

total assay time required less than 10 minutes. The technique is readily automated to handle batches of samples. Each sample (plasma and bronchial washings) was measured three times by preparing three dried films. This procedure was used to determine the variation of sample preparation and the spectral reproducibility. The results indicated that the spectra are highly reproducible with acceptable variations.

5.1.3 Spectral Characterization of Bronchial Washings

The typical spectrum of a normal bronchial washing sample is presented in Fig. 5.1.1C. IR spectra of bronchial washings share many common features with the spectra of other biofluids and in particular, with that of plasma and bronchial alveolar lavage fluid. Proposed bands assignments in bronchial washing fluids is based on the references given in Table 3.2.1.

In order to construct bronchial washings spectral signatures from ARDS patients, we investigated three patients from the Surgical Intensive Care Unit. These patients met all the clinical criteria for ARDS. For consistency, samples from these patients were collected following the same protocol introduced previously, as were sample preparation and IR measurement protocols.

Fig. 5.1.1 compares IR spectra of a patient's bronchial washing fluid with no apparent lung injury (4 hours after receiving a 500 cc of PENTASPAN®) versus the IR spectrum of a control (no HES infusion and normal lung function). Fig. 5.1.2 presents a comparison of IR spectra from the bronchial washings, plasma and bronchoalveolar lavage fluid of an ARDS patient.

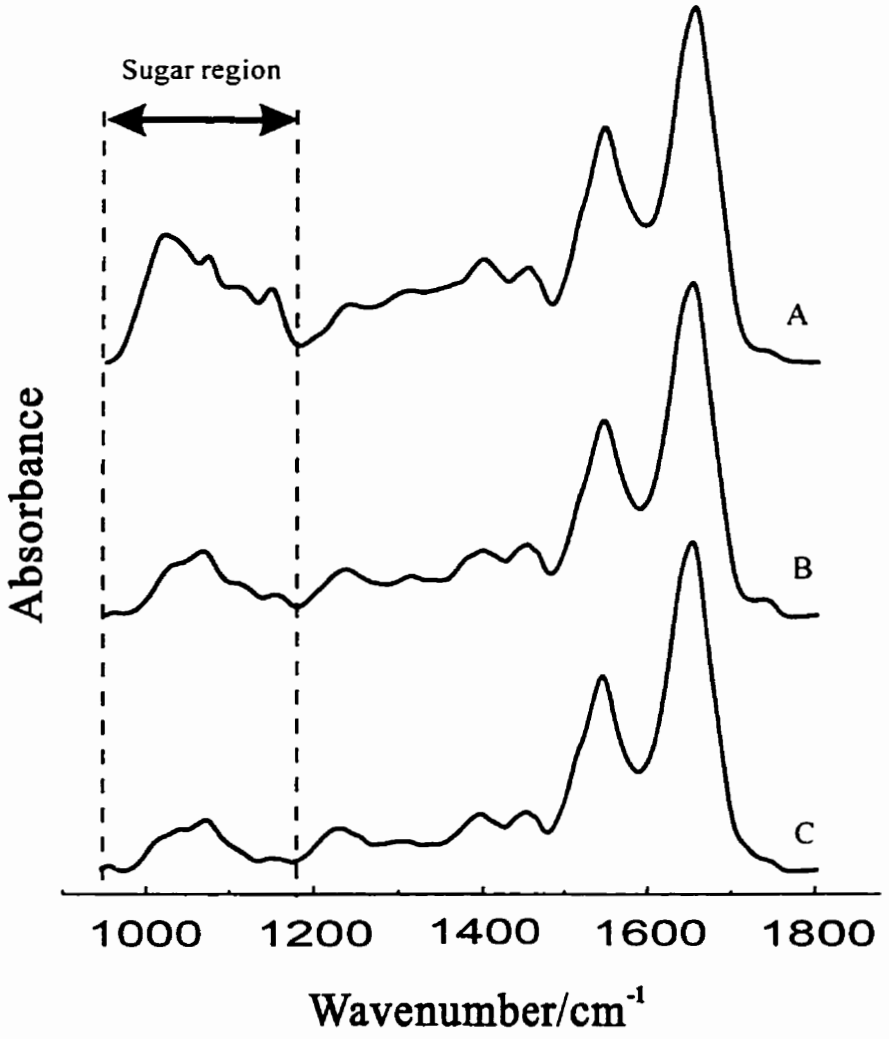

Fig. 5.1.1 Comparison of IR spectra of a non-injury patient's plasma and bronchial washing fluid. A: plasma spectrum 4 hours after receiving 500 cc of PENTASPAN; B: patient's bronchial washing spectrum, no significant starch accumulation; C: a control bronchial washing spectrum (no PENTASPAN infusion)

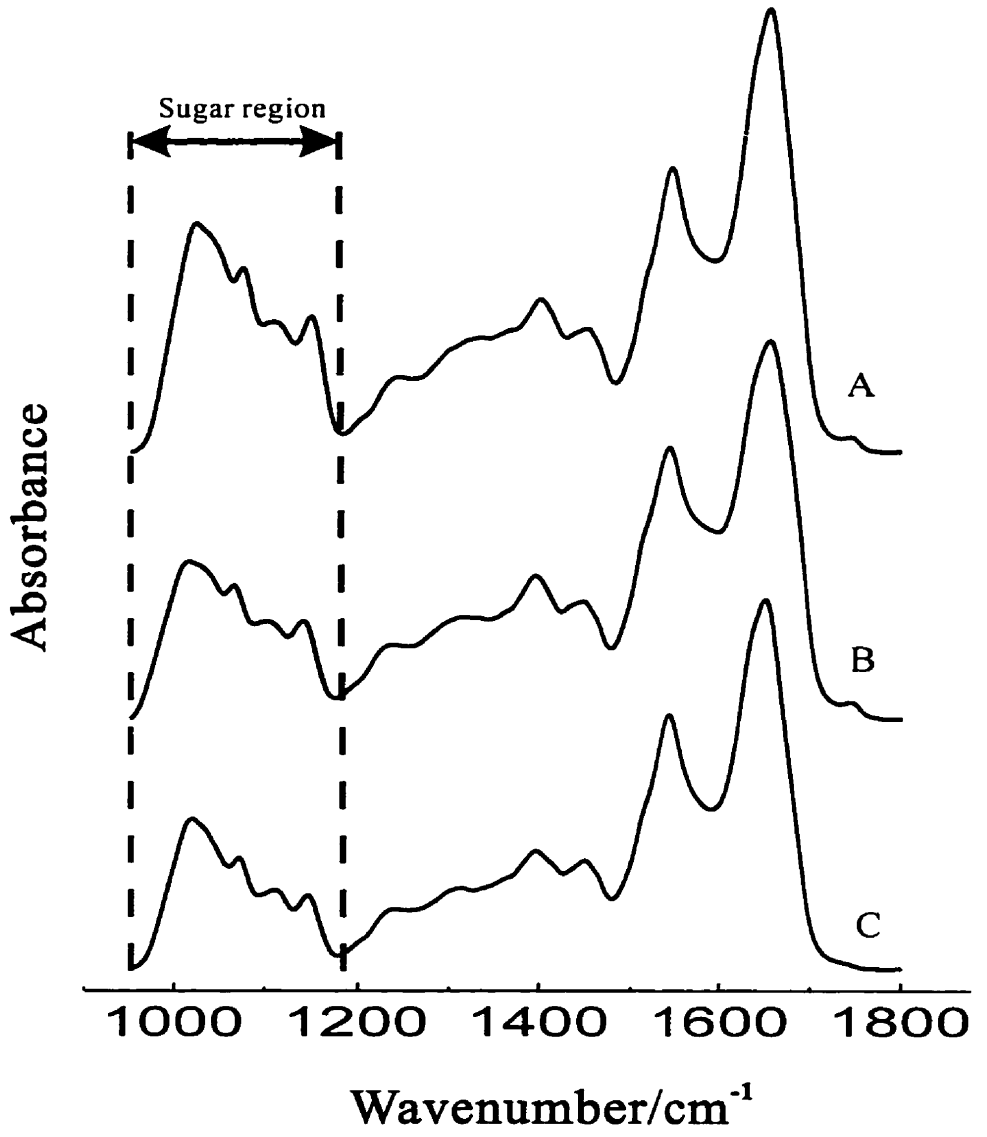

Fig.5.1.2 Comparison of IR spectra of an ARDS patient's plasma and bronchial washing fluid. A: plasma with extensive PENTASPAN loading; B:matched patient's bronchial washing spectrum, significant starch accumulation can be seen; C: lung fluid spectrum from the same patient.

The spectrum of BALF and bronchial washings are similar, particular in the sugar region. This strongly indicates that the determination of alveolar leakage by analyzing bronchial washings from ALI/ARDS patients yields the same diagnostic information as BALF.

The alveolar HES concentration depends on the levels of circulating HES as well as on the pulmonary capillary permeability and surface area. Both Figures provide a simple means of grossly estimating the leakage of the pulmonary vasculature. As exemplified in Fig. 5.1.2, the alveolar HES concentration differs markedly from the plasma HES loading in patients with no apparent lung injury. In a healthy lung, only a very low molecular weight fraction of infused HES would be expected to diffuse between the alveolar and intravascular space. Rapid elimination of HES by the kidneys leads to only minor steady-state concentrations of a low molecular weight fraction of HES in the alveolar spaces, over the analysis period. Increasing pulmonary capillary permeability results in a high molecular weight HES fraction gaining access and penetrating into the alveolar space. As a result, the lung fluid and bronchial washing fluids of an ARDS patient show an accumulation of HES, Fig. 5.1.2 B and C, which is an indicator of increased pulmonary capillary permeability. An increased pulmonary permeability surface area results in faster intravascular-alveolar HES exchange. The determination of HES in bronchial washings may be of value in clinically evaluating and diagnosing the progression of ALI/ARDS.

5.1.4 Problems in Analyzing Bronchial Washing Fluids

Although bronchial washing specimen collection is simple to perform and provides similar diagnostic information to BALF, two problems involved in collection of bronchial washing fluids occur, which strongly affect the analytical results.

(1) Failure to provide quantitative results. Two factors contribute to this problem. The first one is due to the unknown dilution factor involved in the sample collection procedure. The recovered fluids obtained through the washing procedure vary from time to time, and from patient to patient. This largely depends on the patient's clinical situation. In some situations, the washing procedure is easy to perform and rich fluids can be obtained. In other cases, the washings are difficult to perform. Such a problem makes it impossible to provide quantitative results that truly reflect the quantity of leakage.

The second factor is that the location of samples collected may not be at the precise location where leakage occurred. In contrast to the BALF technique, recovery of samples by bronchial washings is a blind procedure. This indicates that using bronchial washing fluids to determine pulmonary permeability yields information on leakage with reference to the non-leak situation, and produces a qualitative result. Although this qualitative analysis only provides a 'leak' or 'non-leak' answer to the problem based on the detection of HES in the fluids, it is crucial clinically to providing information on the pathophysiological changes of ALI/ARDS

The key providing a qualitative result is the detection of HES signature in the fluids. It is known that the IR absorption band shape in the sugar absorption region will change depending on the amount of HES contained in the fluid. This suggests that

analyzing the change of band shape in this region may provide information on the capillary leakage of HES.

(2) *Poor correlation of plasma and bronchial washing fluids:* Although the interstitial HES level depends on the HES level in the circulatory system, the appearance of HES in a patient's plasma and bronchial washings exhibits a phase difference (a time course difference). Generally, infused HES takes a very short time to flow into most organs in the body; however, the time for HES to infiltrate the interstitium from capillaries takes much longer than that in the circulatory system. In addition, HES in the circulatory system has a much shorter half-life than in the interstitium, since α-amylases present in the tissue and in the circulation act at different rates. This implies that measuring plasma HES concentration and comparing that to fluid from bronchial washing might not truly represent the degree of leakage. This is especially true when HES concentration in the circulation is lower than in the bronchial washings.

This problem largely depends on establishing the best time to collect bronchial washings after HES infusion, so that it has an optimal correlation with plasma HES concentration. The answer is still unknown from this study. In addition to this, the best times vary from patient to patient. In order to avoid this problem, it is suggested that for evaluating pulmonary permeability or capillary leakage, one should analyze HES in bronchial washing fluid without necessarily correlating it with the plasma. However, it is necessary to know the HES concentration profile in the circulation in order to have a general idea of the amount of tracer remaining in the system.

5.2 Spectral Pattern Recognition Approach

In order to achieve the recognition of HES signatures in bronchial washing fluids, a new spectroscopic data evaluation technique is introduced. The technique is based on a multivariate statistical analysis methodology which is used to distinguish spectral patterns; it is referred to as spectral pattern recognition. This technique was developed for classification and comparison of spectra based on chemical absorption fingerprints in a certain spectroscopic region.

5.2.1 Pattern Recognition Methods

Classification, a basic human conceptual activity, has played an important role in the development of many areas of science and medicine. A classification scheme may simply represent a convenient method for organizing the patterns in a large set of data so that the repossession of information may be made more efficiently. Describing patterns of similarity and differences among objects under investigation and grouping them by means of their class may provide a very convenient way to analyze the data set.

There are number of methods available for spectral pattern recognition and classification. These methods can be grouped into two categories: unsupervised spectral pattern recognition and supervised spectral pattern recognition. Unsupervised pattern recognition is used to construct a sensible and informative classification of an initially unclassified set of data, using the variable values observed on each individual. These techniques are good for exploratory analysis of the data set. They allow for analyzing raw spectral data to find inter-spectral variations and for group classification according to these variations. The most widely used method for unsupervised pattern recognition is

cluster analysis. This technique is extremely useful in case the classification is not so well defined, and the method may be used to determine the number and membership of the main groups.

Although unsupervised pattern recognition is very useful for investigating unclassified data sets, the interest is not just in exploring a set of multivariate data for evidence of the existence of separate groups of individuals, but in deriving rules for allocating new data to one of a set of *a priori* defined classes or diagnostic groups in some optimal way. The technique for this purpose is called supervised pattern recognition, also referred to as hard modelling. In a supervised pattern recognition method, each assignment or discrimination technique has a basic training set, which is a series of variables (data) collected from samples in which the classification has already been confirmed. These training sets serve to establish the characteristics of each group. A new sample is then classified or diagnosed by determining in some way or other to which group this sample belongs. The most commonly used assignment techniques are *linear discriminant analysis* and *neural networks*.

In this application, it is of particular interest to determine HES in a patient's bronchial washing fluids based on its IR absorption signature. This is a two class classification problem. In dealing with this two class problem, the training set contains two groups, the starch (or leak) group and the non-starch (or non-leak) group. Based on the *a priori* information of starch in the spectrum, a powerful prediction model is established using linear discriminant analysis.

5.2.2 Linear Discriminant Analysis – Two Classes Problem

This section provides an overview of the mathematics of linear discriminant analysis (LDA) for the two class problem. LDA was developed by Fisher (Fisher, 1936), as a technique to determine which linear combination of variables best discriminantes between two or more naturally occurring (or *a priori* defined) groups.

Let us assume that the two groups have the same covariance matrix but distinct mean spectra, and work with samples of spectra $\mathbf{y}_{11}, \mathbf{y}_{12}, \ldots, \mathbf{y}_{1n_1}$ and $\mathbf{y}_{21}, \mathbf{y}_{22}, \ldots, \mathbf{y}_{2n_2}$ from the two groups. Consider each spectra y_{ij} as consisting of measurements on p variables. The discriminant function is the linear combination of these p variables that maximizes the distance between the two (transformed) group mean vectors. A linear combination transforms each observed spectrum, considered as a vector, to a scalar:

$$z_{1j} = \mathbf{a}'\mathbf{y}_{1j} = a_1 y_{1j} + a_2 y_{1j_2} + \ldots + a_p y_{1j_p} \quad (j = 1,2,\ldots,n_1) \qquad 5.2.1a$$

$$z_{2j} = \mathbf{a}'\mathbf{y}_{2j} = a_1 y_{2j_1} + a_1 y_{2j_2} + \ldots + a_p y_{2j_p} \quad (j = 1,2,\ldots,n_2) \qquad 5.2.1b$$

where the first coefficient refers to group 1 or group 2. Therefore the n_1+n_2 observation spectra in the two groups, $\mathbf{y}_{11}, \mathbf{y}_{12}, \ldots, \mathbf{y}_{1n_1}$ and $\mathbf{y}_{21}, \mathbf{y}_{22}, \ldots, \mathbf{y}_{2n_2}$ are transformed to scalars, $z_{11}, z_{12}, \ldots, z_{1n_1}$ and $z_{21}, z_{22}, \ldots, z_{2n_2}$, and one can find the means $\bar{z}_1$ and $\bar{z}_2$ by

$$\bar{z}_1 = \sum_{j=1}^{n_1} \left(\frac{z_{1j}}{n_1} \right) \qquad 5.2.2a$$

$$\bar{z}_2 = \sum_{j=1}^{n_2} \left(\frac{z_{2j}}{n_2} \right) \qquad 5.2.2b$$

We wish to find the vector **a**, as discriminant function, that maximizes

$$\mathbf{a} = \frac{\left[\mathbf{a}'(\bar{\mathbf{y}}_1 - \bar{\mathbf{y}}_2)\right]^2}{\mathbf{a}' S_{pl} \mathbf{a}} \qquad 5.2.3$$

Here, S_{pl} is the pooled sample covariance matrix; and

$$\mathbf{S}_{pl} = \frac{(n_1 - 1)\mathbf{S}_1 + (n_2 - 1)\mathbf{S}_2}{n_1 + n_2 - 2} \qquad 5.2.3$$

where S_1 and S_2 are the sample covariance matrices for group 1 and group 2;

$$S_i^2 = \frac{1}{n_i - 1} \sum_{j=1}^{n_i} \left(y_{ij} - \bar{y}_i\right)^2 \qquad 5.2.3a$$

and $\bar{y}_i$ is the mean spectrum of the group, given

$$\bar{y}_i = \frac{1}{n_i} \sum_{j=1}^{n_i} y_{ij} \quad (i = 1,2; j = 1,2,\ldots n_i) \qquad 5.2.3b$$

The maximum of Eq. 5.2.3 occurs when $\mathbf{a} = \mathbf{S}_{pl}^{-1}(\bar{\mathbf{y}}_1 - \bar{\mathbf{y}}_2)$ or when $\mathbf{a}$ is any multiple of this vector. It should be noted that in order for $\mathbf{S}_{pl}^{-1}$ to exist we must have $n_1+n_2-2>p$, which puts a constraint on the minimal number of sample spectra required to do the analysis. If we now have a sampled spectrum but do not know to which of the two groups it belongs, we can use the discriminant function described above to classify the spectra. We have, in particular,

$$z = \left(\bar{\mathbf{y}}_1 - \bar{\mathbf{y}}_2\right)' \mathbf{S}_{pl}^{-1} \mathbf{y} \qquad 5.2.4$$

where y is the vector of measurements on the new sampling spectra that we wish to classify.

Let us denote the two groups by G_1 and G_2, we can then evaluate Eq. 5.2.4 for each observation y_{1j} from the first sample and obtain $z_{11}, z_{12}, \ldots, z_{1n_1}$, which implies that

$$\bar{z}_1 = \sum_{j=1}^{n_1}\left(\frac{z_{1j}}{n_1}\right) = (\bar{\mathbf{y}}_1 - \bar{\mathbf{y}}_2)' \mathbf{S}_{pl}^{-1}\bar{\mathbf{y}}_1 \qquad 5.2.5a$$

Similarly,

$$\bar{z}_2 = (\bar{\mathbf{y}}_1 - \bar{\mathbf{y}}_2)' \mathbf{S}_{pl}^{-1}\bar{\mathbf{y}}_2 \qquad 5.2.5b$$

Fisher's linear classification procedure assigns y to G_1 if z is closer to $\bar{z}_1$ than to $\bar{z}_2$, and assigns y to G_2 if z is closer to $\bar{z}_2$. This is illustrated in the Fig. 5.2.1. One can see, for this particular configuration, that z is closer to z_1 if $z > \frac{1}{2}(\bar{z}_1 + \bar{z}_2)$. This is true in general because $\bar{z}_1$ is always greater than $\bar{z}_2$ which can be shown as follows

$$\bar{z}_1 - \bar{z}_2 = (\bar{\mathbf{y}}_1 - \bar{\mathbf{y}}_2)' \mathbf{S}_{pl}^{-1}(\bar{\mathbf{y}}_1 - \bar{\mathbf{y}}_2) > 0 \qquad 5.2.6$$

because $\mathbf{S}_{pl}^{-1}$ is positive defined. Therefore $\bar{z}_1 > \bar{z}_2$ now since $\frac{1}{2}(\bar{z}_1 - \bar{z}_2)$ is the midpoint, $z > \frac{1}{2}(\bar{z}_1 - \bar{z}_2)$ implies that z is closer to $\bar{z}_1$.

To express the classification rule in terms of y, first, we express $\frac{1}{2}(\bar{z}_1 + \bar{z}_2)$ in the form:

$$\frac{1}{2}(\bar{z}_1 + \bar{z}_2) = \frac{1}{2}(\bar{\mathbf{y}}_1 - \bar{\mathbf{y}}_2)' \mathbf{S}_{pl}^{-1}(\bar{\mathbf{y}}_1 + \bar{\mathbf{y}}_2) \qquad 5.2.7$$

The classification now: assigns y to G_1 if

$$z = (\bar{\mathbf{y}}_1 - \bar{\mathbf{y}}_2)' \mathbf{S}_{pl}^{-1}\mathbf{y} > \frac{1}{2}(\bar{\mathbf{y}}_1 - \bar{\mathbf{y}}_2)' \mathbf{S}_{pl}^{-1}(\bar{\mathbf{y}}_1 + \bar{\mathbf{y}}_2) \qquad 5.2.8a$$

and assigns y to G_2 if

$$z = (\bar{\mathbf{y}}_1 - \bar{\mathbf{y}}_2)' \mathbf{S}_{pl}^{-1}\mathbf{y} < \frac{1}{2}(\bar{\mathbf{y}}_1 - \bar{\mathbf{y}}_2)' \mathbf{S}_{pl}^{-1}(\bar{\mathbf{y}}_1 + \bar{\mathbf{y}}_2) \qquad 5.2.8b$$

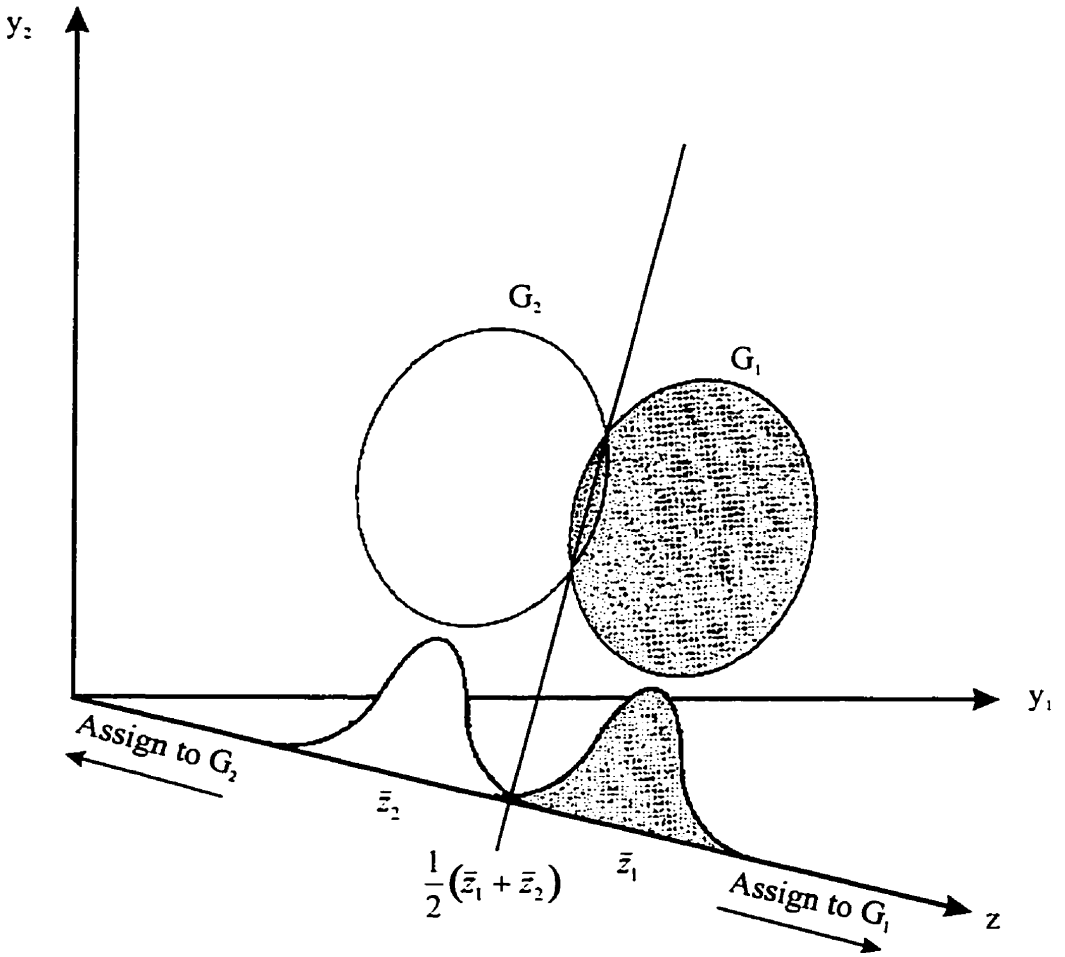

Fig.5.2.1. Fisher's procedure for classification into two groups

5.3 Establishing a Prediction Model

The prediction model is established by a supervised pattern recognition technique. In supervised pattern recognition, the classification scheme is known *a priori* and the problem is now to devise rules for assigning unclassified individual objects to one of the known classes, i.e. predicting the unknowns by the known classes.

The classical approach to spectral pattern recognition begins by selecting a training set. The training set must be truly representative of the properties of the entire population with a high degree of confidence. The class membership in the training set can be built based upon the known information of samples from experimental results or based upon the fuzzy classification technique, known as fuzzy *cluster analysis*. Once the training set is in place, a number of test sets will be used to test the training set in order to gain confidence in the model. Then, this classification model will be used to classify new spectra.

For spectral multivariate statistical analysis, spectral data processing procedures need to be standardized. The data standardization includes both data recording and data reprocessing procedures. The purpose of data recording standardization is to keep experimental conditions and recording parameters the same. Generally, this should suffice for application of the spectral pattern recognition technique. However, in certain applications, data-reprocessing standardization is necessary in order to maintain certain spectral properties. In this study, spectral data reprocessing standardization is applied.

5.3.1 Spectral Standardization

The spectrum standardization in this application involves two steps, spectrum truncation and spectrum normalization.

1. Truncation: The original individual spectrum was recorded from the spectral region 900-4000 cm^{-1}, and contained 3214 data points. Since the sugar region represents the region involving the highest diagnostic value in the spectrum, all spectra were truncated between 970 and 1170 cm^{-1}. The final spectra for analysis consisted of 208 data points. The baseline of all spectra was also corrected and offset during this procedure.

2. Normalization: A large variation in absorption intensities is the major problem for bronchial washing spectra classification. This is due to a variable and unknown dilution factor. In order to produce a reliable classification, the influence of this unknown dilution factor in absorption intensity must be eliminated. Band area normalization is one way to resolve such a problem.

Band area normalization is based on an integration method. For this method, we first define an area constant in the spectroscopic region of interest, so that every individual spectrum will ratio to this area constant in that region, and, in this way we obtain a fraction factor. The normalized spectrum is then obtained by multiplying the fraction factor to that spectrum in the defined region. In doing so the band's area for all individual spectra will be the same as the defined constant area. This treatment will keep the band shape unchanged, but offset all spectra to a reference value. Such treatment can be considered as a process of artificially correcting the dilution factor. Although this corrected dilution factor is meaningless in providing quantitative analysis results, it is a

very important step for spectra classification that eliminates the intensity variations caused by various dilution factors.

In this study, all recorded spectra of bronchial washings used for the analysis were truncated in the spectral region of 970 and 1170 cm^{-1}. All the spectra for analysis were also processed by band area normalization with an area normalization constant of 100 (absorption/cm).

5.3.2 Establishing a Training Set for HES Pattern Recognition

Linear discriminant analysis of IR spectral data is based on the determination of discriminatory features in a set of reference spectra, known as the training set. The training set is used to set up a *class model* in which the discriminatory features can be used to classify new objects (unknown). The features that are used for spectral classification can be a combination of specific peak frequencies, absorption bandwidth, or relative intensities which uniquely characterize the spectral data set in a given class. In this study, we are particularly interested in determining the HES leakage in a patient's bronchial washing fluids, thus the training set must represent the two groups of patients, leak and non-leak, and allow the characteristics of each group to be determined.

Based upon the presentation of HES in bronchial washing spectra, LDA will examine the training set for the peak frequencies, bandwidth and the relative peak intensities that will strongly identify the signature of HES as having arisen from the spectra. The ideal training set should be established on a complex biofluid matrix that involves complex IR absorption signals. The purpose of establishing a training set is to find the HES absorption signal in that complex absorption system. For this application, a

computer-generated training set is constructed based on the human bronchial washing fluids which were collected from the baseline study.

Method: In order to determine the HES signal in bronchial washing fluids, the training set involves two groups, the starch group and the starch free group. This computer-generated training set is based on the bronchial washing fluid spectra and the spectrum of PENTASPAN®. In the starch-free group, there are 100 IR spectra. Due to the limitation of sample size, these 100 starch-free spectra were created from 42 bronchial washing IR spectra by mixing two spectra non-repeatedly. These 42 spectra were measured from 14 bronchial washing samples, and these 14 patients were not infused with PENTASPAN®. These 14 patient's bronchial washings represent the sample's compositional variations. Each of these samples was measured three times to determine the spectral reproducibility. These three measurements represent the sample's experimental variation.

In the starch group, 100 spectra are included which were constructed from these 100 starch-free spectra. The various concentrations of PENTASPAN® in these bronchial washing spectra were built in, by artificially adding the PENTASPAN® spectra with different mixing factors, to the starch-free bronchial washing spectra. The mixing factors represent various amount of starch in the fluids. The method of evaluating the amount of starch in the bronchial washings is explained as following:

(1) The original pure PENTASPAN® (100 mg/ml) was diluted with distilled water by a dilution factor of 1:25 for optimized spectroscopic measurement. This dilution factor resulted in the pure PENTASPAN® solution containing 4 mg/ml of starch.

(2) 3 μl of this diluted solution was used for measurement. This 3 μl of solution contained 0.012 mg of starch.

(3) This amount (0.012 mg) of starch gives 0.40 IR absorbance units (A.U) at 1021 cm^{-1} in the sugar region. By normalizing this 0.4 A.U to 1.0 A.U, this normalized 1.0 A.U of starch absorbance (2.5 times of 0.4 A.U) represents 0.03 mg of starch.

(4) In the next step, this amount of starch absorbance is multiplied by the mixing factor 0.001 to 0.1 continuously. The IR spectra of PENTASPAN®, after multiplication by the mixing factor, then represent the starch concentrations from 0.03 to 3 μg in 0.03 μg steps.

(5) By mixing these various amounts of starch spectra with the starch-free bronchial washing spectra, the spectra of the starch group are created.

5.3.3 Spectral Region Selection for Space Reduction

The difficulty involved in using LDA to classify IR spectra is that of dimensionality. Generally, the complete spectra to be analyzed consist of hundreds of attributes (the frequencies), which form a sparse set in a high-dimension (total data points), with relatively small intrinsic dimension (total sample size in the data set). This makes it difficult to perform the spectral classification. Such a problem can be resolved by applying so called "attribute selection" methodology. The purpose of this methodology is to reduce the dimension (data points) by selecting certain regions in the spectral range of interest which contain the most diagnostic information for classification. Conventional methods of this so called "Attribute selection" in spectral analysis include curve fitting, and principal component analysis. With the development of computer technology, the Genetic Algorithm (GA) method was introduced into the spectral region selection for the purpose of space reduction. A near-optimal region selection for feature space reduction, GA-ORS, was used for spectral sub-region selection (Nikulin, *et al.*, 1998).

Genetic algorithm: A *genetic algorithm* is a mathematical algorithm that is used to transform a set (population) of individual mathematical objects into a new population (the next *generation*) with an associated fitness value. The algorithm simulates Darwinian evolutionary processes and naturally occurring genetic operations on chromosomes. In nature, variety is exhibited as variation in the chromosomes of the individuals in the population. Such variation is presented by variability in both the structure and the behavior of the individual in its environment. In turn, this variation in structure and behavior is represented by differences in the rate of survival and reproduction. Generally, entities that are better able to perform tasks in their environment (fitter individuals) survive and reproduce at a high rate; less fit entities survive and reproduce at a lower rate. By adapting this evolutionary process to natural and artificial systems, any problem can be generally formulated in genetic terms. Once those terms are formulated, such a problem can be often solved by a genetic algorithm.

In practice, the genetic algorithm iteratively performs the operations on each generation of individuals to produce new generations of individuals until some termination criterion is satisfied. For each generation, the algorithm first evaluates each individual in the population for fitness. Then using this fitness information, the algorithm performs the operation of reproduction, crossover, and mutation with the frequency specified by the probabilities of reproduction, crossover and mutation, P_r, P_c and P_m respectively. The mutation operation is used in the conventional genetic algorithm operation on fixed-length strings but it is used very sparingly. The termination criterion is sometimes stated in terms of a maximum number of generations to be run (koza).

The subset selection procedures define the criteria (features) for the selection, and an objective (fitness) function.

Feature selection: To perform the region selection, certain criteria must be applied during the subset selection procedures. The goal of this sub-region (subset) selection option is to construct, from the spectra, a limited number of features which will ensure reliable, robust classification. Therefore, the features that are selected for the analysis must maintain their spectral identity in the set. No general theoretical basis is available for this process. The selection of features is thus highly dependent on the *a priori* knowledge of an interpreter. The validity of feature selection can be checked only by the classification results. Criteria that are often used include; average intensity, ratios of averaged intensity, and variances, etc. Practically, the most common form used for region selection is that of the use of average intensity, i.e. replacing the intensities in the sub-region by their mean value. This average intensity is then taken as the new feature. In the present application, this averaging criterion is used for sub-region selection.

Objective (Fitness) function: An objective function is applied to the subset in order to simultaneously maximize the overall accuracy for the training set and to produce crisper (less fuzzy) class assignments (Nikulin, *et al.*, 1998). The criterion of the fitness function is the use of the mean square error between the training set classification result (the probability that spectrum is in a defined class) and an *a priori* classification indicator for that spectrum. Mathematically, this fitness function is defined as

$$F = \frac{1}{N \times C} \sum_{P=1}^{C} \sum_{I=1}^{N} \left(P_{ia} - I_{ia} \right)^2 \qquad 5.3.1$$

where P_{ia} is the probability that spectrum i is in class a. I_{ia} is the *a priori* class indicator for that spectrum; it equals 1 if the spectrum is in that defined class, and equals zero otherwise.

Input parameters for the algorithm: The input parameters for the algorithm include the size of the population, the maximum number of sub-regions allowed to select the number of generations and the probabilities of mutation and crossover. For the present application, the parameters that are input for the analysis include: population size, P = 300, i.e. the total number of runs of the classification methods will be 300 multiplied by the number of generations (eg.15,000 for 50 generations); the number of points in the spectra is 208 (N=208), the number of generations is 20 (G =20), and the number of sub-regions to be selected is 3 (S=3). The probability of crossover is 0.66 and the probability of point mutation is 0.001. The GA_ORS was applied to the computer-generated training set, and three sub-regions, 1005-1006, 1085-1092, and 1162-1164 cm^{-1}, were determined by the algorithm, which suggested to be the best diagnostic region with acceptable confidence, as indicated in Fig. 5.3.1. The three sub-regions in the representative spectra of bronchial washings in case of non-starch, and contain 0.03, 1.5, 3.0 and 15 μg starch display in Fig. 5.3.2.

The changes of bandwidth and band shift, due to compositional variations, are more sensitive than the band intensity, therefore bandwidth and band shift are significant parameters to detect the compositional variation in spectroscopic analysis. Due to this reason, it is not surprising that the regions selected by the GA_ORS appeared on the shoulder region of absorption band rather than in the center of the band (see Fig.5.3.2).

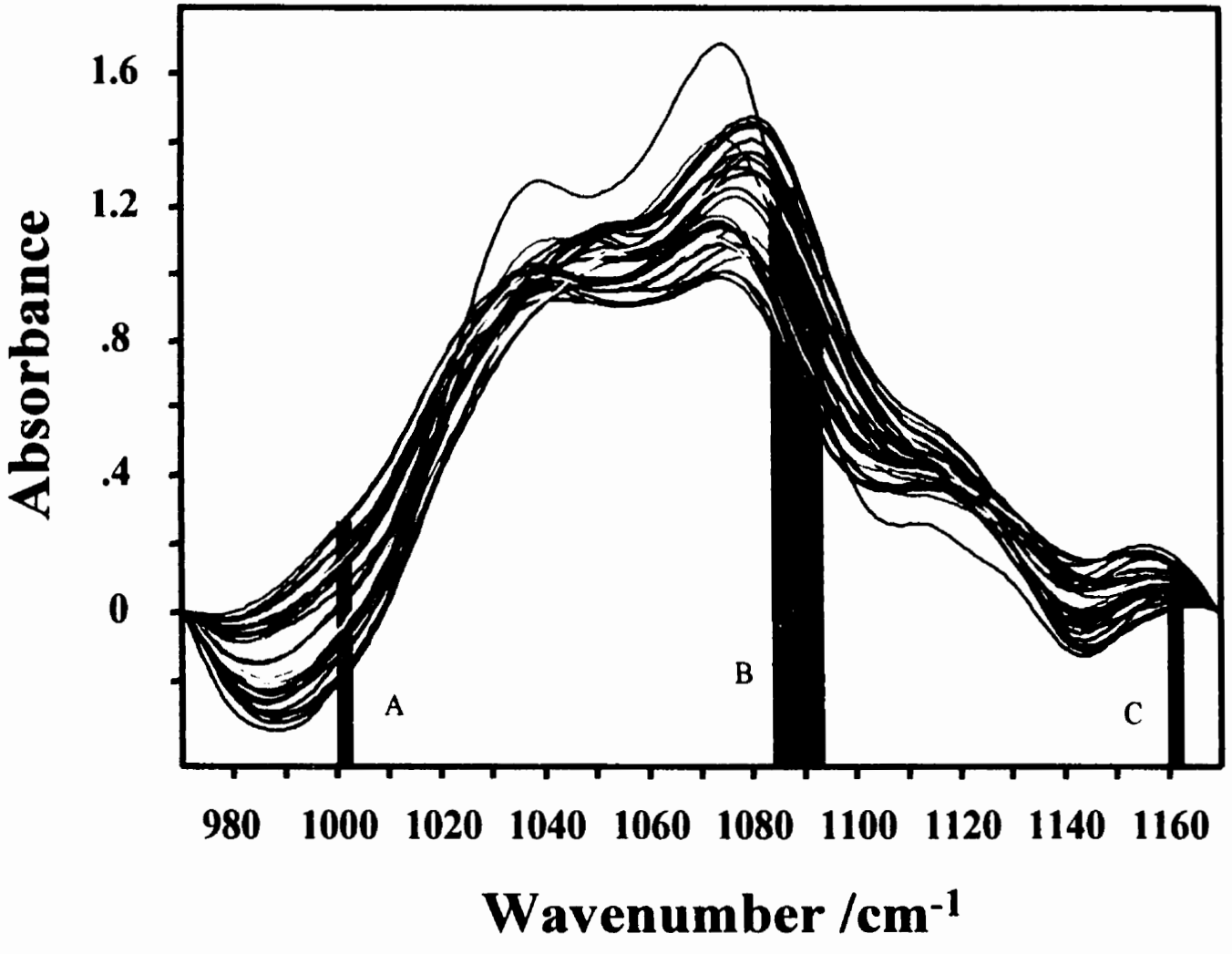

Fig. 5.3.1 Demonstration of three sub-regions selected by GA_ORS which best detect the starch signal in 30 bronchial washings spectra from the training set. A: 1005-1006 cm^{-1}; B: 1085-1092 cm^{-1} C: 1162-1164 cm^{-1}

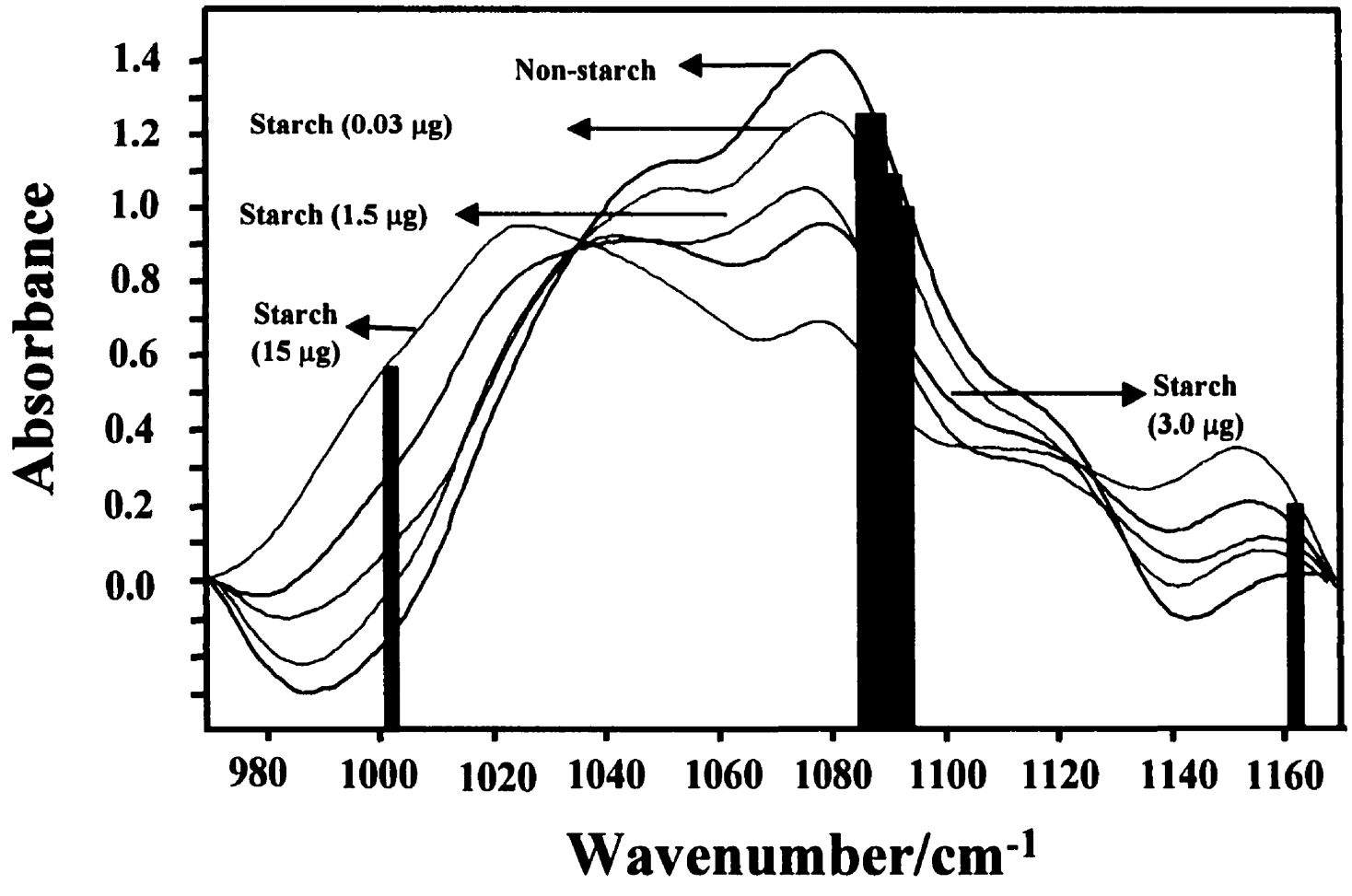

Fig. 5.3.2 Representative bronchial washings spectra in the three sub-regions selected by GA_ORS, in case of Non-starch; and four spectra contain 0.03, 1.5, 3.0 and 15 μg starch. Spectrum contains 15 μg starch was not included in the training set.

5.3.4 Linear Discriminant Analysis of the Training Set

Linear discriminant analysis was then performed using only the regions which were selected after applying the genetic algorithm to the training set.

We are essentially treating each sample spectra (y_{i1}, y_{i2}, ... y_{ip}) as p-vector, for i = $1,2,...n$. As discussed early that the LDA analysis is based on the pooled sample *covariance matrix*, which is determined by the covariance matrix of each class (Recker, 1995). The covariance matrix, classically, is defined as

$$\mathbf{S} = (s_{jk}) = \begin{pmatrix} s_{11} & s_{12} & \cdots & s_{1p} \\ s_{21} & s_{22} & \cdots & s_{2p} \\ \vdots & \vdots & \vdots & \vdots \\ s_{p1} & s_{p2} & \cdots & s_{pp} \end{pmatrix} \qquad 5.3.2$$

where the j^{th} diagonal elements s_{jj} is the sample variance of the j^{th} variable:

$$s_{jj} = \frac{1}{n-1}\sum_{i=1}^{n}\left(y_{ij} - \bar{y}_j\right)^2 \qquad 5.3.2a$$

The off-diagonal elements s_{jk} in 5.3.2 is the sample covariance of the j^{th} and k^{th} variables:

$$s_{jk} = \frac{1}{n-1}\sum_{i=1}^{n}\left(y_{ij} - \bar{y}_j\right)\left(y_{ik} - \bar{y}_k\right) \qquad 5.3.2b$$

In our application, the parameters that were determined from LDA are given in the following matrices: the sample covariance matrix of the leak group, class 1, is

$$\mathbf{S}_1 = \begin{pmatrix} 0.0191 & -0.0036 & -0.0128 \\ -0.0036 & 0.0010 & 0.0028 \\ -0.0128 & 0.0028 & 0.0102 \end{pmatrix} \qquad 5.3.3$$

the sample covariance matrix of the non-leak group, class 2, is

$$\mathbf{S}_2 = \begin{pmatrix} 0.0229 & -0.0025 & -0.0126 \\ -0.0025 & 0.0005 & 0.0012 \\ -0.0126 & 0.0012 & 0.0082 \end{pmatrix} \qquad 5.3.4$$

The diagonal elements these 3×3 matrices are the variances of the three spectral sub-regions which were selected by the GA_ORS. The pooled sample covariance matrix is then calculated by Eq. 5.2.3, and obtained as

$$\mathbf{S}_{12} = \begin{pmatrix} 0.0210 & -0.0030 & -0.0127 \\ -0.0030 & 0.0007 & 0.0020 \\ -0.0127 & 0.0020 & 0.0092 \end{pmatrix} \qquad 5.3.5.$$

The distance (*Mahalanobis* distance) between two groups is calculated by

$$D_{12}^2 = (\bar{y}_1 - \bar{y}_2)^T \mathbf{S}_{12}^{-1} (\bar{y}_1 - \bar{y}_2) \qquad 5.3.6$$

and it is determined to be

$$D_{12}^2 = \begin{pmatrix} 0.0000 & 4.9016 \\ 4.9016 & 0.0000 \end{pmatrix} \qquad 5.3.6a$$

. The discriminant functions of the training set are given by

$$y_1 = -236.75 + 366.34x_{11} + 558.86x_{12} + 403.30x_{13} \qquad 5.3.7a$$

$$y_2 = -202.24 + 340.82x_{21} + 507.85x_{22} + 363.12x_{23} \qquad 5.3.7b$$

Cross-Validation test: The cross-validation test on the spectral training set is performed by the Leave-One-Out method which is commonly used for evaluating the prediction ability of the training process. The method operates on the training set, and is an independent test from that performed on the test set. The method is performed by sequentially removing a single spectrum from the training set, and training the classifier on the remaining spectra in the training set (200 spectra). Prediction is then made for that single test spectrum. This process is repeated for each single spectrum in the training set,

the classifier being returned to the training set after each test so that the training set remains the same size (199 spectra). The strategy of this cross-validation test is to improve the probability that the training set truly represents the full population of the study.

The Leave-One-Out method was built into the Genetic Algorithm program, so that once the analysis was done for the training set, the test of the training set will also be performed. The test results of individual members in the training set are given in terms of the probability of belonging to a given class, which is called the *posterior* probability. The *posterior* probability is the probability, based on the knowledge of the values of other variables, that the respective case belongs to a particular group. The class membership in the training set is then assigned based on the *posterior* probability that is determined during the LDA algorithm's performance. In this study, the two groups defined and given as group 1 and group 2, represent the leak (starch) and the non-leak (non-starch) groups respectively. The *posterior* probability is the determination of leakage. If the probability is greater than 0.50, then this sample is assigned in the leak group (group 1). Otherwise, it belongs to the non-leak group (group 2).

Summary of the training set: A common method used in order to determine how well the current classification function predicts group memberships is to examine the classification matrix. The matrix shows the number of cases that were correctly classified and the number that were misclassified. The classification results of the training set are presented in Table 5.3.1. The *posterior* probabilities for the training set are calculated and given in Table 5.3.2. A plot of the *posterior* probabilities vs. the amount of starch in the sample is illustrated in Fig.5.3.3. The high accuracy of predicting the non-leak (non-

starch) group (98%) with an acceptable prediction rate of the leak (starch) group (80%) in the matrix indicates that the training set does indeed provide a satisfactory answer. As indicated in the table, the mis-classified spectra (20) involve low concentrations of starch, ranging from 0.03 to 0.66 μg in 0.03 μg intervals, which is the prediction limit of the training set.

Table 5.3.1 LDA Classification Table for the Training Set

Group		Actual		Percent correct
		Group 1 Starch (leak)	Group 2 Non-starch (Non-leak)	
Predicted	Group 1 Starch (Leak)	80	20	80%
	Group 2 Non-starch (non-leak)	2	98	98%

There are also two spectra that were mis-classified in the non-starch group, which is due to the spectral variations. Although these non-starch spectra of bronchial washings should represent both compositional and experimental variations, a spectral absorption profile that differs from these in the training set will give a mis-classification result. One way to avoid this problem is to increase the database of the training set.

To optimize the training set performance, two parameters play an important role; the input of the number of generations and the input of the number of regions that the genetic algorithm is looking for. Generally, increasing the number of generations and the sub-regions GA is looking for, will increase the sensitivity of the training set. However, it could result in the problem that the training set is over-trained and the results might no longer be reliable. In this study, if we continuously search for higher accuracy of

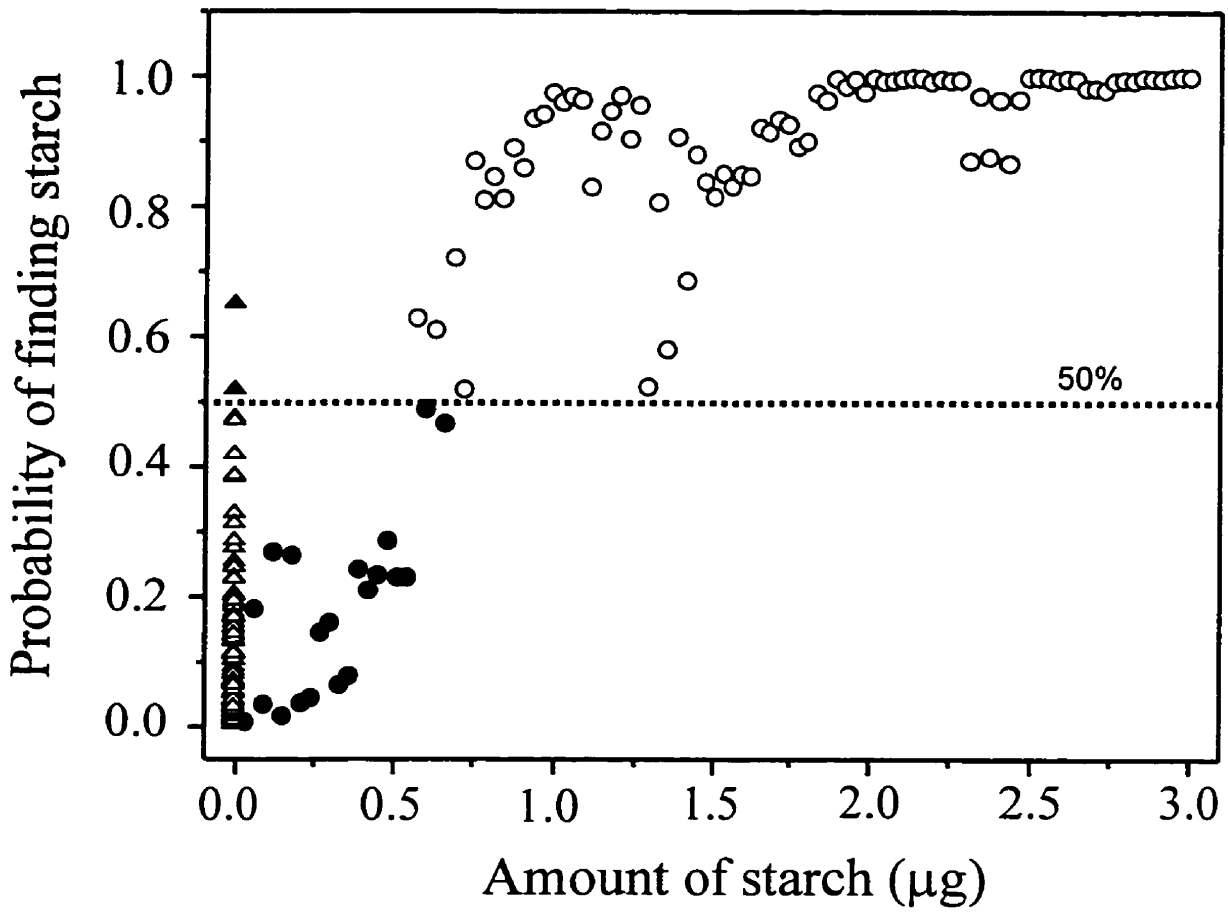

Fig.5.3.3 A plot of the posterior probabilities vs the amount of starch in bronchial washings. The triangles represent the non-starch group, and circles represent the starch group. The mis-classification cases are indicated by solid circles/triangles.

prediction for the leak (starch) group, by increasing the number of generations and the number of regions to allocate, this will result in increasing the mis-classification of cases in the non-leak group. The criterion used to evaluate the training set is to eliminate the mis-classification of cases in the non-leak population as much as possible with an acceptable accuracy rate of classification for the leak population. In other words, the prediction for the non-leak population should be as accurate as possible, and with an acceptable sensitivity with respect to the prediction of the leak population. Otherwise, the training becomes so sensitive that it might lead to incorrect interpretation of a real sample.

5.3.5 Testing of the Training Set

The quality of pattern recognition results must be carefully and critically checked after establishing a training set, in order to provide a reliable prediction model. Although the Leave-One-Out method has been applied to the training set, it is necessary to test the model by using it to predict the classification of an independent data set. Generally, the test set should not contain the same samples which were used in the training set and it is used for direct testing of the classifier performance. Two test sets were generated for the purpose of determining starch in the spectra. One was a computer-generated test set based on the spectra of bronchial washing fluids, and the other one was experimentally constructed from human and animal plasma (sera) samples. In both test sets, the spectra that were used for the non-leak group contained absolutely no PENTASPAN®.

1. A Computer-Generated Bronchial Washing Test Set: These bronchial washing spectra were obtained from those in the baseline study. Eight patients' bronchial washing

samples in that study were used to build the test set with a total of 24 spectra. These patients were not infused with PENTASPAN® for the samples collected.

Method: These 200 spectra were included in the test set and were divided into two groups: the starch group, and the starch-free groups. Each group contained 100 spectra. In order to obtain 100 spectra for the non-starch group, a computer-generated database was used. This database was created from those eight patient's bronchial washing spectra which did not involve PENTASPAN®. The test set involved 24 original spectra from these eight patient's bronchial washing samples. These 24 spectra were then used to create 100 individual spectra, in a manner similar to that in which the spectra were created in the training set, i.e. by adding two spectra non-repeatedly. In the starch group, 100 spectra with various amounts of starch were constructed exactly as in the training set with the same amount of starch in the spectra (in the range from 0.03 to 3μg in 0.03 μg intervals).

Summary of Test Result: Applying the training set to the test set, gave the results shown in Table 5.3.2, as a classification matrix. The matrix indicates, based on *a priori* knowledge of these spectra that the accuracy of predicting leak (starch) is 92%, and the prediction accuracy of non-leak (non-starch) is 91%.

Table 5.3.2 LDA Classification for Test Set of Bronchial Washings

Group		Actual		Percent correct
		Starch (leak)	No starch (Non-leak)	
Predicted	Starch (Leak)	92	8	92%
	No starch (Non-leak)	9	91	91%

2. Experimental Test Set: The experimental test set was constructed from human and animal plasma samples. The set was also divided into two groups, the starch group and the non-starch group. The test set contains 101 starch free spectra measured from 34 human and animal plasma samples, and 111 spectra with various amount of PENTASPAN® which were generated from two human sera (starch free). One contained low glucose concentration (70 mg/dl) and one high glucose (150 mg/dl) concentration.

Method: From the low glucose containing serum, a total of 51 spectra were recorded from 17 different starch concentration samples, each of these samples were measured three times for the purpose of checking spectral reproducibility. The amount of starch in the measured sample (3μl drop) were in the range 0.06 to 1.0 μg in 0.06 μg intervals. From the high glucose containing serum, 60 spectra were recorded in 20 different starch concentrations ranging from 0.06 to 1.2 μg, also in 0.06 μg intervals. The mixed solutions then were recorded under the same spectroscopic conditions (parameters) which were introduced in the experimental protocol for bronchial washings in the baseline study.

Test Result: The test result of the experimental test set is presented in Table 5.3.3. As indicated in the classification matrix, 86.5% accuracy was obtained in predicting starch in plasma and 100% accuracy in classifying the non-starch group.

The high accuracy rate of prediction in the plasma samples is not surprising, since the probability distribution of the training set which was created from bronchial washings has a wide distribution profile. The probability of finding starch in plasma on the test set is distributed narrowly.

Table 5.3.3 LAD Classification for Experimental Test Set

Group		Actual		Percent correct
		Starch	No starch	
Predicted	Starch	96	15	86.5%
	No starch	0	101	100%

This is largely due to the compositional nature of the fluids. The bronchial washing fluids represent a complex biofluid matrix that involves many components contributed from the fluid and cells. The plasma is a homogenous solution that has fewer components which contributed to IR absorption signatures than the bronchial washings. The components in the bronchial washings, such as glycoproteins, glycolipids, surfactant, and other carbohydrate components found in the cells, result in a more complicated absorption profile in the sugar absorption region than that in the plasma spectrum. Such a compositional influence on IR absorption spectra will result in a wider distributed data profile in the classification analysis, as indicated in the training set built from bronchial washing fluids. This problem will also lower the sensitivity of detecting starch in the fluid. Therefore, the training set that is generated from bronchial washing fluids can be used as a prediction model for any other simple fluid matrix which has a narrower data distribution, such as plasma shown in this experimental test set. However, using plasma as a base to generate a training set and then using it to predict bronchial washings will not work well, and a large number of mis-classifications will occur. The detection limit is also dependent on the absorption profile in the sugar absorption region. The less the compositional variation, the higher the sensitivity of detecting HES in the fluids.

The establishment of the training set is crucial to the development of a direct method of diagnosing and monitoring ALI/ARDS. Once the test of the training set is completed and the results are satisfactory, the training set is then ready to be used to examine clinical data.

Low sensitivity, time-consuming, invasive procedures and inconsistent results complicate estimation of the severity of lung injury in the current clinical setting. The bronchial washing-IR assay method assessing pulmonary permeability introduced is intended to provide a simple and direct technique. The usefulness of this methodology in clinical investigations will be discussed in the following chapter, where the method will be applied in a safe and rapid fashion at the bedside, for early diagnosis and continued monitoring of critical ill patients.

Chapter 6

Clinical Investigations

The purpose of clinical investigation is to explore the possibility of applying the IR-bronchial washing technique to cases in clinical practice. A number of investigations will be reported in this chapter including an IR histochemical investigation of autopsy tissue from ARDS patient, a prospective study of the bronchial-washing assay method on a random patient population, as well as case investigations. Under these clinical investigations, the relationship between clinical diagnostic criteria and the IR measurements of pulmonary leakage will be evaluated. The significance of this new technique will also be discussed.

6.1 History and Definition of ALI/ARDS

Acute respiratory failure has been described in the literature as early as World War I, initially presenting following thoracic trauma. At the time of World War II, the syndrome was identified in conjunction with severe trauma sustained during wartime. In 1967, Ashbaugh (Ashbaugh, *et al.*, 1967) formally described this syndrome in 12 patients. Their attempt was to identify and unite a clinical presentation representing a common pathway of damage to the lungs. Ashbaugh and colleagues were the first to recognize ARDS as a distinct clinical entity. They noted that this condition had a mortality rate of 58%. Other terms such as "Shock lung" and "Da Nang lung" were also

used to describe the syndrome in the late 60s and early 70s. At that time, it appeared that the majority of patients succumbed from complications directly related to respiratory failure. Since then, a number of studies have focused on the survival rates associated with the syndrome. Despite advances in medical care, current studies have failed to show significant improvements in mortality rate (60-70%).

Recent studies (1994) demonstrate that 150,000 cases occur annually with overall mortality rates of 50 to 60 %. For ARDS patients, the time course of presentation indicates that 50% develop this syndrome within 24 hours, 80% within 72 hours and 90% within 5 days (Marinelli, *et al.*, 1994). The local experience with ARDS at the Health Sciences Center of the University of Manitoba consists of 687 cases diagnosed over ten years (1984-1994) with overall mortality rates of 37%. Among these patients, 60.4% were males and 39.6% were females. The average age of these patients was 61 with a range from 18 to 98 years.

Recently, a new term Acute Lung Injury (ALI) has been used frequently in the literature. The term first introduced in 1987 by J.F Murray whereby he attempted to ascribe a classification system in order to grade the severity of injury. The consensus conference (1992) has defined acute lung injury as "significant deterioration in lung function due to characteristic pathologic abnormalities in the lung's normal underlying structure or architecture". ARDS is defined as a severe form of acute lung injury. It is formally defined as "a specific form of injury characterized pathologically by diffuse alveolar damage and by breakdown in both membrane barriers. Alterations in the gas exchange functions of the lung result in proteinaceous alveolar edema and hypoxemia" (Bernard, *et al.*, 1993). The etiology of ARDS has still not been completely elucidated.

ARDS has been associated with diverse clinical conditions as a secondary process and, often predates the syndrome of multi organ failure. This definition includes two groups of patients with respiratory failure associated with increased pulmonary permeability, ALI and ARDS. ALI encompasses a much broader group of patients who may develop severe respiratory failure on the basis of the same pathologic mechanism as ARDS. However, these patients may not experience such a profound impairment in respiratory function, ventilatory dynamics and chest radiograph abnormalities classically associated with ARDS.

The introduction of ALI as a precursor to ARDS is intended to provide for early diagnosis and treatment. The focus of current medical therapy has shifted to early recognition and diagnosis of ARDS. Although there has been much effort directed at diagnosis and treatment, what has emerged is a broad consensus concerning issues of clinical presentation and supportive care in the ICU. There have been few clinical studies identifying the primary feature of ALI/ARDS: increased pulmonary capillary permeability. To demonstrate this finding in the clinical setting would certainly add a great diagnostic advantage to this controversial disease.

6.2 Diagnosis of ALI/ARDS

The Consensus Conference definition of ALI/ARDS suggests that better criteria are needed to establish a diagnosis of ARDS. Based on the definition, the main criteria diagnosing ARDS must include the following factors: the diffuse alveolar edema; significant increase in pulmonary vascular permeability; and pathologically, diffuse alveolar damage. Clinically, such diagnostic criteria are very difficult to obtain at the

bedside and, alternative methods must be used. The most widely accepted set of diagnostic criteria for ARDS was proposed by Murray and colleagues in mid 1980's, and is referred to as the Lung Injury Score (LIS) (Murray, *et al.*, 1988). The scoring system employs four parameters: chest X-ray evaluation, a hypoxemia score, respiratory system compliance score and positive end-expiratory pressure score (See Table 6.2.1). A study, based on 14 patients, showed that a significant correlation exists between the LIS and bedside measurements of lung vascular permeability (Sinclair, *et al.*, 1994). This study, however, includes only a small sample size. In order to establish an early diagnosis of ARDS, the Consensus Conference distinguishes criteria between ALI and ARDS that are based on the differences of PaO_2/FiO_2 ratio. $PaO_2/FiO_2 < 300$ mmHg is defined as ALI, and $PaO_2/FiO_2 < 200$ mmHg is ARDS in addition to the presence of bilateral infiltrates on chest X-ray, pulmonary arterial wedge below the hydrostatic pressure and underlying disease compatible with lung injury. Furthermore, Krafft (Krafft, *et al.*, 1996) argued that PaO_2/FiO_2 is the most important defining parameter in assessing ARDS severity. This may help in defining different states of acute lung injury. These measurements basically determine the pulmonary function. Although there is a relationship between pulmonary function and vascular leakage, the lung injury score alone fails to provide direct information on the vascular permeability during the edema process, the important pathophysiological figure of ALI/ARDS. In addition, the LIS has been shown to be unreliable on day 1(ARDS, Evans and Haslett, 1997) .

Several methods have been suggested to measure pulmonary permeability. These methods rely on the use of radioactive isotopes as tracers. Indicator-dilution methods introduce specifically labeled components, typically $^{3}H_2O$, ^{14}C-urea, ^{125}I-albumin and

^{51}Cr labelled red blood cells, into the blood stream (Goresky, *et al.*, 1967; Rinaldo *et al.*,1986; Harris, *et al.*, 1990). The time course of these tracers in the blood stream is then followed in a single pass requiring rapid and precisely timed arterial blood sampling. Based on partitioning models for the variously labeled components, permeability surface area for urea and extravascular volume of lung water (EVLW) can be determined. However, the soundness of model assumptions upon which the permeability surface area and EVLW measurements are based, is difficult to establish clinically. This is especially the case across the critical care population where vascular tone and tissue permeability characteristics vary considerably. The indicator dilution method has been found tedious and unreliable in practice at the bedside. External pulmonary gamma counting has the advantage of providing a more direct measure of tracer infiltration into the lung (Sugerman, *et al.*, 1980; Putensen, *et al.*, 1990). However, the technique is cumbersome and thus ill suited to routine patient monitoring in an intensive care unit environment. The reliance of both of these methods on radioactive tracers carries with it some safety questions as well as the associated ethical issues concerning the use of these tracers on a control population.

Consequently, the only way to accurately diagnose ARDS is by open lung biopsy a procedure which is usually not the best option, considering that this population of patients is too ill and usually deemed unsuitable for an operative procedure. Clearly, a better method is warranted to effectively diagnose ALI/ARDS, a procedure which is also minimally invasive and causes a minimal amount of trauma to these already critically ill patients.

Table 6.2.1. Murray's Lung Injury Score

Descriptions	Value
Chest Radiograph score:	
No Alveolar consolidation	0
Alveolar consolidation in 1 quadrant	1
Alveolar consolidation in 2 quadrants	2
Alveolar consolidation in 3 quadrants	3
Alveolar consolidation in all 4 quadrants	4
Hypoxemia score:	
$PaO_2/FiO_2 \geq 300$	0
PaO_2/FiO_2 225-299	1
PaO_2/FiO_2 175-224	2
PaO_2/FiO_2 100-174	3
$PaO_2/FiO_2 < 100$	4
Respiratory system compliance score (when ventilated) (ml/cm H_2O):	
≥ 80	
60-79	0
40-59	1
20-39	2
≤ 19	3
PEEP* score (when ventilated) (cm H_2O):	
≤ 5	0
6-8	1
8-11	2
12-14	3
≥ 15	4
The final score is obtained by dividing the aggregate sum by the number of components that were used:	
No injury	0
Mild to moderate injury	0.1-2.5
Severe injury (ARDS)	> 2.5

* **FiO_2 is the fraction of inspired oxygen and PEEP is the positive end-expiratory pressure.**

6.3 IR Histochemical Examination of Autopsy Tissue

IR histochemical analysis of lung tissue from an acute lung injury patient was performed by IR microspectroscopy. In this investigation, the IR microspectroscopic technique was

used to assess an acute lung injury patient's autopsy to determine HES distribution in the tissue.

6.3.1 Clinical Presentation

A 49-year–old–male patient presented to the trauma service at the Health Sciences Center, Winnipeg, Canada. He was involved in a motor vehicle accident resulting in a tractor-trailer rolling over him and sustained a fractured pelvis associated with a significant retroperitoneal hematoma. Over a 48-hr period, the patient developed acute lung injury/acute respiratory distress syndrome. He received antibiotics, ventilatory support and continuous venovenous hemodialysis. Low molecular weight hydroxyethyl starch, PENTASPAN®, was administered for oncotic manipulation. Analyzing the patient's bronchial washing fluids by IR spectroscopy demonstrated the presence of PENTASPAN®. The patient died four days post injury. Autopsy examination histologically showed evidence of ARDS.

6.3.2 Autopsy Tissue Preparation and IR Mapping

The autopsy specimen was obtained from the pathology department of Health Sciences Center, Winnipeg. Histological examinations of the specimen showed acute diffuse alveolar damage with hyaline membranes consistant with ARDS and a superimposed bronchopneumonia. See Fig. 6.3.1. For IR histochemical examination, the fresh tissue was quickly frozen in liquid nitrogen. The tissue was then kept in an –80 °C freezer until used. The fresh tissue was cut in 10 μm thick slices which were placed on a calcium fluoride window and allowed to dry at low temperature (-20 °C) in order to avoid diffusion of PENTASPAN®. No further tissue preparation was necessary.

Fig. 6.3.1 Microscopic section from autopsy lung showing acute diffuse alveolar damage with hyaline membrane (arrows) and superimposed bronchopneumonia (arrowhead). **4×magnification**

The IR microspectroscopic measurements of the lung tissue were performed with the EQUINOX 55 spectrometer attached an IR Microscope (Bruker, Germany) equipped with a MCT detector. An eyepiece with magnification of 4×, and a standard 15× IR objective were used for the IR microscopic measurements. Each IR spectrum was recorded at a resolution of 4 cm^{-1}, co-adding 64 scans. Measurement time was about 2 min/spectrum. Tissue sections to be examined were first viewed by the optical microscope objective in order to identify the areas of interest. The IR spectra were recorded by using a rectangular aperture size of 30 × 30 μm.

Spectra were recorded from two areas from the sliced tissue. The first area was 300×300 $(\mu m)^2$, and the second was 510×510 $(\mu m)^2$. These areas were randomly selected from the sliced tissue. The two maps respectively consisted of 100 and 289 individual spectra.

6.3.3 IR Microspectroscopic Analysis

The IR spectra of tissue share many features with biofluids. The major absorption bands are due to the protein, lipids and carbohydrate components. In order to investigate HES distribution on the tissue, the height of the peak at 1030 cm^{-1} (baseline corrected between 970-1186 cm^{-1}) was used as a parameter for the entire map. As discussed previously, the band at 1030 cm^{-1} is raised from the PENTASPAN®, and increasing rapidly as PENTASPAN® concentration increased. Fig. 6.3.2 shows two-dimensional spectroscopic images of the mapping areas as well as the sliced tissue (4× magnification). These spectroscopic images demonstrate that high concentration of PENTASPAN® is present and diffuse patterns can be seen in all of the tissue areas.

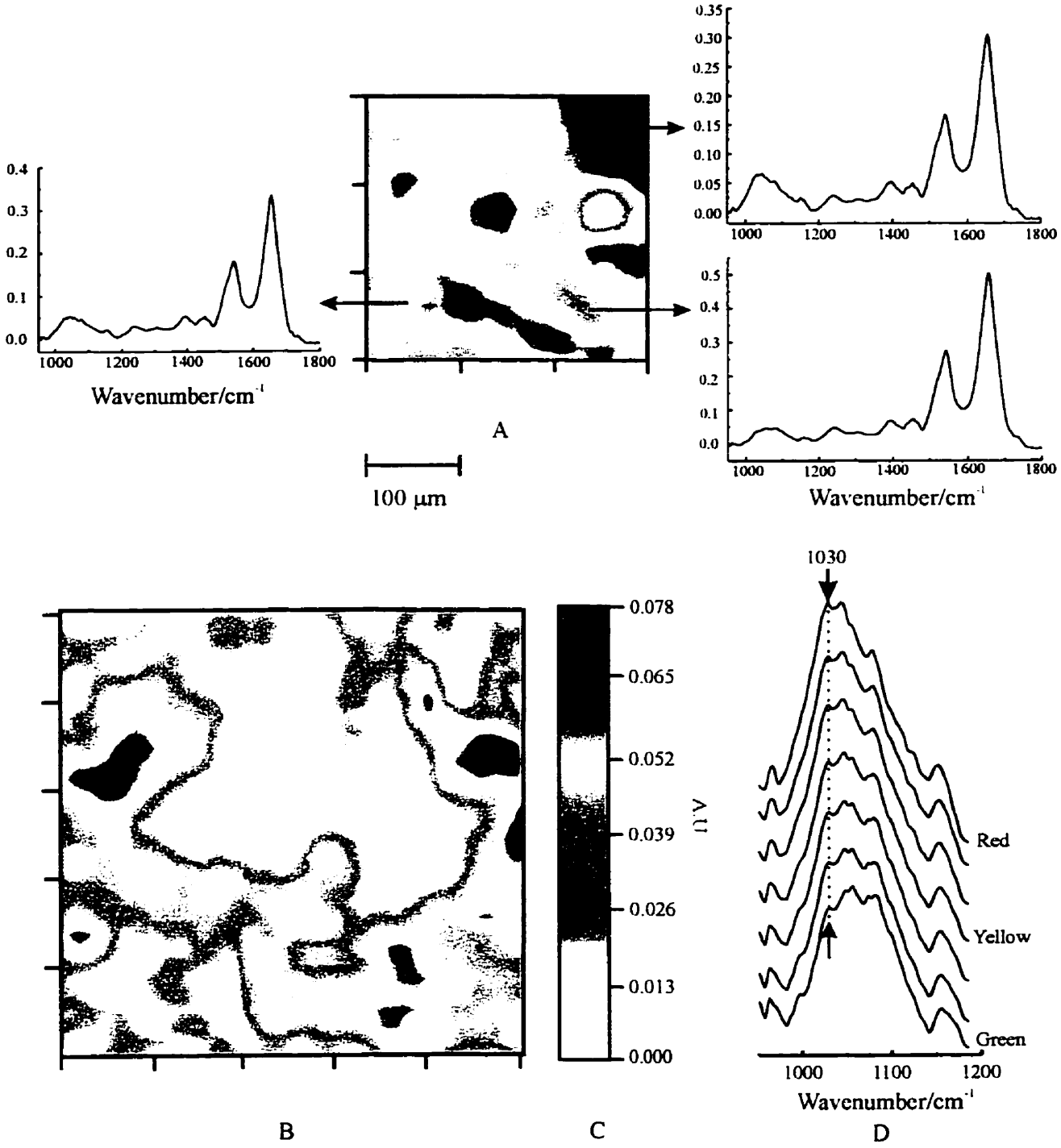

Fig. 6.3.2 IR microspectroscopic investigation of injured lung tissue. A, and B are the histochemical image of IR spectroscopic mapping based on HES distribution on the tissue. C is the color code and the corresponding intensities. D shows the representative spectral signature of color code.

In this investigation, use of a 30 × 30 μm aperture size produces sufficient quality of spectra with high signal-to-noise ratio. This aperture size defines the spatial resolution of the map by 30 × 30 μm. Generally, capillary size is less than approximately 10 μm. Only larger vessels have a size that is greater than 40μm. This spatial resolution will not be high enough to determine HES within the capillaries or the interstitial spaces. It is also not sensitive enough to evaluate small leakage. However, when the capillary membrane barriers are damaged as in a severe case, the HES will penetrate into tissue to a certain depth. If the diffused distance is greater than the spatial resolution of IR microscopy, HES is then detectable. Based on the evidence from the animal studies in chapter 4, PENTASPAN® does not leak out in uninjured tissue, so that when it is present in the tissue in large areas, this is highly suspect for an injury situation. In this investigation, the fact that HES was detected in tissue confirms a severe pathologic stage. The HES is diffused over 50 μm spatially in the tissue section, see Fig. 6.3.2.

The accuracy of determination of the severity of leakage in the tissue is limited by the spatial resolution of IR microscopy. Although the spatial resolution can be improved by reducing the IR aperture size, the signal-to-noise ratio of the spectrum, however, will be poorer as the aperture size decreases. Spatial resolution is restricted by diffraction limit. As the aperture size become smaller, high photon scattering are expected which results in fewer photons reaching the detector that the noise level of the spectrum will increase.

This investigation of autopsy tissue from an acute lung injury patient provides pathologic information of tissue injury. Indeed this is the first case of IR pathologic investigation of tissue microvascular injury. In contrast with pathology, the IR microscopic technique is operator independent once the methodology is in place. A

pathologic specimen requires a pathologist to interpret the slides. Although the diagnosis is based on pathologic evidence and rigid criteria, the actual diagnosis is always subject to the pathologist's own interpretation. Often there can be controversy and the final diagnosis may not be so clear. The advantage of IR microspectroscopy is such that it eliminates the subjectivity of interpretation. If starch is present in the tissue in sufficiently large area (much greater than the actual size of the capillaries), then there must be considerable injury to the capillary endothelium compatible with ARDS. Furthermore, IR microspectroscopy can be an aid to the pathologic diagnosis, especially when the pathologic indices are ambiguous.

The significance of this autopsy investigation is not the precise determination of HES distribution in injured tissue, rather it is the pathologic confirmation that using IR spectroscopy to assess pulmonary permeability in acute lung injury through analyzing bronchial washing fluids. A prospective investigation on a random patient population will be illustrated in next section.

6.4 Prospective Study of a Random Population

The investigations of bronchial washing fluids from ARDS patients clearly demonstrate the potential of determining capillary-alveolar leakage from these fluids. A prospective investigation in a randomized patient population was then designed. The objective of the study was to evaluate as a randomized trial, the diagnostic potential of the IR-bronchial washing technique for the determination of pulmonary permeability.

6.4.1 Study Design

The study was designed to evaluate a general patient population admitted to the Intensive Care Units (ICU) at the Health Sciences Centre, and ICU at the St. Boniface General Hospital, Winnipeg, Canada, during the period July 1995 to April 1996. The total population involved in the study was 85 patients. This study was approved by the University of Manitoba Ethics Committee for Human Research (*E95-28; "Comparative study of fluid removal versus oncotic agents in the management of ARDS"*). The study patient population was comprised primarily of postoperative and trauma patients. All patients enrolled in the study were scored according to the Murray criteria. More detailed information on patient population and diagnoses is provided in Table 6.4.1.

Patients enrolled in the study were divided into two groups; a risk group and an injury group. In the risk group, patients were selected with normal values of PaO_2/FiO_2 (> 300 mmHg). These patients were potentially at risk to develop acute lung injury based on the clinical impression of the attending physician. In the injury group, patients had PaO_2/FiO_2 < 300 mmHg. According to the Consensus Conference definition, these patients are defined as ALI and ARDS. Three sub-groups in this injury group were further stratified; the patients with $0 < PaO_2/FiO_2 < 100$ mmHg, $100 < PaO_2/FiO_2 < 200$ mmHg and $200 < PaO_2/FiO_2 < 300$ mmHg.

For ARDS patients, all of the criteria had to be met within 5 days of admission to the ICU for the case to be diagnosed as ARDS. These criteria include: (1) $PaO_2/FiO_2 <$ 200 mmHg with LIS ≥ 2.5. Patients who had PaO_2/FiO_2 slightly over 200 mmHg but LIS > 2.5 also considered as ARDS by clinical decision. (2) bilateral infiltrates seen on anteroposterior chest radiograph, and (3) no clinical evidence of increased capillary

wedge pressures (pulmonary artery occlusion pressure ≤18 mmHg) in order to exclude patients with hydrostatic edema and (4) underlying disease compatible with ARDS. All patients admitted into the study were intubated, and received PENTASPAN® (DuPont Pharma.). Some patients received PENTASPAN® in multiple doses. Most of them were on positive pressure ventilation. Bronchial washing samples were collected within 26 hours of PENTASPAN® infusion and following the same protocol as used in the baseline study. Samples were immediately refrigerated and assayed within 24 hours of collection. The sample preparation and IR measurement also follow the same protocol as was introduced in the baseline study.

6.4.2 Data Analysis

A total of 72 spectra were recorded successfully from 85 patients. Samples from 13 patients were not used for analysis due to the poor spectral quality, including low IR absorption and drug contamination, which changes the spectral signature. In addition, a number of 5 spectra were withdrawn from these 72 spectra since 10 patients contributed samples twice over a short period of time. Although these spectra can be used for classification purposes, the lung injury score and PaO_2/FiO_2 ratio, however, did not change during that period. It would not be appropriate to use these data for comparison. Thus, 67 patient spectra were used for data analysis in the study. Applying the training set established previously, the probability of leak is determined and presented in Table 6.4.1.

Using the criteria introduced in the Consensus Conference, a comparison can be made based on the PaO_2/FiO_2 and the probability of leakage, which was determined by IR method. Patients were divided into two groups in this comparison: the injury group

Table 6.4.1

Probability of Leakage and Clinical Data for Patients in the Study

Patient ID	Probability of Leakage	LIS	PaO_2/FiO_2 (mm Hg)
1	1	3.5	84
2	0.9979	2.75	215
3	1	3.5	58
4	0.9988	2	152
5	0.7918	3.25	74
6	0.9998	3.25	72
7	0.999	3.25	86
8	0.6807	3	124
9	0.9995	2.5	94
10	1	2.75	55
11	0.8472	0.75	290
12	0.7983	0	480
13	0.8951	0.75	225
14	1	1	150
15	0.4308	1.75	255
16	0.9998	0.5	283
17	0.2781	1.75	230
18	0.0388	0	452
19	0.1695	2	164
20	0.2279	1.75	170
21	0.556	0.33	280
22	0.0443	0.33	275
23	0.8292	1	218
24	0.0718	1.67	113
25	0.1241	0.5	406
26	0.4747	0.5	320
27	0.1862	1.25	155
28	0.1623	1.5	136
29	0.9682	1.75	370
30	0.5688	1.33	197
31	0.2205	1.7	180
32	0.3279	2.67	123
33	0.564	1.75	206
34	0.2	1.3	173
35	0	1.25	223

Patient ID	Probability of Leakage	LIS	PaO_2/FiO_2 (mm Hg)
36	0.5003	2.23	132
37	0.9994	2.5	152
38	0.9786	1.75	170
39	0.924	1.75	235
40	0.8002	1	192
41	0.5552	1.25	295
42	0.01	0.75	354
43	0.9354	0.75	242
44	0.8352	1.25	214
45	0.9781	2.5	74
46	0.9583	2.5	96
47	0.9932	2.5	150
48	0.541	1.5	310
49	0.9993	2.25	90
50	0.7834	1	366
51	0.9798	2.25	111
52	0.2495	2.25	160
53	0.9905	0.5	320
54	0.9347	1	267
55	0.5487	2	170
56	0.9897	2.25	242
57	0.9847	2.25	147
58	0.42	1	268
59	0.912	0.75	378
60	0.0649	1.25	337
61	0.8666	0.3	247
62	0.305	1.5	170
63	0.9981	2.25	242
64	0.8874	1.5	220
65	0.6857	1.5	155
66	0.9844	1.5	292
67	0.9122	1	350

and the risk group. Patients who had $PaO_2/FiO_2 < 300$ mmHg were considered as injured and including both ARDS and ALI, a total of 55 patients are in this group. Patients having $PaO_2/FiO_2 > 300$ mmHg are in the risk group, 12 patients involved in this group. A general 2×2 contingency table is constructed based on PaO_2/FiO_2 and IR spectra classification, see Table 6.4.2.

Table 6.4.2. Comparison of Clinical Data and Leakage

	Injury Group (PaO_2/FiO_2<300 mmHg)	**Risk Group (PaO_2/FiO_2>300 mmHg)**
IR Positive for Leakage	40	7
IR Negative for Leakage	15	5
Total	55	12

- Note: those patients with probability of leakage greater than 50% are considered as IR-positive (leak patients) and these with probability less than 50% are considered as IR-negative (non-leak patients).

To evaluate the relationship between PaO_2/FiO_2 and IR measurements, the sensitivity and specificity of the data set were calculated. According to the Table, 40 of 55 injured patients show IR positive for leakage, which given the sensitivity of 72.7%, and 5 of 12 risk patients apparently show IR negative for leakage, the specificity is 42%. These results represent a strong relationship between the ratio of PaO_2/FiO_2 and the IR measurements for ARDS and ALI patients with high sensitivity. This implies that in most of the injured patients, IR detected the leakage. The technique was successful in identifying patients with this lung pathology.

Since it is well known that ARDS may take up to 48 hours (Marinelli) to demonstrate overt clinical features, for example, classic chest X-ray findings, these

patients may have very well developed later into the classic ARDS models. Furthermore, the group at risk may still be susceptible to developing ARDS/ALI and the IR method detected leakage in these patients at an early stage in the course of their disease. Already, there is much evidence supporting the theory of "ARDS prophylaxis".

The significance of identifying a leak in the "at risk" group can not be underestimated since this would imply aggressively treating these patients in order to prevent future complications and further lung insult. There are many reasons as to why the patients in the risk group may be subject to a low leakage rate, since many clinical conditions may cause even indirect injury to the lung through inflammatory mediators (cytokines and leukotrienes).

In order to evaluate the leakage associated with the degree of injury, an additional comparison was made on patients within the injury group (55 patients). In this comparison, patients are subdivided into three groups; (1) a group of patients with severe ARDS who had PaO_2/FiO_2 ratio between 0 and 100 mmHg (10 patients included in this sub-group). (2) A group of ARDS patients with PaO_2/FiO_2 ratio between 100 and 200 mmHg, 23 patients involved in this sub-group. (3) A group of patients with ALI who had the PaO_2/FiO_2 ratio between 200 and 300 mmHg, 22 patients are included. Results of this comparison are presented in Table 6.4.3. With severe cases of ARDS ($0<PaO_2/FiO_2<100$ mm Hg), all patients (100%) were found IR-positive for HES leakage by using the IR-bronchial washing method. In the group $100<PaO_2/FiO_2<200$ mmHg, 56.5% patient population showed IR-positive for HES leakage. This finding indicates that using the PaO_2/FiO_2 ratio to define ARDS patients is not pathophysiologically specific for syndrome. 77.3% patient population in the group $200<PaO_2/FiO_2<300$ mmHg identified

IR-positive for leakage, which significantly indicated the methodology has an early diagnostic value.

Table 6.4.3 Comparison of Leakage in the Injury Population

	$0<PaO_2/FiO_2<100$ (mmHg)	$100<PaO_2/FiO_2<200$ (mmHg)	$200<PaO_2/FiO_2<300$ (mmHg)
IR positive for Leakage	10	13	17
IR negative for leakage	0	10	5
Total	10	23	22

Table 6.4.2 shows that 58% of non-injured patients (7/12) also presented leakage. A number of reasons can be used to explain this result. First, patients in the risk group had a high potential for developing acute lung injury. Therefore, finding that these patients are associated with leakage might suggest that these patients actually had a low degree of injury due to the defect of capillary-alveolar membrane barriers. In the clinical setting, this suggests that the IR method may be a useful screening test in the early diagnosis of patients who are suspected having an acute lung injury.

As mentioned earlier, the ratio of PaO_2/FiO_2 measures the pulmonary function rather than addressing the pathophysiologic changes in pulmonary vascular permeability. In this sense, the IR technique could provide an additional parameter in diagnosis of ALI/ARDS. If this technique is to obtain clinical validity in the diagnosis of ARDS and in the identification of at-risk patients, then its application must also be balanced with the clinical picture.

6.4.3 Regression Analysis Approach

The purpose of applying regression analysis is to explore the relationship between clinical criteria and the permeability parameters obtained from IR measurements in terms of probability of leakage. The clinical diagnostic criterion is the PO_2/FiO_2 since it is easier to obtain clinically, and it is the definition of ARDS and ALI according to the consensus conference.

A linear regression analysis was performed on the data set by using commercially available software (*Statistica*™, StatSoft, Tulsa, OK). The probability for leakage was chosen to be the independent variable and PaO_2/FiO_2 to be the dependent variable for the analysis. The regression coefficient is determined to be R^2=0.4692 with p<0.0783 (statistically, p<0.05 considered to be significant). Thus, an obvious conclusion is that there is a poor correlation between the PaO_2/FiO_2 ratio and the probability of leakage. The regression equation therefore cannot be used for prediction. Considering that the sample size is small, the statistical significance may be improved by increasing the patient population.

The fact that nearly all ARDS patients can be detected HES leakage by the IR-bronchial washing assay method. The regression analysis indicates the PaO_2/FiO_2 ratio and the IR assessment of pulmonary permeability provide two independent parameters in diagnosing ALI/ARDS. As discussed previously, neither the PaO_2/FiO_2 ratio nor the LIS are reliable predictors for ALI and ARDS. These parameters provide a measure of the patient's pulmonary function abnormality and the IR-bronchial washing assay method provides pathophysiological evidence of acute lung injury. In cases where the patient's LIS was not classically diagnostic of ALI/ARDS, the IR assay method did indicate these

patients were susceptible to the pathophysiological changes of ALI/ARDS, implying damage to the pulmonary alveolar-capillary membrane barrier. Therefore, one can suggest that, rather than using one parameter to predict another, it might be more useful to use both parameters to complement each other in diagnosing and monitoring ALI/ARDS patients.

The prospective study concludes that the IR-bronchial washing assay method is highly sensitive in determining the pulmonary leakage in the cases of ARD. It also has a high sensitivity for evaluating the pulmonary leakage in those patients who have acute lung injury, the early stage of ARDS. This strongly suggests that the method has a high value for the early diagnosis of ARDS, which is especially important for supportive treatment. The overall specificity in the study was not high (42%). This is largely due to the data size in the risk group. The specificity would improve, presumably, by increasing the size of the study population.

6.5 Case Investigations

Over the past three years, a number of ALI/ARDS patients were investigated by the recently introduced IR-bronchial washing technique. In most of these case studies, the IR method proved worthwhile in providing information on alveolar permeability. In this chapter, we will report two of these cases in which the new methodology has been applied.

6.5.1 Monitoring of the Double-Lung Transplant Patient

Lung transplant has become a standard treatment modality in endstage pulmonary disease. A number of complications may occur in the transplant lung recipients. In the

period immediately posttransplant, patients are followed closely in the ICU, being particularly at risk for the development of acute lung injury or ARDS. Therefore, during this period, it is crucial to diagnose ALI/ARDS in order to prevent future complications. In investigating the possibility of ARDS in this patient, the IR-bronchial washing methodology was applied to the patient over a 30-day period posttransplant. The IR-bronchial washing technique has proven invaluable as an aid in monitoring whether the patient undergoes pathophysiological changes of ALI/ARDS during the period of stay in the ICU. In the investigation, both plasma and bronchial washing samples were collected and analyzed, as well as other clinical parameters including plasma COP, LIS and PaO_2/FIO_2.

Case presentation: The patient was a forty-nine year old female with endstage emphysema. Her past medical history included only hypertension for which she was placed on propanolol. This patient had extreme exertional dyspnea, being unable to walk up a flight of stairs without experiencing shortness of breath. She had only a twenty-pack year history of smoking. She was then referred for double lung transplantation for chronic emphysema. She underwent surgery on August 1, 1994. The surgery itself was uncomplicated. Postoperatively, the patient developed worsening oxygen exchange and respiratory decompensation. She was reintubated in the intensive care unit and her PaO_2/FiO_2 ratio was < 100 mmHg, with bilateral hazy infiltrates seen on chest films. A clinical diagnosis was made at this time of adult respiratory distress syndrome. The bronchial washing fluids were collected start from August 5, 1994, 4 days post operation.

Analysis: During the time of patient stay in the ICU, a number of clinical data were collected for the analysis in both diagnosis and oncotic fluid management purposes. The

data include PaO_2/FiO_2 and plasma colloid oncotic pressure. The patient's pulmonary alveolar-capillary leakage is given by *posterior* probabilities that were predicted by using the training set introduced in last chapter. Fig. 6.5.1 presents patient's data post transplant over 30 days period during the time of staying at ICU. Fig. 6.5.1 A is a plot of PaO_2/FiO_2 ratio, the period of ARDS is indicated ($PaO_2/FiO_2 < 200$ mmHg). Fig. 6.5.1 B illustrates the probability of HES leakage, the high probability of leak agrees with the period that patient developed ARDS. Fig. 6.5.1 C and D are the PENTASPAN® concentration profile, and patient's plasma osmotic pressure profile during the time of IUC monitoring respectively.

Clinical Relevance: Any transplanted lung will develop some form of membrane permeability defect in the early postoperative period. Depending on the adequacy of preservation, pulmonary edema can be observed in up to one-third of lung transplant recipients (Shennib, *et al.*, 1994). This early edematous state has been termed the pulmonary postimplantation response and has been attributed primarily to ischemia reperfusion injury that occurs during organ procurement and implantation. Thus, the underlying diagnosis is an important patient management issue immediately posttransplantation. The postoperative ICU period is a critical time for lung transplant recipients. During this period, intensive care monitoring, ventilatory support, and fiberoptic bronchoscopy are important in the management of patients in respiratory failure. The major contributory factors to postoperative complications in the post transplant period are immunosuppression, reperfusion injury and rejection. ALI/ARDS is a devastating potential postoperative complication in these patients, which must be recognized and treated early (Cooper, 1989).

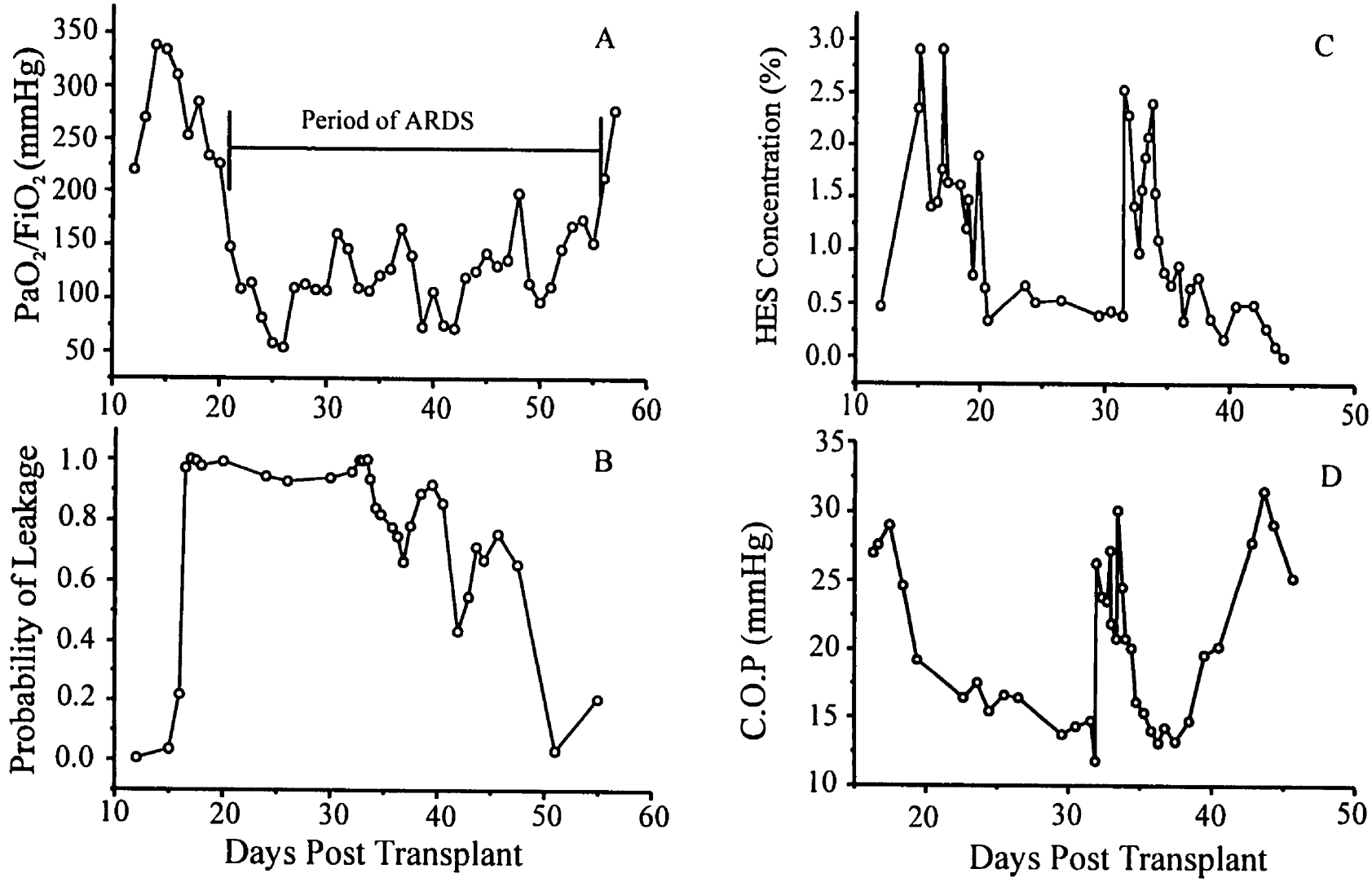

Fig. 6.5.1 Patient's data post transplant. A: PaO_2/FiO_2, B: Probability of HES leakage; C: HES concentration profile (%); and D: Plasma C.O.P (mmHg).

Often there is also an associated risk of acute rejection, it then becomes very difficult to distinguish between ARDS and rejection, which implies entirely different management decisions. It cannot be overemphasized why an early diagnosis would benefit the patient. Pulmonary transplantation results in alterations in lung physiology that are not normally seen under ordinary circumstances. The occurrence of acute lung injury in lung transplant patients, physiologically, is believed to be due to the ischemic insult, as well as from injury occurring at the time of reperfusion of the ischemic donor organ.

A number of experimental models of acute lung injury implicate oxygen free radicals as a factor in the genesis of reperfusion injury. A significant early change in lung permeability is seen after an ischemic period followed by reperfusion (Greenfield, *et. al.*, 1993).

6.5.2 ARDS Patient on Oncotic Manipulation

Case history and presentation: A 61 year-old man presented to Health Sciences Center, Winnipeg on October 6, 1997 with iron deficiency anemia and haematemesis for which he underwent gastroscopy. At the time of endoscopy, the patient aspirated a large amount of gastric contents, resulting in respiratory distress and decreased level of consciousness. The patient has a past medical history of noninsulin-dependent diabetes mellitis, for which he was managed alone with oral hypoglycemics and had a previous left below knee amputation for peripheral vascular disease. The patient had a 50 pack-year history of smoking, and no other associated medical conditions. The family denied symptomatic heart disease. The patient also had known colon cancer for which a sigmoid resection was planned in early January.

The patient was managed presumptively on the ward as having aspiration pneumonia after chest x-ray showed bilateral lower lobe infiltrates. He was placed on intravenous antibiotics, namely, a third generation cephalosporin, and treated with chest physiotherapy. Four days later, the patient was noted to be in worsening respiratory distress. His oxygen saturation on 50% inspired oxygen was only 88%; in addition, he was tachypneic, with increased respiratory excursions.

The patient was intubated, and transferred to the Medical Intensive Care Unit at November 16, 1997. At this time, optimal PEEP was 8, and the compliance was 32, well below the normal of 80. In addition, despite albumin+diuretic therapy, the patient had a PaO_2/ FiO_2 ratio of 120. At 14:00 November 17, 1997, his lung injury score was 3.0, classifying him as having severe lung injury compatible with ARDS. After a family discussion, we obtained informed consent. Consequently, we enrolled him randomly into our comparative management trial. The patient died on Dec 17, 1997, of complications unrelated to ARDS; namely, nosocomial pseudomonas pneumonia on a medical ward acquired 4 weeks after he was successfully treated with hyperoncotic manipulation. The patient's death was considered unrelated to his initial diagnosis of ARDS in the ICU. The family consented to withdrawing treatment and declined autopsy.

Sample collection and IR spectra analysis: The patient received the first PENTASPAN at 23:00 hours November 17, 1997. A blood sample was collected before the infusion for the baseline. The bronchial washings were collected start from 00:45 hours and then continuously collected at one, two, four, eight, twelve and twenty-four hours time interval. Samples were analyzed within 12 hours following collection. Table 6.5.1 gives the probability of leakage and the classification. The classification information in the

table is predicted by the LDA training set introduced previously. Fig 6.5.2 is the clinical data illustration for the patient over the period of time during oncotic manipulation and probability of leakage in the first 24 hours.

Clinical Significance: The IR-bronchial washing method aids in determining the pulmonary leakage and benefits an early diagnosis of ALI/ARDS. The patient in this study was well defined as having ARDS and closely followed by the new methodology. The fact that the first hour after PENTASPAN® infusion verifies that IR measurement can already indicate the leakage of HES. This strongly supports that at a severe degree of acute lung injury as ARDS, supporting that the technique does indeed provide a fast and early identification of severe pulmonary leakage.

This patient was randomized to the treatment arm of the study. He was aggressively diuresed to achieve a fluid balance of negative 17.0 L. Early fluid restriction improved his PaO_2/FiO_2 ratio and the patient had a well above normal PaO_2/FiO_2 following early aggressive treatment. Despite the continued leakage of PENTASPAN® identified by IR, the patient improved all his Murray parameters and respiratory mechanics within the first 24 hours of diagnosis and treatment. The actual lung injury was likely still present. Once treatment was initiated, the patient improved dramatically (see Fig. 6.5.2A). The insult to his lungs was not immediately reversible and continued leakage of PENTASPAN® in the bronchial washings does not imply treatment failure, rather, this patient demonstrates that early recognition of lung injury benefits early aggressive support. (Marino, ICU book, First edition, Lea and Febiger Lit, 1991,)

In the previous case, the patient's bronchial washings were used primarily for monitoring of the progression of her disease. In the latter case, the prospective study is

aimed at the identification of HES *prior to* active treatment as a diagnostic tool. We would anticipate, had further samples been retrieved that the lung injury would continue to improve. It is well documented that the PaO_2/FiO_2 is the parameter most subject to change in the course of this disease.

Table 6.5.1 Probability of leakage in 24 hours

Samples	Time of collection (Hours)	Probability of leak	Classification *
1	0 (baseline)	0.2396	2
2	1	0.5575	1
3	2	0.6403	1
4	4	0.8702	1
5	8	0.9922	1
6	16	0.9957	1
7	24	0.9999	1

* Classification "1" and "2" represent "leak" and "non-Leak" group respectively

Table 6.5.2 Patient's clinical information

Time (Hours)	PaO_2/FiO_2 (mmHg)	Murray LIS	HES Infusion (ml)
0	120	3	
4	98.46	3	500
8	136.67	2.75	1500
12	127.14	2.5	
16	173.33	2.25	1500
20	216	1.75	
24	327.5	1	1500

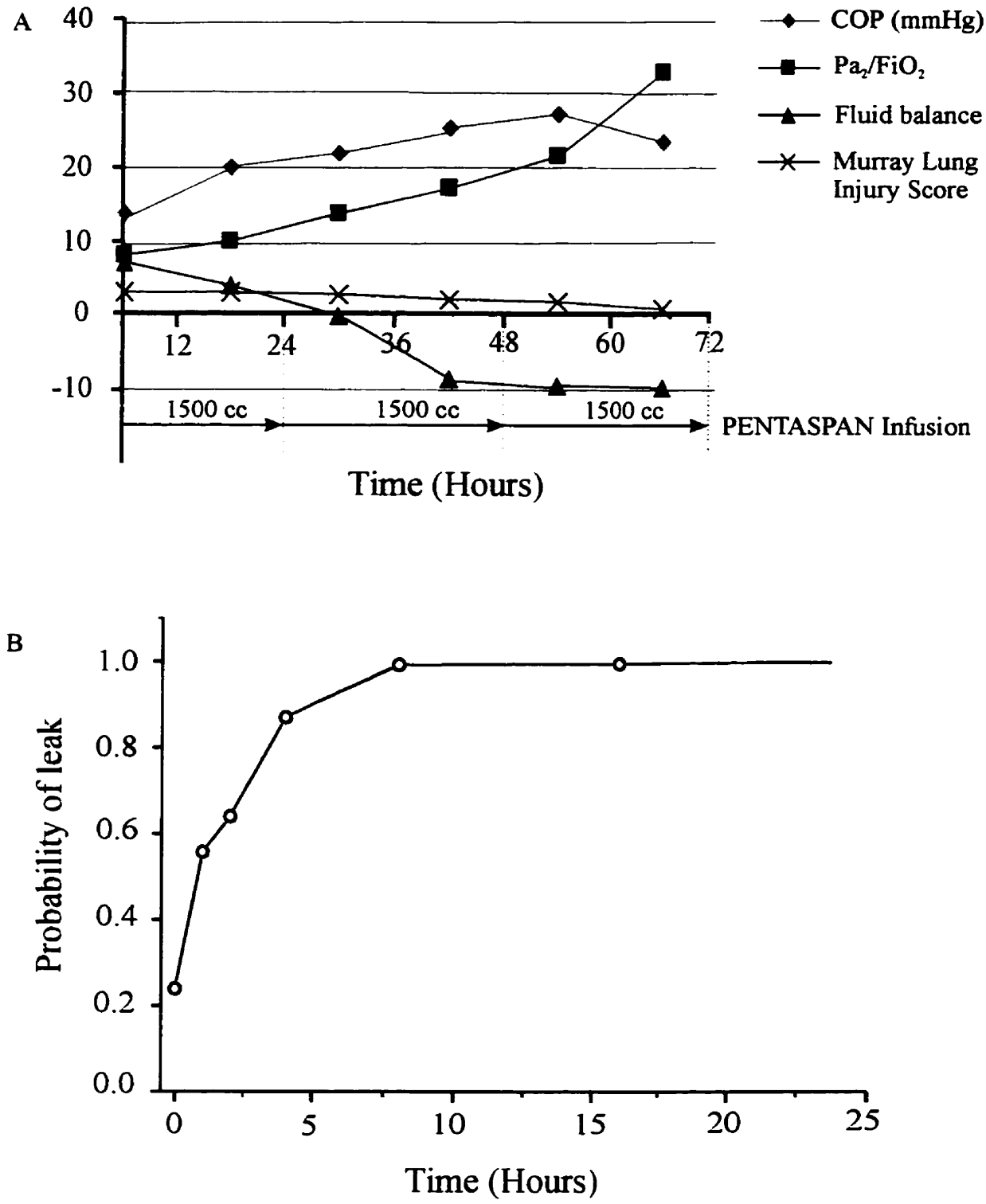

Fig. 6.5.2. A: Clinical data illustrations for the patient over the period of time during oncotic manipulation. B: time course of the probability for leakage in first 24 hours.

Conclusion

This research has introduced a novel and direct approach to determining capillary-alveolar permeability in acute lung injury. To comprehend this new methodology, the background and pathophysiology of acute lung injury was thoroughly discussed. In order to understand capillary leakage and pulmonary edema, forces governing fluid transport across transcapillary membrane barrier and capillary-alveolar membrane permeability properties were introduced. The theory and mathematical expressions of transvascular fluid flux illustrate the physical model of macromolecular exchange across the capillary membrane barrier. Manipulation of fluid filtration rates at the microvascular level based on the physical model is an application of the theory and is an important treatment strategy in noncardiogenic pulmonary edema in critically ill patients. The introduction of hydroxyethyl starch into this treatment strategy is critical to the success of this new diagnostic and treatment methodology.

The use of the IR spectroscopic technique in the assessment of capillary-alveolar permeability is a major development. Through experimentation using isolated canine lobes, the technique and sampling collection protocols were established and standardized. The thiourea-induced injury has profound similarities to ALI/ARDS in the acute consequences, and has been confirmed by pathologic evidence, as well as by a more recently introduced IR microspectroscopy. The animal injury model has confirmed that bronchial fluid collection and content identification through IR spectroscopy is feasible. Classically, animal research has predated clinical trials. Determining HES in human bronchial washing fluids with a high sensitivity index is more complex than using animal

biofluid, however, the strength of the animal studies has encouraged this research to progress further into the clinical setting. The use of the generic algorithm for near optimal IR spectral regional selection (for feature space reduction), and spectral pattern recognition illustrates a new dimension of spectroscopic diagnosis. The probability of pulmonary leakage parameter, determined by spectral pattern recognition, provides useful information as to the presence of a permeability-induced lesion in the ICU patient.

Despite advances in supportive care, survival rates for ARDS remain unchanged since the syndrome was first described. To date, there has been very little research addressing the primary pathophysiology. The IR-bronchial washing method, introduced for assessing permeability at the bedside, will facilitate an early diagnosis of ALI/ARDS in the ICU setting and improve monitoring of patients treated by hyperoncotic manipulation. Early intervention may be the only way to reduce the high mortality associated with this condition and possibly prevent failure of other organ systems, which is the eventual cause of death in this population. Although many methods have already been introduced for this purpose, they have failed to meet clinical requirements. The advantage of the IR-bronchial washing assay method is the high sensitivity and accurate reflection of the true pathophysiologic changes of acute lung injury. It is a safe, noninvasive, inexpensive, operator independent and rapid technique. A number of clinical dilemmas, as demonstrated in chapter 6, have been resolved using this technique. The method has performed well in diagnosis and monitoring, which suggests that the technique has great potential for clinical application because it is able to function at both these levels. In addition, the sample collection does not require a physician. Although, using bronchial washings has proven slightly less sensitive when compared to BALF, this

technique is included in the daily pulmonary toilet of all intubated ICU patients. In effect, the use of this assay method does not require an additional procedure, eliminating any further trauma or risk to the patient.

This method is a new application for IR spectroscopy in clinical science. It will likely prove to be valuable in patient diagnosis and monitoring of acute lung injury. As with most other diagnostic strategies which have been introduced, areas exist which can be improved upon in the future.

From a future perspective, improving the sensitivity of the prediction model will likely mandate a larger non-leak study population. Increasing the randomized prospective study population with ALI patients is necessary in order to expand our knowledge and improve specificity. Given that the study was conducted at a single institution, recruitment of patients was substantially smaller than anticipated. The ideal validation would be for this study to continue as a multi-center trial to generate a large database and improve the sensitivity of assessing this direct technique in diagnosing ALI/ARDS. There is every confidence that this technique will prove invaluable in the diagnosis of this controversial and often misdiagnosed disease.

Bibliography

Adair, T. H., Moffatt. D. S., Paulsen, A. W., and Guyton, A. C., Quantitative of changes in lymph protein concentration during lymph node transit. *Am. J. Physiol.* **243** (Heart circ. Physiol. 12): H351-H359, 1982.

Alberle, D. R., Wiener-Kronish, J. P., Webb, W. R. and Mattay, M. A., Hydrostatic versus increased permeability pulmonary edema: Diagnosis based on radiographic criteria in critically ill patients. *Radiology*, **168**: 73-79,1988.

Anderson, J. L. and Malone, D., Mechanism of osmotic flow in porous membranes. *Biophysical Journal*, 14: 957-982, 1974.

Ashbaugh, D. G., Bigelow, D. G., Petty, T. L., Acute respiratory distress in adults. *Lancet* **2:** 319, 1967.

Basran, G. S., Byrne, A. J. and Hardy, J. G., A noninvasive technique for monitoring lung vascular permeability in man. *Nuclear Medicine Communications*, **3:** 3-10, 1985.

Bernard. G. R., Artigas, A., Brigham, K. L., Carlet, J., Hudson, L., Lamy, M., LeGall, J. R., Morris, A., Spragg, R., The consensus Committee. Report of the American-European consensus conference on ARDS: definitions, mechanisms, relevant outcomes and clinical trial coordination. *Intensive Care Med*, **20**: 225-232, 1994.

Blake, L. H. and Staub, N.C., Pulmonary vascular transport in sheep: A Mathematical model. *Microvascular Reserach*, **12**: 197-220, 1976.

Fawcett, D. W, *A textbook of Histology*, 20Th edition, Chapman & Hall, New York, 1994.

Baughman, R. P., Bosken, C. H., Loudon L. G., Hurtubise P., and Wesseler, T., Quantitative of bronchoalveolar lavage with methylene blue. *Am. Rev. Respir. Dis.* **128**: 226-270, 1983.

Braude, S., Nolop, K. B., Hughes, J. M. B., Barnes, P. J. and Royston, D., Comparison of lung injury vascular and epithelial permeability indices in the adult respiratory distress syndrome. *Am. Rev. Repir. Dis.* **133:** 10002-1005, 1986.

Brereton, R. G. *Chemometrics; application of mathematics and statistics to laboratory systems* Ellis Horwood Limited, West Sussex, England, 1990.

Byrne, K., and Sugerman H. J., Experimental and clinical assessment of lung injury by measurement of extravascular lung water and transcapillary protein flux in ARDS: A review of current techniques. *Journal of Surgical Research* 44**:** 185-203, 1988.

Cael, J., Koenig, J. and Blawell, J., Infrared and Raman spectroscopy of carbohydrates. 3. Raman spectra of the polymorphic forms of amylose. *Carbohydrate Res.* **29:** 123-34, 1973.

Carlson, R.W., Schaeffer, Jr. R. C., Whigham, H., Rattlesnake venom shock in the rat: development of a method. *Am. J. Physiol.* **229**: 1668, 1975.

Carlson, R.W., Schaeffer, Jr. R. C., Puri V. K., Hypovolemia and permeability pulmonary edema associated with anaphylaxis. *Crit. Care Med.* **9:** 883, 1981.

Carlson, R.W., Rattan, S., Haupt, M. T., Fluid resuscitation in conditions of increased permeability. *Anesthesiol Rev.* **17**: 14, 1990.

Centeno, J. A., Johnson, F. B., Microscopic identification of silicone in human breast tissue by infrared microspectroscopy and X-ray microanalysis. *Appl. Spectrosc.* **47**: 341-345, 1993.

Choo, L. P., Wetzel, D. L., Halliday, W. C., Jackson, M., LeVine, S. M. and Mantsch, H. H., In situ characterization of β-amyloid in Alzheimer diseased tissue by synchrotron Fourier transform infrared microspectrscopy. *Biophysical Journal*, **71**: 1672-1679, 1996.

Cooper, J. D., Lung Transplantation. *Ann. Thoracic Surg.* **47**: 28, 1989.

Cotran, R. S., Kumar, V., Robbin, S. L., *Pathologic basis of disease; Chapter 15.* 5th edition, V.B Saunders Company, Philadelphia, Pennsylvania, 1994.

Dauber, I. M., Pluss, W. T., VenGrondelle, A., Trow, R. S. and Weil, J. V., Specificity and sensitivity of noninvasive measurement of pulmonary vascular protein leak. *J. Appl. Physiol.* **50**: 564-574, 1985.

DeFouw, D. O., Meyenhofer; M. F., Rizzo, V. J. and Henry, C. B. S., Ultrastructural aspects of capillary barrier functions after injury. *In Reperfusion injuries and clinical capillary leak syndrome*, edited by Zikria, Futura Publishing Company, New York, 1994.

Demling, R. H, The modern version of adult respiratory distress syndrome. *Annu. Rev. Med.* **4**: 193-202, 1995.

Doyle, R. L., Szaflarski, N., Modin, G. W., Identification of patients with acute lung injury. *Am. J. Respir. Crit. Care Me.*, **152**: 1818-1824, 1995.

Drake, R., Gaar, M. K. A. and Taylor, A. E., Estimation of the filtration coefficient of pulmonary exchange vessels. *Am. J. Physiol.* **234** (*Heart Cric. Physiol.* 3): H266-H274, 1978.

Drake, R. E., Smith, J. H. and Gabel, J. C., Estimation of the filtration coefficient in intact dog lungs. *Am. J. Physiolo.* **238** (*Heart Cric. Physiol.* 7): H430-H438, 1980.

Drake, R., Giesler; M., Laine, G., Gabel, J. and Hasen, T., Effect of outflow pressure on lung lymph flow in unanesthetized sheep. *J. Appl. Physiol.* **58**: 70-76, 1985.

Drinker, C. K. and Hardenbergh, E., Acyte effect upon the lungs of dogs of large intravenous doses of alpha-naphthyl thiourea (ANTU). **15**: 35-43, January 1949

El-Hinnawy, S. I., El-Saied, H. M., Fahmy, A., Infrared and X-Ray Analysis of Hydroxyethyl starch. *Starch/Stärke*, **34**: 92-95, 1982.

Eysel, H. H., Jackson, M., Nikulin, A., Somorjai, R. L., Thomson, G. T. D., and Mantsch, H. H., A novel diagnostic test for arthritis: Multivariate analysis of infrared spectra of synovial fluid. *Biospectroscopy*, **3:** 161-167, 1997.

Fabian, H., Jackson, J., Murphy, L., Watson, P. H., Fichtner, I and Mantsch, H. H., A comparative infrared spectroscopic study of human breast tumors and breast tumor cell. *Biospectroscopy*, **1**: 27-45, 1995.

Fein, A; Grossman, R. F; Jones, J. G; Overland, E; Pitts, L; Murry, J. F; Staub, N. G. The value of edema fluid protein measurement in patietns with pulmonary edema. *The American Journal of Medicine* **67**, 32-38, July 1979.

Fisher, R.A., The use of multiple measurements in taxonomic problems. *Annals of Eugenics*, **7**: 179-88, 1936.

Frostell, C. G., Lung permeability and other pathophysiological lung problem in shock. *Acta Anaesthesiol Scand* **37**: Supplementum **98**: 11-13, 1993.

Gaar, Jr. K. A., Taylor, A.E., Owens, J. L. and Guyton, A. C., Effect of capillary pressure and plasma protein on development of pulmonary edema. *Am. J. Physiol.* **213:** 79-82, 1967.

Gaar, Jr. K. A; Taylor, A.E; Owens, J. L; and Guyton, A. C. Pulmonary capillary pressure and filtration coefficient in the isolated perfused lung. *Am. J. Physiol.* **213:** 910-914, 1967.

Gaar, Jr. K. A; Taylor, A.E; and Guyton, A. C. Effect of lung edema on pulmonary capillary pressure. *Am. J. Physiol.* **216:** 1370-1373, 1969.

Goresky, C. A., Cronin R. F. P. and Wangel, B. E., Indication dilution measurements of extravascular water in the lungs. *The Journal of clinical Investigation*, **48**, 487-501, 1969.

Gorin, A.B., Kohler,J. and DeNardo, G., Nonivasive measurement of pulmonary transvascular protein flux in normal man. *J. Clin. Invest.* **66**: 869-877, 1980.

Greenfield, L. J., Surgery: Scientific Principles and Practice. Edited by Greenfield, J. B Lippincott Company, Philadelphia, 1993.

Griffiths, P. R., and de Haseth, J. A., *Fourier transform infrared spectroscopy*, Wiley, New York, 1986.

Guyton, A. C. and Hall, J. E., *Textbook of medical physiology*, 9th edition, W.B. Sanders Company, 1996.

Guyton, A. C., Concept of negative interstitial pressure based on pressures in implanted perforated capsules. *Circ. Res.*, **12**: 399, 1963.

Guyton, A. C., Interstitial fluid pressure: II. Pressure-volume curves of interstitial space. *Circ. Res.*, **16**: 452, 1965.

Guyton, A. C. et al., Interstitial fluid pressure pressure: III. Its effect on resistance to tissue fluid mobility. *Circ. Res.*, **19**: 412, 1966.

Guyton, A. C. et al., Interstitial fluid pressure pressure: IV. Its effect on fluid movement through the capillary wall. *Circ. Res.*, **19**: 1022, 1966.

Guyton, A. C. et al., Circulatory Physiology II. Dynamics and control of the body fluids. Philadephia, W. B. Saunders Co., 1975.

Guyton, A. C. Granger, H. J., Taylor, A. E., Interstitial fluid pressure. *Physiol. Rev.*, **51**: 527, 1971.

Guyton, A. C. et al., Forces governing water movement in the lung. In Fishman, A. P., and Renkin, E. M. (eds): Pulmonary edema. Baltimore, Waverly Press, p65, 1979.

Hancock, B. J., Hoppensack, M. and Oppenheimer, L., Do transvascular forces in isolated lobe preparation equibrate? *J. Appl. Physiol.*, **67**: 628-635, 1989.

Hardt, N.S., Yu., L. T., La Torre, G., Steinbach, B., Fourier transform infrared microspectroscopy used to identify foreign material related to breast implants. *Mod. Pathol.* 7: 669-676, 1994.

Harms, B. A., Rosenfeld, D. J., Pahl, A. C., Conhaim, R. L.and Starling J. R., Pulmonary transvascular fluid filtration response to hypoproteinemai and Hespan infusion. *Journal of Surgical Research*, **48**: 408-414, 1990.

Harris, T. R., Bernado, G. R., Brigham K. L., Higgins, S. B., Rinaldo, J. E., Borovetz, H. S., Sibbald, W. J., Kariman, K. and Sprung, C. L., Lung microvascular transport properties measured by multiple indicator dilution method in patients with adult respiratory distress syndrome. *Am. Rev. Respir Dis.* **141**: 272-280, 1990.

Hayat, M. A., Principles and techniques of electron microscopy: Biological applications. Baltimore, MD: University Park, 1981.

Heise. H. M., Marbach. R., Koschinsky, T., Gries. F. A., Heise. H. M., Multicomponent assay for blood substrates in human plasma by mid-infrared spectroscopy and its evaluation for clinical analysis. *Appl. Spectrosc.* **48**: 85-95, 1994.

Heise. H. M. and Bittner, A., Investigation of experimental errors in the quantitative analysis of glucose in human blood plasma by ATR-IR spectroscopy. *J. Mol. Struct.*, **348**: 21-24, 1995.

Herzberg, G., Molecular spectra and molecular structure. II Infrared and Raman spectra of polyatomic molecules. Published by Van Nostrand Reinhold Company, New York, 1945.

Hineno, M., Infrared spectra and normal vibrations of β-D-glucopyranose. *Carbohydrate Res.* **56**: 219, 1977.

Hudson, L. D., Milberg, J. A., Anardi, D. and Maunder, R. J., Clinical risks for development of the acute respiratory distress syndrome. *Am. J. Respir Crit. Care Med.* **151**: 293-301,1995.

Jackson, M., Mantsch, H. H., The use and misuse of FT-IR spectroscopy in the determination of protein structure. *Critical Reviews in Biochemistry and Molecular Biology*, **30**: 95-120, 1995.

Joris, I., Majno, G., Ryan, G. B., Endothelial concentration in vivo: a study of rat mesentery. *Virchows Arch B Cell Pathol.* **12**: 73, 1972.

Joris, I., Majno, G., Corey, E. J., The mechanism of vascular leakage induced by leukotrience E4: endothelial contraction. *Am. J. Pathol.* **126**:19, 1987.

Kalasinsky, V.F., Biomedical applications of infrared and raman microscopy. *Applied Spectroscopy Reviews*, **31**: 193-249, 1996.

Kedem, O. and Katchalsky, A., Thermodynamic analysis of the permeability of biological membranes to non-electrolytes. *Biochimica et biophysica acta*, **27**: 229-246, 1958.

Kenton, J. A., Kalasinsky, V. F., Johnson, F. B., Vinh, T. N., O'Leary, T. J., Fourier transform infrared microscopic identification of foreign materials in tissue sections. *Lab. Invest.* **66**: 123-131, 1992.

Koza, J. R., *Genetic programming: On the programming of computer by means of natural selection.* The MIT press, Combridge, Massachusttes, London, England, 1980.

Krafft. P., Fridrich, P., Pernerstorfer, T., Fitgerald, R. D., Koc, D., Schneider; B., Hammerle, A. F., Steltzer, H., The acute respiratory distress syndrome: definitions, severity and clinical outcome. An analysis of 101 clinical investigations. *Intensive Care Med.*, **22**: 519-529, 1996.

Kreuzfelder, E., Koka, T., Keinecke Heinz-otto., Obertacke, U., Schmit-Neurbrg, K-P., Nakhosteen J. A., Paar, D. and Scheiermann, N., Adult respiratory distress syndrome as a specific manifestation of a general permeability defect in trauma patients. *Am. Rev. Respir. Dis.* **137**: 95-99, 1988.

Laine, G. A., Allen, S. J., Katz, J. W., Gabel, J. C., Drake, R. E., A new look at pulmonary edema. *News Physiol. Sci.*, 1: 150, 1986.

Landis, E. M., Heteroporosity of the capillary wall as indicatedby cinematographic analysis of the passage of dyes. *Ann. NY Acad. Sci.* **116**: 765-773, 1964.

Landis, E. M. and Pappenheimer, J. R., Exchange of substances through the capillary walls. In: *Handbook of Physiology. Circulation,* edited by W. F. Hamilton. Sec. 2, Vol. II Chapter 29, p. 961-1034, Washington, DC: *Am. Physiol. Soc.*, 1963.

Lasch, P. and Naumann, D., FT-IR microspectroscopic imaging of human carcinoma thin section based on pattern recognition techniques. *Cellular and Molecular Biology*. **44**: 189-202. 1998.

Levick, J. R. and Michel, C. C., Permeability of individually perfused frog mesenteric capillaries to T-1824 and T-1824-Albumin as evidence for a large pore system. *Q. J. Exp. Physiol.* **58**: 67-85, 1973.

Lui, K-Z., Ahmed, M. K., Dembinski.. T. C., Mantsch, H. H., *J. Gynec. Obstetrics* **57**: 161, 1997.

Macnaughton, P. D., Pulmonary physiology of acute lung injury. In *ARDS: acute respiratory distress in adults*. Edited by Timothy, W.E and Christopher H. Chapman and Hall Medical, 1996.

McGrath, A., Conhaim, M. R. L., Myers, G. A. and Harms, B. A., Pulomonary vascular filtration of starch-based macromolecules: Effects on lung fluid balance. *Journal of Surgical Research*, **65**, 128-134, 1996.

Majno, G., Palade, G. E., Schoefl, G. I Studies on inflammation; The site of action of histamine and serotonin along vascular tree: a topographic study. *J. Biophys. Biochem Cytol.* 11:697, 1961.

Majno, G., Sea, M. S., Leventhal, M., Endothelial contraction induced by histamine-type mediators: an electron microscopic study. *J. Cell Biol.* **42**: 647, 1969.

Mantsch, H. H and Jackson, M. Molecular spectroscopy in biodiagnostics. *Journal of Molecular Structure*, **347**: 187-206, 1995.

Marinelli, W. A; and Ingbar D. H., Diagnosis and management of acute lung injury. *Clinics in Chest Medicine*, **15**: 517-546, September, 1994.

Mathlouthi, M and Koenig, J. L., Vibrational spectra of carbohydrates. *Advances in Carbohydrates Chemistry and Biochemistry*, **44**: 7-89, 1986.

McGrath, A. M., Robert, L. C., Myers, G. A. and Harms, B. A., Pulmonary vascular filtration of starch-based macromolecules: effect on lung fluid balance. *Journal of Surgical Research*, **65**: No.2, 1996.

McNamee, J. E. and Staub, N. C., Pore models of sheep lung microvascular barrier using new data on protein tracers. *Microvascular reasreach*, **18**: 229-244, 1979.

Meyer, B. J., et al., Interstitial fluid pressure V. Negative pressure in the lungs. *Circ. Res.*, **22**: 263, 1968.

Mikulecky, D. C., On the relative contribution of viscous flow vs diffusinal (frictional) flow to the stationary state flow of water through a "tight" membrane. *Biophysical Journal*, **7**: 527-534, 1967.

Milici, A. J., Watrous, N. E., Stukenbrok, H. and Palade, G. E., Transcytosis of albumin in capillary endothelium. *J. Cell.Biol.* **105**: 2603-2612, 1987.

Mintun, M. A., Warfell, T. E. and Schuster, P. D., Evaluating pulmonary vascular permeability with radiolabeled proteins: an error analysis. *J. Appl.Physiol.* **68**: 1696-1706, 1990.

Murray, J. F., Matthay, M. A., Luce, J. M. and Flick, M. R., An Expanded Definition of the adult respiratory distress syndrome. *Am. Rev. Respir. Dis.* **138:** 720-723; 1988.

Nikulin, A. E., Dolenko, B., Bezabeh. T. and Somorjai, R. L., Near-optomal region selection for feature space reduction: novel preprocessing methods for classifying MR spectra. *NMR in Biomedicine*, **11**, 209-216, 1998.

Oppenheimer, L., Lung fluid movement and its relevance to the management of patients with increased lung water. *Clinical Intensive Care, the International Journal of Critical and Pulmonary Care Medicine*, **1**: 103-110, 1990.

Oppenheimer, L., New approaches to the measurement of pulmonary capillary permeability and pulmonary edema. *The Canadian Journal of Surgery*, **25**: No. 4, 1982.

Oppenheimer, L. and Huebert, D., Near-infrared spectrophotometric devices to measure fluid exchange in blood-perfused organs. *J. Appl. Physiol.* **74**: 2205-2213, 1993.

Oppenheimer, L. Interstitial space and pulmonary oedema, Adult respiratory distress syndrome, Chapter 17, *Current concept on adult respiratory distress syndrome*, Zopol Lamare Artigaf, Churchill Inc., 193-207, 1984.

Oppenheimer, L., Goldberg, H. S., Pulmonary circulation and edema formation. In *Heart-lung interactions in health and disease*. Edited by Scharf, S. M and Cassidy S. S, Marcel Dekker, Inc, New York, 1989.

Oppenheimer, L., Unruh H. W., Skoog; C. and Goldberg H. S., Transvascular fluid flux measured from intravascular water concentration changes. *J Appl. Physiol.*: **54**: 64-72, 1983.

Oppenheimer, L; Smit, A. and Palomar, A., Pulmonary edema reabsorption: New therapeutic strategies. In *"The pulmonary circulation: Moving from passive to active control"*. Edited by Pinsky, M.R et al. W.B.Saunders Company Ltd, 1996.

Owens, C., M; Evans, T. W., Keogh, B. F. and Hansell, D. M., Computed tomography in established adult respiratory distress syndrome, correlation with lung injury score. *Chest* **106**: 1815-1821, December, 1994.

Pappenheimer, J., Passage of molecules through capillary walls. *Physiol. Rev.* **33**: 387-423, 1953.

Parker, J. C., Guyton, A. C., Taylor, A. E., Pulmonary interstitial and capillary pressure estimated from intra-alveolar fluid pressure. *J. Appl. Physiol.*, **44** (2): 267, 1978.

Parker, J. C., et al., Pulmonary transcapillary exchange and pulmonary edema. In Guyton, A. C., and Young, D. B. (eds): International Review of physiology: Cardiovascular Physiology III. Vol. 18. Baltimore, University Park Press, p. 261, 1979.

Patlak, C. S., Goldstein, D. A., and Hoffman J. F., The flow of solute and solvent across a two-membrane system. *Journal Theoretical Biology*, **5**: 426-442, 1963.

Parker, J. C., Ryan, J. and Taylor, A. E., Plasma-lymph albumin kinetics, total lymph flow, and tissue hematocrit in normally hydrated dog lungs. *Microvasc. Res.* **28**: 254-269, 1984.

Pepe, P. E., Potkin, R. T., Reus, D. H., Hudson, L. D., Carrico, C. J., Clinical predictors of the adult respiratory distess syndrome. *The American Journal of Surgery.* **144**: 124-130, July 1982.

Peterson, B. T., Permeability: theory vs practice in lung research. *Am. J. Physiol. (Lung cell. Mol Physiol.* **6**: 243-256, 1992.

Pickere, J. A., Lung connective tissue: location, metabolism, and response to injury. Boca Raton, Fl., CRC Press, 5-100, 1981.

Putensen, C., Mutz, N., Himmer, G., Himmer, G., Neumann, M., Waibel, U., Putz, G., Braunsberger, B., Oberladstätter, M., Gamma scintigraphic imaging of lung microvascular permeability in adult respiratory distress syndrome. *Crit. Care Med.* **18**: 807-812, 1990.

Quon, C. Y., Clinical pharmacokietics and pharmacodynamics of colloidal plasma volume expanders. *J Cardiothoracic Anesthesia* **2**: 13-23, 1988.

Rabinovici, R., Yue, T. L., Vernick, J., PAF, Eicosanoids and Cytokines. PAF and TNFα interaction in the pathophysiology of septic shock. In: *Cell-Cell interaction in the release of inflammation mediators, Eicosanoids, Cytokines and Adhesion.* Edited by Wong Y-K, Sherhan C.N. New York, NY: Plenum Press; 193, 1991

Reid, L. M., Pathology of Adult respiratory distress syndrome and experimental injury, with emphasis on vascular changes. *Seminars in respiratory medicine supplement issue* 29-35, Oct. 1986, Thieme Medical Publishers, Inc., New York.

Rencher. A. C., Method of multivariate analysis. A Wiley-Interscience Publication. John Wiley & Sons, Inc. 1995.

Rencker. Method of multivariate statistics, Wiley Interscience, 1995.

Rigas. B., Morgallo, S., Goldman, I. S. and Wong, P. T. T., *Proc. Natl. Acad. Sci.* USA **87**: 8140, 1990

Rinaldo, J. E., Borovetz, H. S., Mancini, M., Hardesty R. L. and Griffith B. P., Assessment of lung injury in the adult respiratory distress syndrome using multiple indicator dilution curves. *Am Rev. Respir.Dis.* **133**: 1006-1010,1986.

Renkin, E. T. and Curry, F. E., Endothelial permeability: pathways and eodulations. *Annals New York Academy of Sciences*, 248-258, 1982.

Rennard, S., Basset, G., Lecossier, D., O'Donnell, K., Martin, P. and Crystal, R. G., Estimation of volume of epithelial lining fluid recovered by lavage using urea as a marker of dilution. *J. Appl. Physiol.* **60**: 532-538, 1986.

Romeo, M., Urden F., Quinn; M., Wood, B. and McNaughton, D., Infrared microspectroscopy and artificial neural network in the diagnosis of cervical cancer. *Cellular and Molecular Biology*, **44**: 179-188, 1998.

Russnyak, I., Foldi, M. and Szab , G., Lymphatics and lymph circulation: Physiology and Pathology, 2nd edition Oxford, UK: Pergamon, p971, 1967.

Rubin, E., and Farber, J. L., Pathology, 2nd edition, J.B Pillicott Company, Philadelphia, 1994.

Sakuma, T., Okaniwa, G., Nakada, T., Nishimura, T., Fujimura, S., and Matthay M. A., Alveolar fluid clearance in the resected human lung. *Am. J. Respir. Crit. Care Med.* **150**: 305-310, 1994.

Sandiford, P., Province, M. A., and Schuster, D. P., Distribution of regional density and vascular permeability in the adult respiratory distress syndrome. *Am. J. Respir. Crit. Care Med.* **151**: 737-742, 1995.

Schultz, C. P., Liu, K. Z., Jonston, J. B. and Mantsch H. H., Study of chronic lymphocytic leukemia cells by FT-IR spectroscopy and cluster analysis. *Leukemia Research.* **20**: No. 8 649-655, 1996

Schultz, C. P., Khalique, A. M., Dawes, C. and Manstch, H.H., Thiocyanate levels in human saliva: quantitation by Fourier transform infrared spectroscopy. *Analytical biochemistry*. **240**, 7-12, 1996.

Schultz, C. P. and Manstch, H.H., Biochemical imaging and 2D classification of keratin pearl structure in oral squamous cell carcinoma. *Cellular and Molecular biology*. **44**: 203-210, 1997.

Schuster, D. P., What is acute lung injury? What is ARDS? *Chest* **107**: 1721-1726, 1995.

Sinclair, D. G., Braude, S., Haslam, P. L. and Evans T.W., Pulmonary endothelial permeability in patients with severe lung injury. *Chest*, **106**: 2, 535-539, 1994.

Shaw, R. A., Kotowich, S., Mantsch, H. H. and Leroux, M., Quantitation of protein, creatinine, and urea in urine by nera-infrared spectroscopy. Clinical biochemistry, **29**: No. 1, 11-19, 1996.

Shennib, H. and Tector. J. Reperfusion injury in lung transplantation. *Reperfusion Injuries and Clinical Capillary Leak Syndrome*. Edited by Zikria, B.A. and Carlson R. W. Armonk, NY: Futura Publishing Company, 1994.

Spendding, H., Infrared spectroscopy and carbohydrate chemistry. *Advances in Carbohydrate Chemistry*, **19**: 23-49, 1964.

Sprung, C. L., Rackow, E. C., Fein, A.., Jacob, A.I., and Isikoff, A. K., The spectrum of pulmonary edema: differentiation of cardiogenic, intermediate, and noncardiogenic forms of pulmonary edema. *Am. Rev. Respir. Dis.* **124**: 718-722, 1981.

Starling, E. H., On absorption of fluid from the connective tissue spaces. *J. Physiol.* **19**: 312-236, 1896.

Staub, N. C., Pulmonary edema. *Physiological Review* **54**: (3) 678-811, 1974

Staub, N. C., Bland, R. D., Lbrigham, R. W. C., Demchronic lung lymph fistulas in sheep. *J. Surg.* **19**: 315-320, 1975.

Staub, N. C., Pulmonary edema due to increased microvascular permeability. *Annu. Rev. Med.*, **32**: 291, 1981.

Staub, N. C., Interstitial volume regulation and lymphatic clearance. *Plasma volume expansion*. Edited by Jea-Francois Baron, Arnette, Paris, 1992.

Sugerman, H. K., Hirsch, J. I., Pharm, D., Strash, A. M., Kan, P. T., Sharpe, Jr. A. R., Stoneburner, J. and Greenfield, L. J., Gamma camera detection of oleic acid alveolar-capillary albumin leak. *Journal of Surgical Research.* **29**: 93-99, 1980.

Tanaka, H., Dahms, T. E., Bell, E., Naunheim, K. S. and Baudendistel, L. J., Effect of Hydroxyethyl starch on alveolar flooding in acute lung injury in dogs. *Am. Rev. Respir. Dis.* **148**: 852-859, 1993.

Unruh, H. W., Goldberg, H. S. and Oppenheimer L., Pulmonary interstitial compartments and tissue resistance to fluid flux. *J. Appl. Physiol.* **57**: 1512-1519, 1984.

Ulrich, K. Kroemer, H. Clinical Pharmacokinetic considerations in the use of plasma expanders. *Clinical Pharmacokinetics*, **12**: 123-135, 1987.

Vasko, P. D., Blackwell, J., and Koenig, J. L., Infrared and Raman spectroscopy of carbohydrates, Part I. *Carbohydrate Res.* **19**: 297-310, 1971.

Vasko, P. D; Blackwell, J. and Koenig, J. L., Infrared and Raman spectroscopy of carbohydrates, Part II. *Carbohydrate Res.* **23**: 407-416, 1972.

Véronique bellon-maurel, Vallat, C. and Goffinet, D., Quantitative analysis of individual sugar during starch hydrolysis by FT-IR/ATR spectrometry. Part I: Multivariate calibration study-repeatability and reproducibility. *Applied spectroscopy* **4**: Number 5, 1995.

Wang, J., Sowa, M., Mantsch, H. H., Bittner, A., Heise, H. M., Comparison of different infrared measurement techniques in the clinical analysis of biofluids. *Trends in analytical chemistry*, **15**: No. 7, 286-295, 1996.

Webb, A. R., Tighe, D., Moss, R. F., Al-Saady, N., Hynd, J. W., Bennett, E. D., Advantage of a narrow-range, medium molecular weight hydroxyethyl starch for volume maintenance in a porcine model of fecal peritonitis. Critical Care Medicine, **9**: 409-416. 1991.

Weibel, E. R., Morphological basis of alveolar-capillary gas exchange. *Physiol. Rev.* **53**: 419-495,1973.

Weinbaum, S. and Curry, F. E., Modelling the structure pathways for transcapillary exchange. 323-345, 1995.

Weigelt, J. A., Management of the patient with the adult respiratory distress syndrome. *Seminars in respiratory medicine supplement issue* 54-58, Oct. 1986, Thieme Medical Publishers, Inc., New York.

Willoughby, D. A., Mediation of increased vascular permeability in inflammation. In: *The inflammatory process*. Edited by Zweifach B.W, Grant L, McClusky R.T. New York, NY: Academic Press; **2**: 303, 1973.

Wong, P. T., Wong, T. R. K. and Fung, M F. K., Pressure-tuning FT-IR of human cervical tissues. *Appl. Spectrosc.* **47**: 1058, 1993.

Yoffey, J. M. and Courtice, F. C., Lymphatics, lymph and the lyphomyeloid complex. *London: Academic*, 1970.

Zikria, B. A., King, T. C., Stanford, J. and Freeman, H. P., A biophysical approach to capillary permeability. *Surgery*, **105**: 625-631, 1989.

IMAGE EVALUATION
TEST TARGET (QA-3)

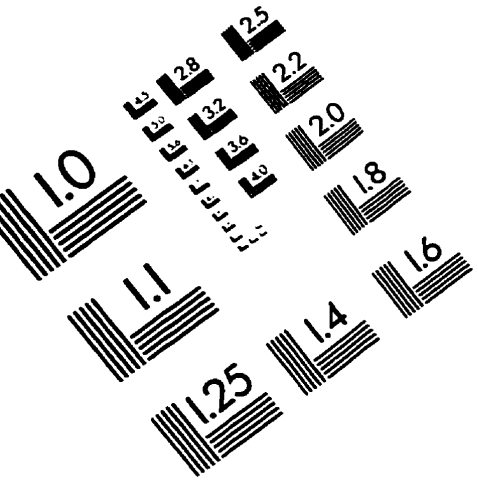

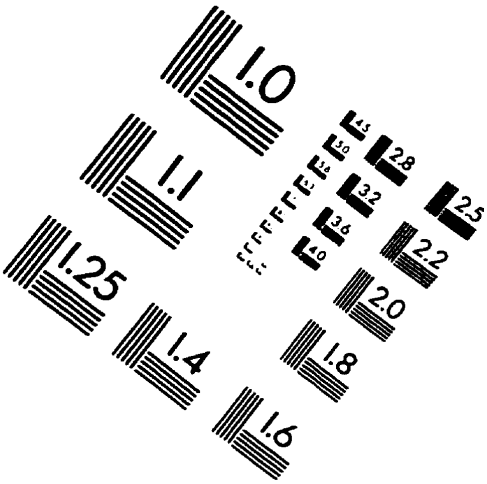

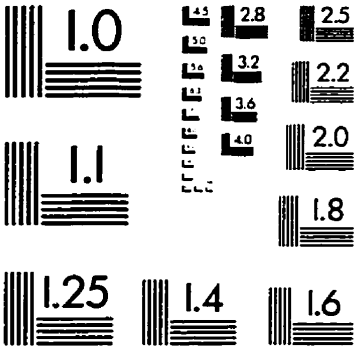

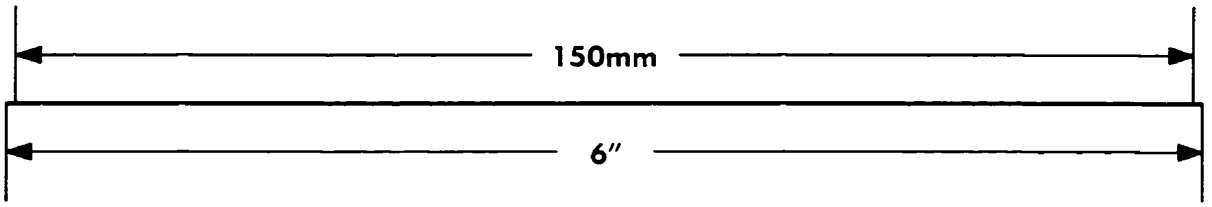

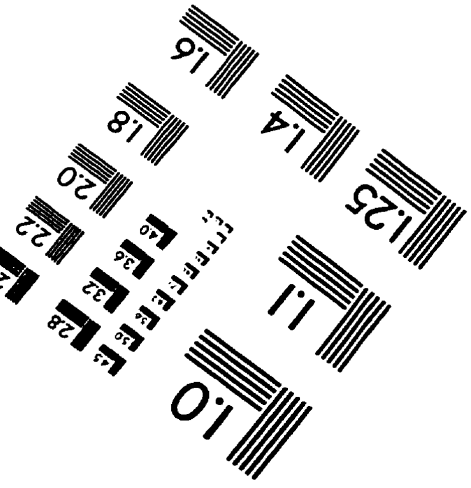

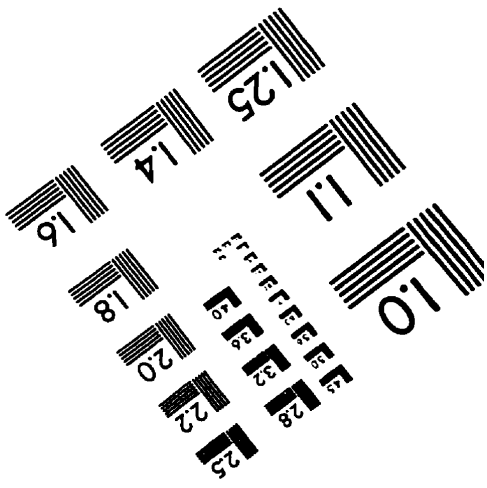

APPLIED IMAGE, Inc
1653 East Main Street
Rochester, NY 14609 USA
Phone: 716/482-0300
Fax: 716/288-5989